In compliance with the
Canadian Privacy Legislation
some supporting forms
may have been removed from
this dissertation.

While these forms may be included
in the document page count,
their removal does not represent
any loss of content from the dissertation.

REAL-TIME RAINFALL ESTIMATION AND PREDICTION

By

MOHAMED GAD, B.SC., M.SC.

A Thesis

Submitted to the School of Graduate Studies

in Partial Fulfilment of the Requirements

for the Degree of

Doctor of Philosophy

McMaster University

REAL-TIME RAINFALL ESTIMATION AND PREDICTION

DOCTOR OF PHILOSOPHY (2002) McMaster University

(Civil Engineering) Hamilton, Ontario

Title:	Real-Time Rainfall Estimation and Prediction
Author:	Mohamed Gad, B.Sc (Ain Shams), M.Sc (Ain Shams)
Supervisor:	Professor I.K. Tsanis
Number of pages:	xxv, 323, A.60

ABSTRACT

In this study the two problems of rainfall estimation and forecasting using data from weather radars and rain-gauges are studied. A GIS multi-component interface is developed for the analysis of weather radar precipitation data. This interface performs different operations, such as loading and redelivering radar and satellite data, projecting geographical features into the radar coordinate system, and overlaying data from multi-sensor into a common coordinate system. Additional features include accumulating radar rainfall depths, radar comparison with rain-gauge data, animating storm evolution on top of geographical features, and tracking and forecasting rainfall fields.

Accurate measurements of rainfall duration, timing, location, and intensity are important for different water resources applications. Weather radars can provide valuable information on the space-time variations of rainfall. However, there are uncertainties in the radar measurements of precipitation. Thus rain-gauges are used to calibrate Z-R relations, which are used to convert from radar reflectivity Z to rainfall rate R. Sampling errors cause differences between rainfall estimated by radar and that estimated by rain-gauges. These errors constitute a limitation for use of radar data for high resolution applications such as urban applications. A methodology is developed to address and correct the effects of these errors. The results prove that correction for these errors reduces the variation between the two sensors. In addition, given that the radar is properly calibrated, correction for sampling errors can provide temporally detailed radar rainfall fields that can be used for high resolution hydrological applications.

The comparisons between two Canadian radars (King City and Exeter) show

that there is good agreement between rainfall fields estimated by the two radars. The comparisons between radar rainfall intensities estimated by the two radars and the corresponding rain-gauge intensities show that the classical Z-R equation used by the National Canadian Radar Network is biased and can lead to serious underestimation of rainfall. An optimum Z-R relation is calibrated using surface rain-gauge data to be used for unbiased rainfall estimation by the two radars.

A new radar-based model is developed for quantitative short-term forecasting of rainfall fields. The new model is called the AARS (Automated Adaptive Rainfall Simulator). The AARS model employs an optimization strategy for performing the cross-correlation analysis that reduces the run time significantly and makes the technique attractive for real-time applications. In addition, the model tracks and forecasts the changes in rainfall intensities in space and time and produces forecasted rainfall fields for the specified lead time. The AARS model employs the adaptive exponential smoothing algorithm for real-time parameters estimation. Performance comparisons between the AARS model and the Canadian short-term prediction model SHARP (Short-Term Automated Radar Prediction) show that the AARS is superior in terms of tracking run time and slightly better in terms of accuracy for forecasting lead times up to 30 minutes. The application of the AARS model for rainfall forecasting in Hamilton-Wentworth Region shows promising results for forecasting lead times less than 60 minutes.

ACKNOWLEDGMENTS

First, I wish to acknowledge my academic advisor, Dr. I. Tsanis of the Department of Civil Engineering, for suggesting this research and for supervising the thesis. I wish also to acknowledge my supervisory committee members, Dr. S. Moin from the Dept. of Civil Engineering and Dr. M. Woo from the School of Geography and Geology for their help and guidance over the past four years. Dr. Norman Donaldson from King Weather Radar Group and Mr. Mark Stirrup from the Regional Municipality of Hamilton-Wentworth are acknowledged for several insightful discussions. I would like to thank the faculty members and staff of the Civil Engineering Department at McMaster University, The Regional Municipality of Hamilton-Wentworth for providing rain-gauge data from the regional network, King Weather Radar Group for providing the real-time feed of radar data, Ontario Climate Center for providing rain-gauge data in Southern Ontario, and the Meteorological Service of Canada for providing GOES-8 satellite images. I am grateful to the CIS staff, M. Hollamby-Lane, P. Monger, and T. Pfaff for their technical support in managing the real time feed of radar data.

Finally, I am unable to find the right words to say to my parents, who always support me. Without you, I might not have had the ability to complete this graduate degree.

TABLE OF CONTENTS

LIST OF FIGURES

LIST OF TABLES

LIST OF SYMBOLS AND ABBREVIATIONS

Symbols

English Alphabet (uppercase followed by lower case letters)

A	Radar Z-R constant.
$A(c)$	State vector of a radar rainfall pixel at time c.
$A_{c,c}$	Updated state vector at time c, this state-vector is used for forecasting the next forecast.
$A_{c-t,c-t}$	State vector at the previous time step.
a'	Half the major axis of the ellipse.
b	Radar Z-R constant.
b'	Half the minor axis of the ellipse.
C_R	The radar constant which depends on many factors including the transmitted power, antenna gain, horizontal and vertical beam widths, pulse length, and wave length.
CSI	Critical Success Index.
D_o	Raindrop diameter in mm at the subcloud level.
D_t	Raindrop diameter in mm at the ground level.
d_{tg}	One minute TB rain-gauge accumulation at time t_g (mm).
d'	Separation between the tangent plane at the radar location and a parallel plane at the pulse volume height.
e	Eccentricity of the ellipse.
E_c	The error between the observed value $R(c)$ at time c and the t-step ahead forecast $R_{c,c-t}$ made at time c-t.
ER	Earth radius.

FCC	Forecasting cross-correlation between a forecasted rainfall field and its corresponding measured field.
$Ferr$	Average forecasting error between a forecasted rainfall field and its corresponding measured field.
$FRMS$	Forecasting Root Mean Square error between a forecasted rainfall field and its corresponding measured field.
h	Length of the pulse volume in space.
h_N	Distance from the center of the ellipsoid and the projection of the pole on the parallel plane.
H_o	The length of a line drawn from the radar location perpendicular to the equatorial plane, i.e, perpendicular separation between a parallel circle at the radar and the equator.
H_p	The length of a line drawn from the point being projected perpendicular to the equatorial plane, i.e, perpendicular separation between a parallel circle at the point and the equator.
H'	Smoothing coefficient vector.
I_g	Rain-gauge rainfall intensity.
I_r	Radar rainfall intensity.
K_A	The complex index of refraction.
$M(t)$	Transition Matrix.
$N_o(D_o)$	Raindrop size distribution (a density function) in number of drops per cubic meter of air per unit size interval at the subcloud level.
$N_t(D_t)$	Raindrop size distribution in number of drops per cubic meter of air per unit size interval at the ground level
O	The radar Location.
P	Location of the point being projected.
P_r	Radar returned power.
Q_p	The intersection of a line drawn from point P perpendicularly to the ellipsoid and the minor axis of the ellipsoid.
$\overline{Q_p P}$	Length of a line drawn from point P perpendicularly to the ellipsoid

	towards its intersection with the minor axis of the ellipsoid, i.e, the radius of curvature of the ellipsoid in a plane perpendicular to the meridional plane at the point being projected.
r	Range from the radar location.
r_p	Range of point P with respect to the radar planar coordinate system.
R	Rainfall rate.
$R2$	Coefficient of determination.
$R(c)$	Rainfall observation obtained at the current time c.
$R_{c,c-t}$	The t-step ahead forecasted value made at time c-t.
$R(t)$	Rainfall Intensity at a radar pixel at time t.
R_o	Radius of a circle passing thought the radar location on the spheroid surface and parallel to the equatorial plane.
R_p	Radius of a circle passing thought the point being projected on the spheroid surface and parallel to the equatorial plane.
t	Time.
T	Accumulation period.
T_{drop}	The time required for a rain drop to fall to the ground
V	Speed of rainfall patterns.
W	Gravity potential.
$w_t(D_t)$	Drop terminal velocity.
x_p, y_p	Cartesian Coordinates of the projected point with respect to the radar planar coordinate system.
$Xshift$	Cartesian shift in X direction of the current radar rainfall grid with respect to the previous radar rainfall grid.
$Xshift_{opt}$	Optimum Cartesian shift in X direction of the current radar rainfall grid with respect to the previous radar rainfall grid.
x,y	Cartesian Coordinates.
$Yshift$	Cartesian shift in Y direction of the current radar rainfall grid with respect to the previous radar rainfall grid.
$Yshift_{opt}$	Optimum Cartesian shift in Y direction of the current radar rainfall grid

	with respect to the previous radar rainfall grid.
y'_p	A specific distance in the radar data plane.
Z	Radar reflectivity.

Greek Alphabet (uppercase followed by lower case letters)

γ_p	An angel in the plane defined by the three points P, Q_p, and u_p. Where u_p is the normal projection of point P on a plane defined by the radar location and the minor axis of the ellipsoid.
$\Delta \lambda_p$	Difference in longitude between the point being projected and the radar.
ΔS	Spatial shift of the current radar rainfall grid with respect to the previous radar rainfall grid.
ΔS_{opt}	Optimum spatial shift of the current radar rainfall grid with respect to the previous radar rainfall grid.
β	Radar elevation angel.
β'	Exponential smoothing coefficient.
α_p	Azimuth of point P with respect to the radar planar coordinate system.
α	Radar azimuth.
ρ	Correlation coefficient.
σ	Standard deviation.
ΔH_p	Distance between the intersection of the normal to the ellipsoid at point P and the minor axis of the ellipsoid, and the center of the ellipsoid.
θ_p	An angel in the plane of the radar and the minor axis of the ellipsoid.
θ	An Integer.
λ_o	Longitude of the radar location.
λ_p	Longitude of the point being projected.
Φ_o	Geodetic latitude of the radar location.
Φ_p	Geodetic latitude of the point being projected.
Φ'_o	Geocentric latitude of the radar location.
Φ'_p	Geocentric latitude of the point being projected.

ψ	The earth centered angle corresponding to a great circle arc drawn between P (the point being projected) and O (radar location) in their plane with the earth's center.
η	Halting percent of the starting tabu search in the initialization scan.
r_p , α_p	Polar coordinates of the projected point with respect to the radar planar coordinate system.

Abbreviations

AARS	Adaptive Automated Rainfall Simulator
AFGWC	Air Force Global Weather Central.
AGL	Above Ground Level.
ANN	Artificial Neural Network.
ASCII	American Standard Code For Information Interchange.
c/w	Mixed-type Rainfall (more convective + Widespread)
c	Convective.
CAPPI	Constant Altitude Plane Position Indicator.
CC	Cross-correlation between two scans from two different radars.
DBF	Data Base Format.
DBZ	Units of Radar Reflectivity in Decibels (on a logarithmic scale).
DLL	Dynamically Linked Library.
ESRI	Environmental Systems Research Institute.
FMH	Federal Meteorological Handbook.
GIF	Graphics Interchange Format.
GIS	Geographical Information System.
GOES	Geostationary Operational Environmental Satellite.
GPP	Gravitational Planar Projection.
GPS	Global Positioning System.
HRAP	Hydrologic Rainfall Analysis Project.
IDW	Inverse Distance Weighted Interpolation.

IEEE	Institute of Electrical and Electronics Engineers.
IR	Infra Red.
JPEG	Joint Photographic Experts Group.
MOS	Synoptic Scale Models Using Model Output Statistics.
MCS	Mesoscale Convective System.
NASA	National Aeronautics & Space Administration.
NEXRAD	Next Generation Weather Radar.
NGM	Nested Grid Model.
NMC	National Meteorological Center.
NOAA	The National Oceanographic and Atmospheric Administration.
NWP	Numerical Weather Prediction Models.
NWS	National Weather Service.
QPF	Quantitative precipitation forecasting.
RMS	Root Mean Square Error.
RMSRED	Relative Reduction in The Mean Square Error.
RS	Response Surface Search.
SHARP	Short-Term Automated Rainfall Prediction
TB	Tipping Bucket Rain-Gauge.
TS	Time shift (Chapter 6).
TS	Tabu Search (Chapter 7).
UPS	Universal Polar Stereographic system.
UTC	Coordinated Universal Time. This is the modern equivalent of Greenwich Mean Time.
UTM	Universal Transverse Mercator Projection.
w/c	Mixed-type Rainfall (more Widespread + Convective)
w	Widespread Rain
WGS84	World Geodetic System of 1984.

CHAPTER 1

INTRODUCTION

The existence of water in the liquid state makes the earth unique among the known planets. The earth has a great amount of water: over 70% of the surface is covered with water or ice. Water is continually evaporating, condensing, transported, and precipitating in a never-ending cycle known as the hydrological cycle. The hydrologic cycle involves many hydrometeorological elements. One of these elements-Precipitation-constitutes the main variable in most water resources and hydrological applications. Precipitation is the primary input to the different rainfall-runoff simulation models. Accurate precipitation analysis is important for applications such as severe rainfall and flash flood forecasting (Georgakakos and Hudlow, 1984; Seo and Smith, 1992; and others), long term water resources planning and management (Newsome and Collier, 1991), crops-yield forecasting, studies of probable design storms and floods (Hardaker and Collier, 1995), and land-atmospheric water budget studies. One of the most important applications for precipitation analysis is the real-time control of urban drainage systems (Einfalt et al. 1990; Green, 1991; Cluckie et al., 1995; and others), which requires detailed spatial and temporal information on rainfall intensity distribution. In urban combined sewer

systems, precipitation represents a health concern as precipitation analysis is used to minimize the discharge of untreated sewage into local receiving water bodies. The untreated sewage overflows occur in cases of severe rainfall events for which no prior rainfall forecast is available. Knowledge of rainfall and resulting flows at key points in the combined sewer system in advance is essential to minimize combined sewer overflows.

Severe weather, including heavy rainfall events, exact a heavy toll in both lives and property damage. For example, according to recent statistics performed by Environment Canada, poor weather conditions cause on average 220 fatal car accidents and more than 11,500 severe injuries in Canada each year. The storm in Vancouver and Victoria in December 1996 had an economic impact of $200 million and the hail storms which hit Calgary and Winnipeg in July 1996 resulted in property losses of close to $300 million.

Using data from weather radar, hydrometeorologists aim to provide more accurate information on where a storm will hit and the amount of snow or rain the area is likely to receive in advance. This information is valuable to organizations such as municipalities and conservation authorities in charge of flood control and for the management of combined sewer overflow and storm water run-off in cities and towns. In addition, information on the place, time, and amount of rainfall predicted could help municipal and provincial road crews with protection strategies against flash floods. During severe weather events, when every minute counts, improved event prediction will give us more time to protect our environment, families, and

property.

1.1 Precipitation

Precipitation occurs as a result of different atmospheric processes interacting on different spatial and temporal scales. These scales are usually classified into four main categories: the micro-scale, mesoscale, synoptic scale, and the climatological scale. Each category is also subdivided into sub-categories (refer to Orlsnski, 1975 for more details). Table 1.1 (briefly) shows the spatial and temporal resolutions of these four main scales.

Table 1.1 Meteorological Scales Definition

Classification	Spatial Scale	Temporal Scale
Micro-Scale	20 - 2000 m	seconds - few minutes
Mesoscale	2 - 200 km	few minutes - few hours
Synoptic-Scale	200 - 2000 km	few hours - few days
Climatological-Scale	2000 km - 10000 km	days - few months

This study is concerned with precipitation estimation and forecasting on a fine scale important to hydrological applications (1-10 km spatial , and 1 to 10 minutes temporal resolution). This scale is usually referred to in meteorology as the meso-γ scale. It should also be noted that the term mesoscale will be used throughout the thesis to refer to a resolution of 50-100 km, and 2-4 hours.

For the purpose of this study, precipitation may be classified by its

mechanism and the level of intensity into three main types: (1) convective precipitation; (2) widespread precipitation; and (3) orographic precipitation.

Convective Precipitation (Thunderstorms)

Convective precipitation is associated with towering cumulus clouds. This type of precipitation is most dominant in Southern Ontario. Thermal uplifting of moisture-laden air causes this type of precipitation. There are three known subcategories :(1) scattered convective cells develop through strong heating of the land surface in summer; (2) showers of rain that may form in cold, moist, unstable air passing over a warmer surface; and (3) convective activities associated with the passage of cold fronts, which commonly referred to as squall lines.

Convective precipitation is characterized by high level of rainfall intensity and is highly variable in space and time. It is possible for such rain to fall at rates of 38-50 cm/h for short periods of time. Rainfall amounts of 15-30 cm in one hour from a convective storm are not uncommon. The size of a convective storm is usually quite small. Such storms can be as large as 1600 km^2, in cases of mesoscale convective system MCS (MCS are systems composed of large number of storm cells traveling together in groups and covering large areas), but usually range from 5-8 km^2 up to 1000 km^2 (Singh, 1992). In convective precipitation rainfall rates may vary by tens of millimetres per hour in one minute and over distances of few hundred meters (Bader et al.,1983; Collier 1989; and Tsanis and Gad 2001). The small size of convective storms relates significantly to the flood producing storms for small

drainage basins. Convective storms can cover small drainage basins, but cannot completely cover large drainage basins.

In terms of spatial configurations, thunderstorms are sub-classified into single cell storm, multicell clusters, squall lines (or multicell lines) , and supercell storms (refer to Figure 1.1) . Thunderstorm cells exhibit a circular or oval shape that is generally preserved throughout their life cycle. This pattern and intensity is illustrated in Figure 1.2. Figure 1.3 illustrates a typical mature thunderstorm cell hyetograph measured at a fixed point on the ground. It should be noted that the high spatial and temporal variability of convective precipitation makes it is very difficult to estimate/forecast its detailed structure accurately in space and time with the resolutions required for fine hydrological applications (1-10 km spatial , and 1 to 10 minutes temporal resolution).

A convective storm cell undergoes three stages (known as growth, maturity, and dissipating) in its life cycle. The longer a storm preserves its structure the higher its predictability in the future. This is because the current rainfall structure can be projected into the future with high degree of confidence. The life cycle of a single convective cell takes usually from 30 to 60 minutes on average, which associates it with very low predictability beyond these times. The squall lines and supercell storms are more predictable than cases of single cells as they are associated with atmospheric conditions that usually preserve their nature for longer durations. For more details on the classifications and life cycle of thunderstorms, refer to Tsanis and Gad (1999).

Stratiform Precipitation (widespread precipitation)

In comparison with convective rainfall, stratiform rainfall is typically characterized by lighter and more uniform rainfall rates, more extensive spatial coverage, and longer duration. Stratiform precipitation is referred to in other terminology as widespread precipitation. The stratiform cloud can be associated with, for example, stable ascent in synoptic systems or weak ascent within segments of mesoscale convective systems (e.g. the extensive "trailing stratiform region" often observed to follow the intense and narrow line of convective rainfall in squall-line systems). Another example of widespread precipitation occurs in cases of cyclonic precipitation in a low-pressure systems. This type of precipitation occurs as a consequence of warm moist air being drawn into the low-pressure system, where it is elevated aloft and circulated over cold air behind the front. The amount of moisture drawn into the low pressure system depends on the intensity of the low and the available source of moisture. The intensity of rainfall from such a condition is light to medium. Figure 1.4 illustrates a typical rainfall hyetograph produced from widespread rainfall. In comparison with convective precipitation, widespread rainfall preserves its state for relatively longer durations.

Orographic Precipitation

When a parcel of warm and moist air reaches a mountain range it is lifted up the mountain slope, cooling as it rises. It then becomes saturated with water. That water begins to fall as rain, snow or hail, depending on the temperature of the

surrounding air. This process is known as orographic lifting and the cooling of the air often results in large clouds, precipitation, and even thunderstorms in some cases. This type of precipitation is not dominant in Southern Ontario although the effect of the Niagra Escarpment may account for its existence locally.

1.2 Precipitation Measurements

In traditional water resources rain-gauges have been considered the main rainfall measuring sensor. Rain-gauges provide direct rainfall measurement over small area and time intervals in the order of seconds or minutes. A rainfall network, even a fairly dense one, can miss significant rainfall, especially rainfall associated with convective storms. No rain-gauge network can observe, in real time, precipitation distribution and its variation over large areas (order of 200×200 km^2) with the accuracy required for operational flood forecasting. Thus there is a strong need for real-time precipitation analysis that is not totally dependent upon rain-gauge observations.

Development of procedures for using radar data to measure precipitation has progressed from manual techniques, to fully automatic techniques. Radar does not measure rainfall directly, rather, it measures the energy that backscatters from the meteorological target, which can be related indirectly to the precipitation rate. The distance from the radar site to the precipitation area is measured by the time between emission of the radar pulse and receipt of the echo. Thus the precipitation field can be located from the measurements of distance and direction. Radar produces an

estimate of the precipitation field in the form of a grid covering an area approximately 480×480 km^2. The spatial resolution of the radar grid is 1-4 km and the temporal resolution is 5-15 minutes (i.e., the time between measurements over the same grid point).

It is not possible to accurately determine the rainfall intensity from radar alone due to some uncertainties and bias in the radar measurements. Hence, use of radar, in conjunction with rain-gauge data as a calibrating device, can provide more accurate estimates of rainfall fields.

1.3 Scope of the Thesis

This research focuses on issues related to precipitation estimation and forecasting using data from radar and rain-gauges. In order to differentiate between the two problems, let *VARIABLE* denote a certain variable (precipitation intensity for example). The estimation problem means providing accurate computation of the current or previous values of *VARIABLE* by using measurements from all available sensors that already have measured *VARIABLE*. On the other hand, the forecasting problem involves calculating the future expected value of *VARIABLE* using information from the history of *VARIABLE*. The two problems become difficult when an estimate/forecast of *VARIABLE* in space with high resolution is required. In addition, other difficulties arise from the fact that there are uncertainties in the measurements of *VARIABLE* due to some sources of errors and due to the complicated nature of *VARIABLE*.

In this study the estimation problem deals with the accuracy of radar estimation of rainfall and the possible techniques to improve such estimation by use of rain-gauges as a calibration sensor. The second problem, i.e., the problem of quantitative precipitation forecasting (QPF) arises from the need to provide prediction of the expected amount of precipitation that will fall in the future (< 2 hrs lead time). Both the estimation and the forecasting problem studied in this dissertation aim to estimate/forecast rainfall fields in high spatial and temporal resolutions (1-4 km, 1-10 minutes). Within this main framework, attempts are made to answer several fundamental questions such as:

1- How do we overcome the difficulties of managing and processing the large amount of radar data? How can these data be incorporated into a geographical reference system?

2- Is it possible to track rainfall fields in areas not covered by radar by using data from rain-gauges only?

3- How should we study and address the sources of fluctuation between the values of precipitation measured by radar and rain-gauges?

4- Can radar data be used for high resolution hydrological applications, i.e., urban applications for example?

5- For the purpose of rainfall estimation, are the regional Canadian radars (King City and Exeter) estimating rainfall accurately? Is there a significant difference in rainfall estimation between the two radars and between the two

radars and the ground rain-gauge estimation?

6- Is improvement in real-time tracking and forecasting of rainfall fields possible? If so, how significant can this be? What is the achievable forecasting accuracy in a small area such as Hamilton-Wentworth Region?

The next chapter (Chapter 2) reviews the work done on both the rainfall estimation and prediction problems. At the end of Chapter 2, the main objectives of this thesis are formulated.

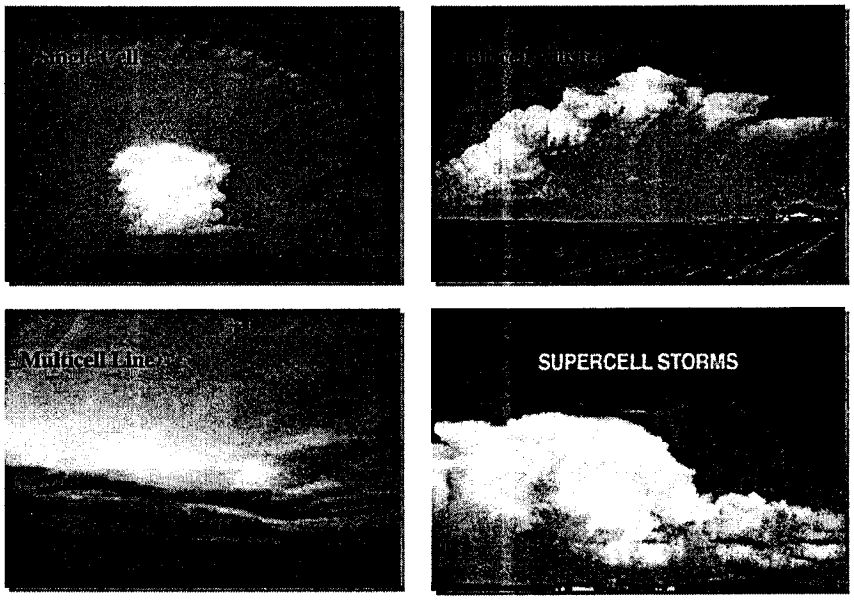

Figure 1.1 Typical thunderstorm configurations.

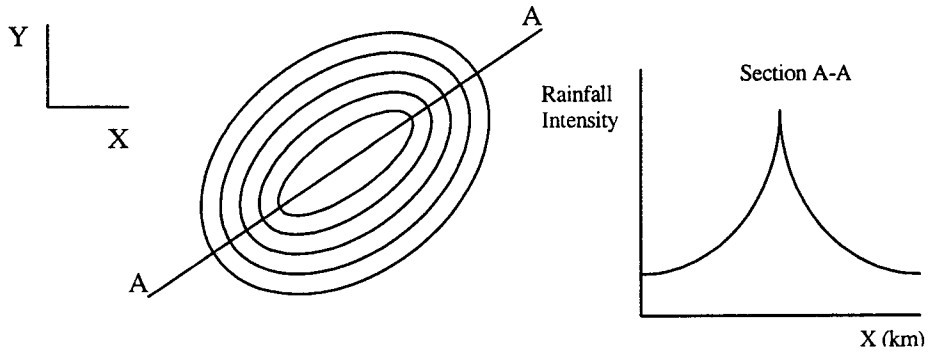

Figure 1.2 Pattern and intensity distribution of a single cell thunderstorm.

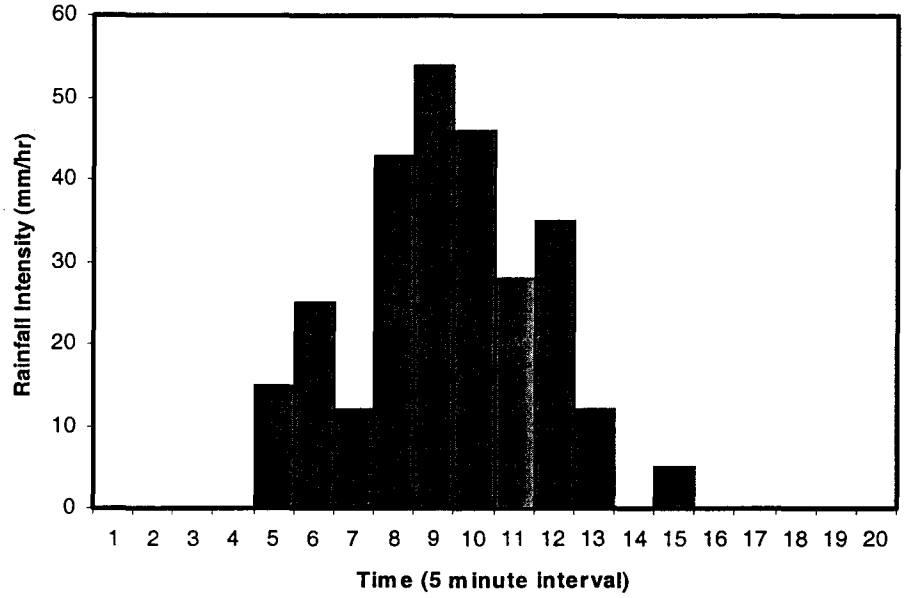

Figure 1.3 Typical mature thunderstorm cell hyetograph.

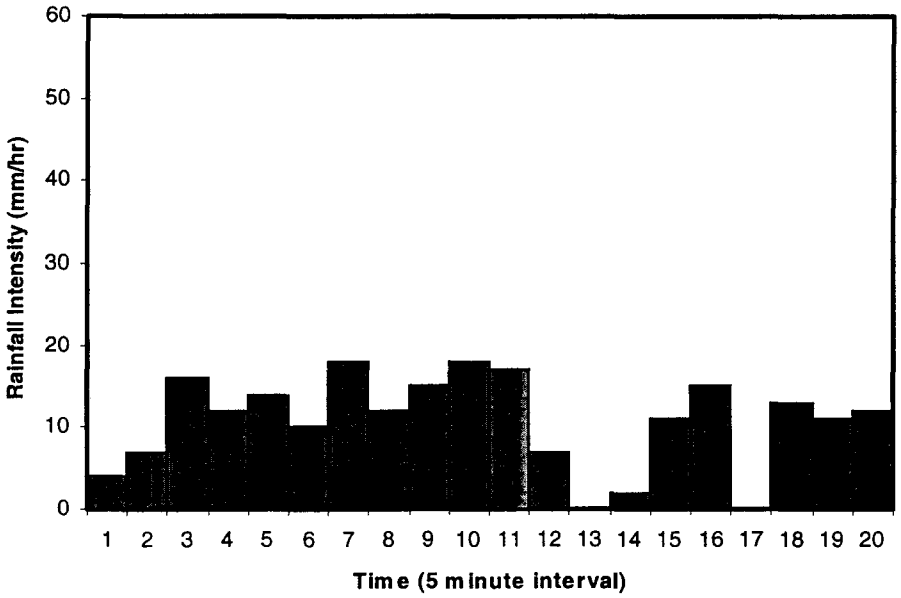

Figure 1.4 Typical widespread rainfall hyetograph.

CHAPTER 2

REVIEW OF WEATHER RADAR OBSERVATIONS AND APPLICATIONS

2.1 Introduction

Radar can estimate precipitation over a large area (of order 240 km radius) with high spatial (of order 1-4 km) and temporal (of order 10 minute) resolution. Rain-gauges, the standard measurement of rainfall, make essentially sparse point measurements. A very dense network of rain gauges is required to match the radar detected precipitation fields due to the spatial and temporal variability of rainfall. This is costly and not practical. It is only recently that radar has been able to provide adequate estimates of precipitation. There are many choices, issues and assumptions made when using radar for precipitation monitoring. These range from theoretical, empirical, technological and processing considerations. A review of the basic radar theory and implementations as they relate to precipitation measurements, and previous research in the problem of radar/rain-gauge estimation and forecasting of rainfall is discussed in this chapter.

2.2 Radar-Rainfall Measurements Process

The principles of radar and the observation of weather phenomena were established in the 1940's. Since that time great strides have been made in improving equipment, signal and data processing and its interpretation. Most meteorological radars are pulsed radars, that is, electromagnetic waves at fixed preferred frequencies are transmitted from a directional antenna into the atmosphere in a rapid succession of short pulses. Figure 2.1 is a schematic diagram showing a directional radar antenna emitting a pulse-shaped beam of electromagnetic energy over the curved earth surface to illuminate a portion of a meteorological target. Many of the physical limitations and constraints on the observation technique are immediately apparent from the diagram. For example, there is a limit to the minimum altitude that can be observed at far ranges due to the curvature of the earth.

A parabolic reflector in the antenna system concentrates the electromagnetic energy into a conical shaped beam, which is highly directional. The width of the beam increases with range. For example, a nominal 0.5 degree beam spreads to 0.44, 0.9 and 1.75 km at ranges of 50, 100, and 200 km, respectively. The short bursts of electromagnetic energy are absorbed and scattered by any meteorological targets encountered. Some of the scattered energy is reflected back to the radar antenna and receiver. Between successive pulses, the receiver listens for any return of the wave. The return signal from the target is commonly referred to as the radar echo. The strength of the signal reflected back to the radar receiver from the target is a function of the concentration, sizes and water phase of the precipitation particles comprising

the target. The power return, P_r , therefore provides some measure of the characteristics of the meteorological target and is, but not uniquely, related to a precipitation rate for any given rate of precipitation. The radar range equation relates the power-return from the target to the radar characteristics and parameters of the target. Greater details on weather radar theories can be found in different references such as: Skolnik (1970) for engineering and equipment aspects; Sauvageot (1982) Battan (1981), and Collier (1989) for meteorological phenomena and applications; Atlas (1964, and 1990) for general review; Rinehart (1991) for modern techniques; and Doviak and Zrnic (1993) for Doppler radar principles and applications. The radar measurements of precipitation can be summarized in two main steps: (1) conversion of the power return (P_r) to reflectivity factor (Z) through the radar equation, and (2) conversion of the reflectivity factor into rainfall rate. A brief summary of the principles follows.

2.2.1 The Radar Equation

The amount of energy backscattered from the hydrometeors depends upon the number of particles within the pulse volume of the radar beam, their size, composition, relative position, shape and orientation. The total backscattered energy is the sum of the energy backscattered by each of the scattering particles. Burgess and Ray (1986) provide a concise summary of scattering theory. When the drop diameter is small in comparison with the wavelength the scattering is known as Rayleigh scattering and the reflectivity factor Z can be related to the returned power through

the radar equation (Battan, 1981):

$$Z = \frac{\overline{P_r} \times r^2}{C_R \times |K_A|^2} \tag{2.1}$$

Where:

Z = The reflectivity factor.

r = Range to the target.

C_R = The radar constant which depends on many factors including the transmitted power, antenna gain, horizontal and vertical beam widths, pulse length, and wave length.

K_A = The complex index of refraction.

Many pulses must be averaged in the radar processor to provide a significant measurement; the pulses can be integrated in different ways but usually in a digital form, and must allow for the logarithmic scale to account for the wide range of power covered. In practice, for a typical system, the signal at the antenna is received (i.e., the returned power), amplified logarithmically, averaged over many pulses, corrected for (log) averaging, then converted to a reflectivity factor using the radar range equation. This operation is done automatically by the radar processor. The reflectivity factor is the most important parameter for radar interpretation. The factor is derived from the Rayleigh scattering model and is theoretically defined as the sum of particle (or drop) diameters to the sixth power per unit volume.

$$Z = \sum_{\substack{Unit \\ Vol}} D_o^{\,6} \tag{2.2}$$

2.2.2 Rainfall-Reflectivity Relationship

The second step in radar rainfall estimation is to convert the estimated reflectivity factor to rain rate. It can be proven (refer to Wilson and Brandes 1979) that the reflectivity factor at the subcloud level (Z) and the rainfall rate at the ground level (R) can be expressed as following:

$$Z = \int_0^{\infty} D_o^{\,6}\, N_o(D_o)\, dD_o \tag{2.3}$$

$$R = 6\pi \times 10^{-4} \int_0^{\infty} D_t^{\,3}\, N_t(D_t)\, w_t(D_t)\, dD_t \tag{2.4}$$

Where:

Z = Reflectivity factor in mm^6/m^3.

D_o = Raindrop diameter in mm at the subcloud level.

$N_o(D_o)$ = Raindrop size distribution (a density function) in number of drops per cubic meter of air per unit rain drop size interval at the subcloud level.

R = Rainfall rate in mm/hr.

D_t = Raindrop diameter in mm at the ground level.

$N_t(D_t)$ = Raindrop size distribution in number of drops per cubic meter of air per unit rain drop size interval at the ground level

$w_t(D_t)$ = Drop terminal velocity in m/s.

Establishing a physically based Z-R relation from the above two expression is difficult. There are two main obstacles: (1) The drop size distributions can not be estimated from the reflectivity factor alone; and (2) even if we assume one of the distributions is known, the other can not be derived unless the two can be related with a process model. There is no process model that is widely accepted. The reason is that such a model is required to capture the physical processes (such as collision, breakup, coalescence, evaporation, and advection) occurring between the subcloud level and the ground. Thus, in practice, empirical approximation is used to convert the estimate of reflectivity factor to radar rainfall rate. This empirical Z-R relation is in the form of:

$$Z = AR^b \tag{2.5}$$

Where:

Z = Reflectivity factor in mm^6/m^3.

R = Radar rainfall rate in mm/hr.

A,b = Parameters.

An empirical Z-R relation can be obtained from measured drop-size distributions (Marshall-Palmer, 1948). However, differences in radar calibration could lead to

different Z-R relationships for the same drop size distribution. An alternative is to compare Z measured aloft by the radar with R measured at the ground by rain-gauges. The advantage of the latter approach is that it reflects any differences between the radar detected precipitation aloft and that which reaches the ground. It also has the advantage of taking into account errors in the radar calibration, although the result is not a fixed Z-R relationship and it may not apply to other radars. The parameters (A, b) may vary according to storm type and geographical location. The possibility of accounting for part of the variability of Z-R relation by stratifying storms according to rain type (such as convective, stratiform, orographic) has received a good deal of attention (Battan, 1981). Figure 2.2 shows the variation in empirically determined Z-R relationships. In spite of all of this work, it has been difficult to displace the Marshall-Palmer relationship given by $Z = 200\ R^{1.6}$. From Figure 2.2 , the MP relationship roughly falls in the middle of all the measurements. However, if we assume the Z-R conversion is free from calibration error, significant differences between radar and rain-gauge measurements are still common. These differences may be attributed to different sources of errors.

2.3 Sources of Errors in the Radar-Raingauge Comparisons

The sources of errors leading to the variability in the difference between radar and rain-gauges are classified into two main groups: (1) measurement errors; and (2) sampling errors. Figure 2.3 schematically illustrates the problems in interpreting radar measurements. These errors are briefly described below.

2.3.1 Measuring Errors

The measuring errors are those associated with problems with either the sensor setup and calibration or specific environmental conditions. The measuring errors are stated below. For details on the measuring errors refer to Browning (1987), Zawadzki (1984), and Donaldson (1990). The measuring errors include: radar beam filling, non uniformity of vertical distribution of precipitation, attenuation by intervening precipitation, beam blocking , attenuation due to a wet radome, electromagnetic interference, ground and other clutter, anomalous propagation, antenna accuracy, electronics stability, processing accuracy, and rain-gauge measurements errors. However, the measurement errors do not seem to allow for rigorous mathematical modelling and their effect on the accuracy of radar rainfall estimation is known only qualitatively. In practice, some measurement errors can be identified and removed by quality control procedures. Other measurement errors such as attenuation exist in almost all the data in significant rainfall events. Attenuation occurs due absorption and scattering of the microwave energy by substances in the air. The more space a beam travels, the more energy that is absorbed. The energy backscattered from a storm near the radar will be greater than the energy backscattered from a distant storm (i.e., due to loss of energy). This causes rainfall intensity to be measured higher at small ranges from the radar as compared to far ranges. No operational approach is yet in place to correct for attenuation. Measurements errors (especially attenuation) and the methods used for "cleaning" the data from these errors are very active research areas.

2.3.2 Sampling Errors

If the radar observations of the reflectivity factor are assumed error-free, i.e. the measurements errors are negligible, the radar rainfall estimates obtained using a Z-R relation can still contain an error with respect to rain-gauges due to: (1) failure to account for the natural variability of the drop size distribution, and (2) neglect of the differences between the sampling characteristics of the two sensors.

The differences between the sampling characteristic are both spatial and temporal. Radar measures volume-averaged returned power and converts it to estimates of spatially averaged rainfall by projecting onto the earth's surface. On the other hand, rain-gauges measure point rainfall on the ground. Also, radar rainfall is obtained from a discrete-time integration over the period of interest, whereas rain-gauge measurements are from a relatively continuous-time integration. These fundamental differences in the sampling strategies of radar and rain-gauges limit the use of rain-gauges in the assessment of radar accuracy. These sampling differences have been acknowledged by many researches (Austin, 1987; Joss and Waldvogel, 1990; Kitchen and Blackall, 1992; Fabry et al., 1994; Seed et al., 1995; Ciach and Krajewski, 1999; and others). Accordingly, the observed difference between radar and rain-gauge can not be treated as pure radar error because part of the observed difference is due to sampling differences between the two sensors. Kitchen and Blackall (1992) noted that the small-scale structure of rainfall introduces representativeness errors (sampling errors) in the comparison between rain-gauges and radar estimated rainfall rate. They used a dense rain-gauge network, covering a

distance from 0.7-10 km, in order to investigate the effect of the small-scale rainfall variability. They argued that representativeness errors may account for a significant part of the radar rain-gauge scatter.

In this thesis, the effects of the sampling errors on the differences between radar and rain-gauges and on the Z-R calibration will be addressed in Chapter 6. It should be noted that, due to the temporal and spatial sampling strategy of the radar, there are concerns regarding its uncertainties for use in rainfall estimation for high resolution applications (such as urban areas). Such high resolution applications require detailed rainfall input (1 minutes accumulations for example) and radar can not provide this level of temporal detailing. This subject also is dealt with in Chapter 6 of this thesis.

2.4 Rainfall Estimation From Optimal Multi-Sensors Merging

The estimation of rainfall from multi-sensors arose from the fact that rainfall measurements can be obtained from several sources. The most important sources are multiple radars, rain-gauge networks, and satellites. In addition, output from cloud models can be used as a rainfall estimator. Many studies have considered the problem of merging rainfall estimates from multi-sensors (Ahnert et al., 1983; Krajewski, 1987; Seo et al., 1990[1,2] , and others). A statistical merging procedure (Krajeweski, 1987, and Seo et al., 1990[1,2]) is employed in the NEXRAD (Next Generation Weather Radar) system in the United States. This procedure merges data from multiple radars with rain-gauges by using the co-kriging optimal interpolation to

produce a second stage (Stage-II) of rainfall accumulations products. Co-kriging is an interpolation technique that uses the spatial structure of two correlated fields together with their cross-correlation structure to develop a more precise field of the variable being studied. This procedure is the only procedure for this purpose being employed operationally. Satellite visible and infra red data are used only for quality control purposes in order to eliminate errors in the ground-based radar estimations. For example, if radar detects rainfall in a place for which satellite data indicates no clouds, then the radar estimate is replaced by zero (Fiore et all, 1986, and FMH, 1991). One concern about the statistical merging procedures of data from radars and rain-gauges is the smoothing of the estimated fields. On the other hand, the advantage of this procedure is that statistical merging guarantees rainfall estimates with minimum error variance. Therefore, it is only applicable for applications that require quantitative information on the mean rainfall and the uncertainty of its estimation. For applications requiring detailed resolution rainfall fields, however, this approach can smooth out the original detailed structure of precipitation obtained from the raw radar data.

2.5 Real-Time Radar Rainfall Tracking and Forecasting Algorithms

When the objective is the real-time quantitative precipitation forecasting (QPF), the problem becomes more complicated. Rainfall forecasting is usually classified into short, medium, and long range forecasting. In short range forecasting the lead time is less than 2 days ahead. Medium range forecasting is 2-14 days ahead,

and long range forecasting is months ahead (Bengtsson, 1985; and Collier , 1989). As shown in Figure 2.4, short range forecasting is sub-classified into nowcasting, mesoscale forecasting, and synoptic scale forecasting (Browning, 1980). In nowcasting, the forecast is for a few hours ahead with high spatial scales (< 10 km). Mesoscale forecasting (spatial scale 20-500 km, temporal scale 2-50 hrs) is done using numerical weather prediction models (NWP). Forecasts based upon synoptic scale models using model output statistics (MOS) are of spatial scale, 500-5000 km, and temporal scale, 50-500 hrs. NWP and MOS models are not readily compatible with the high spatial and temporal resolutions (a few minutes and a few kilometers) required for applications such as nowcasting applications (Georgakakos and Hudlow, 1984). Two approaches are commonly used for nowcasting: (1) the extrapolation approach; and (2) the simplified dynamical approach.

2.5.1 The Extrapolation Approach

This type of short-term QPF is based upon the extrapolation of current weather. The extrapolation of a current state of a rainfall field requires a tracking process of the echos. One method used to study the storm motion tracks the center of gravity of the rain area (Wilk and Gray, 1970; Barclay and Wilk, 1970; Zittel, 1976; Bjerkaas, et al., 1980; and others). If echoes can be delineated easily this procedure might be the simplest and most effective pattern-matching procedure. This approach is employed operationally in the FRONTIERS tracking system in England and in the NEXRAD storm tracking system in the United Sates. The FRONTIERS

tracking system, as described by Conway and Browning (1988), is a rainfall field centroid interactive method. A composite picture of the radar network image is assembled interactively by the operator. The operator delineates the rainfall pattern into a number of clusters. The boundaries of the selected clusters are specified by the operator. The velocities of the chosen clusters are determined from the positions of the centroid in connective frames. These centers are then extrapolated individually. It should be noted that the limits of the human capacity make it difficult for the operator to track several clusters simultaneously. The NEXRAD tracking system employs an automatic centroid tracking algorithm. This algorithm identifies regions of significant reflectivities in each elevation angle. It then computes a 3D center of mass and projects it onto the horizontal plane. The movement of identified storms is monitored by relating all storms found in the current volume scan to storms from the previous scan using a matching procedure. Constraints, such as the minimum and maximum speed used to establish a search region for the next storm centroid to be marked as the same storm, are imposed to aid the matching procedure (FMH, 1991). A problem with this algorithm exists because of the limited number of storms that can be tracked. The default maximum number of storms in the NEXRAD system, for example, is 20. Generally, problems usually arise in using the centroid tracking methodology because of the variable nature of rainfall (birth, growth, and decay), which affects the location of the center of gravity and may lead to ambiguities in the estimated storm characteristics. Other problems appear in cases of widespread rainfall patterns that produce difficulties in isolating storm clusters.

Another method of estimating the kinematics of rainfall cross-correlates a portion or the whole radar domain with subsequent scans. This procedure has the advantage of taking into account the detailed shape of the echo being tracked, thus decreasing the chances of mismatching echoes (Wilson, 1966; Zawadzki, 1973; Austin and Bellon, 1974; Hill et al., 1977; Yoshino and Kozeki, 1985; Collier, 1989; and others). This technique is used operationally in both the Canadian Short-Term Automated Radar Prediction (SHARP) model (Bellon and Austin, 1976) and the Japanese short-term prediction model (Ishizaki et al., 1989). This technique utilizes a cross-correlation analysis to determine the average translation vector. Based on the obtained average translation vector, the latest rainfall field is extrapolated into the future. This methodology is useful for those storms where the changes in rainfall intensity over time are not significant However, in cases of severe convective storms, the growth and decay of storms produce a pronounced rain intensity variation within the rainfall field, which can not be accounted for by this type of model. Bellon and Austin (1984) used the SHARP technique to forecast precipitation for the city of Montreal. Their experiment showed a mean absolute deviation varying from 50 to 60% for 0.5 to 3 hrs forecasts. They based their assessment on comparison with rain-gauge ground values.

Alaka et al. (1979) used a linear extrapolation methodology to model the growth and decay of rainfall. They compared the current rainfall field with the most recent rainfall field after displacing it to the 'current time' position using the determined displacement vector. The differences (including the sign) between the

two consecutive fields were then added to the current echo in order to find the new echo at the new forecast lead time. This approach considers only the most recent change in the rainfall field evolution and does not account for the historical trend in the rainfall field evolution. Accordingly, this methodology can introduce significant errors especially for longer lead times.

Chen and Kavvas (1992) introduced a radically new technique. The technique decomposes the radar image of the rain field into constituent polygonal contours, whose evolution in time and space is tracked through subsequent radar images and then projected into the future via an adaptive exponential smoothing scheme. By recomposing the projected contours at a desired lead time, a prediction of the rain field is obtained. The technique was validated for lead times up to 30 minutes on historical radar data from one storm with encouraging results. The technique is computationally demanding and the polygon model used was not described clearly in their work. Describing rainfall contours using a polygon model has a smoothing effect, which can lead to information loss of the detailed rainfall field structure. In addition, rainfall contours do not follow a clear trend that can be modeled over long forecasting lead times (i.e., more than 30 minutes)

Rinehart and Garvey (1978) developed the TREC (Tracking Radar Echoes by Correlation) method. The method is basically the same as the cross-correlation method mentioned above, but it is applied to small partitions of a storm system instead of the whole radar domain. The small partitions are typically boxes (each is 10 km $\times$ 10 km for example). The method had originally been developed for the

purpose of retrieving wind fields within radar echoes. The TREC method involves some difficulties attributed to the noisy velocity vectors that appear due to mismatching boxes and due to contaminations in the data itself (Rinehart, 1981), in addition to the run time requirements. Li et. al. (1995) described the COTREC improvement to reduce noisy velocity vectors from the TREC velocity field. They determined the regions of growth and decay using a simple comparison of the average rainfall inside a box and its corresponding matched box. Regions with a positive difference are marked growth, and those with a negative difference are marked decay. The application of the method for quantitative precipitation forecasting was not done using test cases in their work. They suggested for future works that, in order to use the TREC method for forecasting purposes, the TREC velocity field and the growth and decay field should be extrapolated separately.

The general problem with all extrapolation forecasting models is the inability to predict the birth of new rainfall cells, or account for rapid growth or decay. This problem has attracted researches to search for another approach that tries to model the physics of rainfall. This approach is known as the simplified dynamical approach.

2.5.2 The Simplified Dynamical Approach

The simplified dynamical approach was originally proposed by Georgakakos and Bras (1984[1,2]). This approach is based on mass conservation of liquid water applied to a column of the atmosphere. This work focuses on describing the primary processes within a column of the atmosphere associated with a convective cloud and

does not explicitly address interactions between cloud columns, which is a simplification of the physical processes. A comprehensive presentation of the complete set of differential equations for meteorologic modelling is given by Pielke (1984). However, the solution of the complete set of governing equations at high spatial and temporal resolution is impractical, if not impossible , with the current meteorological sensors and hardware technology (French and Krajewski, 1994[1]). Hence, several simplifications of the set of continuity equations are made: microphysical precesses are not explicitly described, condensed water immediately transforms into precipitating water, i.e., the cloud water content is in a steady state, the presence of snow or ice is not addressed, and moisture input to the column from the sides is neglected (Andrieu et al., 1996). Georgakakos and Bras (1984[1,2]) and Lee and Georgakakos (1991) discuss the assumptions leading to the set of simplified equations.

The general idea of the simplified dynamical approach is that air rises pseudo-adiabatically in the cloud column with updraft velocity (possibly height-varying) producing an input rate of condensed water mass equivalent. The input mass of condensed water is distributed to various droplet diameters according to an exponential distribution. Due to the action of the updraft at the cloud top, a portion of the input water mass leaves the top of the column. The larger droplets fall through the cloud bottom having a certain precipitation rate. The precipitation rate at the ground is computed by subtracting the loss caused by evaporation. In summary, the simplifications include consideration of only the governing equations of conservation

of water mass together with a pseudoadiabatic parameterization to determine the mass of condensate.

Lee and Georgakakos (1990) developed a two-dimensional version of the spatially lumped model developed by Georgakakos and Bras (1984[1,2]). Based on surface pressure, surface temperature, and surface dew point temperature, the model is parametrized to give the precipitation rate as an output. The model derives an advection scheme using mid-level wind predictions from the synoptic-scale NGM (Nested Grid Model) run by the NWS (National Weather Service) in the United States. The model relies on hourly rain-gauge data for sate estimation. Lee and Georgakakos (1990) suggested using radar data instead of rain-gauge data for state estimation.

Seo and Smith (1992) derived a simplified dynamical QPF model using the same approach of Lee and Georgakakos (1990) with the additional characteristic of incorporating radar observations for state estimation. Testing and validation were limited due to lack of data. The authors showed that the model performs better than PERSISTENCE for 1 hour ahead forecasts. PERSISTENCE extrapolation means that the latest available radar observations are the forecasted rainfall field. Thus, in PERSISTENCE, there is no translation of the field in space and neither growth nor decay of rainfall intensity in time.

French and Krajewski (1994[1,2]) used the same approach followed in the studies described above with additional characteristics. Instead of determining the cloud top pressure empirically in terms of the updraft velocity, they introduced the

use of IR (Infra Red) satellite data to determine the cloud top temperature and pressure. In addition, they used a cross-correlation analysis on radar data as a horizontal advection scheme. In their updating algorithm, the state estimation was performed using radar data. They concluded that the developed model performed well compared with two alternative real-time forecasting strategies: PERSISTENCE and the SHARP Canadian advection model. Their comparison did not include run time requirement, which makes their model questionable for real-time application. However, this work is unique in its emphasis on using of observations from radar and satellite to define the model state and the boundary condition respectively.

Andrieu et. al. (1996) adapted the same simplified dynamical approach for modelling precipitation in a mountainous region in France characterized by orographic precipitation. Based on the analysis of two storm events, they concluded that the simplified dynamical approach performs as well as, or slightly better than the PERSISTENCE and SHARP models.

Based on the above review of the forecasting work done using the simplified dynamical approach, one can conclude that this approach is still not adequately proven to outperform the operational extrapolation techniques. In addition, the simplified dynamical approach requires meteorological data that are difficult to obtain especially in real-time with a high temporal and spatial resolution. However, this approach can be useful for providing spatially and temporally averaged rainfall forecasts with relatively poor resolution. With future advances in computations and remote sensing, this approach may take a prominent place operationally.

2.5.3 Statistical Regression and Neural Network Techniques

The development of statistical techniques arose as the difficulties of the physical modelling, owing to the diversity of climatic processes in different scales and the lack of detailed understanding of the rainfall producing mechanism, were recognized. These techniques are based on the so-called "black box regression" technique. These techniques try to relate the probability of precipitation (POP) to the levels of some "explanatory variables". Because statistical methods focus on statistical correlations between predictors and predictands, they can make no direct statement about physical cause-and-effect. The localization of the large-scale numerical models can be attempted by use of regression models (National Weather Service, Meteorological Service Division, 1981). However, the use of statistical regression to partially bridge the gap between the mesoscale and the scales resolved by the large scale numerical models involves difficulties such as: (1) the identification of all the relevant meteorological variables that will be used as 'explanatory' variables, and (2) the absence of high temporal correlation in the station precipitation records (French et al, 1992). An alternative to the statistical regression models is the use of Artificial Neural Networks.

Artificial Neural Networks (ANNs) provide a methodology for extracting patterns from noisy data. They have been applied to a wide variety of problems, including cloud classification (Bankert 1994) and tornado warnings using doppler radar data (Marzban and Stumpf, 1996) in a meteorological context. The advantages and disadvantages of neural networks in comparison to other statistical techniques

for pattern extraction are discussed in Marzban and Stumpf (1996). The standard procedure for use of a neural network involves "training" the network with a large sample of representative data. The network has some number of input and output "nodes" representing the predictor and predictand variables, respectively. In between, there are a number of hidden nodes arranged in layers. The number of hidden nodes and layers is usually determined empirically to optimize performance for a particular situation. Each connection between nodes on a particular layer and the layer above can be represented by a weight, which indicates the importance of that connection between the two nodes. The training phase of the neural network is designed to optimize the weights so that the mean squared error of the output is minimized. The network then can be used to make predictions based on new input values.

The first contribution to ANNs application in rainfall forecasting was done by French et al. (1992). They developed a three-layer learning network with input, hidden, and output layers. Training was conducted using back propagation, where the input and output rainfall fields were presented to the network as a series of learning sets. The neural network was then used to forecast rainfall intensity fields with a lead time of 1 hr, using only the current field as input. Rainfall fields were generated using a space-time mathematical rainfall simulation model, and the forecasted fields were compared to the perfectly known model-produced field. Comparisons with true mean areal intensities and percent areal coverage indicated that, in most cases, the method performed well when applied to events used in the training. They concluded

that the network performed at a level comparable to PERSISTENCE and the SHARP schemes. Their network did not outperform the extrapolation techniques; rather, it provided merely a first step towards understanding and evaluating a role for ANN in the investigation of complex geophysical processes. The authors recommended that many more studies be performed before a conclusive statement can be made regarding the applicability of ANNs in short-term rainfall forecasting.

It should be noted that ANNs have shown considerable success when used to improve the NWP models output for mesoscale rainfall forecasting (Brooks and Doswell, 1997). However, for short-term QPF, ANNs are still far from being successfully employed. The lack of success is attributable to the same difficulties experienced in using the regression techniques. An additional difficulty appears because of the amount of data required to train the network in order to account for all possible precipitation meteorological scenarios.

2.6 Rain-Gauge Tracking Techniques

In the last two decades radar data have recently become available to the wide number of researchers in the field of meteorology and hydrology. Radar data were not as available as rain-gauge data in the past and the available records are short. Hence, for applications that require a historical analysis of the rainfall kinematics, rain-gauge data are more available. In addition, the radar beam finds some areas inaccessible. Thus hydrologists have developed and investigated methods to determine the kinematic characteristics of rainfall from rain-gauge networks (Briggs et al. 1950;

Felgate and Read 1975; Hindi and Kelway, 1977; Shearman, 1977; Marshal, 1980; Drufuca, 1978; Niemczynowicz and Jönsson, 1981; Shtifter, 1981; Scheckenberger 1983; Shaw 1983; James and Scheckenberger 1983; Niemczynowicz and Dahlblom 1984; and others).

All storms are comprised of "cells", with each cell has its own characteristics. Cells can vary in size and shape, and vary in the level of precipitation intensity. When a storm cell has a given level of rainfall intensity, the actual amount of rainfall that falls on any point will depend on the speed of the cell's movement. A slow moving cell will drop more rain on a given point than will a fast moving cell with the same level of rainfall intensity.

One of the methods used to determine the speed and direction of the storms using rain-gauge measurements was introduced by Shtifter (1981), who studied the movement of 22 storms in the Hamilton-Wentworth area in Southern Ontario. Data were collected from 3 precipitation gauges. The time to peak was then calculated for the 3 hyetographs as a basis for evaluating the direction and speed of the storms. Scheckenberger (1983) also studied the dynamics of storms in the Western Shore of Lake Ontario and developed a software package to process rain-gauge observations in order to estimate storm cell characteristics such as speed and direction of motion, spatial dimensions, and growth/decay functions. These estimated properties are then used to model rainfall produced by one or more storm cells. Nimmrichter (1986) investigated the storm cell kinematics for two major urban centers on the western shore of lake Ontario. In the Hamilton-Wentworth Region storm, he found that cells

originating from the west at a speed of approximately 25 km/hr were most frequent. Similar findings were obtained for the City of Toronto, where storm cells traveling from west to east at a slightly higher speed of approximately 30 km/hr were the most frequent.

In the above studies (Shtifter, 1981; Scheckenberger, 1983; and Nimmrichter, 1986), the same technique (named The Three Points Method that was originally developed by Hindi and Kelway, 1977) was used to estimate the kinematic characteristics of the storm from rain-gauge observations. This technique is based on the observed time to peak of the hyetograph measured at every three gauges. This method assumes constant storm velocity vector and uses triangulation between three gauges to compute the velocity vector . A triangle is constructed among the three gauges and the storm direction is obtained in terms of the angles of the triangle and the measured times to peak at the three gauges. When more than three gauges exist, a velocity vector is produced by using every combination of three gauges. A simple or weighted average is then calculated. The shortcomings of this technique are the time consuming work required to extract the time to peak at each gauge, and the complex nature of thunderstorms (multi-cell structures), which produces multi-peak hyetographs, making it difficult to specify exactly which time-to-peak should be used from each gauge. However, this can be avoided by employing methods of hyetograph separation, which are also complex and time consuming. The Three Points Method is an example of a group of rain-gauge techniques called 'the rigid methods'. The term 'rigid' is used because they are rigid in the sense that they use

only one feature from the hyetograph. Examples of typical features include the peak intensity, as followed in the Three Points Method, and the pause between two peaks.

Another method called "full correlation analysis", developed by Briggs et al. (1950), was extended later by Felgate and Read (1975) and Shaw (1983). This method uses the so called "characteristic ellipse" to give indirect information about the size, the shape, and the lifetime of the rainfall cells. The results of this method are difficult to interpret physically and involve uncertainties (refer to paper by Niemczynowicz 1987 for more details).

A third group is the so-called lag-correlation analysis, which was developed in different versions by Marshall (1980) (latest version) and investigated by several researchers (Sherman 1977; Niemczynowicz and and Jönsson, 1981; Niemczynowicz 1987). These methods are based on the fact that, although the rainfall hyetographs at adjacent gauges are often similar, there is a time lag from one gauge to the next. The apparent consistency of these lags suggests that they represent the drift of the rain storm across the catchment. The latest version of the method is based on determining the sample cross-correlation between all pair-wise combinations of gauges at a known applied time lag . Using the assumption of spatial stationarity, the problem can be reduced to the (U',V') space representing the relative coordinates between gauges. A correlation surface is interpolated for every applied time lag on the (U',V') space and the velocity vector is determined by tracking the point of maxima of the correlation surfaces (refer to Marshall, 1980 for details). These correlation-based methods have some advantages over the rigid methods in the sense

that they use all available information from the hyetographs to determine the velocity vector. However, these methods are affected by the multiple existence of storm cells over the rain-gauge network, which can cause a misleading high correlation between two gauges lying in the path of two different rain cells. In addition, the approach also requires manual interpretation of the results in order to specify and track the point of maximum correlation.

Niemczynowicz (1987) compared the three known rain-gauge tracking methods (the three point method, the cross-correlation method, and the lag-correlation method). He concluded that these methods of varying complexity seemed to work well only for single-peak rainfalls. When more than one rainfall cell were simultaneously present over the rain-gauge network all methods failed and the so-called objective methods lost their objectivity.

2.7 Discussion

This chapter presents a literature survey that briefly covers the two problems of rainfall estimation and prediction. The estimation problem is covered in sections 2.2 to 2.4, in which the difficulties of accurate estimation of rainfall from the radar sensor are brought to the readers attention. It can be concluded from these sections that calibrating radar estimation of rainfall using rain-gauge data is essential to remove any bias from the radar estimation of rainfall before using it in hydrological modelling. Another important conclusion is that there are significant differences between the radar and rain-gauge estimation of rainfall. These differences may be

attributed to the differences in the sampling strategies of the two sensors. The effects of the sampling errors on the difference between the two sensors and on the calibration of the radar Z-R relation may constitute a significant factor that has to be studied. Radar has a great advantage because it provides a detailed spatial structure of rainfall. The temporal resolution of the radar scans is 10 minutes that may not be suitable for high resolution hydrological applications (urban applications for example). Hence, the use of radar rainfall data for such applications is still limited. A benefit to this field will be attained if a methodology for improving the temporal resolution of the radar derived rainfall data is established and verified.

Section 2.5 of this chapter reviews the research done on the radar short-term prediction problem (nowcasting), or the short-term QPF using radar data. The QPF problem, in this thesis, means providing quantitative precipitation forecasting of rainfall for lead times less than two hours and for spatial resolutions less than 4 km. Rainfall is one of the most difficult elements of the hydrological cycle to forecast. This is due to the tremendous range of variability it displays over a wide range of scales in both space and time. Generally, two main approaches have been followed for QPF: (1) the extrapolation approach, and (2) the simplified dynamic approach. The simplified dynamic approach tries to simplify the precipitation dynamics in a column of the atmosphere considering only mass conservation. The extrapolation approach is based on extrapolating the current weather conditions into the future. Based on the literature survey, and using the current technology of remote sensing and hardware capabilities, the simplified dynamic approach can not be considered to

significantly outperform the extrapolation approach. Hence, it can be concluded that the extrapolation approach is still more attractive because it requires less computations and data, making it more suitable for real-time QPF. A question then arise: is improvement in real-time QPF using the extrapolation approach achievable?

Finally, section 2.6 reviews the work done on the problem of rainfall tracking using only rain-gauge data. Although the use of rain-gauge tracking methods has been relatively displaced by the radar methods, it still has some important applications, such as the historical analysis of rainfall kinematics and the storm trajectory based interpolation using rain-gauge data (refer to Chapter 3 for more details). In the review of the available rain-gauge tracking methods, it has been shown that there are difficulties associated with using these techniques. These difficulties are mainly attributable to the inability of the rain-gauge techniques to deal with the multi-peak structure of rainfall. This difficulty requires manual processing of the rain-gauge data, which is time consuming.

2.8 Study Objectives

This dissertation focuses on the rainfall estimation and prediction problems. The information presented in Chapters 1 and 2 emphasizes the need for improving radar rainfall estimation through the proper calibration of radar data using rain-gauges. In addition, it shows the importance of QPF and the need to improve such forecasting in real-time. Within this main framework this study tackles other problems, which can be summarized by the following objectives:

1- Develop a rain-gauge technique for storm tracking to be used in simulating the small-scale structure of rainfall and in estimating the kinematic characteristics of rainfall. Perform a comparative analysis between the rain-gauge and radar techniques for estimating rainfall kinematics. Estimate the regional predominant storm kinematic characteristics in Hamilton-Wentworth Region using the developed rain-gauge technique.(*Chapter 3*).

2- Investigate the problem of geo-referencing radar rainfall data. Develop an accurate projection method for the purpose of evaluating the different projection methods used for projecting radar rainfall data and rain-gauge data. Investigate the problem of the selection of a common coordinate system for rainfall data from multi-sensors. (*Chapter 4*)

3- Developing a multi-component interface using the technology of Geographical Information System to incorporate rainfall data from multi-sensors into a geographical reference system. The tremendous amount of rainfall data from multi-sensors (rain-gauges, radars, and satellite) is a common problem faced by researchers in this field. Hence, the ability of such an interface to overcome the difficulties of managing, processing, and analysing rainfall data from multi-sensors is important. In addition, the results and the techniques developed throughout the thesis are to be incorporated into this interface. (*Chapter 5*)

4- Address the effects of the sampling errors on the radar rain-gauge differences. Address the effect of these errors on the Z-R calibration process. *(Chapter 6)*

5- Evaluate the applicability of radar rainfall data for high resolution hydrological applications that require high spatial and temporal resolution of rainfall. (*Chapter 6*)

6- Assess the accuracy of the two Canadian radars (King City, and Exeter) in terms of rainfall estimation. Perform a calibration analysis using rain-gauge data.(*Chapter 6*)

7- Develop an extrapolation-based model for tracking and forecasting rainfall fields (for short-term QPF) using radar data. The model is required to simulate the growth and decay of rainfall on a cell by cell basis. Compare the developed model to the PERSISTENCE and SHARP forecasting models. *(Chapter 7)*

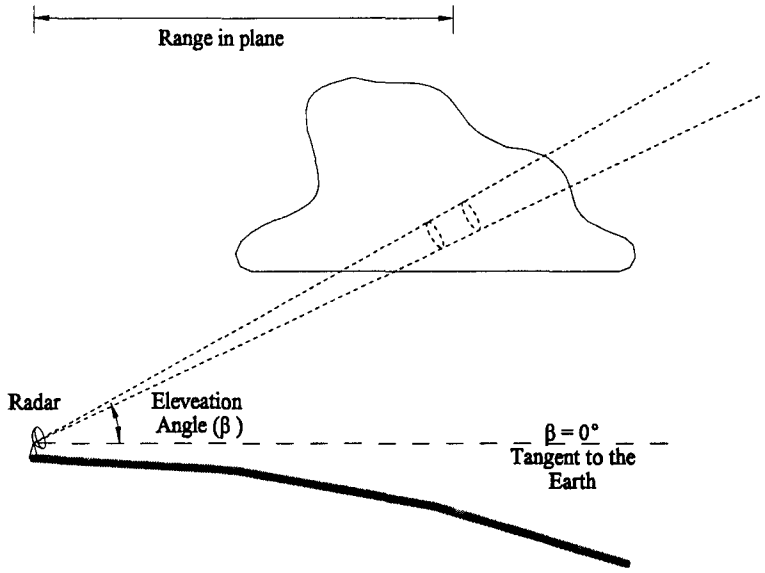

Figure 2.1 Propagation of electromagnetic waves through the atmosphere for a pulse weather radar.

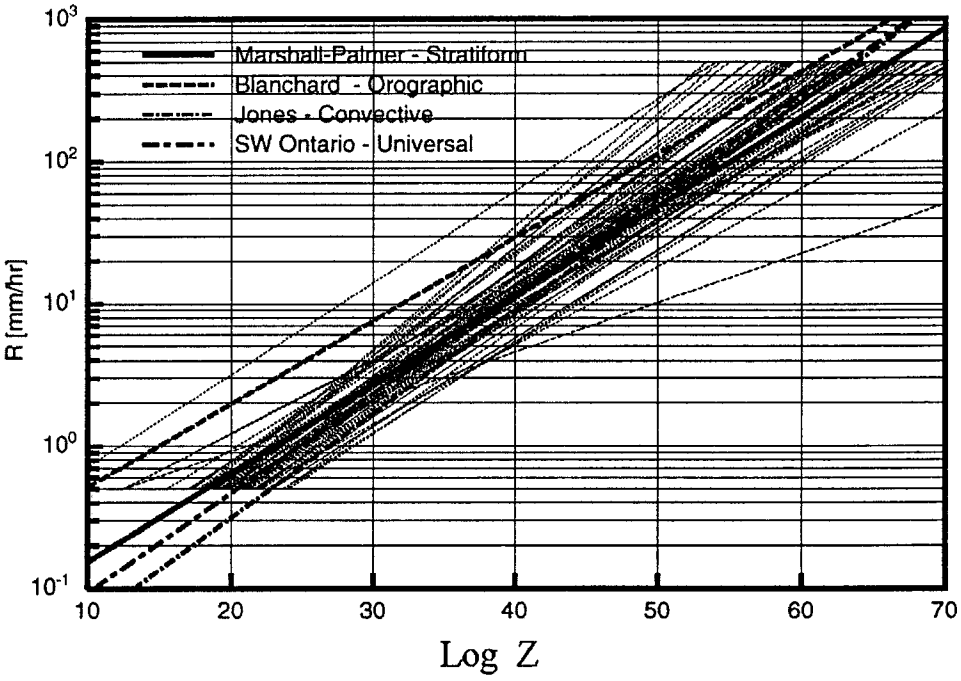

Figure 2.2 A graphical presentation of over 69 Z - R relationships (Battan 1981).

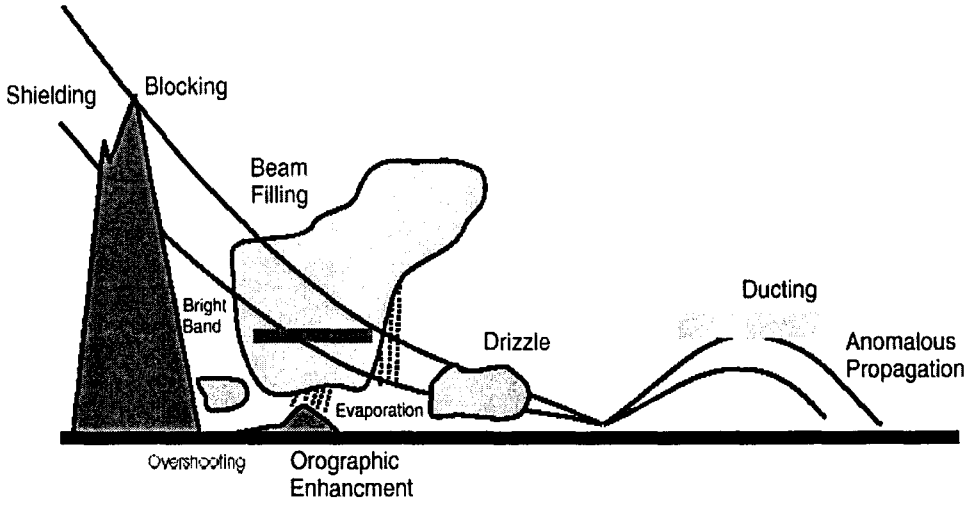

Figure 2.3 A schematic diagram to illustrating some of the possible sources of errors for the radar detection of precipitation. (From Donaldson,1990).

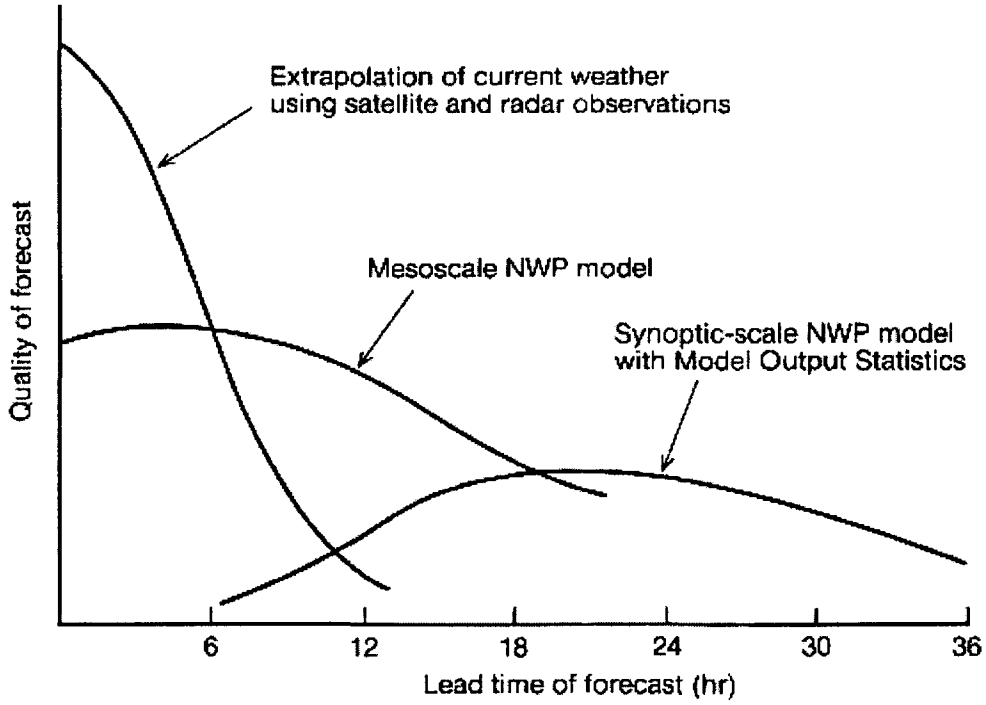

Figure 2.4 Precipitation forecasting models (From Collier, 1989 after Browning,1980).

CHAPTER 3

VISUALIZING AND TRACKING RAINFALL USING RAIN-GAUGE DATA

3.1 Background

In Southern Ontario, thirty to forty "thunder storm days" are reported annually (Kendall and Petrie, 1962). Thunderstorm cells exhibit a circular or oval shape that is generally preserved throughout their life cycle (refer to Figure 3.1). Determining the storm speed and direction is of practical importance to hydrologists in the case of precipitation modelling. During the 1970s and the early 1980s, the problem of estimating storm kinematics (i.e., speed and direction) from the rain-gauge sensor was under extensive investigation (Briggs et al., 1950; Felgate and Read, 1975; Hindi and Kelway, 1977; Shearman, 1977; Marshal, 1980; Drufuca, 1978; Niemczynowicz and Jönsson, 1981; Shtifter, 1981; Scheckenberger, 1983; Shaw, 1983; James and Scheckenberger, 1983; Niemczynowicz and Dahlblom, 1984; and others). The research in this area has slowed considerably since then and moved to the radar tracking techniques. These have received more attention due to the wide spatial coverage that can be achieved under the radar umbrella and uncertainties experienced when using the rain-gauge tracking methods. However, radar data are not as available

as rain-gauge data and the available records are short. In addition, some areas are not accessible by the radar beam. Thus, if a reliable rain-gauge tracking method exists, rain-gauges tracking methods can still be useful. Different applications still require a reliable tracking technique, which is totally based on rain-gauge data. For example:

1- *Off-line processing of historical rainfall data*:

Current technology allows the introduction of storm kinematics into rainfall input used for runoff calculations for the design of water resources systems. Studies of the frequency distribution of the kinematics characteristics of rainfall and their joint probability distribution with other rainfall random variables, such as the event volume, duration, and inter-event time, can be introduced in the design storm concept (Sargent 1981&1982; Foroud et. al., 1984; Ngirane et. al. 1985; Ogden et. al. 1995; Singh 1998; and others). The radar data required for such analysis are not easily available and the available records are relatively short for any historical analysis, while historical information can be obtained from rain-gauge networks using rain-gauge tracking techniques.

2- *Short-term rainfall interpolation:*

The distributed modelling of the rainfall-runoff relationship for small basins, especially urban basins, requires a rainfall input of high spatial resolution and accuracy. Rain-gauge data are used for rain-gauge trajectory based interpolation purposes (Scheckenberger 1983; James and Scheckenberger 1983; Niemczynowicz

and Dahlblom 1984; and others). The trajectory based interpolation is a methodology in which the hyetographs measured at the rain-gauge network are spatially shifted according to the storm velocity vector. A grid is then interpolated from the shifted hyetographs using an interpolation method. The first essential step in such trajectory interpolation methodology is the estimation of the storm kinematics using rain-gauge data.

For the above reasons, and probably for other future urban applications, it would be useful to reconsider the rain-gauges tracking approach. This chapter describes a program developed within ARC-INFO GIS as a set of ARC-macros that can be used to identify storm characteristics from a set of rain-gauges through graphical display. Graphical display of data and related parameters are necessary to the scientist concerned with seeking patterns in the data, generating hypotheses, and assessing the fit of proposed models. Hence, an essential element in data analysis is data visualization.

The main objective of this chapter is to visualize rainfall data in space and time in order to extract some information concerning the storm process under investigation. When the number of rain gauges and the number of time steps increase, it is hard to interpret the spatiotemporal behaviour of the data. The importance of the visualization technique described in this chapter then becomes evident. Three different interpolation techniques (Spline, Inverse Distance Weighted (IDW), and Kriging) are evaluated and used to visualize the spatiotemporal distribution of rainfall. An automated process using mpeg technology that displays

the storms in a movie sequence is developed to analyze the storm characteristics, i.e. speed and direction. The functionality of this method is verified using radar data through a case study for the Hamilton-Wentworth Region in Ontario, Canada. At the end of the chapter, the method is applied to explore the predominant storm characteristics in the study area.

3.2 Study Area and Coordinate System

3.2.1 Study Area and Data

The Regional Municipality of Hamilton-Wentworth, Ontario, Canada, maintains a real-time network of 16 tipping bucket rain-gauges that are distributed in the region for the purpose of rainfall and flow forecasting. The study area is a square area of approximately 8 km × 8 km of the Municipality of Hamilton-Wentworth, which is located on the west end of Lake Ontario. The study area is instrumented with 10 tipping bucket rain-gauges. Due to a malfunctioning gauge, 9 gauges have been selected for use in this study. The rain-gauge group lies approximately 80 km south west of King City weather radar, which is located at 43.96 N latitude and 79.57 W longitude. Figure 3.2 shows the locations of rain-gauges used in this study as well as the location of King City weather radar. Figure 3.3 shows the study area and the complete rain-gauge network operated by Hamilton-Wentworth region with respect to the Regional Municipality of Hamilton-Wentworth.

The manufacturer of the tipping bucket rain-gauges is BWD Industries Ltd. - Melbourne, Australia (Model No. RIMCO 7499200 with no heating option). The gauges are calibrated by an operator on a quite regular basis (every three weeks approximately). The time on the dataloggers of the gauges is set to match the time on the laptop used to communicate with the dataloggers, and the time on the laptop is set to match some approximation of Eastern Time (EST), i.e. set to match someone's watch or a clock in the main office. Over time, all of these sources of time drift from the exact actual EST (at different rates), and then they are reset to again closely match the correct time. Hence, the exact timing of the data can not be found very accurately, but it can be assumed to be within few minutes from the EST time system.

The data sample covers a period of 5 months in the summer of 1989 from both rain-gauges and radar. Additional rain-gauge data cover the summer of 1990. Rain-gauge data are in the form of one minute accumulations and the radar data are the CAPPI (Constant Altitude Plane Position Indicator) reflectivity scans using conventional rather than Doppler data. The data have regular 10 minute temporal spacing. For the format and specifications of the CAPPI data, refer to Chapter 5 (section 5.3). The radar grid resolution is 1 km in this study. It should be noted again that radar data are used in this study to verify the functionality of the rain gauge tracking technique developed in this chapter.

3.2.2 Coordinate Systems

In order to properly compare the velocity vectors estimated from the rain-gauge technique to those observed from radar, both the gauge locations and the radar grid should lie in the same geographical reference otherwise an additional error between the two estimated velocity vectors will result from the difference in coordinate systems. It should be noted that radar CAPPI gridded data are mapped to an oblique azimuthal plane tangential to the globe at the radar location (the origin) with its y axis parallel to the local geographic north at the radar location. Rain-gauge coordinates are usually in decimal degrees. In this study, they were originally referenced in strip 17 of the UTM (Universal Transverse Mercator) coordinate system with its y-axis parallel to the central meridian of strip 17 (81° W). The main error between the two estimated velocity vectors would result from the difference in the y-axis direction rather than the distance distortion of the projected earth curved surface. In other words, there is a coordinate system rotation that could constitute the main error between the two velocity vectors. To avoid the problem of coordinate systems and projections, the rain-gauge coordinates are projected into the radar coordinate system and the whole analysis on both radar data and rain-gauge data are performed in the radar azimuthal coordinate system as shown in Figure 3.4 (Refer to Chapter 4 for the details concerning the geo-referencing problem).

3.3 Problem Formulation

All rain-gauge tracking methods share a common principle of tracking a recognizable feature of the rainfall pattern. Examples of such features are the center of the isohyetal pattern, the peak of the hyetograph, the leading edge of the rain, or the maximum of the lag-correlation surface. Three known tracking methods (the three point method, the cross-correlation method, and the lag-correlation method) were compared in a study by Niemczynowicz (1987) with the main conclusion that these methods of varying complexity seemed to work well only for single-peak rainfalls. When more than one rainfall cell was simultaneously present over the rain-gauge network all methods failed, and the so-called objective methods lost their objectivity (refer to Chapter 2, section 2.6 for a review of the rain-gauge tracking techniques).

The effect of the problem of multi-peak rainfall structure on estimating the velocity vector can be explained by taking the three point method as an example. This method assumes constant storm velocity vector and uses triangulation between three gauges to compute the velocity vector. Input to this method consists of the peak times at three rain-gauges and their coordinates. When more than three gauges exist, a velocity vector is produced by using every combination of three gauges and an arithmetic or weighted average of the velocity vector is determined from such combinations. The three point method suffers from the ambiguities involved in selecting the right combination of peak times and gauges. When many storm cells are simultaneously present over the area in a multi-peak structure it is very difficult

to decide which peak time belongs to a particular storm cell, without manual recognition of the rainfall movement pattern. This problem requires a subjective time-consuming manual procedure in order to decide which combination of peak times and gauges should be used to estimate the storm speed. Figures 3.5 and 3.6 show two storm events illustrating the previous problem on the 9 rain-gauge network used in this study. In Figure 3.5, the number of peaks is high and vary in space and time, causing difficulty in deciding which combination of peaks should be used as input to the three point method. Although Figure 3.6 is supposed to be a single peak case: (a) the group of hyetographs measured at gauges R11, BLO, and RBG have no relation with those hyetographs at the group LEE, DAF, and CHE and (b) both groups have no relation to the group of hyetographs at gauges HAR, R18, and BUN. A wrong estimate of the storm velocity vector would be obtained by using the three point method if one peak from a particular group was selected as part of another group.

The rain-gauge technique presented in this study implements the Geographical Information Systems (GIS) technology and the idea of tracking the isohyetal patterns. The isohyetal pattern method uses these patterns to calculate the storm movement parameters from distance traveled over time. This idea has progressed from time consuming manual processing (Huff, 1967; Clayton and Deacon, 1971) to automatic processing (Shaw and Lynn, 1972; Hindi and Kelway, 1977; Tsanis and Gad 2001, Tsanis et al., 2002). Although the method presented in this study seems to be approximate because it is user dependent, it can solve the

problem of the multi-peak structure of hyetographs.

3.4 Areal Precipitation Methods

Theissen (1911) came up with the first technique to estimate areal average precipitation, a technique which has been commonly applied in hydrology. Another classical work in data analysis is that of Matheron (1971) who introduced the theory of regionalized variables to estimate areal averages considered as realizations of stochastic processes. This theory led to the development of the Kriging technique, which is a modified optimal interpolation technique of Russian origin. A study by Tabios and Salas (1985) was done to investigate the different methods of spatial interpolation techniques for estimating annual precipitation at five selected sites. The comparison was based on the following criteria: the mean and variance of the observed and interpolated annual precipitation, the sum of square errors between the observed and interpolated values of annual precipitation, the proportion of the variance accounted for by the interpolation, the coefficient of determination between the observed and interpolated values and the standard deviation of the error of interpolation. The results of the study show that for estimating annual precipitation, the Kriging technique is the best among all techniques. On the other hand, polynomial interpolation gives the poorest results.

3.4.1 Description of the Interpolation Methods

The three spatial interpolation techniques (Spline, Inverse Distance Weighted (IDW), and Kriging) to be used in the present work are briefly described below. These methods are coded in the ARC-INFO V. 7.2.1, program (ESRI, 1998[1])

IDW: A linearly weighted combination of a set of precipitation sample points, in which the weight is a function of inverse distance, determine the cell values and the interpolated surface. The significance of known precipitation points can be controlled by changing the values of two coefficients: (a) the power and (b) the radius object. A larger power ensures that the nearby data has the most influence, resulting in a rougher and more detailed interpolated surface. A common value of power, which is a positive real number, is 2. A variable or fixed radius object can limit the number of precipitation sample points to be used in the interpolation. Since the influence of input points on an interpolated value is related to distance the resulting interpolated surface is not "ridge preserving" (Philip and Watson, 1982). Hence, a sufficiently dense network is required to accurately simulate or model the local variation. An evenly (spatially) distributed and dense network is required to represent the desired interpolated rainfall surface (Watson and Philip, 1985).

SPLINE : Spline interpolators have been widely used to develop climatic surfaces from sparse observation points. The interpolated surface based on SPLINE (a) passes exactly through the data points and (b) has a minimum curvature. The latter

task is accomplished by minimizing the cumulative sum of the squares of the second derivative terms of the surface taken over each point on the surface. This interpolation is also referred to as thin plate interpolation (Franke, 1982). It ensures both a smooth surface and a continuous first-derivative surface. Rapid changes in gradient or slope (the first derivative) may occur in the vicinity of the data points; hence, this model is not suitable for estimating second derivative (curvature). Mitas and Mitasova (1998) provide a detailed description of the calculation procedure. There are three arguments that are used in the SPLINE interpolation: (a) the "aType" argument modifies the minimization criterion so that the third derivative terms are incorporated into the minimization criteria (b) the "aWeight" argument specifies the weight attached to the third derivative terms during minimization. Higher values of this term lead to smoother surfaces. Values vary between 0 and 0.5 with the higher values leading to smoother surfaces (regularized option). Finally, (c) the "aType" argument modifies the minimization criterion so that first-derivative terms are incorporated into the minimization criteria (tension option). Values vary between 0 and 10.

KRIGING: The Kriging method can be viewed as a classical weighted linear interpolation method that satisfies the same conditions as the Lagrange or the least squares interpolation method. This technique is used regularly in geotechnical analysis and has been applied to hydrologic analysis by a number of authors (Montmollin et al., 1980; Tabios and Salas, 1985; Dingman et al., 1988). The

advantage of Kriging over ordinary least-squares techniques is that the estimated values at observation sites are equal to the actual measurements (Gebhardt et al., 1988). When Kriging is used, precipitation at a site is considered a function of a predictable trend and a random component. Kriging may treat the trend as a constant (simple Kriging), or may describe the trend as a polynomial (Universal Kriging). The variance of the difference between rain-gauge measurements is related to the distance between rain-gauges, called a semivariogram. The direction (of the distance) is assumed not to affect rain-gauge values. Kriging is an advanced interpolation procedure that generates an estimated surface from a scattered set of points with z values. Unlike the other interpolation methods supported by the Spatial Analyst, Kriging involves an interactive investigation of the spatial behavior of the phenomenon represented by the z values before the best estimation method for generating the output surface is selected. Points sets known to have anomalous pits or spikes, or abrupt changes, such as those that might be represented by breaklines in a tin, are not appropriate for the Kriging technique. In some cases, the data can be pre-stratified into regions of uniform surface behavior for separate analysis.

3.4.2 Evaluation of the Interpolation Techniques

Tabios and Salas (1985) recommended Kriging for annual rainfall interpolation, however, not much work has been done on the interpolation techniques for higher spatiotemporal resolution. In a study by Naoums et al. (2002) the three interpolation techniques (Spline, IDW, and Kriging) were compared in terms of their

accuracy for short-term rainfall interpolation. This comparison was performed on the same rain-gauge network used in the analysis of this chapter, using the same one minute rain-gauge accumulations over the same sampling period of 1989 and 1990. The methodology of the comparison was to remove one gauge from the network. A rainfall value was then interpolated at the removed site. The absolute error was calculated between the interpolated value and the observed value. This operation was performed at all the gauging sites and for all 1 minute records. The comparison was based on the average absolute error, the coefficient of determination between the observed and interpolated values, and the standard deviation of the error of interpolation. The results of the study showed that, for short-term rainfall interpolation, the IDW technique was superior among all techniques. On the other hand, Spline interpolation gives the poorest results. The details of this comparative analysis are available in Naoums et al (2002). Accordingly, the IDW technique was recommended in the study area.

3.5 Methodology

A GIS module is developed to spatially incorporate rainfall data for any number of rain-gauges in a geographical reference. Input consists of rainfall station points, storm rainfall data, simulation period, and length of time step. The user can choose to add any additional geographical features in the study area. The module output is in the form of a time series movie file for each storm analyzed.

The main idea of the method is to use an automated process to display the

storm in a movie sequence to simulate it as it moves through the study area. To achieve this task, three macros are developed on GIS Arc-Info to direct input and output through the process. The method can be summarized in the following steps:

1- Rainfall data are extracted in an ASCII file for each gauge.

2- The extracted data are appended and converted to an Arc-Info compatible format.

3- For each time step:

    1- Rainfall data are loaded into Arc-Info and spatially joined to the locations of the gauges.

    2- A rainfall grid is interpolated from the current rainfall intensities using an interpolation method.

    3- The rainfall grid, together with the values of the intensities recorded at each gauge, is displayed on the terminal screen.

    4- A sunraster image is created from the display for this time step.

4- A movie is encoded from the pictures representing the different time steps.

The direction and speed of the different storm cells can be easily determined by displaying the movie. Storm direction can be determined visually by tracking the motion of the peak rainfall intensities in the study area. The 360° azimuth is divided into 16 segments of 22.5 degrees. Accordingly, the estimated direction is one of these 16 segments, although it may not be precisely estimated within the 22.5 segment. By recording the travel time of the peak intensity in a determined direction,

the storm speed can be calculated by simply dividing the traveled distance by time (refer to Figure 3.7 for the distances between gauges). The peak intensity is chosen as the tracked characteristic rather than the start or end of rainfall for two reasons; (1) the start, and especially the end of rainfall, unlike the peak intensity, are highly influenced by environmental conditions; (2) because of the isotropic nature of thunderstorm rainfall, the observed peak intensity is closely correlated with the observed volume of event rainfall at any gaging site (Scheckenberger, 1983). Although the user tracks the peak intensity, other hyetographs characteristics (start and end of rainfall) may be useful in providing more evidence that may be used to estimate the direction.

It should be noted that the output mainly depends on the user's judgement. The user should not take a decision concerning the storm direction without having enough visualization evidence. It should be noted that this visualization method has the following advantages: (1) it is an automated method that does not require pre-processing calculations ; (2) it has the ability to detect multiple cells traveling over the study area, hence avoiding the problem that plague multi-peaked hyetographs; (3) other hyetograph characteristics may provide information in evaluating the storm characteristics; and (4) the consistency of the information from gauges can be visually evaluated, providing additional and useful procedure to assist in the quality control of the data.

3.6 Method Structure

The method consists of three macros on Arc/Info that run in sequence. A brief description of each macro is provided in this section. The technical details and source code of these macros can be found in Gad and Tsanis (1999). It should be noted that the raw rainfall data obtained from the tipping bucket gauges must be prepared first before being loaded into Arc/Info. Two Perl programs are developed to manipulate the raw data obtained from the tipping bucket gauges. The first program summarizes the events in the year and classifies the events into small, medium or large categories. The second program extracts rainfall data in a continuous time format to be compatible for loading into Arc/Info (refer to Gad and Tsanis (1999) for more details). Table 3.1 shows the rainfall format developed by the second Perl program, which constitutes the input to the GIS module. Figure 3.8 shows a logic diagram that explains the structure of the Arc/Info macros.

Table 3.1 Sample Rain-Gauge Input Data

Gauge No	Index	Yr	Month	Day	Hr	Min	Tips/min	Vol (mm)	Cum Tips	Cum Vol (mm)
2	1261	1989	9	22	21	0	2	0.42	143	30.03
2	1262	1989	9	22	21	1	2	0.42	145	30.45
2	1263	1989	9	22	21	2	3	0.63	148	31.08
2	1264	1989	9	22	21	3	2	0.42	150	31.5

SETUP

This Arc-Info macro is used to initialize the simulation process. The macro copies the geographical coverages representing the rain gauges, the geographical

features, and other parameter files and templates from the original location of the data to the user-specified workspace . The macro was developed to keep the original data in a safe place in its original locations. The whole simulation is carried out on the copy that this macro creates in the user-specified directory.

LOAD

This Arc-Info macro is required to load the extracted storm rainfall data of all gauges from the ASCII file developed from the Perl program to an Arc-Info template. This template is needed for compatibility with the system in which tipping bucket rain-gauges work and is subject to the user modifications. For other systems of recording rainfall, the template must be modified by the user. Output is an info file developed using Arc-Tables.

SIMULATE3D

After loading rainfall data into the template, rainfall data from the rain gauges are spatially related to the locations of the rain gauges in order to be used to interpolate a rainfall grid using the user-specified interpolation method. For each time interval, a rainfall grid is interpolated and displayed on the terminal screen. Because the objective is to simulate the storm kinematics, each rainfall grid is deleted after a sunraster image is saved from the display at this time step. The module encodes the produced series of sunraster images into one movie file using mpeg technology. Input consists of:

1- Point coverage representing the rain-gauge locations or a text file containing the x and y coordinates of the rain-gauges together with their rainfall z values.

2- Any additional geographical features in the study area required to be displayed in the output simulation movie.

3- Extracted rainfall data resulting from the module LOAD in ARC-INFO format.

4- Display parameters and files.

Output is in the form of a movie file that can be used to identify the storm kinematics, i.e., speed and direction. Another version of this macro is available to produce the animation in 2D perspective.

3.7 Method Tests

A snapshot of a 2D areal precipitation produced by a thunderstorm is shown in Figure 3.9. The results of the three interpolation techniques (i.e., Spline, IDW, and Universal Kriging) are shown in the figure. It appears that the rainfall interpolation technique has a significant effect on the simulated results in terms of the number and size of storm cells. In addition, the three techniques give estimates that vary within 8% of the average precipitation intensity in the study area. In terms of the storm direction, the effect is small. For the purpose of identifying the storm kinematic characteristics, the method of interpolation has virtually no effect on the result of the

visualization analysis.

A snapshot of a 3D perspective plot of areal precipitation (Spline interpolation) produced by a moving thunderstorm single cell is shown in Figure 3.10. A snapshot of a 3D perspective plot of areal precipitation (IDW interpolation) produced by a moving multicell thunderstorm is shown in Figure 3.11. From animation it was ascertained that one storm cell was entering and another cell was leaving the study area as shown on the snapshots in Figure 3.11.

Figure 3.12 shows a sample series of 2D pictures of areal precipitation from one movie that was produced using spline interpolation. The pictures indicate an attack direction from the west. The series of pictures also illustrates the fast rate of propagation of a storm cell across the study area.

3.8 Verification Using Radar

Rainfall fields contain a complicated mixture of cloud structures that develop and dissipate, draw together and move apart and, in doing so, move across the catchment with the possibility of moving in relatively different directions within the same overall rainfall pattern (Austin and Houze, 1972; Amorocho and Wu, 1977; Gupta and Waymyre, 1979). Because it is possible to have multiple motions within the radar umbrella, the differences between the radar technique and the rain-gauge technique may be due to differences in spatial scale rather than errors in the methods themselves. The radar results give typical motions over a much larger domain than

the gauge network. For this study, radar motions are calculated for an area about 100 km x100 km to the southwest of King City radar.

3.8.1 The Radar Technique

The radar tracking technique used is the cross-correlation technique described in Chapter 7. The radar tracking algorithm works by shifting the current rainfall gridded data relative to the previous grid by a variety of lengths and selecting the shift that maximizes the correlation between the two radar grids. The rainfall grids are obtained by using ($Z=200R^{1.6}$) to convert from reflectivity. A threshold value of 0.06 mm/hr is used, under which the grid cells are marked zeros. The results of the radar tracker are reported as the optimum spatial shift ($XShift_{opt}$, $YShift_{opt}$) in x and y directions, respectively. The resolution of the radar grids is 1 km in this study. The mean motion of the precipitation field in km/hr is given by ($XShift_{opt}/\Delta t$, $XShift_{opt}/\Delta t$) where $XShift_{opt}$ and $YShift_{opt}$ are in kilometers and Δt is the time separation in hours. Refer to Chapter 7 (section 7.3) for more information on the cross-correlation tracker.

3.8.2 The Comparison

Twenty-three storm events from 1989 in which both radar and rain-gauge data are available are selected for the purpose of comparing the two techniques. The storm velocity vectors are estimated from distance and time by displaying the output movies of the rain-gauge technique. Figure 3.13 shows a sample series from a 3D

movie representing one storm event (Sept. 8, 1989). It can be extracted from the figure that the rainfall pattern advances from the SW-W direction. The speed can be found by dividing the traveled distance by time. To explain these calculations, consider the 5 minute time period between 09:04 and 09:09. The rainfall pattern moves a distance of approximately 5.2 kilometers from a midpoint between HAR and LEE to gauge CHE. Accordingly, the calculated speed is 62.4 km/hr. It should be noted that the figure indicates that the rainfall cell recorded at gauges R11 and BLO at the starting time steps belong to an earlier storm cell that partially passed the northwestern corner of the study area and not to the rainfall cells recorded later at the other gauges. It is very important to point out that the larger the time interval used to calculate the speed of the storm the more reliable was the result. The error caused by the sampling resolution of the gauges (1 min) is minimized when using longer distance for calculating the speed.

Figure 3.14 shows an example of a series of radar grids depicting the 10 minute radar scans for the same storm event (Sept 8, 1989). The images agree well with the results obtained from the rain-gauge simulation described above. Velocity vectors are obtained from the radar technique from the optimum spatial shifts corresponding to the different time steps by averaging over the same time period used in the rain-gauge technique. It should be noted that the radar technique is characterized by a small variance of the estimated velocity vector, which ensures high confidence in its estimated velocity vectors.

The rain-gauge visualization technique and the radar tracking technique were

applied to the twenty three storms to determine their kinematic characteristics. The overall results of the twenty three storms (Figure 3.15 and Figure 3.16) show good agreement between the two techniques. The average absolute differences in the estimated speed and direction for the events studied are 8.3 ± 5.49 km/hr, and 9.1 ± 5.48 degrees respectively.

3.9 Method Application

In order to explore the characteristics of storm kinematics and single cell size in the study area one minute rainfall data obtained from the 9 precipitation stations covering a number of 39 storms are used. The 39 storm events occurred during the summers of 1989 and 1990. The developed rain-gauge visualization technique is applied to this set of data. Its results are shown in Table 3.2. The frequency distribution of the storm direction is shown in Figure 3.17.

The predominant storm direction ranges from 202.5 to 292.5 degrees ,i.e., within the S-W quadrant with average speed of 58 ±15 km/hr. It should also be noted that no significant joint correlation between the speed and direction of rainfall is found. However, a conclusion concerning the joint correlation between the storm speed and direction can not be generalized because of the limited number of storms analyzed.

In order to explore the expected size of a storm cell, the hyetographs of the 39 storms are analyzed by separating the bell-shaped hyetographs. Because each storm contained multiple cells, a number of 337 bell-shaped hyetographs are

separated from the 39 storms. Assuming a quasi-circular shape, a cell size can be found by multiplying the duration of its separated-bell-shaped hyetograph by the cell speed. Figure 3.18 shows the frequency distribution of the storm size with an expected average of 3.94 ±1.3 km.

Table 3.2 Estimated Storm Speed and Direction for 39 Storm Events

Storm No.	Direction (Deg.)	Speed (km/hr)	Storm No.	Direction (Deg.)	Speed (km/hr)	Storm No.	Direction (Deg.)	Speed (km/hr)
1	247.5	84	14	247.5	45	27	225	65
2	247.5	58.5	15	225	52	28	270	80
3	247.5	70	16	270	40.5	29	270	80
4	247.5	63	17	270	49.2	30	270	40
5	247.5	70	18	247.5	58	31	270	80
6	247.5	60	19	247.5	63	32	247.5	52
7	202.5	39.6	20	247.5	70	33	247.5	70
8	202.5	39.4	21	270	72	34	292.5	52
9	202.5	41	22	247.5	78	35	225	50
10	247.5	60	23	247.5	70	36	225	72
11	247.5	40	24	225	50	37	225	72
12	247.5	40	25	270	46	38	270	30
13	247.5	42	26	270	75	39	202.5	70

3.10 Closing Remarks

This chapter focuses only on rain-gauge tracking techniques. The reason is that there are areas, mostly urban, that are not equipped with radar or where radar data in real-time are not available. Rainfall in these areas, for practical applications, is observed only by using rain-gauge networks. Another important application of rain-gauge tracking techniques appears when the objective is to perform a historical analysis on the characteristics of the rainfall kinematics. Only rain-gauge networks can provide such historical data. In addition, there are other applications requiring an

estimation of the rainfall kinematics from rain-gauge data, such as rainfall trajectory based interpolation (refer to section 3.1). The following points summarize the results of this chapter:

- A simple and efficient rain-gauge tracking technique is developed for the purpose of estimating the kinematics of rainfall using any number of tipping bucket rain-gauges. The technique is based on visualizing the storm evolution as it moves across a study area by using GIS and mpeg technologies. The developed rain-gauge technique is compared to a cross-correlation radar tracker. The results of the comparison shows good agreement between the two trackers. The average absolute differences between the two trackers in estimating storm speed and direction are 8.3 ± 5.49 km/hr, and 9.1 ± 5.48 degrees respectively.

- The analysis proved that storm size, speed and direction affect the spatial variability of rainfall received on the ground. For example, it is possible to have a gauge recording a high rainfall event , whereas another gauge, 8 km away, which does not fall along the active convective cell route, records no rain. Convective type rainfall and widespread rainfall are the most common types in the Hamilton-Wentworth Region. This result was obtained by inspecting the general characteristics of the hyetographs analyzed (refer to the typical hyetographs of convective and widespread rainfall shown in Figures 1.3&1.4).

- The 1 min rainfall recorders are essential to the purpose of storm tracking in urban areas. Roughly, a high resolution (5 km × 5 km) network of one minute gauges is required.

- The rain-gauge technique presented in this study is applied to explore the predominant characteristics of rainfall in the study area. The results indicated that the predominant storm direction ranges from 202.5 to 292.5 degrees , i.e., within the S-W quadrant with average speed of 58 ± 15 km/hr. Assuming the frequency distribution is symmetrical, the expected size of a storm cell is approximately 3.94 ± 1.3 km in diameter. However, if we consider a positively skewed distribution, it can be said that 85% of the storm cells vary in diameter of 3 to 5 km. In addition, it should be noted that storm speeds can reach up to 120 km/hr in some cases.

This chapter provides an exploration of storm characteristics in Hamilton-Wentworth Region. The results of the predominant storm characteristics obtained in this chapter will be used as supporting statements in the following chapters. In addition, the methodology used within this chapter acts as a quality control analysis of the rain-gauge data. These rain-gauge data will be used in some of the remaining analyses of the thesis.

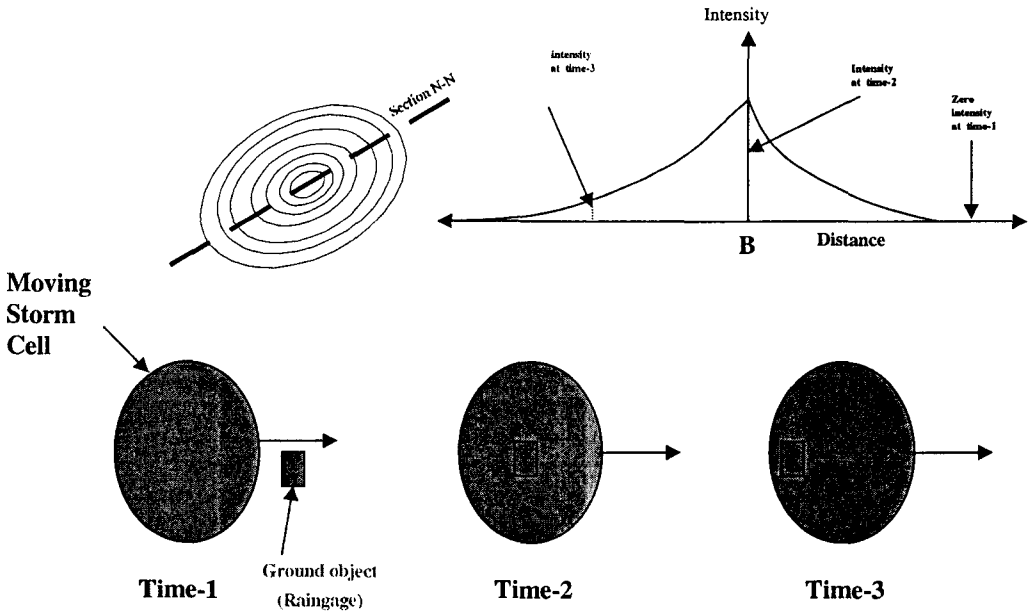

Figure 3.1 Variation of rainfall intensity due to storm cell advance.

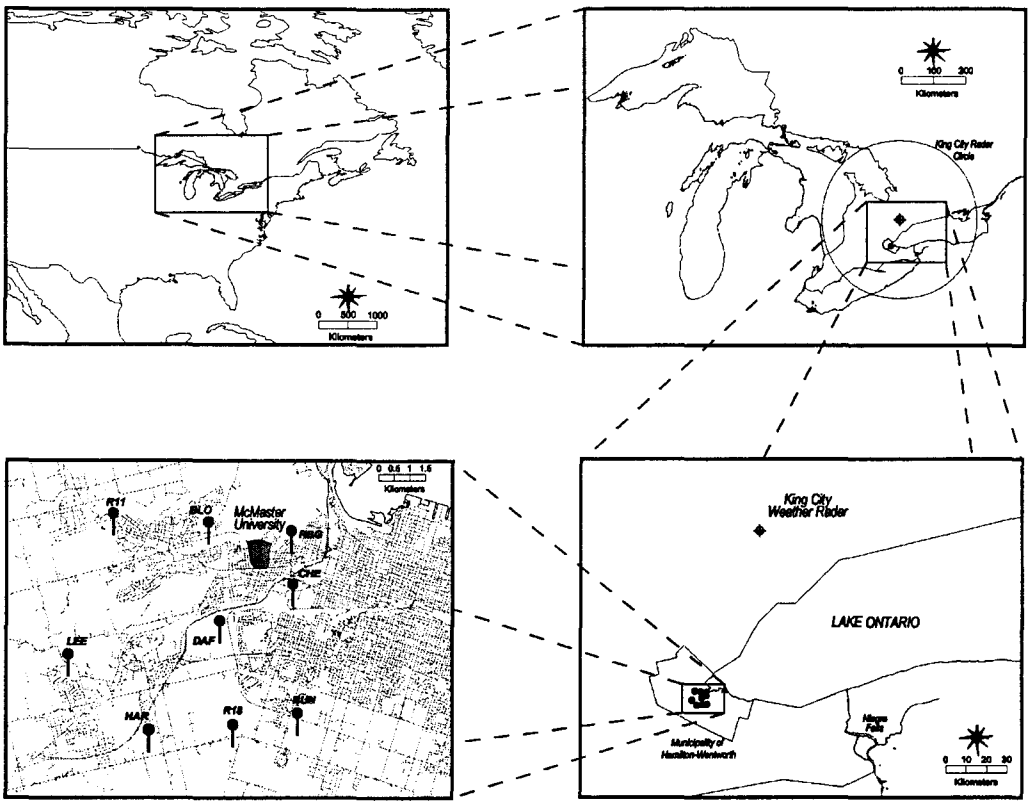

Figure 3.2 The locations of the rain-gauge network and King City weather radar.

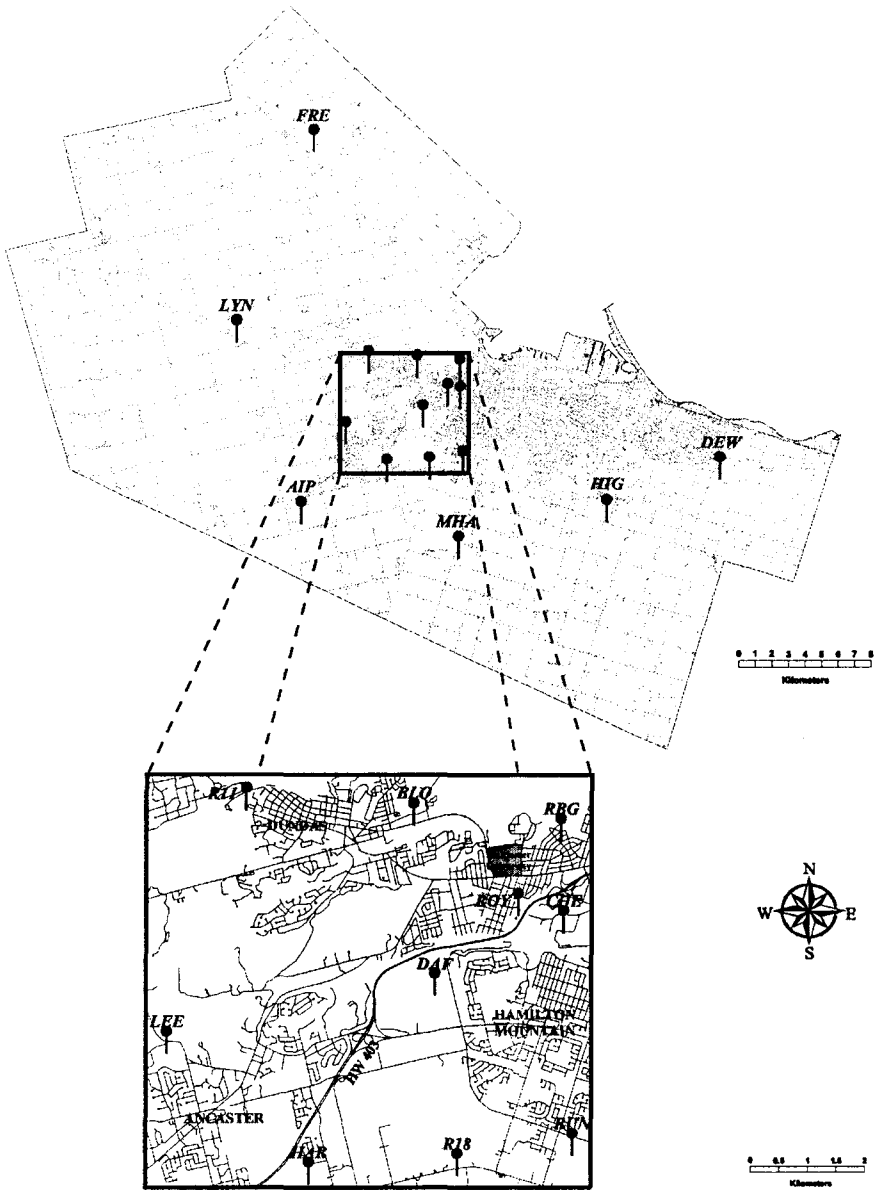

Figure 3.3 Locations of rain-gauge network operated by the Regional Municipality of Hamilton-Wentworth.

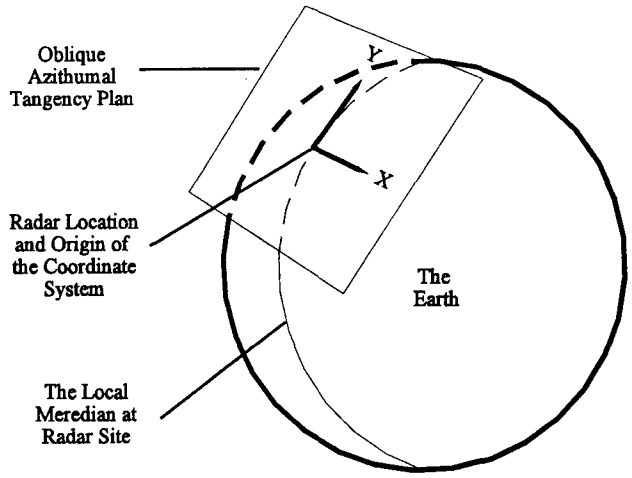

Figure 3.4 The radar azimuthal coordinate system.

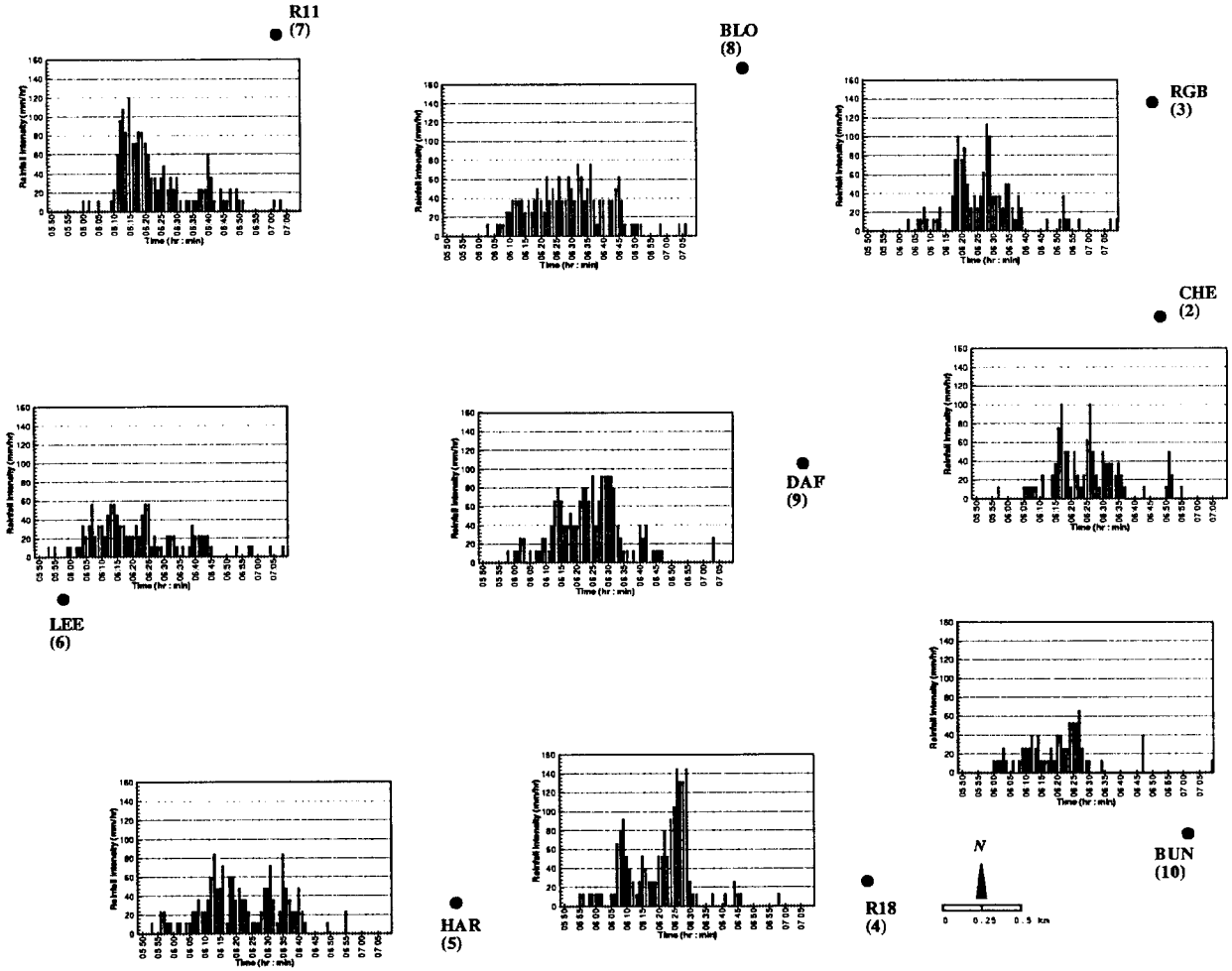

Figure 3.5 Hyetographs recorded at the nine rain gauges for the storm event June 6,1989.

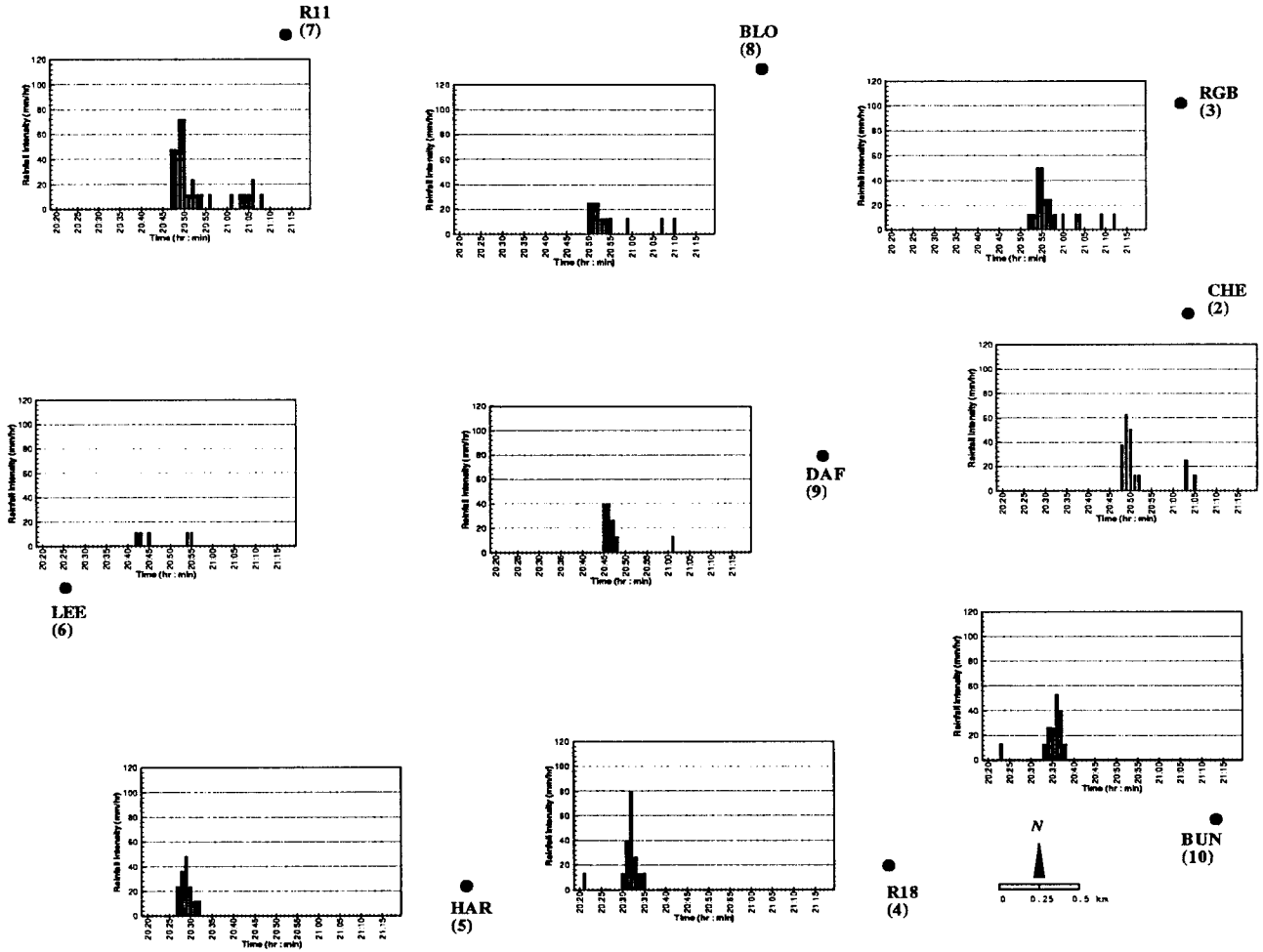

Figure 3.6 Hyetographs recorded at the nine rain-gauges for the storm event May 30, 1989.

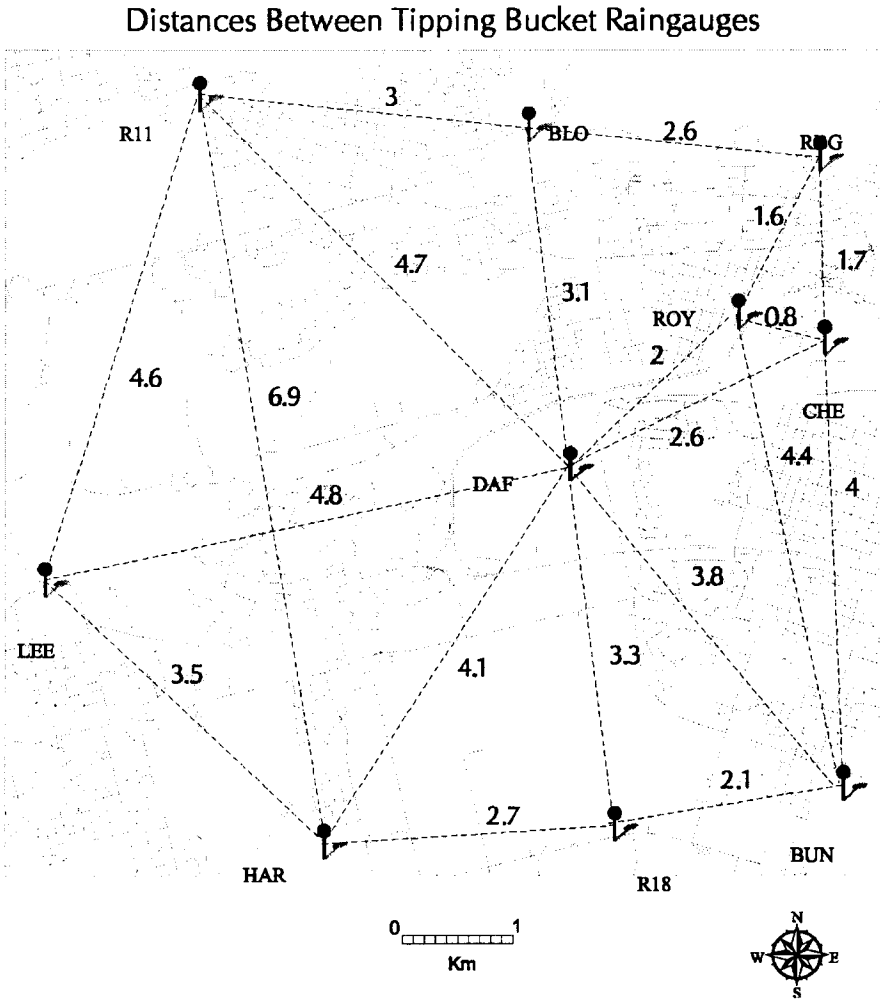

Figure 3.7 Distances (km) between rain-gauges in the study area.

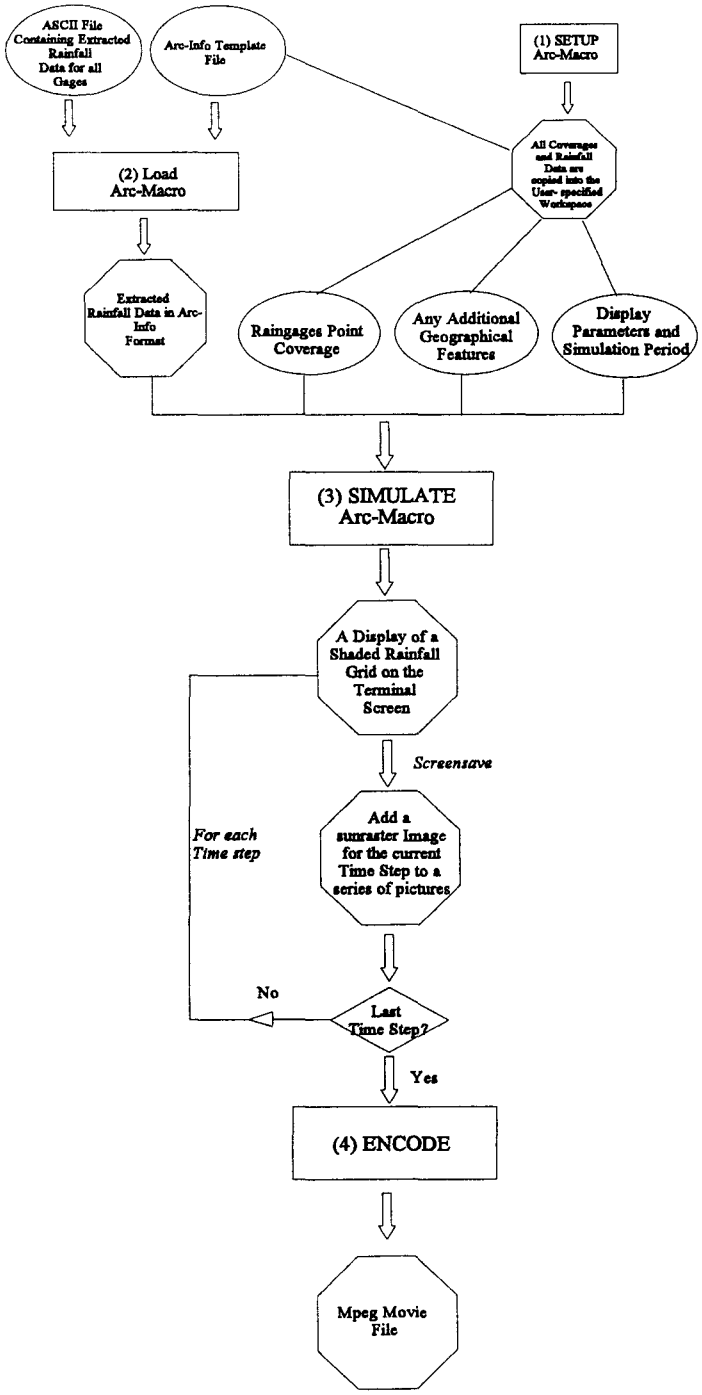

Figure 3.8 Logical diagram of the rain-gauge algorithm used to estimate the speed and direction of the storm cells.

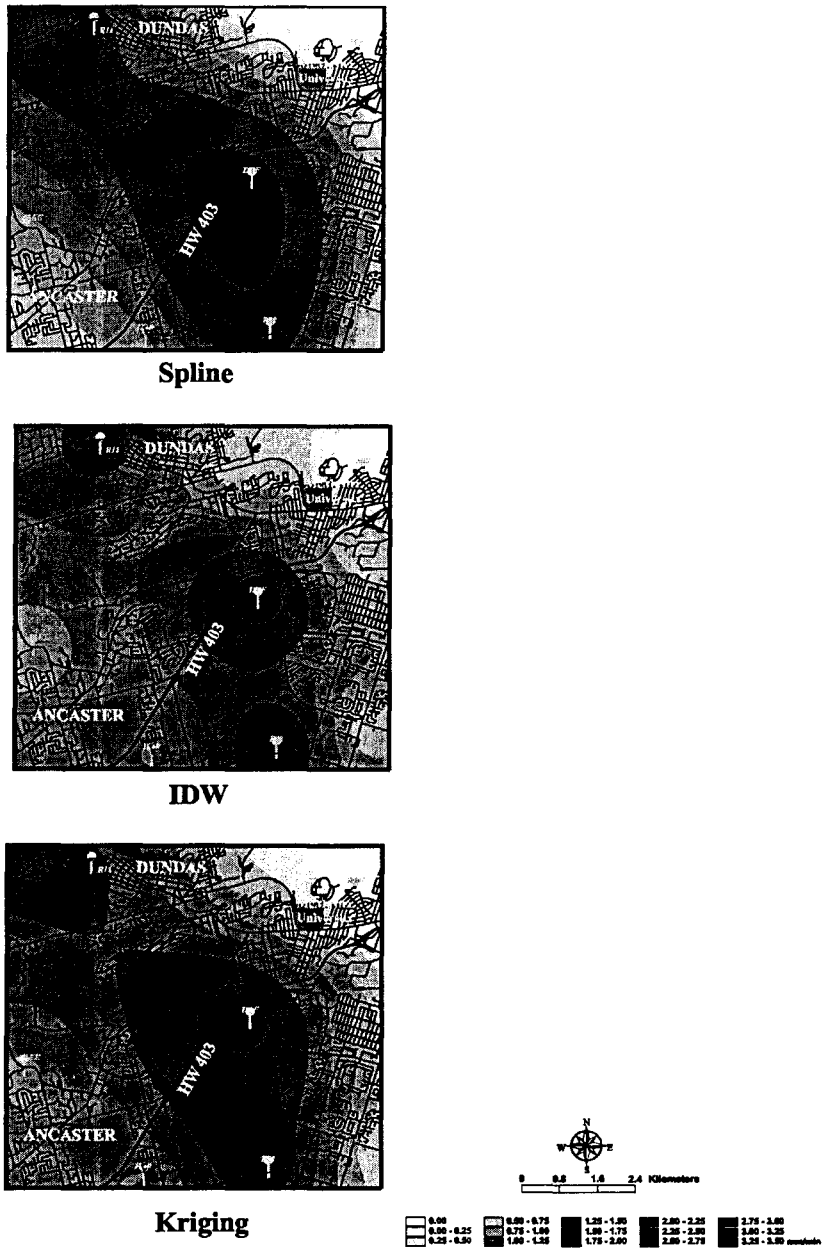

Figure 3.9 Snapshot of a 2D areal precipitation produced by a thunderstorm. Three interpolation techniques are used, i.e., Spline, IDW, and Kriging.

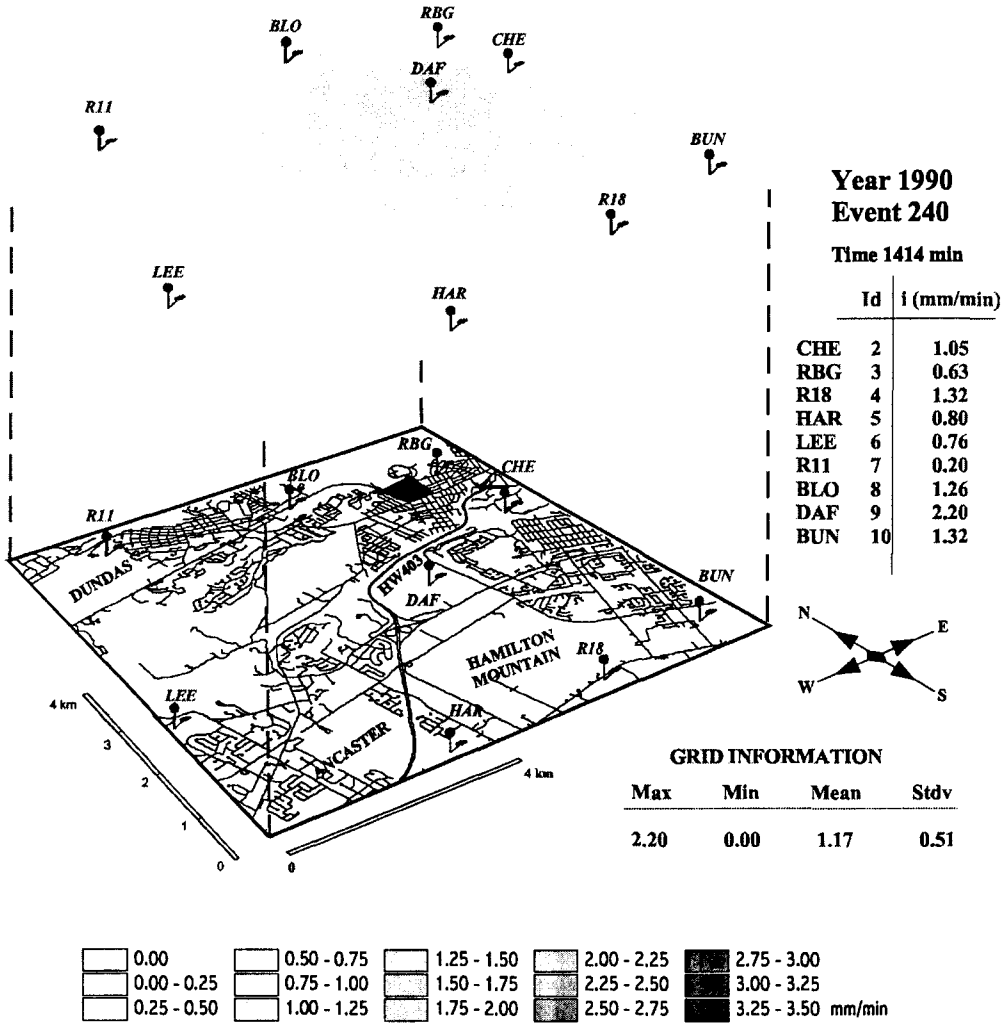

Figure 3.10 Snapshot of a 3D perspective plot of areal precipitation produced by a moving thunderstorm single cell.

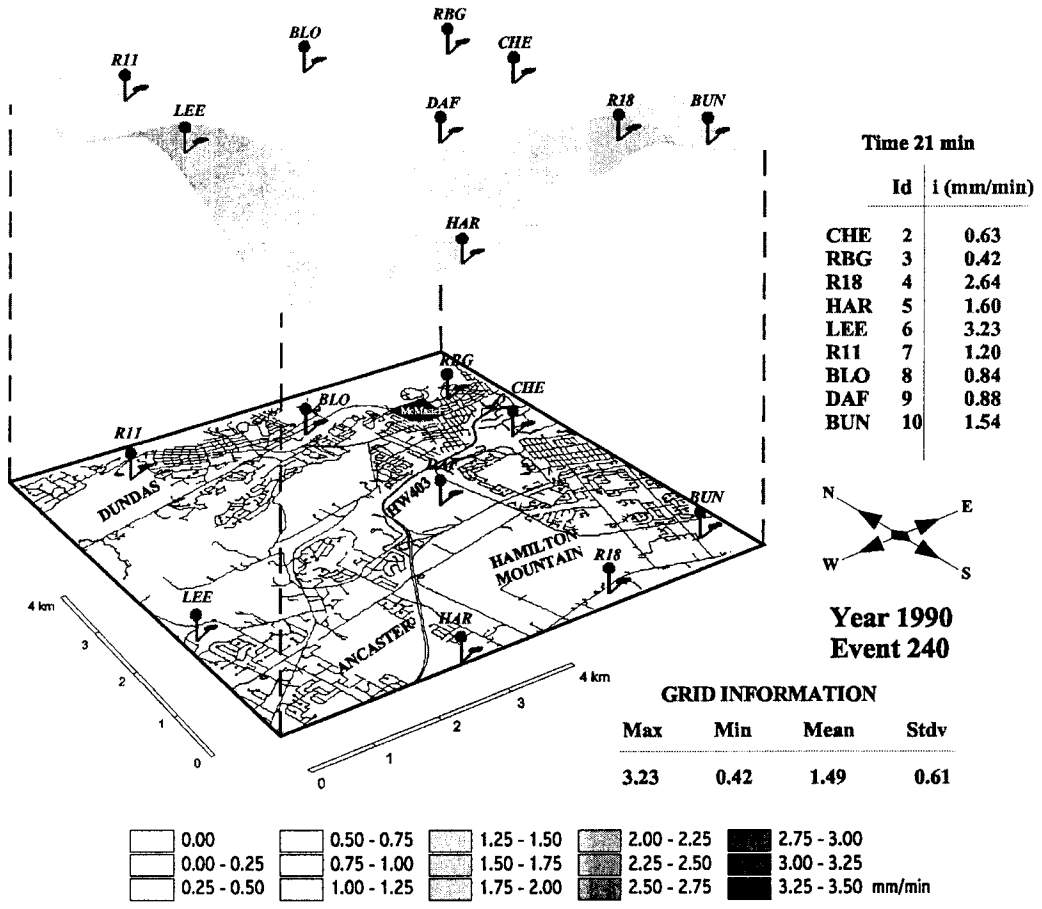

Figure 3.11 Snapshot of a 3D perspective plot of areal precipitation produced by a moving thunderstorm multicell.

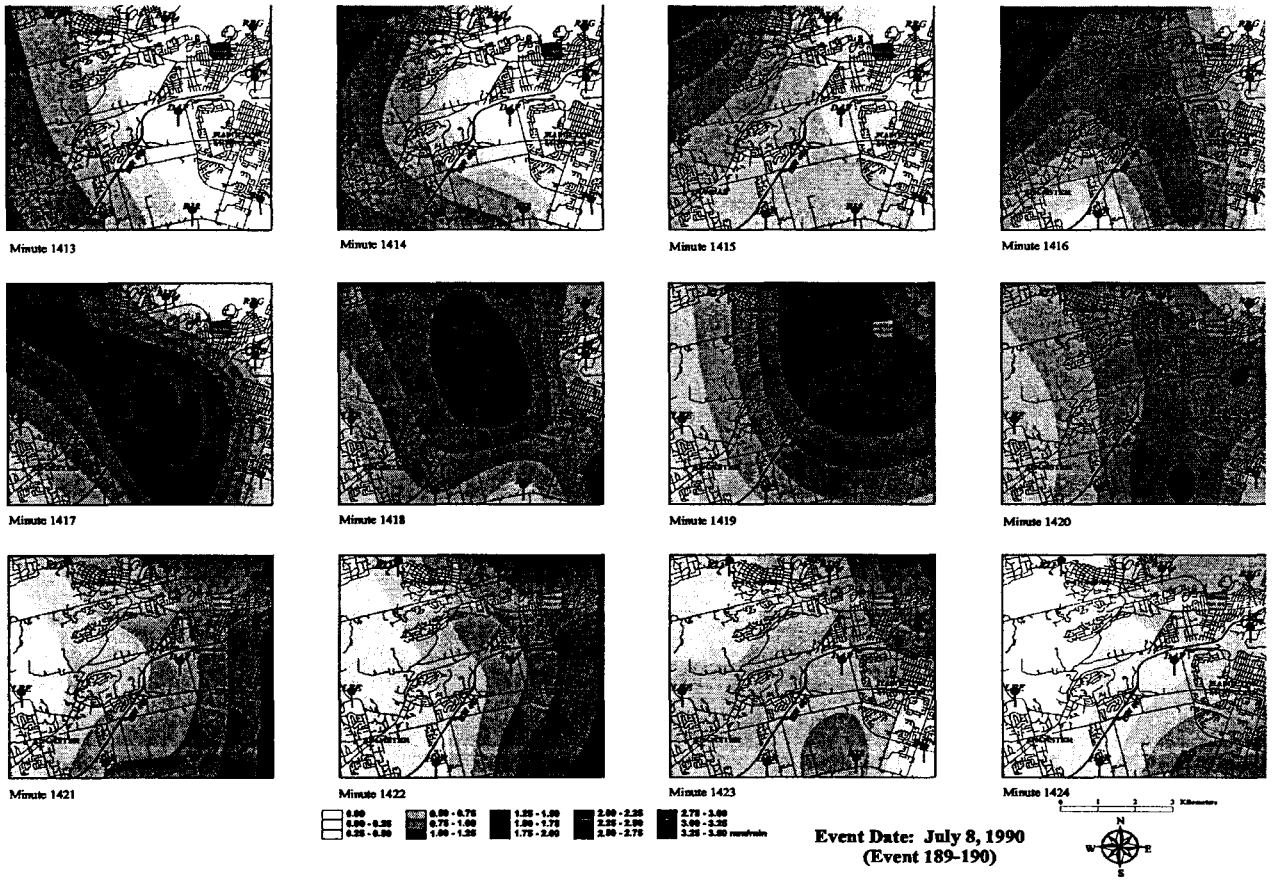

Figure 3.12 Sample series of pictures indicating an attack direction from the west. The series is obtained from one movie representing the event of July 8,1990.

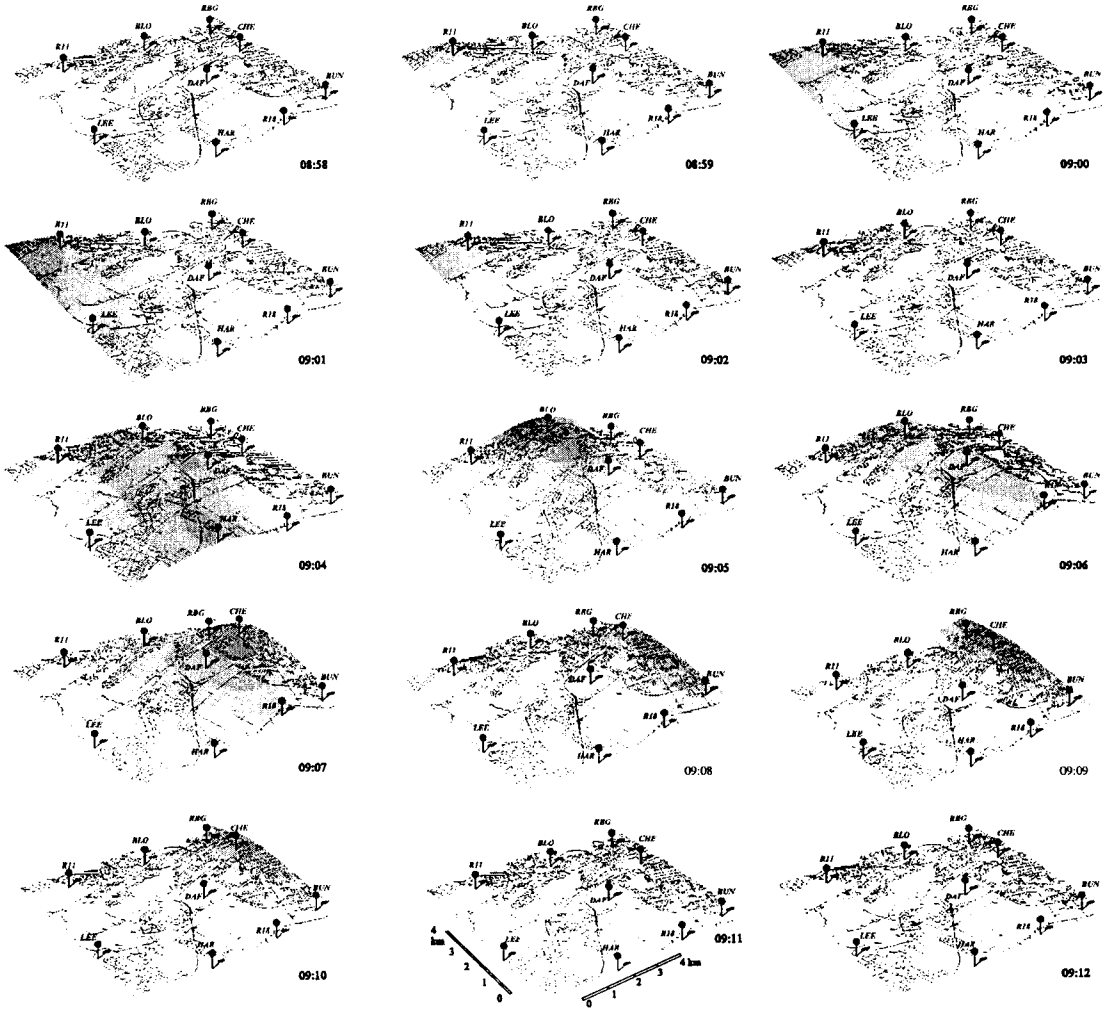

Figure 3.13 A sample series from a 3D movie representing the storm event of Sept. 8, 1989.

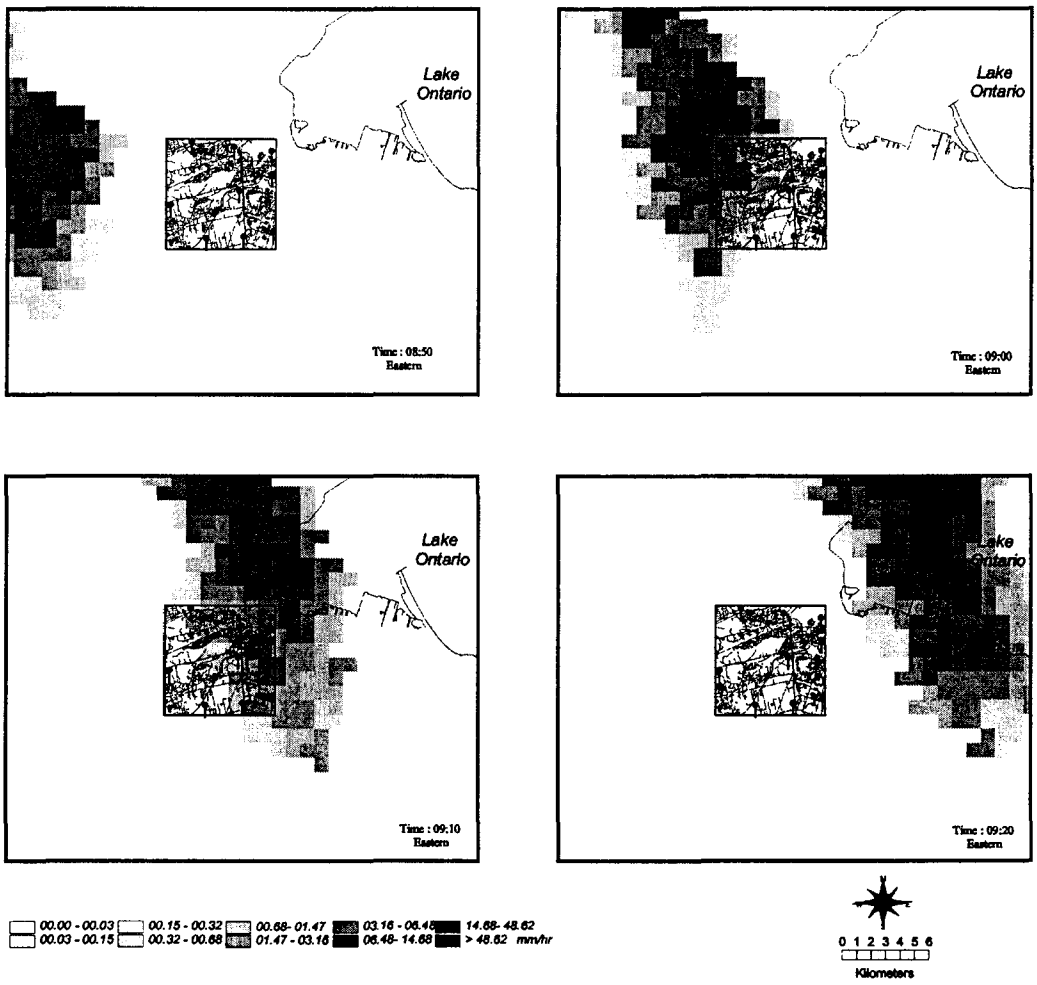

Figure 3.14 A series of radar grids (1 km^2) depicting the 10 min radar scans for the storm event (Sept. 8, 1989).

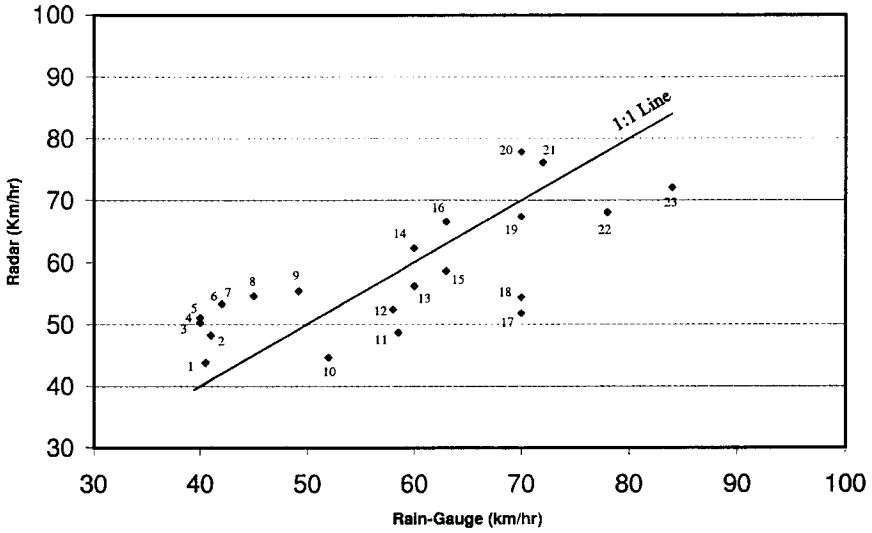

Figure 3.15 Storm speed (km/hr) comparison between estimates based on a the rain-gauge tracker and the radar tracker.

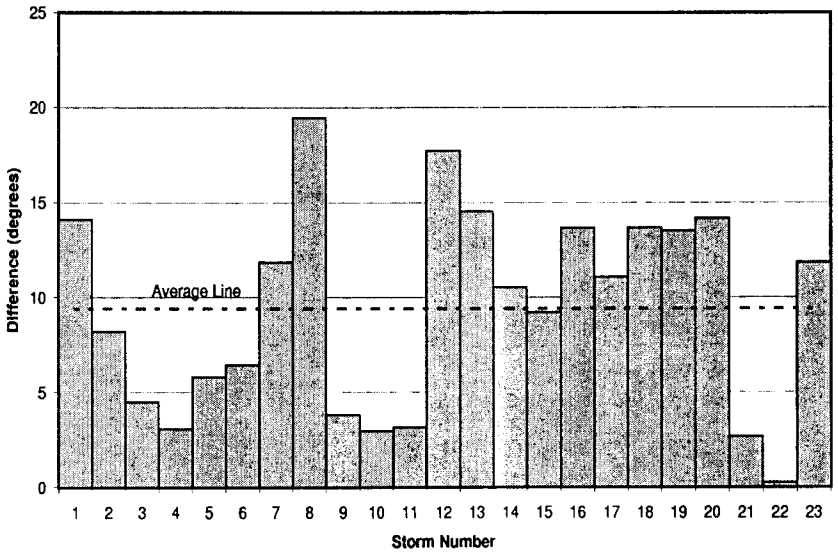

Figure 3.16 Difference in storm direction between the rain-gauge and the radar trackers.

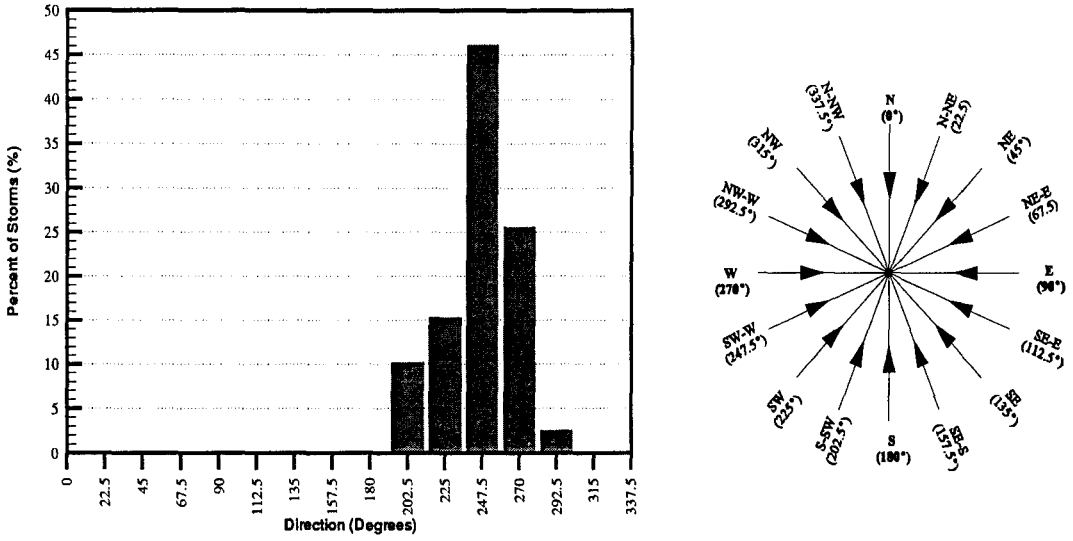

Figure 3.17 Distribution of the storm direction based on 39 storm events in 1989-1990.

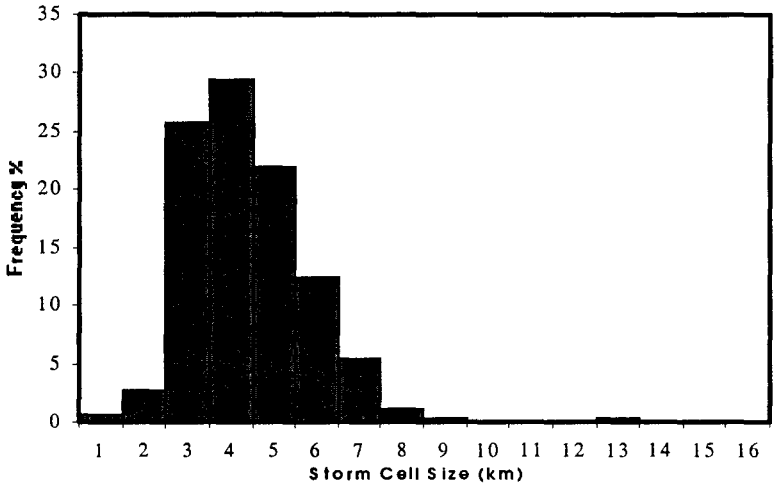

Figure 3.18 Single cell size distribution based on 337 bell-shaped separated hyetographs.

CHAPTER 4

GEO-REFERENCING RAINFALL DATA FROM MULTI-SENSORS

4.1 Introduction

Rainfall data from ground radars and rain-gauge networks are typically in different projection systems. Since it is a common practice to calibrate radar estimated rainfall fields by using rain-gauge data, an accurate positioning of the radar rainfall grid on the locations of rain-gauges, or vice versa, is essential. In addition, rainfall data from multi-sensors (multiple radars, rain-gauges, and weather satellites) are usually referenced in a common coordinate system for different applications such as hydrological modelling, severe storm warning, and meso-scale storm tracking and forecasting. Hence, it is important to assess the accuracy of overlaying the data from the different sensors and to properly select the common coordinate system in which the data are referenced. In this chapter, a new ellipsoidal-based projection method is developed for the purpose of evaluating the accuracy of different sphere-based projection methods typically used for projecting radar data. In addition, the problem of selecting a common coordinate system for data from multi-sensors is investigated and a common coordinate system for the Great Lakes area is suggested. The work

described in this chapter is used in the following chapters for geo-referencing radar rainfall data with respect to rain-gauges and to geo-reference data from multiple radars into a common coordinate system.

4.1.1 Map Projections

A map is a two-dimensional representation of part, or all of the surface of the three-dimensional earth. Map projection is the methodology used to transfer features, or positions, on the earth reference sphere, or ellipsoid, to the corresponding points on a flat sheet of a map or vice versa. All projections produce a certain amount of distortion in terms of distance, angle, shape, or area. The three plotting surfaces in use for practical map projections are: the plane, the cone, and the cylinder. Snyder (1987) and Bugayevskiy and Snyder (1995) have provided detailed discussions on map projections. This study focuses on those map projections that are based on plane projection surfaces, since they provide the closest representation of the CAPPI (Constant Altitude Plane Position Indicator) data, which are mapped in an Earth's tangential plane. Planar projections project earth features onto a flat surface touching the globe. A planar projection is also known as zenithal or azimuthal projection. The plane of projection is usually tangent to the globe at a point, and it may be secant. The aspect of the projection is determined according to the location of the tangential point (polar for the poles, equatorial at the equator, or oblique at any other arbitrary point) as shown in Figure 4.1. The differences between planar projections arise from the method used in the projection. Three known sphere-based planar perspective

projections are the *Gnomonic*, *Stereographic*, and *Orthographic* projections. Figure 4.2 shows the method followed in constructing each projection. In addition, there are some other non-perspective planar projections, such as the *Azimuth Equidistant* and *Lambert Equal-area* projections. Ellipsoidal formulas exist for some of the above named projections (Snyder, 1987).

4.1.2 Radar Projection Methods

The radar rainfall product is either a polar or rectangular grid of precipitation. Let us consider a Cartesian grid that has 480x480 cells. Each cell (i.e, pixel) in this grid is 1km x 1km in size. The radar is located at the centre of this grid, as shown on Figure 4.3a. If the sole consideration for the placement of the rainfall grid on a map is its coincidence with the radar location (as seen in Figure 4.3b), the registration of this rainfall grid becomes a problem. This is because the y-axis of the rainfall grid should be oriented so that it is parallel to the direction of the local geographic north at the radar location on the map, as shown in Figure 4.3c. Another problem is the distortion that results from the projection method used to produce the reference map, which makes it necessary to distort the radar grid by the same amount. In addition, the radar's rainfall grid is not located on the earth's surface but is originally mapped from a constant altitude above sea level to an Earth's tangent plane at the radar location. Hence, the proper transformation of the locations of the radar rainfall cells to the reference map's projection, or vice versa, is essential.

The conventional method used to locate a rainfall cell on the ground assumes

that the earth is a perfect sphere and the planar range of the rainfall cell from the radar coincides with a great circle drawn in the direction of the azimuth from the radar location (FMH 1991; Hoke et al., 1981; Anagnostou, 1997; Tsanis et al., 2002; and others). This method was also used to map data from multiple radars and to reference locations onto NEXRAD map displays (Reed and Maidment, 1999), which use the HRAP (Hydrologic Rainfall Analysis Project) sphere-based projection system. This projection system is used by both the Air Force Global Weather Central (AFGWC) and the National Meteorological Centre (NMC) oof the USA (Hoke et al, 1981). Accordingly, the longitude and latitude of the rainfall cell are obtained in terms of the longitude and latitude of the radar location. This means that the conventional method assumes that the radar grid coincides with the earth's spherical surface.

Some researchers have pointed out that the radar rainfall grid should be treated as a plane tangential to the earth at the radar location. In a study of the use of HRAP rainfall data in GIS-based hydrologic modelling, Reed and Maidment (1995) suggested a *Lambert Equal-Area* projection to represent each radar plane; in another paper in 1999 they suggested an *oblique Stereographic* plane to represent each radar coordinate system before projecting it in the common coordinate system. Tsanis et al. (2002) used an *oblique azimuthal equidistant* plane in a comparative study between a radar and a rain-gauge tracking technique. Hence, a question arises: which projection is more accurate, or in other words are there really significant differences between these planar projections? Also, what shape should the earth be assumed to

be if we are going to represent the radar data in a plane tangential to the earth at the radar location? There are differences between the spherical and ellipsoidal earth datums. The main difference appears between the geocentric and geodetic latitudes, as shown in Figure 4.4. Snyder (1987) defines the *geodetic* latitude (Φ) of a point as the angle between the normal plane to the ellipsoid at this point and the equatorial plane. The *geocentric* latitude (Φ') is the angle between a line drawn from the point and the centre of the ellipsoid and the equatorial plane. For a sphere, the geodetic and geocentric latitudes are the same. These differences typically cause errors when converting between the two datums. Using a sphere-based map, for example, to locate a point with latitude and longitude obtained using a GPS (Global Positioning System), will result in erroneous location because the geodetic-based latitude obtained from the GPS has been interpreted as a geocentric one. The proper way to locate the point on the sphere-based map is to convert the latitude obtained from the GPS to the corresponding geocentric value. This value is then used to locate the point on the sphere-based map.

However, the consequences of using a reference sphere instead of an ellipsoid, as well as the consequences of using the conventional method or any other planar projection on the accuracy of locating rainfall on the ground are not fully understood. Also, insufficient literature exists, and a detailed systematic analysis of such consequences has not been offered thus far. The work described in this chapter is an attempt to fill this knowledge gap.

4.2 The Scanning Strategy and The Radar Rainfall Product

Most meteorological radars are pulsed radars, that is, electromagnetic waves at fixed preferred frequencies are transmitted from a directional antenna into the atmosphere in a rapid succession of a microwave train of pulses. Figure 4.5 shows a directional radar antenna emitting a pulsed beam of electromagnetic energy and illuminating a portion of a meteorological target. The target is uniquely defined in space by measurements of range, azimuth and elevation angles.

A number of conical scans are performed according to the automatic scanning strategy of the radar antenna. The scanning strategy tries to form a constant altitude product at approximately 1.5-2 km above the ground. Different scanning strategies are followed in each radar system (Shed et al., 1991). For example, in King City Weather Radar, Ontario, Canada, the scanning strategy is determined as follows:

1. Data are collected from a number of conical scans, let us say, 24.
2. At each range , the conical surface closest to height, let us say 1.5 km (above ground AGL), can be found by calculations that take into account the spherical earth curvature and the refractive effects. This is usually done by using 4/3 earth model to account for the beam curvature caused by atmospheric refraction. (Donaldson, 2001; Doviak and Zrnic ,1993)
3. The data for that range are extracted from that surface.

Thus the curve of height versus range is a saw-tooth shape (see Figure 4.6a) centered approximately at 1.5 km (ASL), except for ranges beyond approximately 125 km.

The beam corresponding to the lowest elevation angle goes above 1.5 km and finally reaches almost 5 km at the far range. Figure 4.6b and Figure 4.6c show the elevation angle and the distance d' (refer also to Figure 4.5) versus range.

Since the radar measurements have to be represented on a plane for processing and displaying purposes, the data are mapped from the saw-tooth shaped curve to the tangent plane. This mapping is done by means of simple geometrical projection, using the slant range and the cosine of the elevation angle to produce a polar product in the tangent plane. Conversion from polar to Cartesian is then done, usually by a nearest neighbor method.

4.3 The Earth Figure

Intensive work has, and is still, being done in the science of Gravimetry. However, for the purpose of this study, it is essential to introduce some basic definitions concerning the earth's figure and gravity. Consider a body at rest on the earth's surface. The net force acting on this body is the result of the gravitational force and the centrifugal force caused by the earth's rotation. This net force is a vector of magnitude and direction. The direction of this force is the direction of the *plumb line*, or the *vertical*. The total force, the resultant of the gravitational force and the centrifugal force, is called the *gravity* and its potential is called the *gravity potential* (W). The surfaces at which W is constant, called *gravity equipotential surfaces*, are shown in Figure 4.7. The lines (called *plumb lines*) that intersect all equipotential surfaces normally have a slight curvature. The surface of the oceans,

after some idealization, is an equipotential surface. This particular equipotential surface is a part of the known term "the geoid" ($W=W_o$), which is still held by many to be the fundamental surface of physical geodesy (Heiskanen and Moritz, 1967). A reference mathematical surface is essential to represent the geoid for the purpose of geodetic observations in order to specify locations on the earth surface and in order to locate the variations in the geoid itself.

A sphere is a very simple one parameter surface. The earth's departure from a sphere is significant, however, and another mathematical figure adequate for correct representation should be adapted. The reference ellipsoid of revolution, generally referred to as the ellipsoid, or spheroid, is produced by rotating an ellipse about its minor axis, which may not exactly coincide with the axis of rotation of the earth. Although the geoid actually has different variations in space and time, the reference ellipsoid is the best simple surface to represent it. At sea, the geoid coincides with the free unbounded water surface, which might not coincide with the reference ellipsoid. Under the continents, the geoid rises above the ellipsoid by a distance known as the geoid height. The angle between the ellipsoid and the geoid at any point is known as the deflection from the vertical (Pick et al., 1973).

In the last fifteen years satellite data have provided geodesists with new measurements to define the best earth-fitting ellipsoid. The most recently developed and widely used ellipsoid is the World Geodetic System of 1984 (WGS84) on which Global Positioning (GPS) measurements are based. In addition to this ellipsoidal coordinate system, however, thirty or more reference ellipsoids have been developed

all over the world for different uses in different places. The latitude and longitude of a point based on a certain spheroid are not essentially the same as those determined by another and, for this reason, a datum conversion is required.

Based on the above discussion of the gravity field of the earth it is assumed for this study that:

1. The reference ellipsoid is the best simple representation of the geoid.
2. The main force acting on a free falling body is the gravity force as defined above.
3. The direction of gravity at a point on the earth is a line normal to the reference ellipsoid at this point, which is directed to the centre of curvature of the ellipsoid in the plane perpendicular to the meridional plane at this point.
4. Rainfall detected by radar in a pulse volume tends to follow a gravity path, which is assumed to be a line drawn from the centre of the grid cell normal to the reference ellipsoid.

4.4 Formulating the Projection Problem

The Gnomonic projection would be the most appropriate way to represent radar data if the earth was a spherical figure with surface gravity vectors directed towards the centre. The earth, however, is ellipsoidal and the direction of gravity, normal to the ellipsoidal surface is not directed towards the centre of the ellipsoid. The following questions arise: (1) What is the magnitude of error resulting from

locating rain-gauges in the radar tangent plane, or vice versa, if the earth is approximated by a sphere? (2) If representing the earth as a sphere does not lead to a significant error, which sphere-based projection method should be used, and how should it be used? (3) Is there an exact solution to the problem of gravity projection to be used as a reference method to evaluate the other methods? (4) Which coordinate system is more suitable as a common coordinate system for data from multiple radars? And (5) which coordinate system is more suitable as a common coordinate system for satellite based data?

It should be noted that the planar projections of GIS software are only supported on spherical earth representations. There are, however, some special cases, such as the polar aspect of the Stereographic projection followed by the Universal Polar Stereographic system, or UPS. The GIS methodology followed when projecting data from an ellipsoid-based projection into a sphere-based projection is done by interpreting the geodetic coordinates as geocentric coordinates. The approach is described in the following quoted paragraph from ArcDoc 7.0 (1994):

"*Some projections are only supported on a sphere. These projections are meant to be used at small scales. You should not try to project data from a projection on a sphere to a projection on a spheroid. The mathematical transformation does not exist. It is not possible to improve the geodetic precision of data by simply putting it in onto a spherical representation of the earth. However, it is possible to project data from a projection on a spheroid to a projection on a sphere. This will degrade the data by putting it onto a spherical representation of the earth*".

The conventional method, which is widely used to project rain-gauge geographical locations onto the radar Cartesian coordinate system, or vice versa , also employs a spherical figure of the earth. This method assumes that the range in the radar plane and the azimuth measurement of the meteorological target coincide with the earth's surface. To introduce the conventional method, let points O and P represent a radar and a rain-gauge with coordinates (λ_o, Φ_o), and (λ_p, Φ_p) respectively where λ denotes the longitude and Φ is the latitude. The Cartesian coordinates of the rain-gauge (x_p, y_p) with respect to the radar coordinate system can be found by applying the following equations:

$$\Delta\lambda_p = \lambda_p - \lambda_o \tag{4.1}$$

$$\psi_p = cos^{-1}(sin\,\phi_o\, sin\,\phi_p + cos\,\phi_o\, cos\,\phi_p\, cos\,\Delta\lambda_p) \tag{4.2}$$

$$r_p = ER \times \psi_p \tag{4.3}$$

$$x_p = r_p \sin\alpha_p = r_p \times \frac{\cos\phi_p \sin\Delta\lambda_p}{\sin\psi_p} \tag{4.4}$$

$$y_p = r_p \cos\alpha_p = r_p \times \frac{\cos\phi_o \sin\phi_p - \sin\phi_o \cos\phi_p \cos\Delta\lambda_p}{\sin\psi_p} \tag{4.5}$$

where

r_p , α_p = The range and azimuth of point P with respect to the radar coordinate system.

ψ_p = An earth centered angle corresponding to a great circle arc drawn between P and O in their plane with the spherical earth centre.

ER = The Earth's radius.

It is important to mention that, by definition, the same results of this method would be obtained if an *azimuthal equidistant* planar projection tangential to the spherical earth at point O was used to project the spherical coordinates. Hence, the *conventional* method and the *azimuthal equidistant* planar projection are actually the same method.

4.5 The New GPP Method

In this study this method is the exact solution to the problem that represents the gravity path. The *Ellipsoid-based Gravitational Planar Projection* (or *GPP*) (Gad and Tsanis, 2001) is a new ellipsoidal based projection method that is developed in this study to be used as the reference method for evaluating the other sphere-based methods. This method projects rainfall data from their original height in a direction normal to the ellipsoid surface, as shown in Figure 4.8. This section and the following section describe the equations of the forward and inverse transformations, which are valid for any oblique aspect. These equations are not valid for the

equatorial and polar aspects. The cases of equatorial and polar aspects are relatively simple and can be easily determined following the principle of normality to the ellipsoid.

4.5.1 The Forward Transformation

To derive the forward transformation for the oblique case consider a plane tangential to the spheroid at the radar location $O\ (\lambda_o\ ,\ \Phi_o)$, and a plane parallel to the previous plane and separated by a distance d', as shown in Figures 4.9 & 4.10 (note also the definition of d' on Figure 4.5 and Figure 4.8). For a specific ellipsoid, let a represents the major axis and e the eccentricity. It can be proven from the ellipsoid geometry (refer to Ewing and Mitchell, 1970) that :

$$R_o = \frac{a'\cos\phi_o}{\sqrt{1 - e^2 \sin^2\phi_o}} \tag{4.6}$$

$$\phi_o' = \tan^{-1}\left[(1 - e^2)\tan\phi_o\right] \tag{4.7}$$

$$H_o = R_o \tan\phi_o' \tag{4.8}$$

$$h_N = \left(R_o + H_o \tan\phi_o + \frac{d'}{\cos\phi_o}\right) \times \frac{1}{\tan\phi_o} \tag{4.9}$$

Refer to the list of symbols in the beginning of the thesis and to Figures 4.9 & 4.10 for the definitions of the symbols. Consider an arbitrary point $P\ (\lambda_p\ ,\ \Phi_p)$,

representing a rain-gauge on the surface of the spheroid. The objective is to find the corresponding Cartesian coordinates (x_p , y_p) in the radar coordinate system represented in an origin at the radar location and a y-axis parallel to the local geographic north at the radar location. From the known ellipsoidal geometry, it can be proven also that:

$$\phi_p' = tan^{-1}[(1-e^2)tan\,\phi_p] \tag{4.10}$$

$$R_p = \frac{a'\cos\phi_p}{\sqrt{1-e^2\sin^2\phi_p}} \tag{4.11}$$

$$H_p = R_p \tan\phi_p' \tag{4.12}$$

Now, consider Figure 4.10 , from the triangle $n_p u_p Q_p$, the angle θ_p is expressed as following:

$$\Delta H_p = H_p \frac{e^2}{1-e^2} \tag{4.13}$$

$$\overline{Q_p P} = \frac{R_p}{\cos\phi_p} \tag{4.14}$$

$$\theta_p = tan^{-1}\frac{R_p \cos\Delta\lambda_p}{H_p + \Delta H_p} \tag{4.15}$$

Then, the distance y_p' can be obtained from the triangle $u_p' Q_p N$:

$$y'_p = \frac{\sin\theta_p}{\sin(\phi_o + \theta_p)}(h_N + \Delta H_p) \tag{4.16}$$

$$y_p = \frac{R_o}{\sin\phi_o} + \frac{d'_p}{\tan\phi_o} - y'_p \tag{4.17}$$

From the triangle $P'u'_pQ_p$, the following can be obtained:

$$\gamma_p = \sin^{-1}\frac{R_p \sin\Delta\lambda_p}{Q_p P} \tag{4.18}$$

$$x_p = (h_N + \Delta H_p) \times \frac{\sin\phi_o}{\sin(\phi_o + \theta_p)} \tan\gamma_p \tag{4.19}$$

It should be noted that equations from (4.6) to (4.9) have constant output for a specific radar location. The results of the rest of equations vary according to the location of the point being projected.

THE DISTANCE d'

It will be shown later that the parameter d' has insignificant effect on the solution. It can be assumed, for example constant =2000 meters. However, to reach to this conclusion and to see the effect of this parameter, a solution methodology employing variable d' has to be developed.

This solution methodology requires knowledge of the elevation angle corresponding to each range. This relationship is obtained from the scanning strategy of the radar (refer to Figure 4.6c) and can be obtained from the data provider.

Denoting this relationship as:

$$\beta = f(r) \tag{4.20}$$

the solution proceeds as following:

1. Solve all equations starting from (4.6) to (4.18) except (4.9) and (4.17).
2. Assume a starting value for d'_p, let us say 1000 meters.
3. Solve Equation (4.9). Find y_p from equation (4.17), and x_p from (4.19). Then calculate r_p:

$$r_p = \sqrt{x_p^{\,2} + y_p^{\,2}} \tag{4.21}$$

4. Find β from relation (4.20) then calculate d'_{p2} using:

$$d'_{p_2} = r_p \times tan\,\beta \tag{4.22}$$

5. If $| d'_p - d'_{p2} | <$ *heighterr*, then stop, else, take $d'_p = d'_{p2}$ and loop again starting from step 3. The value of *heighterr* in this study is taken as 50 meters.

4.5.2 The Inverse Transformation

The equations required for calculating the geodetic coordinates of points from their Cartesian coordinates (oblique aspect) will only be cited here. Their derivation is provided in Appendix I. Given the radar location O (λ_o, Φ_o) and the Cartesian

coordinates of an arbitrary point $P\ (x_p\ ,\ y_p)$, the corresponding longitude and latitude $(\lambda_p\ ,\ \Phi_p,)$ are calculated. The solution proceeds as following:

1- Obtain R_o , Φ'_o , H_o , and h_N using equations (4.6), (4.7), (4.8) and (4.9), respectively, and solve directly for λ_p using:

$$\lambda_p = \lambda_o + tan^{-1} \frac{x_p}{y'_p \sin \phi_o} \tag{4.23}$$

where

$$y'_p = \frac{R_o}{\sin \phi_o} + \frac{d'_p}{\tan \phi_o} - y_p \tag{4.24}$$

The parameter d'_p can be assumed constant (2000 meters for example) or can accurately be found by relation (4.20).

2- Calculate the following:

$$c_1 = a'^2 (1 - e^2) \tag{4.25}$$

$$c_2 = \frac{1}{1 - e^2} [(y'_p \sin \phi_o)^2 + x_p{}^2] \tag{4.26}$$

$$c_3 = h_N - y'_p \cos \phi_o \tag{4.27}$$

$$c_4 = \frac{e^2}{1 - e^2} \tag{4.28}$$

$$A = c_4^{\,2}, \qquad B = 2c_3c_4, \qquad D = c_2 + c^2{}_3 - c_1c^2{}_4$$
$$E = 2c_1c_3c_4, \qquad G = c_1c^2{}_3 \tag{4.29}$$

3- The solution of the following polynomial provides the corresponding "height" (H_p) from the equatorial plane:

$$AH_p^{\,4} + BH_p^{\,3} + DH_p^{\,2} - EH_p - G = 0 \tag{4.30}$$

4- Once H_p is obtained, the corresponding latitude can be found as following:

$$R_p = \left(\frac{c_1 - H_p^{\,2}}{1 - e^2}\right)^{1/2} \tag{4.31}$$

$$\phi_p = \tan^{-1}\frac{H_p}{R_p(1 - e^2)} \tag{4.32}$$

Equation (4.30) can easily be solved by using an iterative procedure such as Newton-Raphson Using Derivative (refer to Press et al., 1999). The solution converges to the correct root very rapidly by taking the starting point as H_o. More details can be found in Gad and Tsanis (2001).

4.6 The GPP vs Other Planar Projections

In order to evaluate the different sphere-based projection methods, a comparison between the developed *GPP* method (the exact solution) and the other

sphere-based planar projections is presented in this section. The methodology of comparison is done by selecting a set of control points under the coverage of a radar umbrella. The control points are projected into radar coordinates using a certain sphere-based method and then compared to the obtained coordinates using the GPP method. The sphere-based planar projections will be considered in two approaches:

Method 1: Taking the geodetic latitudes of the radar and the control points as they are, i.e, as if they were geocentric ones.

Method 2: Converting the geodetic coordinates of both the radar and the control mesh to geocentric ones before using the sphere-based projection methods.

The Radius of the reference sphere used in the analysis is ER = 6371200 m. The reference ellipsoid for the *GPP* is taken as the WGS1984, which has parameters a' = 6378137 m and e = 0.081819. Two test cases are selected for the comparison. The first is Cold Lake Radar, Alberta, Canada (λ_o = -109.9553°, Φ_o = 54.9133°), and the second is King City Radar, Ontario, Canada (λ_o = -79.5728°, Φ_o = 43.9635°). Figure 4.11 shows the control mesh used around each radar.

To explain the results, let us take one point (λ_p = -112.21°, Φ_p = 54.9133°) which is located in a range of approximately 144 km from Cold Lake Radar location. The x_p, and y_p coordinates, obtained using the different methods, are shown in Table 4.1.

Table 4.1 Coordinates of a Test Point in Cold Lake Radar Coordinate System

	Sphere-based Projections *Method 1*				Sphere-based Projections *Method 2*				The GPP	
	Gnom.	Stereo.	Conv.	Lam.	Gnom.	Stereo.	Conv.	Lamb.	H_{CAPPI} = 1000	H_{CAPPI}= var
$x(m)$	-143797	-143779	-143773	-143770	-144444	-144426	-144420	-144416	-144300	-144295
$y(m)$	2310	2310	2309	2309	2315	2315	2315	2315	2318	2318

Table 4.1 shows that the conventional method (in the manner of method 1) and the GPP method produce a difference in the x-coordinate of approximately 470 meters. This means that the consequences of using the conventional method or any other sphere-planar projection in the manner of method 1 (the commonly used procedure) may place a rain-gauge in the wrong radar rainfall cell. Such a positioning error may affect the radar calibration results. On the other hand, the difference is smaller using method 2, i.e. when converting the geodetic latitudes of both the radar and the rain-gauge to geocentric latitudes before projection. The reason for this difference can be explained by the fact that the distance between any two meridians increases from the poles to the equator. This mainly affects the calculated x. This means that points having the maximum east/west distance from the radar will suffer maximum location error if method 1 is used. Although using method 2 reduces the error significantly , however, there are still small differences that result from the difference between the curvature of the sphere and ellipsoid, the method of projection, and the small effect of d'. However, these small errors are acceptable. Note also the negligible difference between the GPP if d' is taken constant and the GPP in the exact solution (i.e, by

using variable d'). It should be noted that the error of using the sphere-based projections in the manner of method 1 is expected to increase with the latitude of the radar, i.e., the further north the radar is located the greater will be the error values.

For a complete summary of the results of the analysis, refer to Figures 4.12 to 4.19. These figures show the contours of the absolute error for the different methods in the two test cases considered (Figures 4.12 to 4.15 correspond to the Cold Lake test case, and Figures 4.16 to 4.19 correspond to the King City test case). The absolute error is defined as the distance in the tangent plane between the projection of a point using a certain method and its projection using a reference method (the *GPP*). For example, the absolute error in locating the above point using the conventional projection in the manner of method-1 (taking the GPP using variable d' as the reference method) is:

$$Absolute\ Error = \sqrt{(x_{(i)conv1} - x_{(i)GPP})^2 + (y_{(i)conv1} - y_{(i)GPP})^2} \qquad (4.33)$$

$$= \sqrt{[-143773 - (-144295)]^2 + [2309 - 2318]^2} = 522\ meters$$

Figures 4.20 and 4.21 present the absolute error of the GPP method if the parameter d' is considered constant.

4.7 Case of Multiple Radars

Radar data from multiple radars are usually stored in a common coordinate system. They are then merged with data from other sensors (satellite and rain-gauge data) for different applications (FMH, 1991), such as severe weather warnings, mesoscale weather forecasting and storm tracking, river flow forecasting, and future offline hydrological and meteorological analysis. In these cases, the inverse transformation is essential in order to project the radar rainfall products from their original tangent planes onto a common coordinate system. There are two procedures that can be used to resample data from multiple radars into a common coordinate system:

Procedure 1:

- The radar grid is represented by an array of points in which each point is located at the centre of a rainfall cell.
- The points array is projected back into geographical coordinates and then projected forward into the common coordinate system.
- A new fixed resolution grid is resampled from these points in the common coordinate system using a simple average, or bilinear method.

Procedure 2:

- The radar grid is represented by an array of square polygons. Each polygon represents a rainfall cell.

- The array of polygons is projected back to geographic coordinates then projected forward into the common coordinate system.
- A new fixed resolution grid is produced using a weighted averaging method, in which the weights are determined by the percentage of areas of the projected polygons within each new cell of the common coordinate system grid.

Procedure 2 seems to be more accurate in terms of keeping the same orientation and distortion of a rainfall cell with respect to other geographical features. One could ask which application requires this level of precision. The resolution (i.e., the pixel size) of a multiple radar product is greater than the resolution obtained from a single radar product, which means that an averaging method will have to be used when either procedure is employed in order to obtain the pixel values in the multiple radar product. Thus, procedure 1 is more attractive, since it requires considerably fewer computations.

However, a question remains on how to select the common coordinate system. Such selection is influenced by the purpose for which the data are to be used, since no projection can retain all (that is conformal, equidistant, or equal area) properties. Hence, an optimum common Cartesian coordinate system, which is suitable for all applications, can not theoretically exist. Hence, compromises have to be made. These compromises should reflect the main application in which the data will be used.

Hydrological Analysis:

For this purpose, rainfall data from multiple radars are merged with rain-gauge data and Geostationary Operational Environmental Satellite (GOES) data by using optimal methods to improve the quality of such product (OFCM, 1991; Krajewski, 1987; Seo et al., 1990[1&2] ; and others). In this case, the most important characteristic in the common projection system is the datum, which must be the same as the datum of the topographical maps, from which hydrological parameters are obtained for lumped and distributed modelling. Unfortunately, this is not the case in the HRAP (grid of the Hydrologic Rainfall Analysis Project) of the NWS in the US, which is constructed in a sphere-based secant polar plane to reference Stage-II and Stage-III of NEXRAD data (Hoke et al., 1981). On the other hand, most topographical maps are defined in ellipsoid-based projections. Accordingly, two problems occur during the overlaying process. The first is a location problem, which is mainly caused by the differences between the geocentric and geodetic coordinates. The second problem is caused by area and shape distortions with latitude (Reed and Maidment, 1995). An ellipsoid-based Equal-Area with minimum scale error projection is the optimum as a common projection for radar data for regional hydrological analysis. This is because topographical maps will be projected into the common projection system, and the hydrological analysis will be performed using the same projection, preserving land surface area that is an important characteristic for this type of application.

Storm tracking :

This application can be divided into two categories. The first is the nowcasting urban application, in which time plays the most important role. Such an application produces a forecast that has a lead time of one hour or less. Hence, it is more appropriate to perform such an analysis in the same coordinate system of each radar, since the area of interest is usually under the coverage of one radar. The second category is for mesoscale storm tracking, which requires data from multiple radars. For this purpose, the motion of the target being tracked is the crucial aspect. The Mercator projection preserves a very valuable property is that it ensures all rhumb lines (lines of constant azimuth) appear as straight lines, thus removing additional non-linearities from the equations of the target motion. This eliminates some fictitious directions and their corresponding biases in forecasting locations of the storm centroid. For areas in the northern and southern latitudes, a Polar Stereographic projection can be substituted for the Mercator projection.

4.8 A Common Coordinate System for the Great Lakes Area

Environment Canada operates a network of weather radars under the National Radar Project. The network currently consists of 25 radars distributed across the provinces of Canada (as shown in Figure 4.22 and Table 4.2). The objective of this section is to recommend a common coordinate system for the Canadian radars in the area covering the Great Lakes in Ontario. The selected coordinate system is required for performing storm tracking operations, severe weather forecasting, quantitative

rainfall forecasting using data from multiple radars and satellite images. Hence, one of the important properties required in the common coordinate system is to facilitate the overlaying process of multiple radar data with GOES-8 data in the Great Lakes satellite sector.

Table 4.2 The Canadian National Radar Network

Name	*ID*	*Long.*	*Lat.*
Victoria	XSI	-123.756	48.86028
Aldergrove	WUJ	-122.488	49.01606
Spirit River	WWW	-119.234	55.6925
Carvel	WHK	-114.145	53.5605
Strathmore	XSM	-113.398	51.20639
Jimmy Lake/Cold Lake	WHN	-109.955	54.91333
Radisson	XRA	-107.444	52.52056
Bethune	XBE	-105.183	50.57111
Broadview	WIK	-102.683	50.38333
Woodlands	XWL	-97.7783	50.15389
Upsala	WIM	-90.4167	49.03333
Montreal River	WGJ	-84.5958	47.24778
Exeter	WSO	-81.3842	43.37027
Britt	WBI	-80.5328	45.79278
King City	WKR	-79.5742	43.96389
Landrienne	XLA	-77.8081	48.55139
Franktown	XFT	-76.1136	45.04083
McGill	WMN	-73.9361	45.425
Villeroy	WVY	-71.9153	46.45
Lac Castor	WMB	-70.6667	48.58333
Val d'Irene	XAM	-67.6011	48.48028
Mechanic Settlement	WMK	-65.1667	45.7
Gore (Halifax)	XGO	-63.7033	45.09889
Marble Mountain	XME	-57.8342	48.93028
Holyrood	WTP	-53.1786	47.32555

The Meteorological Service of Canada distributes NASA weather satellite images through an agreement with the National Oceanographic and Atmospheric Administration (NOAA) in the United States. These images are generated by geostationary satellites orbiting approximately 35,400 kilometres above the equator. The images include visible, infrared and water vapour channels. Each channel is obtained in three sectors: (1) East North America, (2) Big North America, and (3) the Great Lakes (a regional view remapped to a Polar Stereographic projection).

The Great Lakes sector covers the area of the Great lakes and contains 8 Canadian radars (as shown in Figure 4.23). Fortunately, the satellite channels covering the Great Lakes sector, which are distributed by the Meteorological Service of Canada, are mapped in a Polar Stereographic Projection. This system is selected as a common coordinate system for both satellite data and radar data in order to save the resources of remapping the satellite images into another projection. In addition, the Polar Stereographic projection is the most suitable for the required applications in the northern hemisphere. Finally, in order to check the parameters required to geo-reference the satellite images in the common projection, a set of graticules (a grid of lines of equal latitudes and lines of equal longitudes) was used on both the satellite image and the common coordinate system. A matching procedure was then used to determine the referencing parameters. The results of the matching operation are shown in Table 4.3. The obtained bounding box of the Great Lakes sector is shown in Figure 4.23. It should be noted that satellite images have to undergo image processing operations before being used with radar data. The image processing

operations are described in Chapter 5.

Table 4.3 Parameters of the Great Lakes GOES-8 Images

Parameter	Value
Projection	Polar Stereographic (83 W)
False Easting	0
False Northing	0
Xscale	1606.71 (m)
Negative-Yscale	-1606.71 (m)
Rotation Term-1	0
Rotation Term-2	0
X-coordinate of Upper Left Pixel	-820729.547
Y-coordinate of Upper Left Pixel	-4455922.823

4.9 Summary

- A spheroid-based projection method (*GPP*) is developed in this study for the purpose of evaluating different sphere-based projection methods in terms of the accuracy of locating rain-gauges with respect to radar rainfall data. The different sphere-based planar projections give approximately similar results to the *GPP* if the geodetic coordinates are converted to geocentric ones before projection into the radar coordinate system. If the geodetic coordinates are not converted to geocentric ones before using any sphere-based planar projection, an error in locating the rain-gauge can be introduced. This

error is sufficient such that rain-gauges would potentially not be located in their corresponding radar pixels. This, in turn, may affect any results of high resolution radar-gauge comparison.

- An optimum common coordinate system that is suitable for all applications of radar data can not be found theoretically. However, for nowcasting applications, it is suggested that this analysis be performed in the radar plane. A spheroid-based equal-area projection is suggested for hydrologic modelling and Mercator and Polar Stereographic projections are suggested for mesoscale storm tracking.

- A Polar Stereographic projection (83 W) is suggested as a common coordinate system to geo-reference radar data and GOES-8 satellite data for tracking and forecasting purposes in the Great Lakes area. The parameters of the raster to real-world conversion of the satellite images are determined in Table 4.3.

- The projection method developed in this study is ellipsoid based and recommended for referencing data from multiple radars into any ellipsoid based common coordinate system.

- The projection method developed in this study is coded for use within

a GIS interface for the analysis of radar derived rainfall characteristics. This GIS interface is the focus of Chapter 5. The results of the overlaying process of data from multiple radars with GOES-8 satellite images and the selected coordinate system are also used within this GIS interface.

- The projection method described in this chapter is used in the following chapters for geo-referencing rain-gauge locations with respect to the radar rainfall data. This spatial accuracy is required when working with high resolution radar data, and this is the focus of Chapter-6. In addition, the selected common coordinate system is used in Chapter 6 as a common coordinate system for data from two Canadian radars.

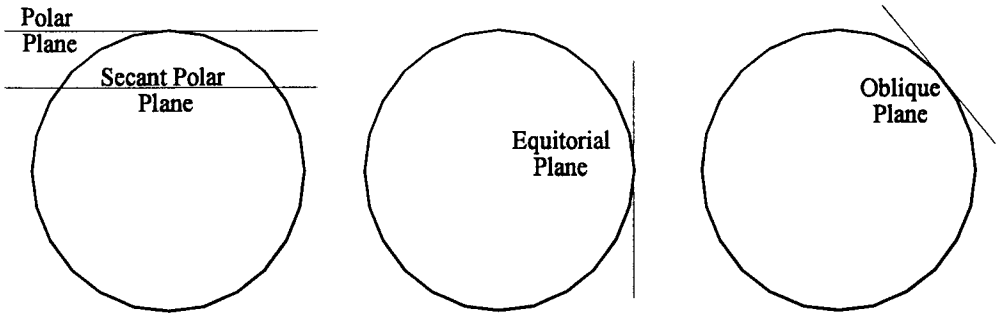

Figure 4.1 The three aspects of the zenithal projection.

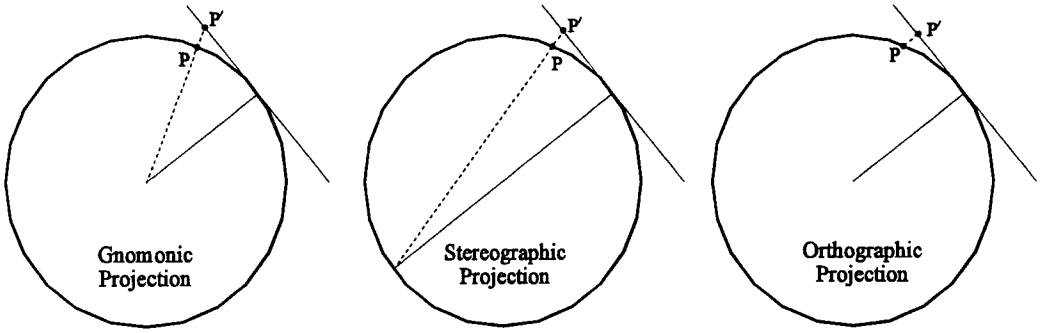

Figure 4.2 Three known sphere-based perspective planar projections.

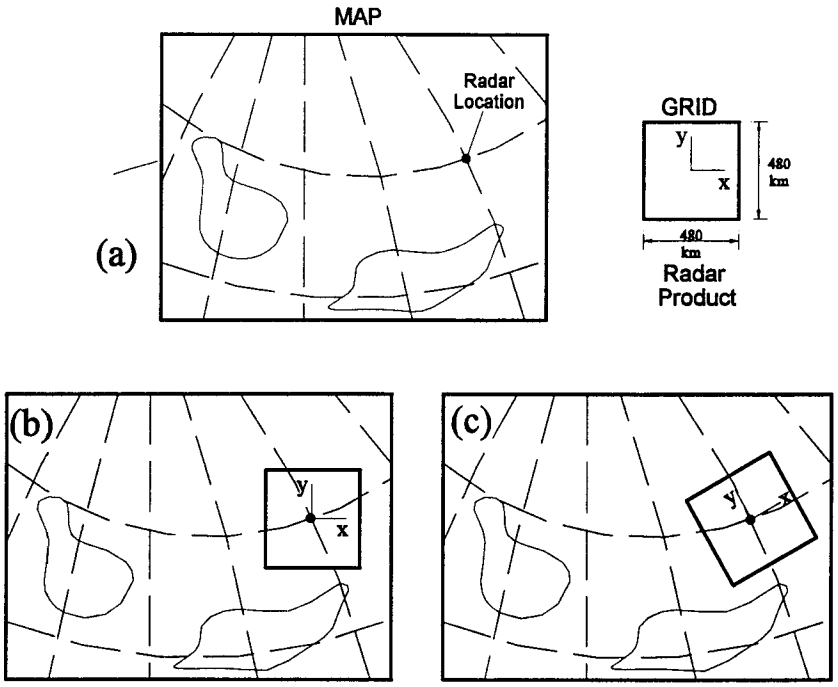

Figure 4.3 Schematic diagram representing the overlaying process of the radar rainfall grid on a map.

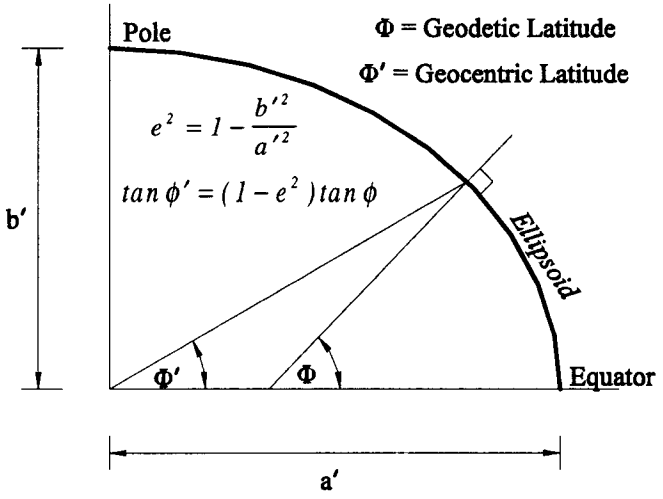

Figure 4.4 Difference and conversion between geodetic and geocentric latitudes.

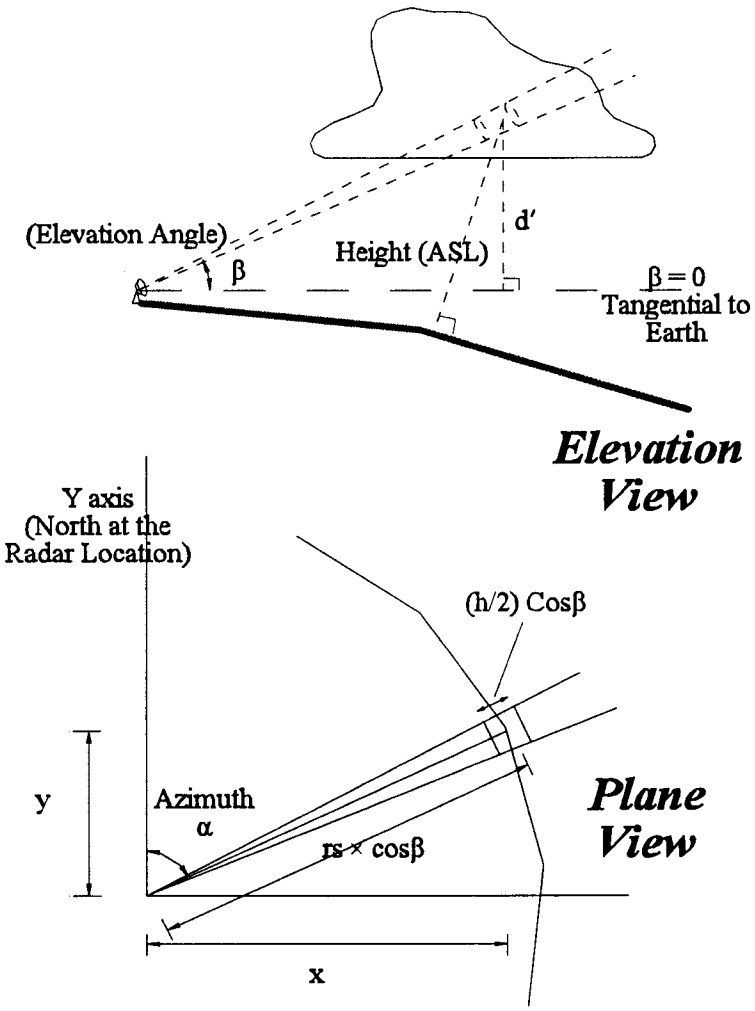

Figure 4.5 Radar detection of meteorological targets and the mapping process from the beam height to the tangent plane.

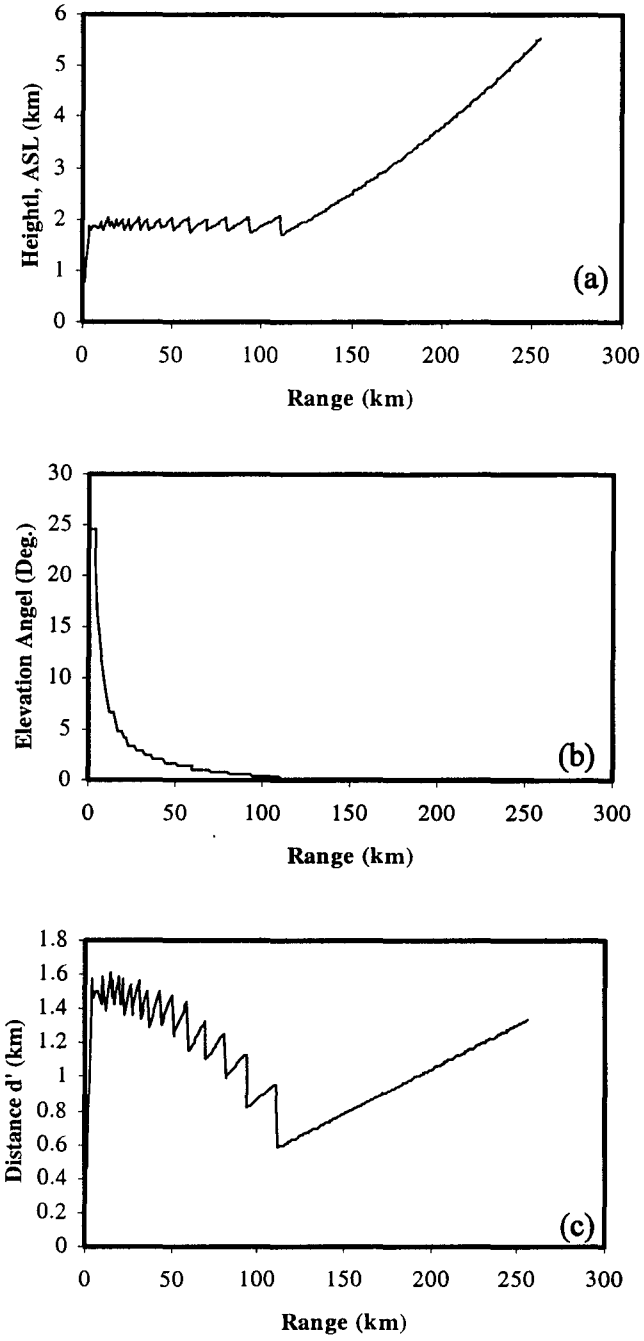

Figure 4.6 CAPPI scanning strategy at King City radar, Ontario, Canada: (a) height versus range ; (b) elevation angle used for each range; and (c) distance d' versus range (refer to Figure 3.5 for the definition of d').

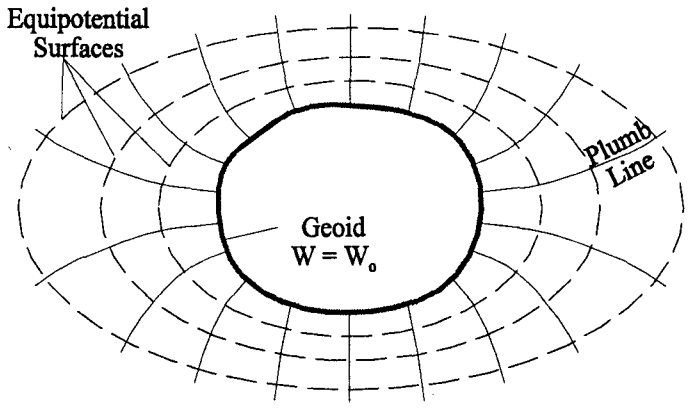

Figure 4.7 The geoid as a gravity equipotential surface.

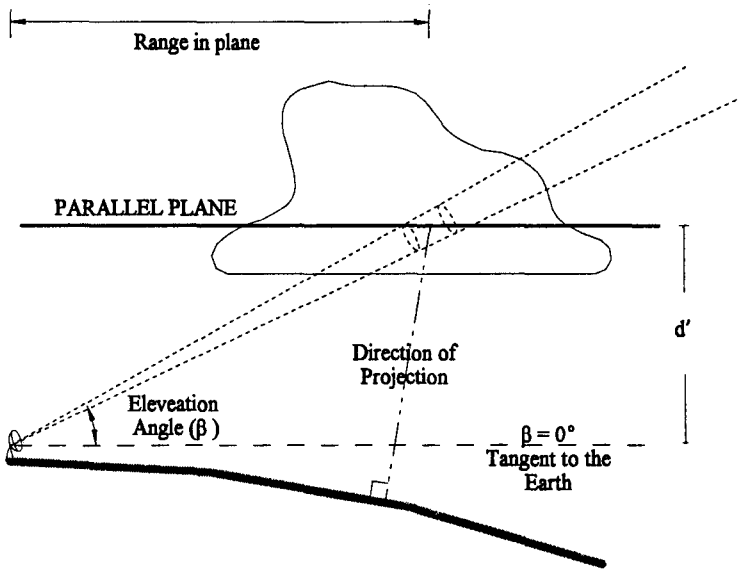

Figure 4.8 The direction of the GPP projection.

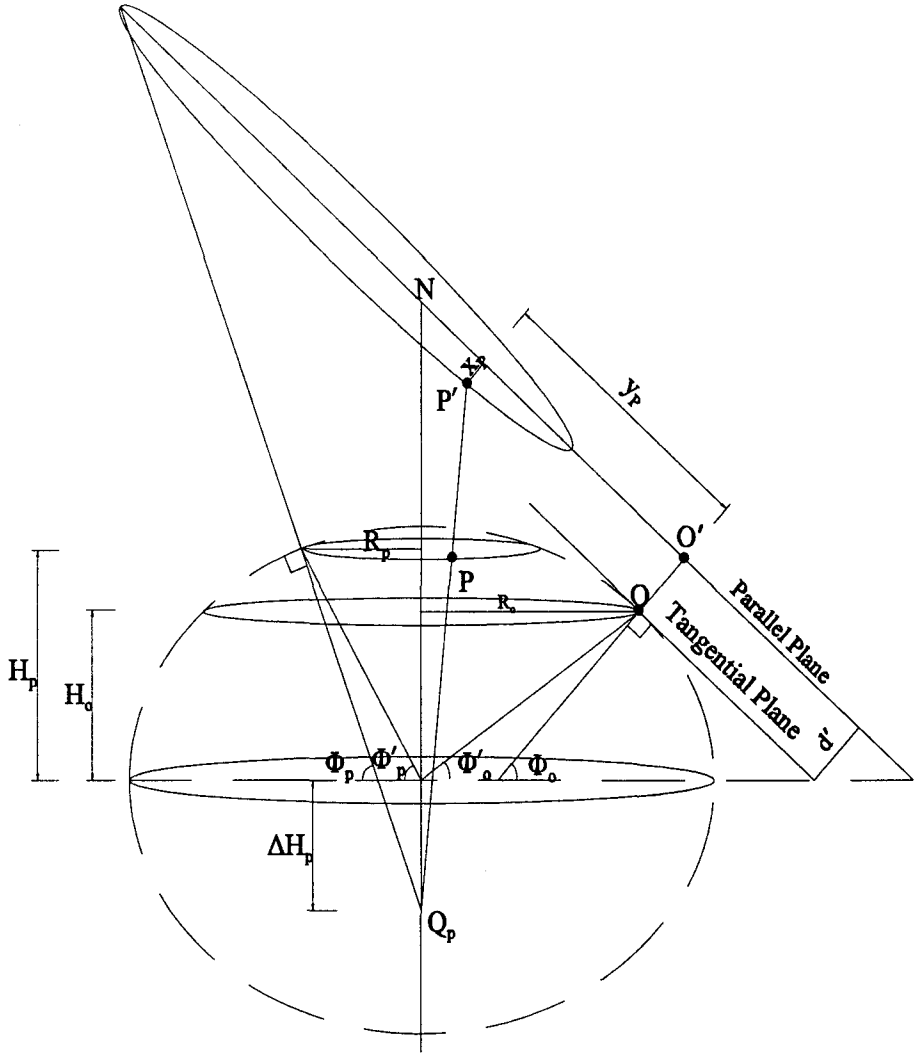

Figure 4.9 Derivation of the GPP (definition of basic symbols). Note that point *O* represents the radar and point *P* is the point to be projected.

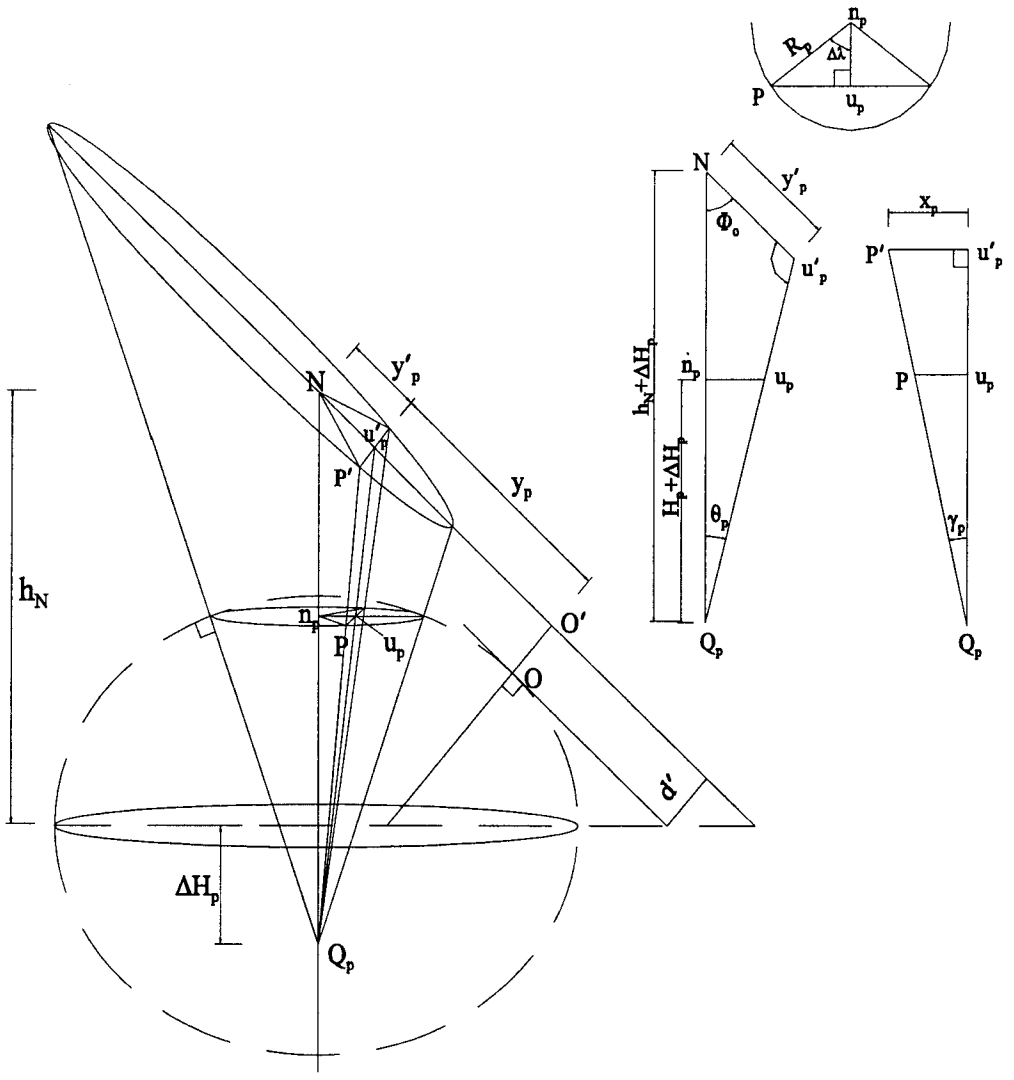

Figure 4.10 Derivation of the GPP (definition of the remaining symbols and construction of the projection).

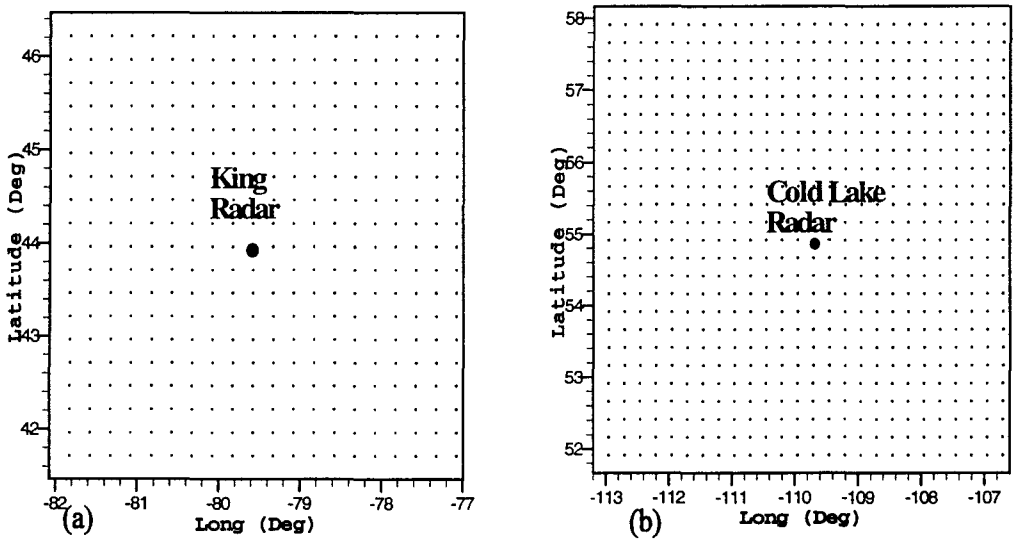

Figure 4.11 The control mesh used in the comparison: (a) mesh around Cold Lake radar site; (b) mesh around King City radar site.

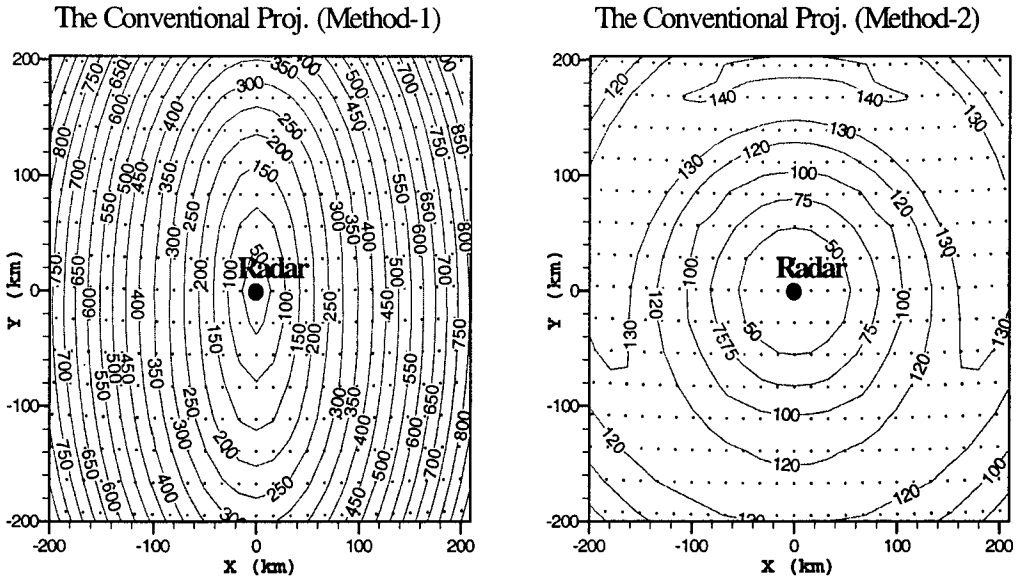

Figure 4.12 Cold Lake test case. The figures present the contours of the absolute error in meters. The left panel shows the error using the conventional projection in the manner of method 1 (no conversion from geodetic to geocentric). The right panel shows the error in the manner of method2 (by converting from geodetic to geocentric before projection).

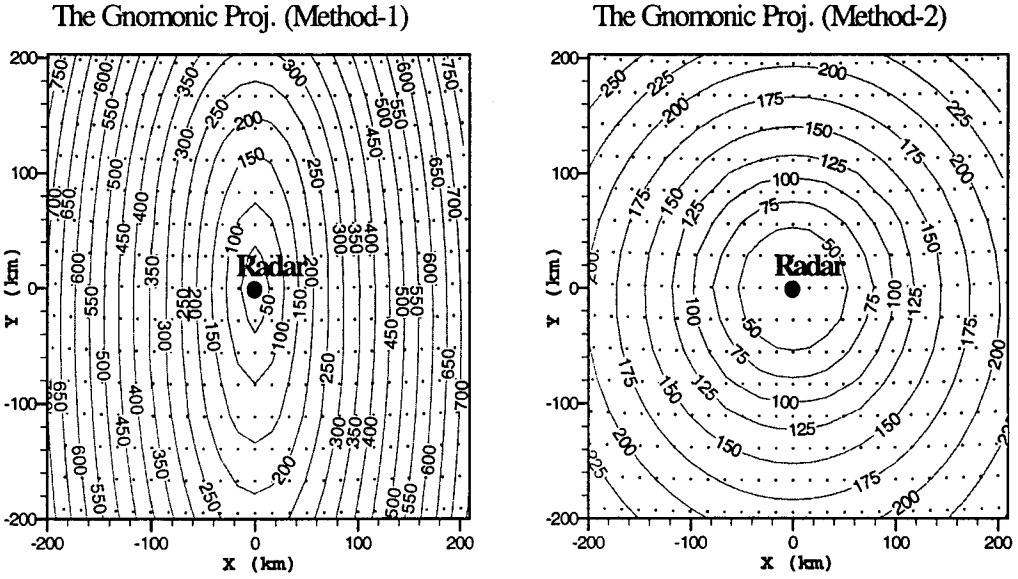

Figure 4.13 Cold Lake test case. The figures present the contours of the absolute error in meters. The left panel shows the error using the Gnomonic projection in the manner of method 1 (no conversion from geodetic to geocentric). The right panel shows the error in the manner of method2 (by converting from geodetic to geocentric before projection).

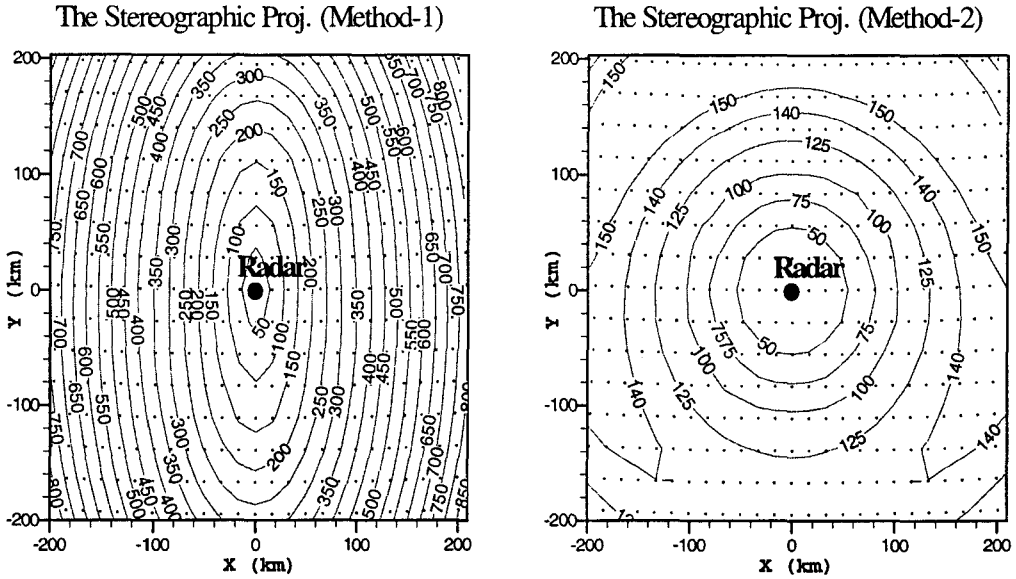

Figure 4.14 Cold Lake test case. The figures present the contours of the absolute error in meters . The left panel shows the error using the Stereographic projection in the manner of method 1 (no conversion from geodetic to geocentric). The right panel shows the error in the manner of method2 (by converting from geodetic to geocentric before projection).

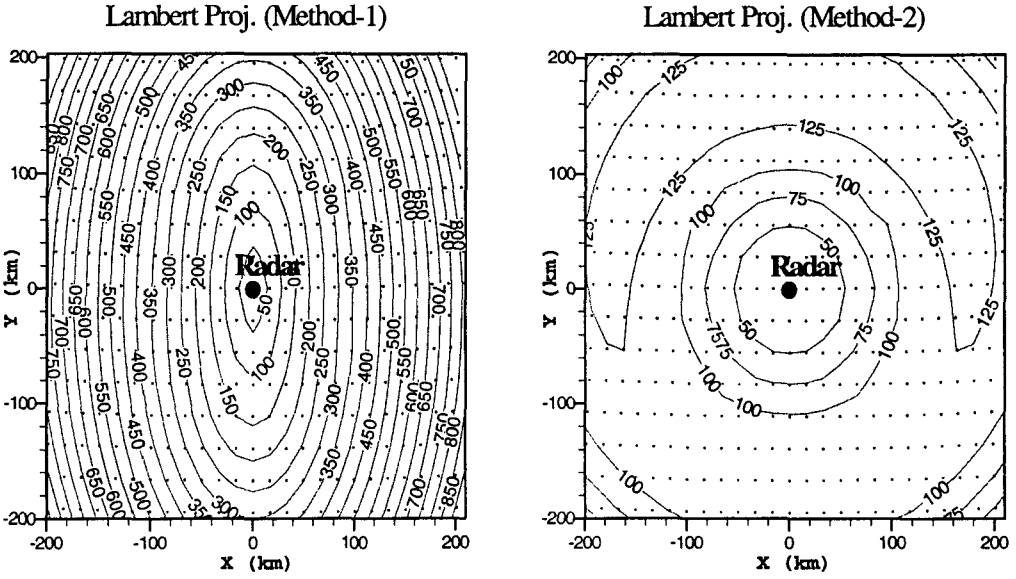

Figure 4.15 Cold Lake test case. The figures present the contours of the absolute error in meters . The left panel shows the error using Lambert projection in the manner of method 1 (no conversion from geodetic to geocentric). The right panel shows the error in the manner of method2 (by converting from geodetic to geocentric before projection).

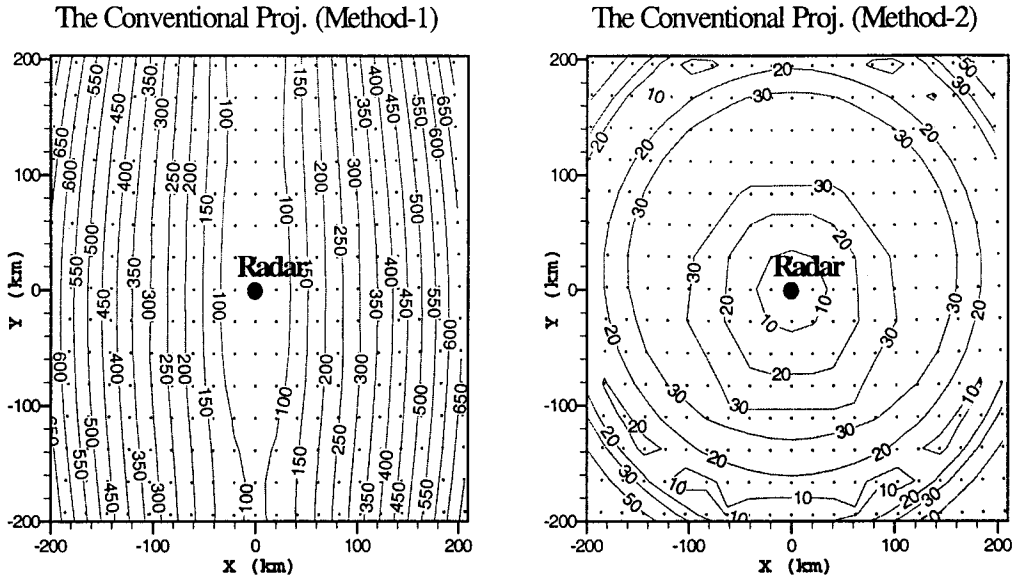

Figure 4.16 King City test case. The figures present the contours of the absolute error in meters. The left panel shows the error using the conventional projection in the manner of method 1 (no conversion from geodetic to geocentric). The right panel shows the error in the manner of method 2 (by converting from geodetic to geocentric before projection).

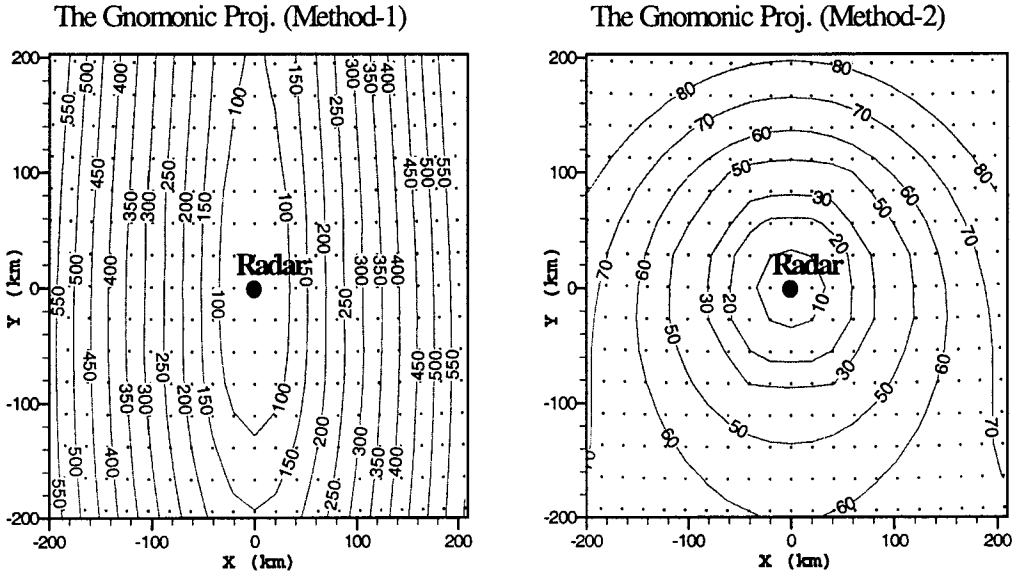

Figure 4.17 King City test case. The figures present the contours of the absolute error in meters . The left panel shows the error using the Gnomonic projection in the manner of method 1 (no conversion from geodetic to geocentric). The right panel shows the error in the manner of method 2 (by converting from geodetic to geocentric before projection).

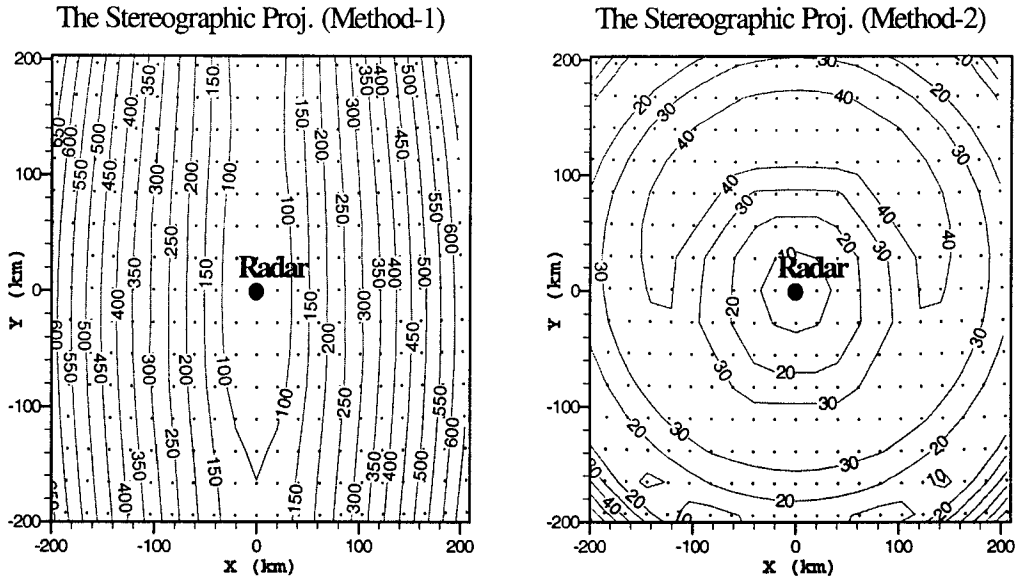

Figure 4.18 King City test case. The figures present the contours of the absolute error in meters. The left panel shows the error using the Stereographic projection in the manner of method 1 (no conversion from geodetic to geocentric). The right panel shows the error in the manner of method 2 (by converting from geodetic to geocentric before projection).

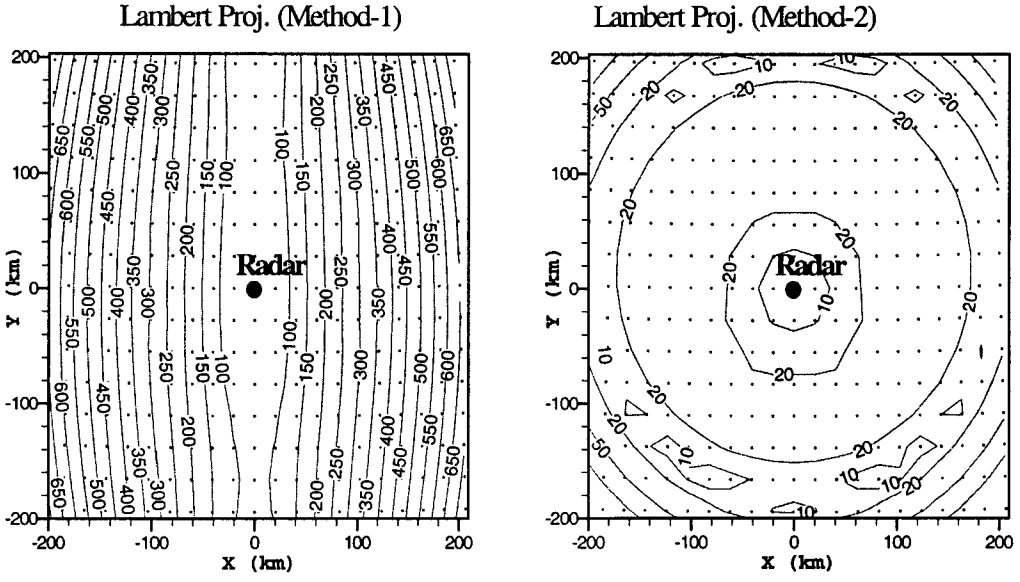

Figure 4.19 King City test case. The figures present the contours of the absolute error in meters. The left panel shows the error using Lambert projection in the manner of method 1 (no conversion from geodetic to geocentric). The right panel shows the error in the manner of method 2 (by converting from geodetic to geocentric before projection).

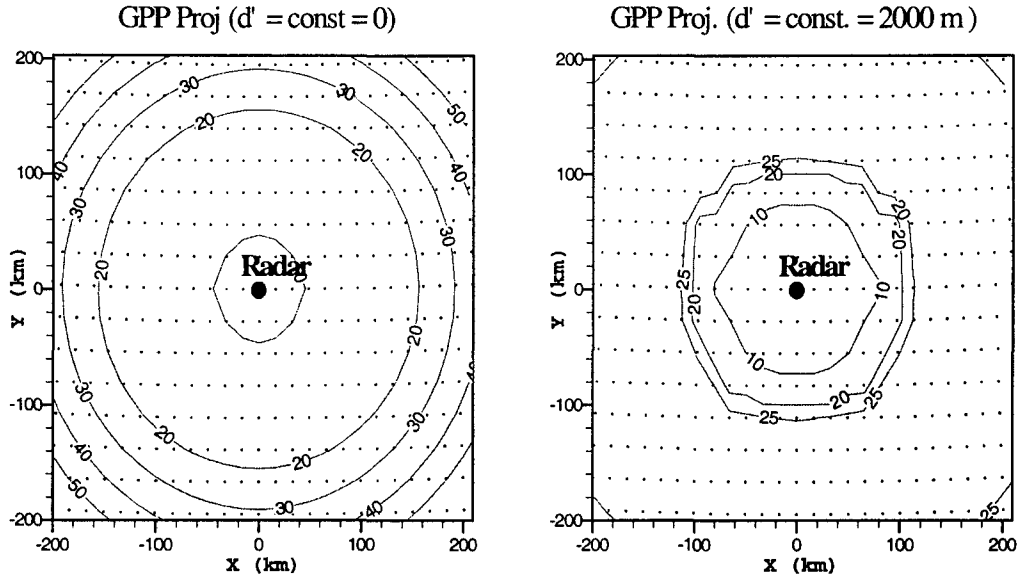

Figure 4.20 Cold Lake test case. The left panel shows the absolute error using constant $d' = 0$ when applying the GPP . Right panel shows the absolute error using constant $d' = 2000$ meters. As shown, the error is negligible.

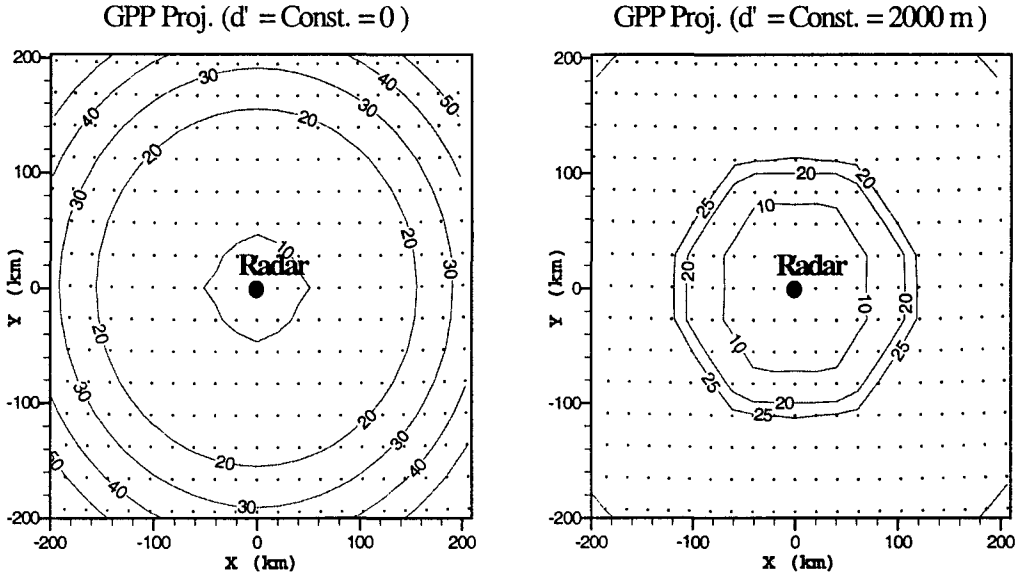

Figure 4.21 King City test case. The left panel shows the absolute error using constant $d' = 0$ when applying the GPP . Right panel shows the absolute error using constant $d' = 2000$ meters. As shown, the error is negligible.

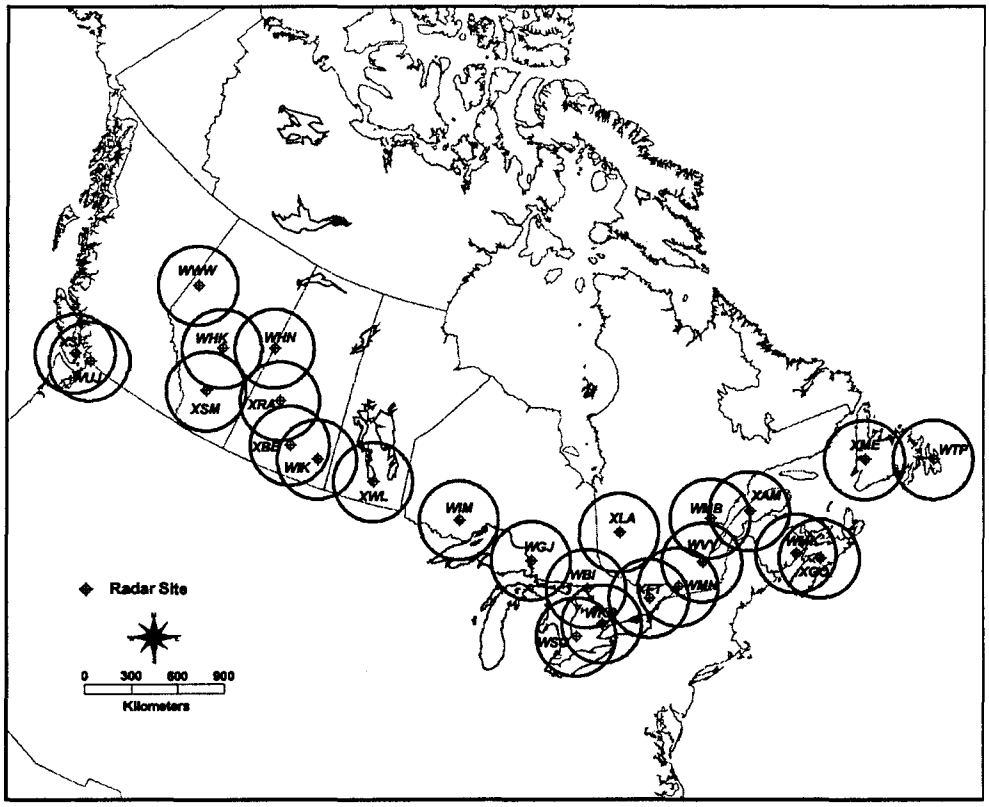

Figure 4.22 The Canadian National Radar Network.

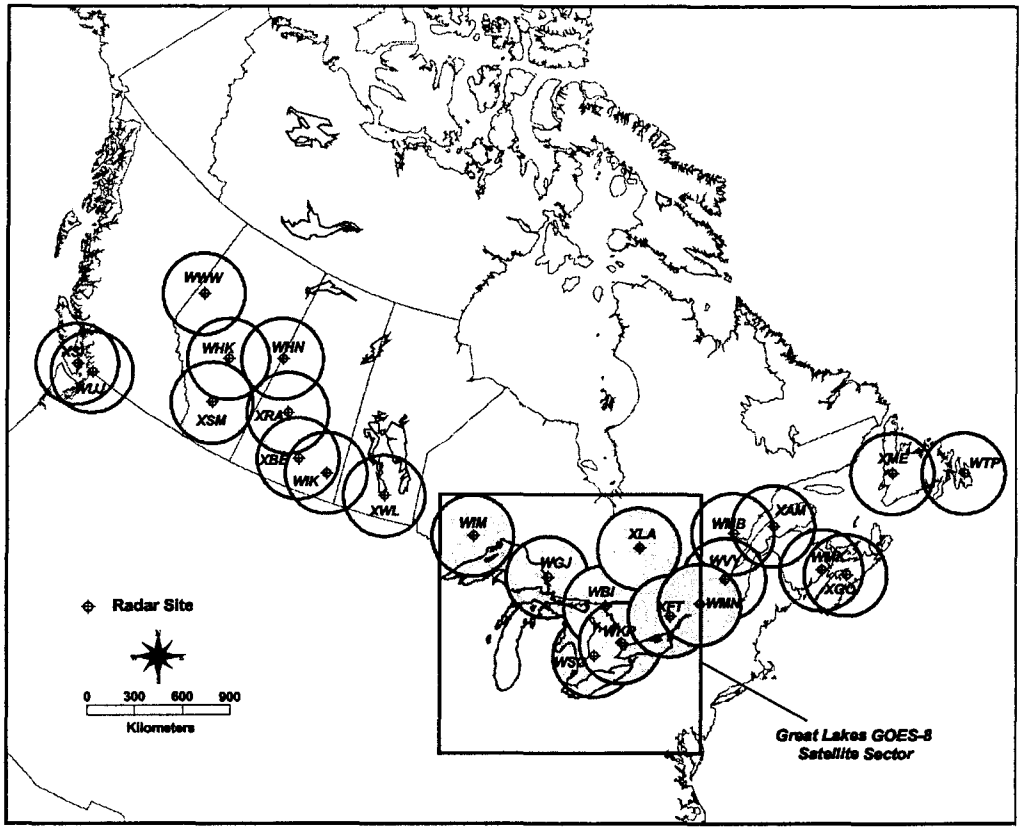

Figure 4.23 The Great Lakes GOES-8 satellite sector with respect to the National Radar Network. The common coordinate system is a Polar Stereographic projection (83 W central meridian).

CHAPTER 5

DEVELOPING GEOGRAPHICAL INFORMATION SYSTEM FOR ANALYSIS OF RADAR RAINFALL DATA

5.1 Introduction

Radar rainfall data are difficult to process and analyse. For example, one radar scan consists of a binary array of 480×480 values. Ordinary spreadsheets can not deal with this amount of data. In addition, the acquisition of a radar scan every 10 minutes makes the total number of scans tremendous. Managing and analyzing weather precipitation data require extensive computer resources. Only a few platforms, therefore, are available for this purpose. One example of these platforms is the Unidata McIDAS-X software developed at the Space Science and Engineering Centre (SSEC) at the University of Wisconsin-Madison. The Canadian radar groups use separate C-routines for the purpose of viewing and analyzing radar data that are problematic in terms of portability and complexity. In this chapter, a GIS multi-component interface (RAINPLAT-GIS) is developed within the ArcView-GIS environment for processing and analyzing weather radar precipitation data. In

addition to radar data, the interface implements components to handle satellite and rain-gauge data. It should be noted that this interface is used throughout the thesis to achieve the different objectives. The results of the different chapters are implemented in this interface. The projection methodologies developed in Chapter 4 and the tracking and forecasting techniques developed in Chapter 7, for example, are coded into this interface. The interface is able to (a) read, process, and geo-reference data from radars, satellite, and rain-gauges; (b) compare radar data with rain-gauge data for the purpose of radar calibration; (c) estimate the kinematics of rainfall patterns; (d) accumulate radar derived rainfall depths; and (e) forecast rainfall patterns over the short-term (less than two hours lead time). By using the spatial capabilities of GIS this interface can accurately locate rainfall on the ground and can overlay the animated storm motion on different geographical features, making the exploration of rainfall characteristics obtained from radar data easier to perform.

In the following sections the advantages of using Geographical Information System as a platform for rainfall data from multi-sensors are discussed, the format of the CAPPI data (Constant Altitude Plane Position Indicator) is described, and the description of the theories and technical details of the different components of the RAINPLAT-GIS interface are explained. Test cases are used to illustrate the functionality of the interface are satellite data using GOES-8 geostationary satellite, radar data from King City (WKR) radar, and radar data from Exeter (WSO) radar (see Figure 5.1). The coordinates of the two radars and the bounding box of the satellite Great Lakes sector are shown on Figure 4.23, Table 4.2, and Table 4.3 in the

previous chapter. Additional details on this interface can be found in Gad and Tsanis, 2002[1].

5.2 The Choice of Geographical Information System

The use of Geographical Information Systems (GIS) was originally limited to applications in the field of geography such as the setup of multi-dimensional information, analysis, utility, and display. Nowadays, it has reached far beyond the limited concept of graphics and provides support for many applications. For example, GIS can provide powerful tools for storing, managing, analyzing, displaying, and modelling different spatiotemporal environmental processes.

Arc-View GIS is a PC-based software that offers a user-friendly interface and powerful functions for spatial operations. One of its extensions, the spatial analyst extension, implements a large number of member functions (analysis requests) within the Grid class. These member functions provide different operations for the analysis of raster data. Examples of these are the local statistical operations, focal and zonal statistical operations, geometric and distance operations, and other global merging and mosaic operations. In addition to these built-in capabilities, ArcView GIS maintains a powerful feature - the ability to establish conversations with externally and dynamically linked libraries (DLLs). The main advantage of such DLLs is that they can extend the functionality of an application without recompiling the original executable because the external modules in this case are dynamically linked to the application at run time. ArcView provides classes and requests that support loading

and calling of procedures in these types of libraries. The advantages described above makes ArcView GIS one of the favorite platforms for studying different point, areal, and especially continuous processes. Rainfall patterns are examples of the continuous processes that can be analyzed in a GIS environment. Rainfall fields contain a complicated mixture of cloud structures that develop, dissipate, and come close to each other or go apart and, doing so, move across the catchment (Austin and Houze, 1972; Amorocho and Wu, 1977; Gupta and Waymyre, 1979; and others). Radar scans can provide different information concerning rainfall characteristics (Huff et al, 1981; Collier, 1989; and others).

The contribution of weather radar to the description of the behavior of precipitation, a major part of the hydrological cycle, has been of considerable interest over many years. Radar data are important to the fields of meteorology and hydrology in measuring and forecasting precipitation, as well as their corresponding uses in watershed modelling and flood forecasting. For those research scientists and engineers who have the opportunity to use radar rainfall data, the difficulties of managing and processing the large amount of radar data are problematic. A further problem relates to the understanding of aspects of the rainfall process as revealed by radar scans. Hence, the aim of this chapter is to provide a flexible and suitable platform for handling radar rainfall data. This platform is the Arc-View GIS.

5.3 Format of the CAPPI Product

After the full 360 degree scan of the radar, a CAPPI product is produced. The time separation between full scans, i.e., between files, is usually 10 minutes, which constitutes the temporal resolution. The corresponding date and time of the data are normally included in the filenames. Note that the date and time are in UTC system. There are two approaches that can be used for importing radar rainfall grided data into GIS: (1) the coverage (vector) approach, and (2) the grid (raster) approach. In the coverage approach the radar product is treated as point coverage, in which each point is located at the centre of a rainfall cell. In the grid approach, the radar product is considered as raster data, i.e., a matrix of rows and columns. The chief advantage of treating radar data as raster data is that, unlike the vector approach, the grid approach requires considerably less computer resources in terms of storage, processing time, and computer memory. The reason for this difference is that in the vector approach, a rainfall cell is represented by three variables (x, y, and rainfall value), whereas in the raster approach a rainfall cell is represented by only one variable (rainfall value). Only one variable is used because the location of one rainfall cell from the whole grid is only required to reference the raster grid. This unique location is usually the lower left corner of the grid. In addition, the GIS vector data require additional computer resources to handle their attributes. Given the above reasons, the raster data approach is used by this interface to manipulate radar data files.

The radar raw data file is structured and formatted so that the file contains a header part followed by a binary stream of one byte unsigned character values representing the records of the grid cells. Accordingly, the values range from 0 to 255, commonly referred to as the Iris N values, are the reflectivity in ½ DBZ (radar reflectivity in decibels, i.e., on a logarithmic scale), offset to -32 DBZ. Such N values can be converted to reflectivity, rain rate, or snow rate using a conversion table or using the corresponding equations. However, in some radar systems, the character values might represent the reflectivity values directly i.e., 1 DBZ data resolution. Hence, one must refer to the data specifications for the variable represented by the one byte character value. The header part is an ASCII (American Standard Code For Information Interchange) text containing some information such as the radar name and location, date and time, and other information. Figure 5.2 shows a typical header for a CAPPI data file. The valid time of the data file is written after a specific time string in the header, and the binary data section starts after another specific data string at the end of the header part. In our case, as shown in Figure 5.2, the time string is "At Valid Time:" and the data string is "#DATA".

Two problems exist in the structure and format of the data that can prevent ArcView GIS from loading the data properly. The first problem is that the data are in the form of binary character values, a format that is not supported by GIS as external grid data sets. GIS supports two formats for importing external grid data sets that are either space delimited ASCII values or IEEE (Institute of Electrical and Electronics Engineers) floating point binary values. The second problem is that the

data file obtained from some radar systems may have been processed in an order incompatible with GIS. To explain the second problem, let us represent the radar image in 480 rows (each row consists of 480 cells). The problem is that the row at the bottom of the actual image is written at the beginning of the binary file in a standard right hand coordinate system. If the data are to be loaded into GIS as a grid data set, GIS assumes the first value in the file to be the upper left corner of the grid and proceeds to the bottom of the grid, i.e., GIS assumes that the first row written in the data file to represent the top row in the grid data. Accordingly, if the data file is loaded in the original order into GIS then the result will be a reversed grid, which is different than the actual radar image.

5.4 Loading and Geo-referencing Radar Data

5.4.1 Loading the Data

A dynamic link library (*cappiload.dll*) and a calling script perform this task. The dynamic link library overcomes the two problems mentioned in section 5.3. It has two procedures for loading radar data. The first procedure handles binary data, and the second handles ASCII data. The binary data procedure:

1- Reads the valid time from the header of the data file.

2- Scans the data file from the beginning to the string "#DATA" and forwards the file pointer to the beginning of the binary data section.

3- Reads the N binary character stream from the data file and converts the

format into N IEEE binary floating points values.

4- Converts the N IEEE values into reflectivity, rain-rate, snow-rate, or keeps the N values according to the user selection and input parameters.

5- Arranges the sequence of the data, if necessary, and writes the output in a temporary binary IEEE floating point file.

6- Returns the valid time and an error checking handler.

A calling script is required to call this DLL and add the DLL's output as grids to ArcView. This calling script:

1- Asks the user to select the radar data files using a dialog.

2- Loads the dynamic link library *cappiload.dll* and defines the signatures of its internal procedures.

3- For each file of the user selected files, the script:

   (a) Calls the loading procedure and passes the path of the raw data file to it.

   (b) Loads the output of the loading procedure as a grid data set.

   (c) Loads the grid data set as a grid theme in the user specified view, and renames it using the corresponding date and time.

4- Drops the DLL.

The ASCII data procedure is similar to the binary procedure except that it accounts

for reading different delimiters. The procedure used is determined from the data format and specifications. Figure 5.3 shows a screen shot of the interface prompting the user to select data files for loading. Figure 5.4 is a screen shot of ArcView taken after the data has been loaded. The source code of the dynamic link library and the calling script is provided in Appendix II. In addition, the process of loading radar data within the interface developed in this study is described in a simple user manual of the interface in Appendix V.

5.4.2 Coordinate System and Projection

In order to properly reference the radar data with respect to other geographical features as well as the rain-gauge locations, both the geographical features and radar data must be referenced in the same projection and must use the same coordinate system. Radar CAPPI grided data lies in an oblique plane tangential to the globe at the radar location (the origin) with its y axis parallel to the local geographic north at the radar location (as shown in Figure 5.5). Geographical features and rain-gauges are usually in geodetic coordinates or in other projection systems. There are two solutions to this problem: (1) projecting the geographical features into the radar oblique plane and performing the analysis in this plane; or (2) projecting both radar data and geographical features into another common projection system.

For applications that require data from a single radar (i.e., radar calibration using rain-gauges, small scale severe weather warning, or storm tracking for urban applications), as recommended in Chapter 4, the first solution is more convenient.

This is because only one off-line projection operation is to be done to project geographical features into the radar coordinate system. Accordingly, radar data will be loaded as it is without projection, thus saving time and computations. In addition, when the objective is the off-line calibration of radar using rain-gauges, the first solution also is more accurate because the re-sampling effect of projection of the radar grid alters the values of the rainfall cells. Although, the re-sampling effect can be eliminated if the grid cells are treated as polygons this procedure is computationally demanding (refer to Chapter 4 for more details). For applications that require data from multiple radars and satellite data, the interface uses a polar stereographic projection as a common coordinate system (refer to Chapter 4). Two methods are coded into the interface for projection. The first method is the GPP projection method developed in Chapter 4. This method is based on the gravity direction that is the normal to the reference ellipsoid at the point being projected. The second method is the conventional projection method, which uses pre conversion of the coordinates from geodetic to geocentric coordinates. Refer to Chapter 4 for the details and equations.

The dynamically linked library (*cappiproj.dll*) is responsible for projecting the user selected shape files into the radar plane. This library is independent of ArcView classes, i.e., it has its own read/write routines for handling shape files. Details of the shape file format can be found in an ESRI (1998[2]). Hence, this library is a stand alone application and can be linked to any other software which supports shape files binary format. The functions of *cappiproj.dll* are:

1- Open the original shape file "*.shp" and index file "*.shx" for binary read access.

2- Identify shape type (i.e., point, line, or polygon).

3- Create the new *.shp and *.shx files for output in binary write mode.

4- For each shape in the input shape file:

   (a) Read the shape into a corresponding temporary shape object.

   (b) Obtain shape vertices.

   (c) Call the projection routine to project all vertices.

   (d) Update vertices and bounding box of the shape object.

   (e) Write the updated shape information into the output shape file.

   (f) Update the header of the shape file.

   (g) Delete the shape object.

5- Copy the input DBF (Data Base Format) file as an output DBF file, and rename it to be consistent with the output *.shp and *.shx file names.

6- Close input/output shape and index files.

A calling script is required to call this library. In addition to the interaction with *cappiproj.dll*, the calling script prompts for the required name and path of the output shape file. It also asks if the projected shape file is to be added to the view. Figure 5.6 shows sample screen shots of the GPP utility prompting for user input. Appendix III contains two simple procedures for the forward and backward transformations associated with the GPP projection. In addition, Appendix V provides a simple user

manual of the GPP projection within the RAINPLAT-GIS interface developed in this study.

5.4.3 Ground Clutter Removal

Ground clutter is a term used to describe the usually large amounts of microwave energy reflected back to the radar from stationary objects on the ground. Such objects could be towers, hills, high tension lines, trees, buildings, etc. Ground clutter is often removable. Since it is usually stationary, it can be recognized as unmoving echoes. Once the unmovable echoes are identified, they can be filtered out of the radar scans. Clutter removal techniques, both in hardware and software, are one of the more active areas of research in radar technology (Cornelius et al., 1995; Pratte et al., 1997; Sachidananda et al., 1998; and others). The interface filters clutter echoes by using composite clutter maps or masks that should be previously generated for each radar system. An automated clutter cancellation routine is used to suppress clutter from the raw scans. This procedure removes ground clutter in two stages: (1) Where radar reflectivities in a raw image are less than those in a clutter map, the former are deleted; (2) Any remaining reflectivity in the radar image which correspond to instantaneous rainfall rates less than a predefined value (equivalent to 1/32 mm/hr) are deleted. The procedure is fully automatic, requiring only an average ground clutter map collected during dry days.

5.5 The Structure of the GIS Interface

After installation, the "Radar" menu is added to ArcView's graphical user interface. The "Radar" menu contains links to launch separate dialogs, which interact both with the user and the components of the interface. The interface is structured into four main components required for (a) accumulating radar rainfall depths, (b) comparing radar accumulations with rain-gauge accumulations, (c) tracking and forecasting of rainfall patterns, and (d) overlaying radar data with GOES-8 satellite data. These four components will be described in the following four sections.

5.6 Accumulating Radar Rainfall Depths

When the user selects the option to load and convert radar data to rainfall rate, the Z-R parameters must be specified. The application of a Z-R relation produces instantaneous rainfall intensity maps. In order to develop maps of rainfall accumulations a method for calculating rainfall depths is essential. The simplest method is the one that employs the assumption of stationary rainfall intensity in space and in time (during the sampling interval). However, the precipitation field moves at approximately constant speed and direction during the sampling interval. In addition, rainfall intensity changes during the sampling interval. The interface component responsible for accumulating rainfall depths implements three methods for calculating rainfall accumulations: 1) assuming no advection, i.e., no velocity vector; 2) taking the velocity vector into account and neglecting the effect of the growth/decay; and 3) taking the effects of both the velocity vector and the

growth/decay of rainfall by assuming linear variation in the rainfall intensity. A brief description of these three methods follows:

5.6.1 Method 1

In this method, the rainfall field is assumed to remain stationary in space during the sampling interval (10 min). Accordingly, rainfall depths during each sampling interval are simply calculated by multiplying the rainfall rates by the sampling interval (10 min). Finally, the accumulation map during a certain accumulation period, or *output interval,* (one hr for example) is obtained by adding the contributions from all sampling intervals included in the accumulation period.

5.6.2 Method 2

The rainfall field is assumed to move and spread into accumulations according to the velocity vector, i.e., the rainfall field is not assumed to be stationary in space during the sampling interval. To account for this, the sampling interval (10 min) is divided into smaller *sub-intervals* of duration called *the analysis step* (1 min for example). At each sub-interval, the original radar rainfall field is shifted according to the advection velocity vector and placed in the resulting grid cells. The accumulations during the sampling interval are the sum of the accumulations of the original field during one analysis step, as well as all other accumulations during the intermediate sub-intervals. Finally, the accumulation map during a certain accumulation period (10 minutes for example) is obtained by adding the

contributions from all sampling intervals maps, or in other words, the accumulations during all analysis steps or sub-intervals within the *output interval.*

5.6.3 Method 3

This method is similar to that of method 2 except that it allows the advected rainfall field to vary linearly in order to reach the final rainfall field at the end of the sampling interval. This is done by weighting (according to the time offset) a copy of the original rainfall field at the beginning of the sampling interval before shifting it to the proposed location. Figure 5.7 shows a schematic diagram explaining the three accumulation methods.

More details and applications of the above three methods can be found in Bellon and Austin (1984), Austin (1987), Blanchet et al.(1991), Brown et al. (1991), and Fabry et al. (1994). The following input is essential to run the interface component: (1) starting and ending times (2) the output interval for calculating radar depths, i.e., time separation between output grids and (3) selection of a method for accumulating the radar rainfall depths.

Methods 2 and 3, described above, require additional user input to specify the speed and direction of rainfall patterns as well as the number of sub-intervals. The kinematic characteristics (speed and direction) of rainfall can be obtained using the kinematic component described in section 5.8. The output of this component of the interface is in the form of a series of GIS grids representing rainfall depths at every output step in the selected period. The new grids are placed in a new view,

which is named according to the user. Figure 5.8 shows a sample output using the three different accumulation methods.

It is important to highlight some points on the selection of the *analysis step* or, in other words, the number of *sub-intervals*. It might be thought that smaller analysis step may increase the accuracy of the calculated accumulations. However, this rule is valid to a certain limit below which no significant improvements in the accuracy of the estimates can be achieved. In addition, a very small analysis step can increase the run time significantly. Accordingly, it is important to properly "exercise judgement" when selecting the analysis step. The selection of the analysis step should be consistent with both the spatial resolution of the radar grid and the velocity vector. For example, for fast moving rainfall fields, a smaller analysis step must be chosen in order to capture the moving rainfall field at all grid cells. On the other hand, a small analysis step for a slow moving rainfall field is unnecessary because it will increase run time without improving the accuracy that would be obtained using a larger analysis step. The user can choose to enter the value of the number of sub-intervals or leave this to be done automatically by the interface. The interface automatically determines the analysis step and the corresponding number of sub-intervals by calculating the time required by the velocity vector to travel a distance equal to the grid resolution. This travel time is then approximated in order to satisfy an integer number of sub-intervals.

It should be noted that care should be taken when interpreting the accumulations calculated using method 2 or method 3 at the edges of the radar domain (the edges from which the velocity vector advances). The reason for this is that zero values are advected at this edge as no radar data exist beyond the edges. Accordingly, there is an uncertainty associated with the accumulations in a strip of width equal to the velocity multiplied by the sampling interval at the edge of the radar domain from which the rainfall pattern advances.

5.7 Radar Comparison with Rain-gauge Data

Radar rainfall accumulations are usually compared to rain-gauge depths. Different factors affect such comparisons. One of the main factors affecting this comparison arises due to errors in the radar measurements. Applying the black box concept, which involves the calibration of the Z-R relation using accurate rain-gauge measurements, reduces the effect of these errors. However, there are other factors affecting this comparison, such as the sampling errors (Kitchen and Blackall, 1992) which are the focus of Chapter 6. Previous and current research focuses on reducing the bias and fluctuations in radar sensation of precipitation. Accordingly, a user-friendly, flexible, and accurate interface for performing such analysis can facilitate such studies and provide a valuable tool for researchers working in this field. The GIS interface component responsible for this analysis performs the typical GIS intersection operation of the point (rain-gauge) locations on the user selected radar rainfall grids and outputs the corresponding radar accumulations in an output text

file. This component of the interface requires the following input from the user: (a) point coverage representing rain-gauge locations, (b) the starting and ending times and (c) name and path of the output text file. This component of the interface is used in the radar calibration analysis performed in Chapter 6

5.8 Tracking and Forecasting Rainfall Fields

One method used to study the storm motion tracks the centre of gravity of the rain area (Wilk and Gray, 1970; Barclay and Wilk, 1970; Zittel, 1976; Bjerkaas et. al., 1980; and others). If echoes can be delineated easily, this procedure might be the simplest and most effective pattern-matching procedure. In the automatic operation of this technique constraints, such as the minimum and maximum speed used to establish a search region for the next storm centroid to be marked as the same storm, are usually imposed to aid the matching procedure. However, problems usually arise because of the variable nature of rainfall (growth and decay), which affects the location of the centre of gravity and may lead to ambiguities in the estimated storm characteristics. Other problems appear in cases of widespread rainfall patterns, which produce difficulties in isolating storm clusters.

Another method of estimating the kinematics of rainfall is by cross-correlating a portion or the whole radar domain with subsequent scans. This procedure has the advantage of taking into account the detailed shape of the echo being tracked and decreases the chances of mismatching echoes (Wilson, 1966; Zawadzki, 1973; Austin and Bellon, 1974; Hill et al., 1977; Yoshino and Kozeki,

1985; Collier, 1989; and others). If the echoes in the radar image move together and there are no significant intensity or shape changes, this technique can be considered the most accurate and simplest matching technique. However, other methods exist for matching echoes at separate times in order to estimate echo displacement vectors such as: minimizing the error sum of squares (Duda and Blackmer, 1972). The GIS module implements two methods for estimating rainfall kinematics: (1) the echo centroid technique, and (2) the cross-correlation technique.

5.8.1 Echo Centroid Method

Because this release of the interface concentrates mainly on offline applications of weather radar data, it was decided to design this module to work in an interactive mode. The task of delineating separate storm areas is left to the user. This is done using the pointing device. The user performs the following to complete a tracking session:

1- Starts a new session.

2- Activates a rainfall grid as the current grid.

3- Delineates the echo under interest.

4- Repeats steps 2 & 3 for all time steps required and finishes the session in order to display the results of the tracking session.

5- Saves the tracking session in a text file.

This module is written using avenue scripts. The functions of the module:

1- Obtain the polygon drawn by the user.

2- Use the obtained polygon to clip the portion under interest from the whole radar domain.

3- Assign zero values to areas below the threshold value, performs a 2D centre of mass for the clipped zone, and adds the x and y coordinates of the centroid to a global list.

4- Calculate the velocity vector from the positions of each two consecutive centroids in the global list and displays both the average velocity vector and its standard deviation after the user clicks the *finish* button.

5- Save a text file containing all details of the session, including the coordinates of the centroid at the different times, the velocity vector at each time, and the final average and standard deviation of the velocity vector after the user clicks the *save session* button.

A threshold can be applied to identify (pre-sets) intensity zones. The interactive C.G tracker dialog that interacts with the user is shown in Figure 5.9.

5.8.2 Cross-Correlation Method

This module is written using avenue scripts and allows for the correlation of selected portions of the whole domain with the corresponding subsequent scan. The module works by shifting the current clipped rainfall grided data by a variety of grid lengths and finding the optimum spatial shift corresponding to maximum correlation

with the grid at the previous time. A threshold value may also be used, under which the grid cells are marked zeros. The results of this tracker are reported as the optimum spatial shift ($Xshift_{opt}$, $Yshift_{opt}$) in x and y directions, respectively, as well as the corresponding velocity vector that maximizes the correlation coefficient between the shifted copy of the current rainfall grid and the previous rainfall grid. The mean motion of the precipitation field, i.e., the velocity vector in km/hr, is given by ($-Xshift_{opt}/\Delta t$, $-Yshift_{opt}/\Delta t$) where $Xshift_{opt}$ and $Yshift_{opt}$ are in kilometers and Δt is the time separation in hours. This module runs automatically, i.e., the user can select radar rainfall grids at different times and the module moves from one scan to the next until it finishes all rainfall grids within the selected time period. Three options are available for performing the search for an optimum spatial shift:

1- The first option tries all possible shifts in x and y that are within the constraints (i.e., min and max speed).

2- The second option is faster than the first one. It performs the full search in initialization. It then, in subsequent scans, allows the module to focus its search in a 90 degrees quadrant around the direction obtained in the initialization scan.

3- The third option is the fastest search method. This employs the principle of response surface analysis to perform the search only on the directions of maximum slope of the correlation surface, i.e., by climbing the short route on the correlation surface to the global maxima (Gad and Tsanis, 2002[2]). This new methodology is based on simulation-based optimization. The

development and application of this method is described in Chapter 7.

5.8.3 Short-Term Rainfall Forecasting

Quantitative rainfall forecasting using radar data is the subject of Chapter 7. A forecasting model is presented in Chapter 7 and compared to the Canadian Short-Term Automated Radar Prediction (SHARP) model. The developed GIS interface implements both models. The new model is based on an adaptive exponential smoothing algorithm for updating the forecasting parameters of a second degree polynomial model representing the evolution of each radar rainfall cell. For this purpose, a moving (Lagrangian) frame of reference is used. The detailed theory and application of the model is described in Chapter 7. The forecasting component of the interface requires the acquisition of three radar scans to initialize the module. In subsequent scans the model is updated each time a new scan is acquired, i.e., every10 minutes. At each time step the model produces two forecasted rainfall fields: (1) a forecasted grid at the time of the next scan (10 minutes); this forecast is used only to update the model to obtain optimal estimates of the parameters when the next scan is acquired; and (2) a forecasted grid at the required forecast lead time.

5.9 Extension to GOES-8 Satellite Data

Detailed information concerning GOES images can be found in GOES I-M DataBook (1996). Satellite images consists of 4 channels: (1) visible, (2) infrared, (3) water vapour. The visible image is the equivalent of taking a black and white photo

of the earth. The bright areas show where the sun is being reflected back into space as a result of clouds or snow cover. Clouds and snow show up white. The thicker the cloud, the brighter the white colour. Land surfaces show up as gray and ocean surfaces nearly black. The major limitation to visible imagery is that it is only valid during daylight. The infrared image (IR) shows heat based radiation from the infrared spectrum. In other words, the warmer the surface, the more infrared radiation it emits. For a satellite image, cooler surfaces are bright and warmer surfaces are dark. Since the atmosphere cools as altitude increases, clouds would show up as bright areas and land surfaces as dark areas. In addition, low clouds will be more gray and higher clouds will show up more white. Tall thunderstorm clouds will show up as bright white, and it will be hard to differentiate between fog and land areas. A large advantage of IR is that it is available twenty four hours a day. The water vapour image shows an infrared band, which is strongly affected by the presence of water vapour. Essentially, the image shows the altitude of the highest moist layer in the atmosphere. Bright areas reflect the location of high clouds either due to jet stream cloudiness or due to thunderstorm activity. The dark areas reflect the location of dry areas at high altitudes. This is associated with dry air intrusion and sinking motion associated with high pressure systems.

Satellite data are relatively less accurate than radar data in terms of rainfall estimation (FMH, 1991). However, recent studies on satellite retrieval methods have shown promising results with regard to the use of satellite IR data in estimating rainfall by itself (Grimes et. al., 1993; Vicente et. al., 1998). It should be noted that

satellite data are still limited operationally to quality control purposes. In NEXRAD system in the US, for example, satellite data are used to check no-rain areas in order to correct radars errors. If radar reports rainfall in areas where satellite images show no clouds, the rainfall cells in this area are corrected. However, with future research, there is a strong hope that satellite retrieval algorithms will be able to provide rainfall estimation from satellite data by itself. This will enable rainfall estimation in areas in which radar data are not accurate or not available in addition to quality control on radar data. On the other hand satellite data can provide help in terms of tracking the motion of clouds, which can assist with radar data in forecasting rainfall motion, especially on a large scale.

The developed GIS interface has an extension for processing, loading, and geo-referencing satellite images. Accordingly, all sensors (radars, satellite, rain-gauges) can be overlayed in one view, which can facilitate any analysis that requires data from these sensors.

5.9.1 Satellite Images Processing

The Meteorological Service of Canada receives and distributes GOES-8 satellite data in Graphics Interchange image format (GIF). The GIF is a standardisation defining a mechanism for the storage and transmission of raster-based graphics information. Details on the GIF format can be found in CompuServe (1987). GIS doesn't support GIF image themes. Accordingly the original GIF satellite images are decoded then encoded into JPEG format (Joint Photographic Experts Group) in

the IS 10918-1 (ITU-T T.81) standard form that is supported by GIS software. For more details on JPEG format refer to Hamilton (1992). Murray and vanRyper (1996) provided additional details on both GIF and JPEG formats.

A GIF decoder and a JPEG encoder are used to convert the real time feed of GIF satellite images, which are received from the Meteorological Service of Canada into JPEG format. The parameters required for the image-to-world transformation to convert the image coordinates to real-world coordinates are set in a world file accompanying the images (refer to section 4.8 and table 4.3 in Chapter 4 for the values of the parameters). Finally, the JPEG satellite images are loaded to ArcView GIS using ArcView's JPEG image extension and converted to ESRI grid format (refer to Gad and Tsanis, 2002[1&3] for more details).

5.9.2 Satellite Data with Radar Data

The satellite images for the Great Lakes sector are stored in a Polar Stereographic projection. For this reason no projection manipulation is performed on the images except for the image-to-world transformation. In order to overlay radar data with satellite data, radar data are remapped from their coordinate systems into the common coordinate system by using one of the projection methods used in the interface (the GPP method or the Conventional method). The interface loads radar data and satellite data per event basis, i.e., each day is loaded in a separate view. Figure 5.10 shows a satellite grid (after conversion to ESRI grid) covering the Great Lakes sector overlayed on the National Radar network. Figure 5.11 shows satellite

data overlayed with radar data from King City and Exeter radar sites.

5.10 Technical Details

An animation component is provided in the interface. This animation module has the advantage of animating storm motion in more than one view at the same time, thus allowing the user to zoom to different scales. This provides a good tool especially when monitoring storm evolution at different scales at the same time. In addition, the animation module allows zooming inside the same view while the animation is running. Another component is available for the purpose of exporting radar data. The aim of this component is to reproduce sets of radar data files clipped in a certain portion under the radar umbrella.

5.10.1 Installation

The module is available in a setup file. The installation effect is summarized in the following:

1- Some dynamic link libraries are extracted to:

"$AVHOME\AV_GIS30\ARCVIE-W\BIN32\.".

2-The extension files "Gauge.avx", "Radar.avx", and "Satellite.avx", are extracted to: "$AVHOME\AV_GIS30\ARCVIEW\EXT32\".

3-The directory "C:\RAINPLAT\" is created and the executable files, legend files, documentation files, as well as the uninstall program are extracted inside this directory.

$AVHOME denotes ArcView installation directory. It should be noted that some of the dynamic link libraries used in this interface are also provided in separate executable versions in the installation package to be used separately from the DOS prompt.

5.10.2 Performance

In order to fully summarize the performance of the different components of the interface, the run time for some operations on a PIII 600 Mhz (256 M.Ram) PC is shown in Table 5.1. Most of the operations performed by the module may be considered to have acceptable run times except for few operations, such as estimating rainfall kinematics using the cross-correlation technique (option 1 and 2). Future improvements are possible by substituting some of the avenue code by external procedures (dynamic link libraries). The reason for this is that some grid requests in ArcView cause the grids to be written to the computer hard drive, which requires more execution time. This is unlike other programing languages such as C where the operations are done from/to memory directly. Subsequent grid operations in GIS need to read the grid data set again from the hard drive. In addition, grid requests in ArcView-GIS treat the grids as a whole (i.e., there is no cell-by-cell access to the grids), which requires more steps for performing a complicated grid operation (such as the cross- correlation analysis). If these disk write/read operations are avoided and the grid requests are replaced by external procedures to allow cell-by cell access, the run time would be expected to decrease significantly. However, the use of search

option 3 decreases the run time to an acceptable level, which will be described in details in Chapter 7.

Table 5.1 Performance of the components of the GIS Interface

Operation			Av. Run Time (Sec)	Written Using
Loading one radar file (480*480 array) in ArcView.	Binary		< 0.5	C++ and Avenue
	ASCII		0.5-1	C++ and Avenue
Processing and Loading one Satellite image			1-2	C++ and Avenue
Projecting a polygon shape file (1000 records, 20 vertices per polygon in average)			2-3	C++ and Avenue
Accumulating Radar depths in one sampling interval	Method-1 :No advection		1-2	Avenue
	Method-2: Advection (no G/D) using 10 sub-intervals.		10-15	Avenue
	Method-3: Advection (taking G/D) using 10 sub-intervals.		15-20	Avenue
Extracting radar data for one image at locations of 100 points.			1-2	Avenue
Storm Kinematics using the whole radar domain for an intermediate sampling interval.	Centroid Module		2-3	Avenue
	Cross-Correlation Module	Search option-1	960-1100	Avenue
		Search option-2	120-240	Avenue
		Search option-3	10-30	Avenue
Extracting portion of one radar image in a data file.	IEEE floating point Binary format		1-2	Avenue
	ASCII space delimited format		2-3	Avenue

5.11 Summary

- A GIS multi-component interface is developed for the analysis of weather radar precipitation data. The interface is a valuable tool that facilitates the exploration and analysis of radar data.

- The interface handles different operations, such as loading and writing radar and satellite data, projecting geographical features into the radar coordinate system and overlaying data from multi-sensors into a common coordinate system, accumulating radar rainfall depths, radar comparison with rain-gauge data, animating storm evolution on top of geographical features, and tracking and forecasting rainfall fields.

- In addition to the interface components described above, the main advantage exists in bringing radar data and satellite data to the GIS environment, in which different useful analysis requests are available.

- The interface is used to perform the analysis throughout the thesis. In Chapter 6 it is employed to study the sampling errors affecting radar-raingauge comparisons and is used for calibrating King City and Exeter radars. In Chapter 7 the Canadian SHARP (Short-term Automated radar Prediction) model and the developed tracking and forecasting model are coded into the interface. The interface is used in Chapter 7 to compare the two models and to assess the forecasting accuracy.

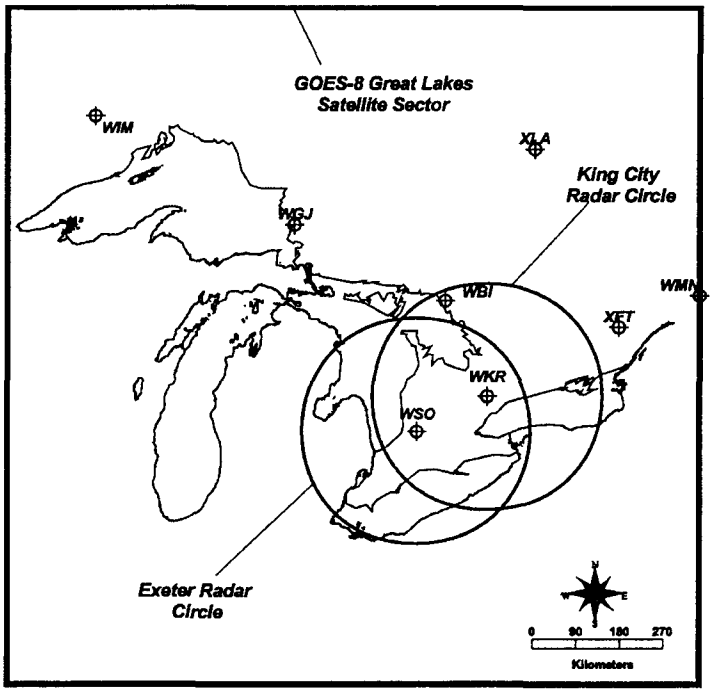

Figure 5.1 Location of King City and Exeter radar sites with respect to the Great Lakes GOES-8 satellite sector.

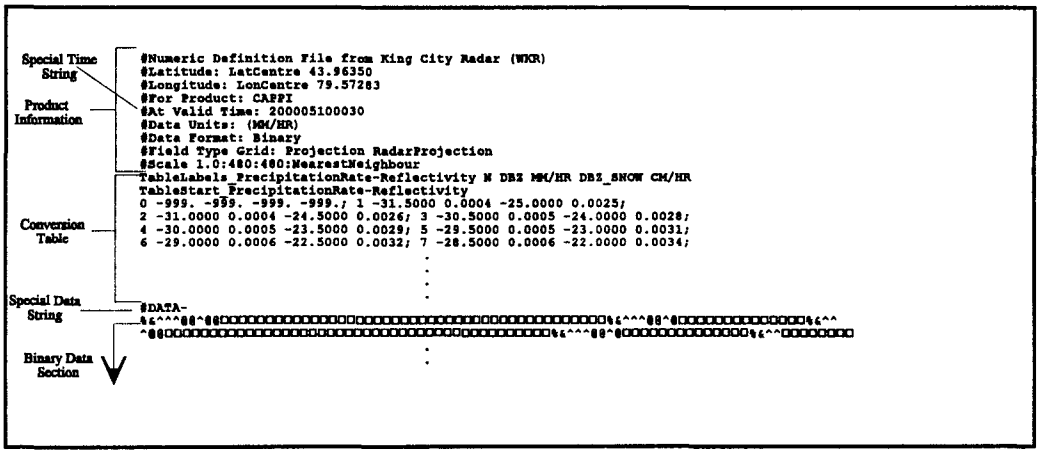

Figure 5.2 A typical header for radar data file.

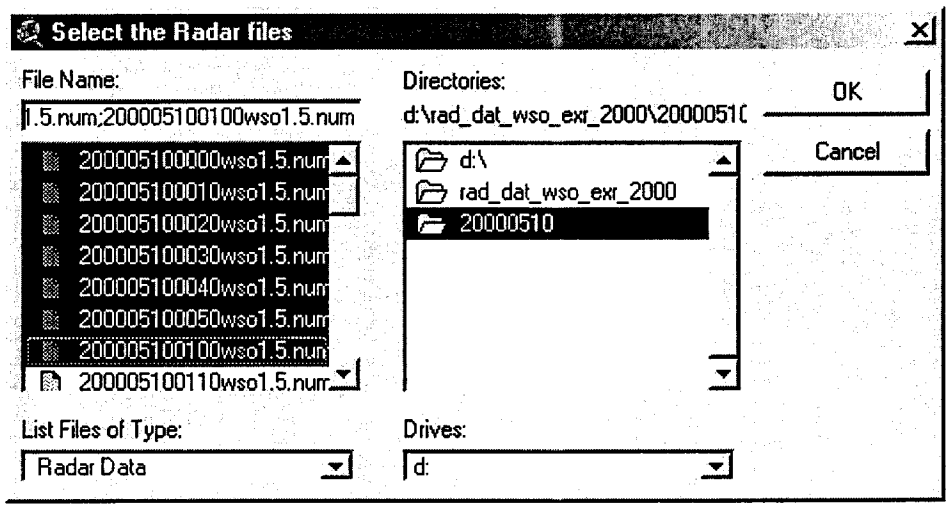

Figure 5.3 Screen shot of the interface prompting for selecting radar data files to be loaded.

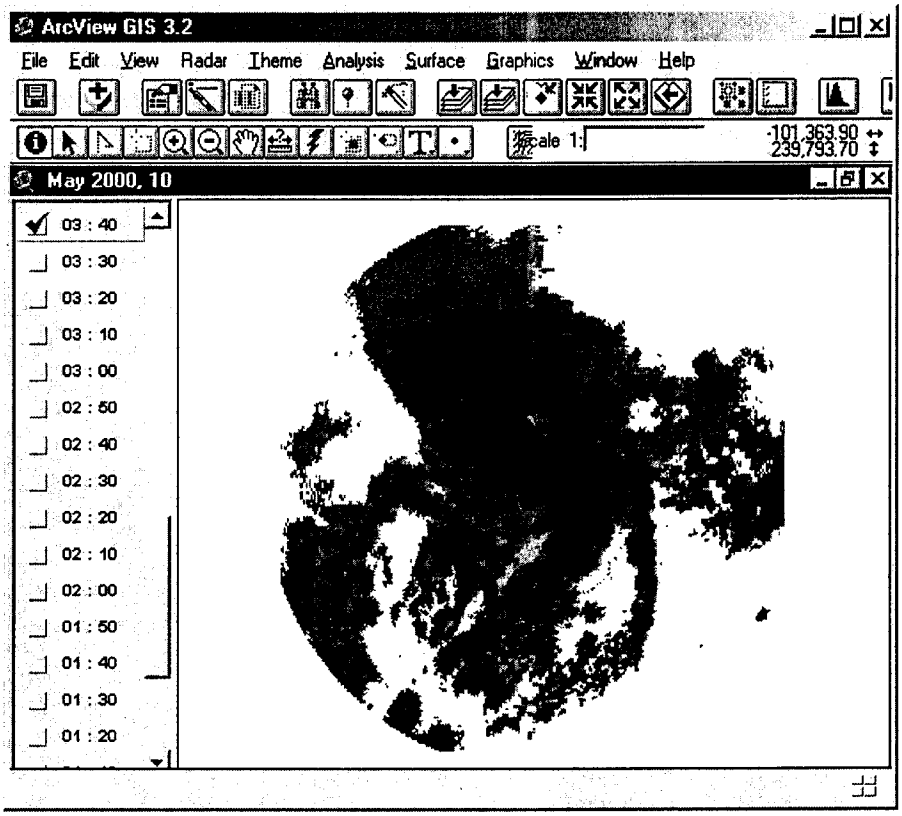

Figure 5.4 Screen shot of ArcView after loading radar data files.

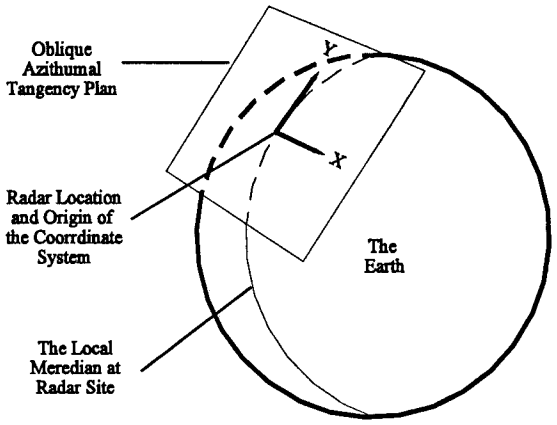

Figure 5.5 The radar coordinate system with respect to the Earth.

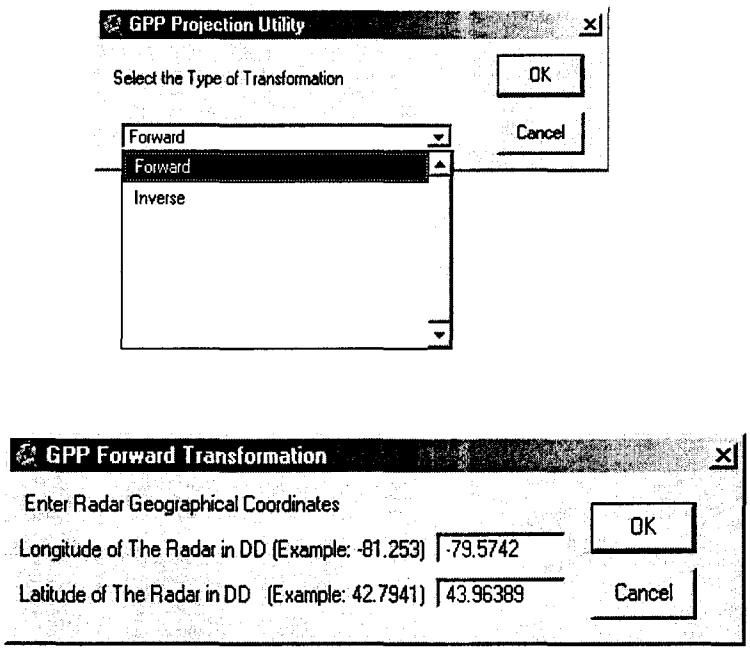

Figure 5.6 Screen shots of the GPP projection utility prompting for user input.

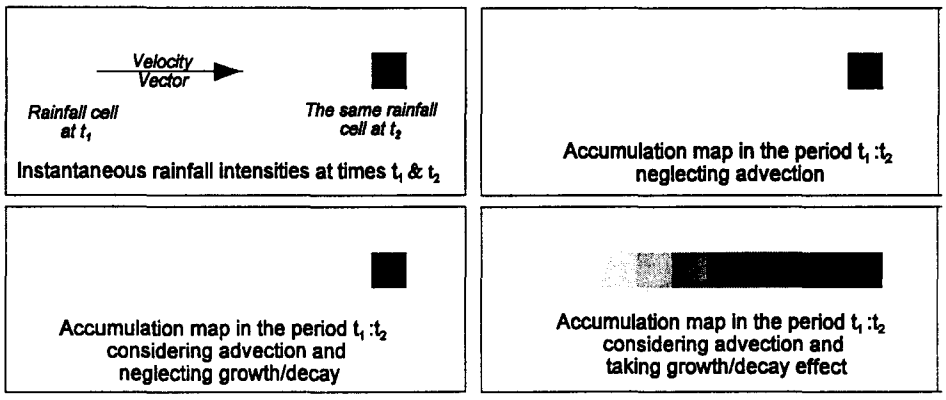

Figure 5.7 A schematic diagram representing the three different methods used for accumulating radar rainfall depths.

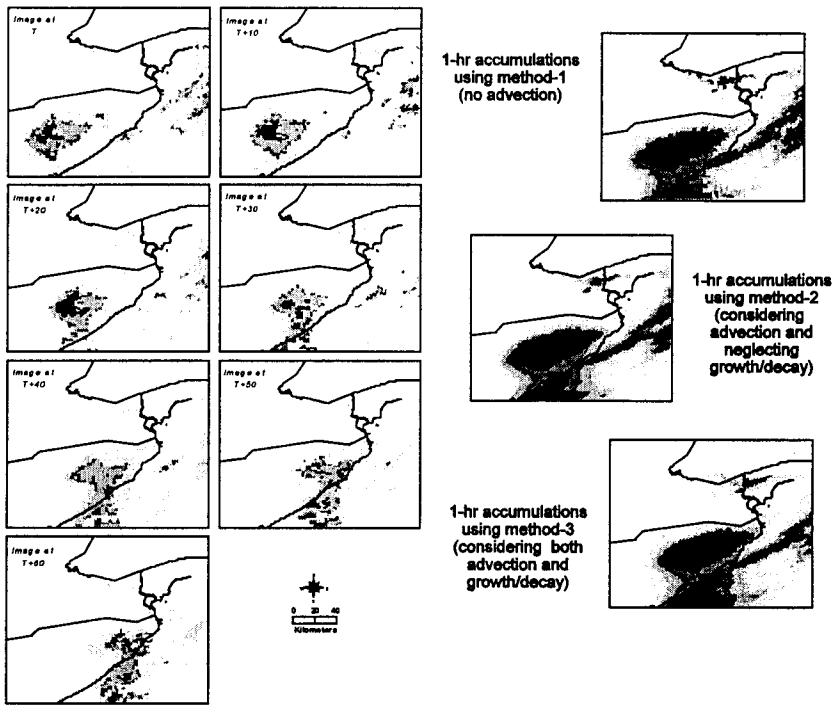

Figure 5.8 A sample case of accumulating 1 hr radar depths. The seven images in the left are instantaneous rainfall intensity maps covering 1 hr, whereas the left three maps are one hour accumulation maps produced using the three different accumulation methods.

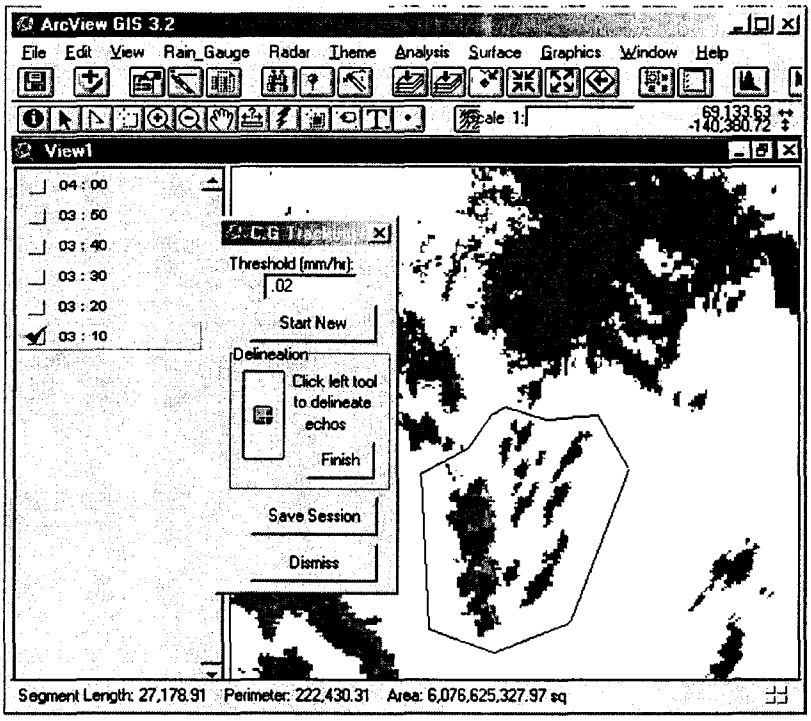

Figure 5.9 Screen shot of the dialog of the interactive C.G tracker.

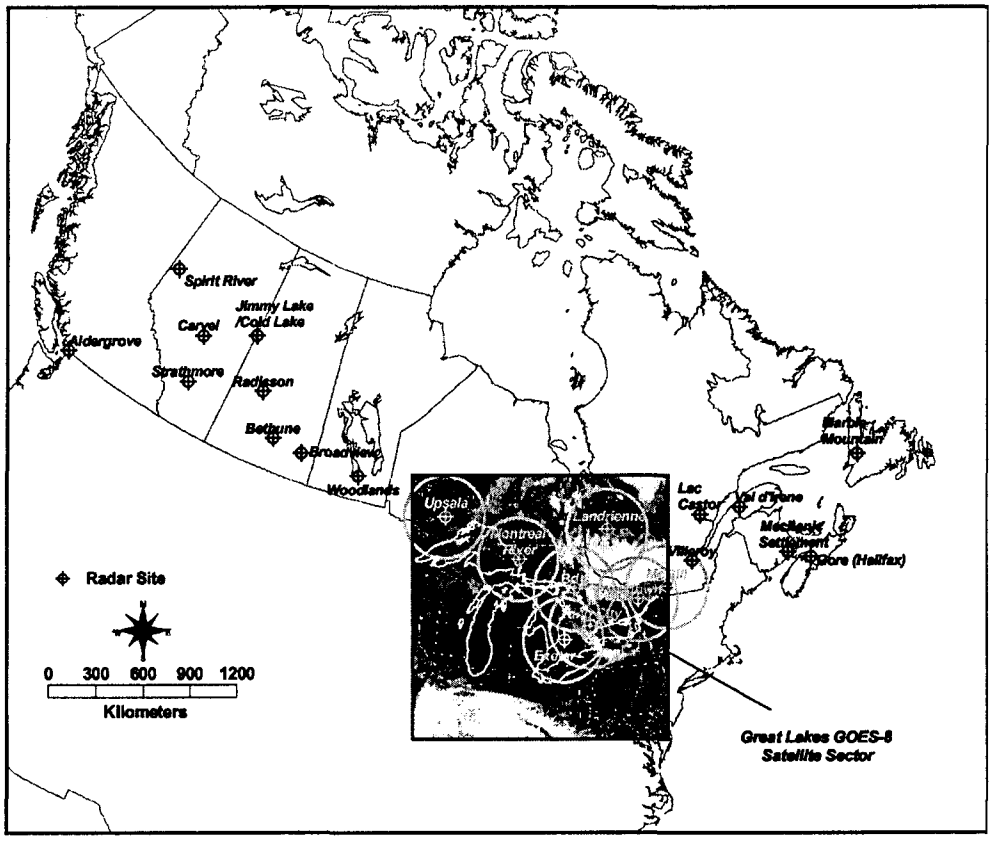

Figure 5.10 GEOS-8 Satellite IR grid (Great Lakes sector) at time 200106031620 UTC. The satellite grid is overlayed on the Canadian National Radar Network. The common coordinate system is a Polar Stereographic projection (83W central meridian).

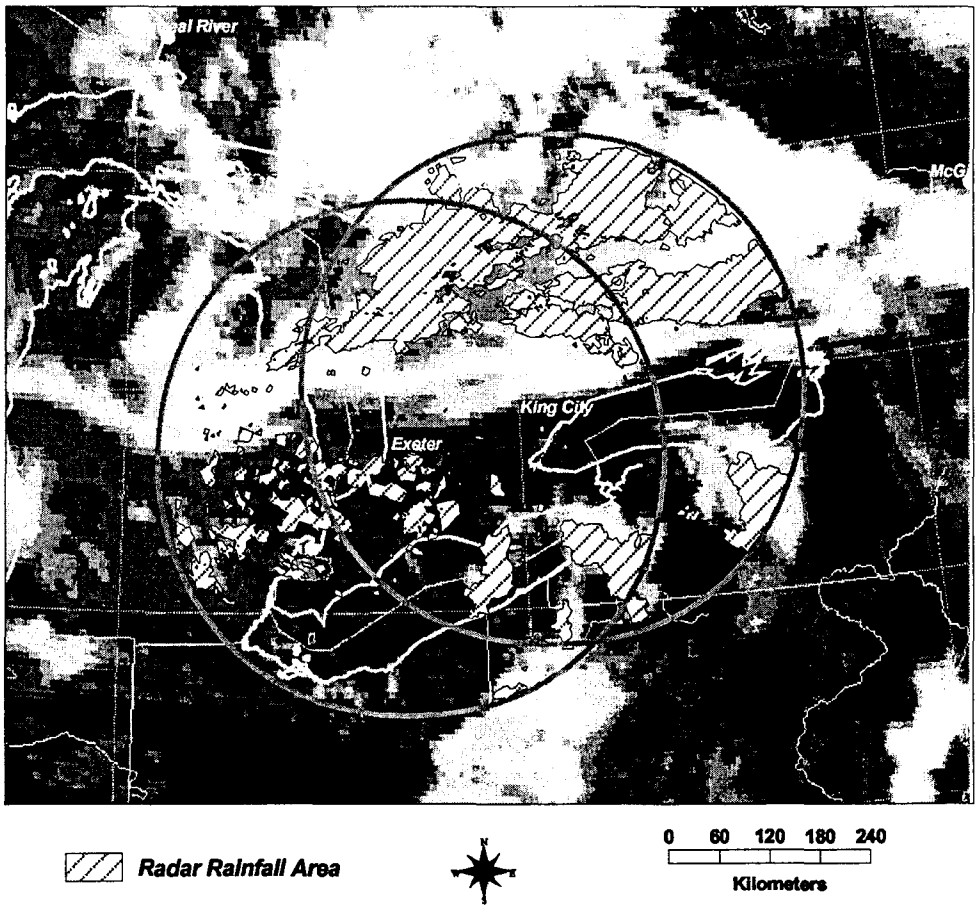

Figure 5.11 Satellite IR grid at time 200105280100 UTC overlayed with mosaic radar data from King City and Exeter radar sites.

CHAPTER 6

RADAR-RAINGAUGE SAMPLING ERRORS AND MEAN FIELD RADAR RAINFALL BIAS REDUCTION

6.1 Introduction

Weather radar does not directly measure rainfall. Rather, it measures the energy that backscatters from the meteorological target. The meteorological target represents the hydrometeors and precipitation particles contained within the radar sampling volume in the atmosphere. The backscattered energy is related to the reflectivity factor (Z) through the radar equation (Probert-Jones, 1962). The reflectivity factor is converted to rainfall intensity through the use of a Z-R relation in the form of:

$$Z = AR^b \tag{6.1}$$

where:

R = the rainfall rate (mm/hr).

Z = radar reflectivity factor (mm^6/m^3).

A, b = constants.

Different Z-R relations are used for the different radar systems. Such Z-R relations are commonly calibrated using ground rain-gauge measurements. The relationship between radar-estimated rainfall and surface rainfall involves different complex factors, and this makes the problem of radar rainfall estimation and calibration very difficult. Many studies have considered this complexity (Hudlow, 1973; Wilson and Brandes, 1979; Doviak and Zrnic, 1993; Zawadzki, 1984; Joss and Waldvogel, 1990; Fabry et. al., 1994; Anagnostou and Krajewski, 1999; and others). These studies concluded that, due to the uncertainties in radar rainfall measurements, there is no unique algorithm that can be applicable for all radar rainfall measurements. Radar/gauge variations of over two orders of magnitude can occur in practice (Collier, 1986). Different factors affect the difference between the two sensors (i.e., radar and rain-gauges). These factors include: (1) errors in the radar measurements; (2) errors in the rain-gauge measurements (Habib et al., 2001); (3) processes taking place between the height of the radar measurements and the ground, such as evaporation and wind drift (Collier 1999); (4) the used Z-R relationship; (5) the difference between point measurements and areal averages (Ciach and Krajewski, 1999); and (6) the advection correction method used in accumulating the radar depths (Fabry et. al., 1994). In order to clarify the different sources of errors and for the purpose of this work, the radar-raingauge error sources are classified into two main groups: measuring errors and sampling errors.

1- Measuring errors:

The group of measuring errors includes:

- Drop size variability from storm to storm and within the same storm.
- Variation of reflectivity with height and beam overshooting of precipitation.
- Radar non-linear averaging of highly variable precipitation over the product pixel, and the method used for averaging.
- Radar signal attenuation, radar hardware miscalibration, and other noise sources (side loops effect, ground clutter, anomalous propagation). For more details, refer to Collier (1989) and Doviak and Zrnic (1993).
- Miscalibration and errors of rain-gauges.

2- Sampling errors:

- Uncertainties in the tipping bucket (TB) rain-gauge accumulations (especially in low rainfall intensities) due to the sampling mechanism of the TB gauges.
- The difference of the spatial sampling volumes of the two sensors. Rain-gauges measure small scale rainfall structures whereas radar averages them. However, this point will be approached in the next section from a new point of view.
- The difference in the temporal resolution of the two sensors (errors

due to temporal variations).

- The difference in the time calibration (two different clocks) and the difference in the locations of the two sample volumes. Radar measures rainfall at a height above the ground surface, whereas gauges measure rainfall at the ground. Some atmospheric processes can affect rainfall rate between the two locations (intensity growth under beam, evaporation, and wind drift).

If good quality radar and rain-gauge data are used, the first group of errors (measuring errors) can be reduced. The measuring errors are not the focus of this study. The second group of errors (the sampling errors) are the main concern of this study. Some researchers reported that sampling effects have a significant contribution to both random and bias errors in radar-raingauge comparisons (Kitchen and Blackall, 1992; Fabry et. al., 1994; and others).

Comparisons between radar and rain-gauges are usually done for hourly or longer accumulation intervals and for spatial resolution of 4 km (the resolution of Stage-II NEXRAD precipitation products). Not much work has been done on a finer spatiotemporal resolution because of the expected significant variations caused by sampling errors (Collier,1986). The commercial radar rainfall accumulation products are also developed for hourly temporal resolutions. Even if raw radar data are used commercially, the highest temporal resolution obtainable is 10 minutes (the temporal spacing between scans). Such temporal resolution constitutes a limitation for use of radar data for the purpose of hydrological modelling for very small watersheds (order

of 1 km × 1 min spatiotemporal resolution). Rain-gauges are the only source of accurate information for such high resolution hydrological applications.

This chapter describes a methodology to address the effects of the sampling errors on the radar-raingauge comparison in addition to their effects on the radar calibration using high resolution rain-gauge data. In addition, this chapter describes a methodology for extracting high spatiotemporal resolution rainfall data from the available radar information. Finally, a calibration analysis will be presented at the end of this chapter. The sampling errors and their effects, as well as the evaluation of radar data for high resolution applications, are presented in sections 6.2 to 6.8. The remaining sections of this chapter assess the accuracy and calibration of King City and Exeter radars in Southern Ontario.

6.2 The Theory in Addressing Sampling Errors

This section discusses the sampling errors considered in this study and their effects on both the difference between the radar and rain-gauge measurements and the Z-R calibration process. The assumptions and main definitions used for addressing the sampling errors are presented in this section.

6.2.1 Uncertainties of Tipping Bucket Rain-gauges

The tipping bucket (TB) gauges operate in a way that falling rain is collected into a fixed-size bucket that tips and drains when it is full. Records of the number of tips, along with information about their time of occurrence, can be used to estimate

rainfall accumulations and rates. The common recording strategy followed to collect the TB data works by recording the number of tips that occur during a specific period of time (e.g., number of tips every minute). The bucket size and how frequently the recording device samples determines the accuracy of the TB gauge. Several studies showed that TB gauge data are corrupted by both random and systematic errors (Sevruk and Lapin, 1993). These errors include losses due to wind, evaporation, wetting, and splashing. TB gauges may also suffer from mechanical and electrical problems, as they may occasionally fail to tip during an event. The chances of occurrence of these measurement errors increase in cases of high rainfall rates. Using quality control procedures, most of the errors mentioned above can be discovered in a data set and eliminated. The quality control procedures depend on the consistency with neighboring gauges (refer to the visualization technique described in Chapter 3).

If we assume the TB data to be free from the above errors, the main important source of error, which appears significantly with low intensities in all TB data in small time scales (e.g, 1 min accumulations), is uncertainty due to the sampling mechanism of the TB gauge. This uncertainty has been reported in different studies (Goldhirsh et al., 1992; Nystuen and Proni, 1996; Steiner, 1996; Yu et al., 1997; and others). Habib et al (2001) showed that the errors associated with this uncertainty are significant for accumulation period less than 15 minutes. However, because the analysis of this study is based on accumulation periods less than 15 minutes, an assumption has to be made when using low intensity TB data for regression purposes.

If a large number of TB readings is used for Z-R regression, then the absolute error attributable to the TB sampling mechanism may be assumed to be normally distributed with zero mean. The error sign is related to the true rainfall value. In other words, in low TB intensities, TB readings may be assumed to overestimate rainfall in low radar intensities and underestimate rainfall in high radar intensities. Hence, if sufficient radar-raingauge pairs are used, this error is assumed to have minimal effect on the regression results (as shown in Figure 6.1). It should be noted that if high intensity events are used in the calibration, this type of error is minimized.

6.2.2 Point and Areal Differences and Errors Due to Temporal Variations

Many studies have considered this difference between the gauge point value and the radar areal average. However, the TB rain-gauge data in this study are considered as areal averages not, as is usually the case, as point measurements. If the velocity vector of rainfall is taken into account TB readings actually represent an average intensity of a strip of the rainfall pattern passing above. For example, consider a rainfall pattern moving with average speed 60 km/hr above a TB gauge of 1 min resolution. In one minute the pattern moves one kilometer and the 1 min reading of the gauge is actually the rainfall accumulation from a 1 km strip taken in the direction of motion above the gauge. In the transverse direction, rainfall value is not expected to vary considerably and rainfall intensity based on 1 min TB accumulation may be considered to represent instantaneous average rainfall over a 1 km by 1 km radar pixel with some degree of approximation. Refer to Figure 6.2 for

a schematic explanation. As shown on the figure, theoretically, the following two equations can be concluded:

$$\int_{x_1}^{x_2} I_r dx = \int_{t_1}^{t_2} I_g dt \tag{6.2}$$

$$|x_2 - x_1| = V \times |t_2 - t_1| \tag{6.3}$$

Where:

I_r = Instantaneous radar rainfall intensity with respect to a Lagrangian coordinate system (with respect to distance) constructed at the height of the radar scan and moving with the storm.

I_g = Instantaneous rain-gauge rainfall intensity with respect to an Eulerian frame of reference (with respect to time) constructed at the gauge location.

x_1 and x_2 = Distance limits on the Lagranian frame of reference.

t_1 and t_2 = Time limits on the Eulerian frame of reference.

The error due to temporal variations appears when rainfall rate variation on time scales less than the period between the radar samples is significant. Accordingly, to a good degree of approximation, both errors due to point and areal differences and temporal variations can be resolved if the rainfall kinematics are taken into account (i.e., correct for advection).

6.2.3 Timing Errors

Radar data are referenced worldwide in an UTC time system, whereas TB gauges are usually calibrated on a local clock. A technician visits the TB gauges frequently to adjust the time of the loggers according to a local watch that may deviate from the correct local time by a few minutes (refer to section 3.2.1). In addition, radar data corresponding to a CAPPI scan are not essentially at the same nominal time. According to the scanning strategy of the radar antenna, variations of the order of a few minutes may exist. Hence, errors of a few minutes may exist between the data times of the two sensors, which represent the timing errors.

6.2.4 Wind Drift

The correction for wind drift is essential for high resolution radar data before any comparisons with rain-gauges. A falling rain drop is subject to two main kinematic components. The first component is the advection speed inherited from the condensing cloud generating it. The second is the induced downdraft horizontal component. In most cases, the two components act in opposite directions. It is assumed that both components act in the vertical plane of the storm movement, i.e. components perpendicular to the storm movement are neglected. For more details on descriptive storm models and cloud dynamics refer to Cotton and Anthes (1989). As it will be shown in the following section, the present study develops a methodology to account for both timing and wind drift errors by introducing one parameter to represent a time shift in rain-gauge data.

6.3 Calculation of Radar and Gauge Rainfall Intensities

Three methods are used to extract radar and the corresponding rain-gauge rainfall intensities. The three methods, with increasing degree of difficulty, try to account for the different sampling errors from method 1 to method 3. The equations presented in this section are applicable to accumulation periods less than the time between radar scans. The three methods are described in sections 6.3.1, 6.3.2, and 6.3.3.

6.3.1 Stationary Rainfall Field with No Timing Errors

This method (method 1) assumes no timing errors and a stationary rainfall field. The radar reflectivity is extracted from the radar pixel just above the rain-gauge location and assumed to be temporally uniform between the radar scans. No correction for timing errors is made. Hence, denoting the radar nominal time as t_{rad} the rainfall intensities from the two sensors can be found from:

$$I_r = \left(\frac{Z_{t_{rad},x=x_G}}{A}\right)^{1/b} \tag{6.4}$$

$$I_g = \frac{1}{T} \sum_{t_g=t_{rad}-\frac{T}{2}}^{t_g=t_{rad}+\frac{T}{2}} d_{t_g} \tag{6.5}$$

Where:

T = Accumulation period (hr).

d_{tg} = One minute TB rain-gauge accumulation at time t_g (mm).

I_r = Radar rainfall intensity (mm/hr).

I_g = Rain-gauge rainfall intensity (mm/hr).

$Z_{trad,x=XG}$ = Radar reflectivity (mm^6/m^3) at radar pixel just above the rain-gauge.

6.3.2 Stationary Rainfall Field with Time Shift

Method 2 is similar to method 1 in terms of the stationary rainfall assumption during the sampling interval except that it allows for a time shift (*TS1*) between radar and rain-gauge data. Accordingly:

$$I_r = \left(\frac{Z_{t_{rad},x=X_G}}{A}\right)^{1/b} \tag{6.6}$$

$$I_g = \frac{1}{T} \sum_{t_g=t_{rad}+TS1-\frac{T}{2}}^{t_g=t_{rad}+TS1+\frac{T}{2}} d_{t_g} \tag{6.7}$$

where:

T = Accumulation period (hr).

d_{tg} = 1 min rain-gauge accumulation at time t_g (mm).

$Z_{trad,x=XG}$ = Radar reflectivity at time of scan t_{rad} and at location $x=X_G$(i.e, pixel just above the gauge location) (mm^6/m^3).

I_r = Radar rainfall intensity (mm/hr).

I_g = Rain-gauge rainfall intensity (mm/hr).

$TS1$ = Time shift between the radar and gauge data (min).

6.3.3 Moving Rainfall Field Allowing Time Shift

This method (method 3) neglects intensity changes between different heights as well as growth and decay of rainfall between radar scans to simplify the computations. Wind drift, the time a rain drop takes to fall to the ground, and timing errors are assumed constant during a storm event. The main idea of this method is that the spatial distribution of rainfall over the cloud with respect to a Lagrangian frame of reference is the same as the temporal Eulerian distribution of rainfall at a rain-gauge location. (refer to Figure 6.2). Hence, the average radar rainfall intensity and the corresponding average rain-gauge intensity over an accumulation period T can be obtained from:

$$I_r = \frac{1}{V \times T} \sum_{x=x_1}^{x=x_1+T\times V} \left(\frac{Z_{t_{rad},x}}{A}\right)^{1/b} \times \Delta x \qquad (6.8)$$

$$I_g = \frac{1}{T} \sum_{t_g=t_1}^{t_g=t_1+T} d_{t_g} \qquad (6.9)$$

where:

V = Storm Speed (m/hr).

T = Accumulation period (hr).

x = Length from the rain-gauge location to the radar pixel under consideration at the time of the radar scan, i.e. , with respect to a Lagrangian frame of reference having its X-axis in the storm direction (m).

Δx = Spatial interval on the radar image in the direction of the storm (Δx = 1 min $\times$V) (m)

$Z_{trad,x}$ = Radar reflectivity at the time of the radar scan t_{rad} and at a location x (mm^6/m^3).

Note that the increment for x is Δx and for t_g is 1 min. To relate the limits of the summations: The starting time at the rain-gauge t_1 which corresponds to radar pixel at x_1 can be related to the nominal time of the radar scan (t_{rad}) by :

$$t_1 = t_{rad} + \frac{X_G - C - x_1}{V} + T_{drop} + \in_t \qquad (6.10)$$

where t_{rad} is the time of the radar scan, T_{drop} is a constant representing the time required for a rain drop to fall to the ground, C is a constant distance representing wind drift, X_G is the coordinate of the rain-gauge with respect to the Lagrangian frame of reference. ε_t is a constant representing the timing errors. Using $x_1 = X_G$ in equation 6.10 (i.e., start the accumulation at the radar pixel just above the rain-gauge), equation 6.10 becomes:

$$t_l = t_{rad} - \frac{C}{V} + T_{drop} + \in_t \tag{6.11}$$

Combining the time due to wind drift, the dropping time, and the timing error in one parameter *(TS2)*:

$$t_1 = t_{rad} + TS2 \tag{6.12}$$

Where:

TS2 = Time shift between the data of the two sensors (min).

Accordingly, to calculate the average radar rainfall intensity and the corresponding average gauge intensity over accumulation period T using method 3, three parameters (A,b, *TS2*) are required giving that the correction for advection is performed. Briefly, the approximation is that rainfall integration over a distance ($T \times V$) on the radar image in the storm direction corresponds to TB rainfall accumulation over a time period T but is shifted by *TS2* from the time of the radar scan.

The advection velocity is estimated using the cross-correlation technique. This procedure has the advantage of taking into account the detailed shape of the echo being tracked, and decreases the chances of mismatching echoes. The technique is described briefly in section 5.8.2 and the complete details of the technique are described in Chapter 7. Instead of using the whole radar domain for estimating the advection velocity a smaller sub-domain, centralized at the rain-gauge network, is used to avoid the effect of any relative motion (internal motions in the rainfall field) in the rainfall field on bigger scales. The sub-domain used for the cross-correlation

analysis is shown in Figure 6.3. The time and space scales used in the application of the cross-correlation are similar to ones used by Landel et. al. (1999) to characterize rainfall variables at very fine spaces and time scales. Note that radar data implies a velocity resolution of 1 km / 10 min or 6 km/hr for motions between consecutive frames.

6.4 Methodology

The methodology used to address the effect of the sampling errors is to calculate the reduction in the radar-gauge scatter due to the introduction of a new parameter. Parameters are used on a one parameter at a time basis. Each parameter accounts for some sources of errors, as described in section 6.2 and 6.3. The three methods of calculating radar and gauge intensities, described in section 6.3 which include some or all of the parameters mentioned above, are to be compared in terms of reducing the variation in the scatter of the two sensors. The calibration using each method is done on a per storm basis and for different accumulation periods. The accumulation periods considered in this analysis are 1, 3, 5, and 10 minutes. For each event, accumulation method, and accumulation period, the parameters are optimized by minimizing an objective function. The reduction in the radar-raingauge scatter is then assessed in terms of the value of the minimized objective function.

6.4.1 The Objective Function

The Z-R parameters and other error parameters are optimized by minimizing an objective function. The objective function is the root mean square (*RMS*) difference between radar and rain-gauge estimated rainfall intensities and is defined as following:

$$RMS_{T,\theta} = [\frac{1}{N_r N_g}\sum_{i=1}^{N_g}\sum_{j=1}^{N_r}(I_{g(\theta,T,i,j)} - I_{r(\theta,T,i,j)})^2]^{1/2} \qquad (6.13)$$

Where:

N_g = The number of rain-gauges.

N_r = The number of radar scans.

θ = An integer representing the method used for calculating rainfall intensities.

T = The accumulation period used for calculating rainfall intensities.

$I_{g(\theta,T,i,j)}$ = Rain-gauge rainfall intensity (mm/hr) based on method θ and accumulation interval T.

$I_{r(\theta,T,i,j)}$ = Radar rainfall intensity (mm/hr) based on method θ and accumulation interval T.

The reason for choosing rainfall intensity in mm/hr instead of accumulations, as is usually done, is to standardize the objective function to operate on different accumulation intervals for comparison purposes. Note that N_g and N_r are constant for each storm and independent of the accumulation period, thus allowing the

comparison of the *RMS* values for the same storm based on different accumulation intervals. Minimizing the objective function provides an estimate of the optimal parameters values. Due to the complexity of the characteristics of the surface of the objective function in multi-parameter space, it was decided to use a full enumeration search strategy that searches the whole parameter space for global minimization of the objective function. This avoids the expected difficulties associated with the objective function. Table 6.1 shows the lower and upper bounds as well as the incremental steps used for the parameters in the full search optimization process.

Table 6.1 Limits of the Parameter Space

Parameter	Lower Bound	Upper Bound	Increment
A	10	300	10
b	0.1	3	0.1
TS1	-6	8	1
TS2	-6	8	1

In case the obtained optimum value lies on the boundary of the parameter space, this bounding limit is expanded and the search continues in the expanded area until the final optimum is enclosed inside the bounding limits (i.e., until it is not on the edges of the parameter space). It should be noted that the calibration is unconditional (i.e, zero radar and gauge values are included).

6.4.2 Evaluation Criterion

In order to assess the improvements in explaining the variations between radar and rain-gauges due to the use of a certain method of calculating rainfall intensities and/or due to the use of a different accumulation interval, the *RMS* is compared to its value using a reference combination. The effect of using a certain method and/or using a different accumulation interval is evaluated by calculating the relative reduction in the radar-raingauge *RMS*. The relative reduction in *RMS* (*RMSRED*) is defined as:

$$RMSRED_{\theta,T} = \frac{RMS_{T,\theta_{opt(Ref)}} - RMS_{T,\theta_{opt}}}{RMS_{T,\theta_{opt(Ref)}}} \tag{6.14}$$

Where:

$RMS_{T,\theta\,opt}$ = Minimum *RMS* using a certain method and certain accumulation period.

$RMS_{T,\theta\,opt\,(Ref)}$ = Minimum *RMS* using a reference.

6.5 The Data Set

The study area is the same area used in Chapter 3 (refer to section 3.2.1). The location of the rain-gauges with respect to the radar rainfall grid were determined according to the gravitational projection method developed in Chapter 4, which is incorporated into the GIS interface developed in Chapter 5. The location of the rain-gauge network with respect to King City Radar is shown in Figure 3.2. The data sample consists of 8 storm events covering a period of 5 months in the summer of

1989. The 8 events are mostly high intensity events, that were selected to minimize the effect of the sampling mechanism of TB gauges. Rain-gauge data are in the form of one minute accumulations and the radar data are the CAPPI reflectivity scans with regular ten minute temporal spacing and one kilometer spatial resolution. Table 6.2 describes the 8 events considered.

Table 6.2 Rainfall events in 1989 used for the sampling errors analysis

Event No.	1	2	3	4	5	6	7	8
Day-Month	30-5	31-5	2-6	9-6	4-8	1-9	8-9	22-9
Type	c/w	c/w	c/w	c	c	c	c	w

w = Wide spread rain

c = Convective

c/w = Mixed-type

6.6 Results of the Sampling Effects

The optimization process is applied on a per storm basis and for accumulation durations of 1, 3, 5, and 10 minutes using the three methods of calculating rainfall intensities described in section 6.3. Eight rainfall events are used, producing a total number of 88 optimization runs. To facilitate the distinction between the different methods and accumulation intervals, the following terminology is used: the letter M is used to denote an accumulation method, and the letter T denotes an accumulation time interval. The integer adjacent to the letter M represents the method's number and the number adjacent to the letter T represents the accumulation period in

minutes. For example, M2T5 represents method 2 using 5 minutes accumulation period. The total number of optimization runs is 88 instead of 96 because the runs for M2T1 are the same as M3T1 by definition, hence the M3T1 results for the 8 storms are taken the same as M2T1 results. The optimum parameters obtained from each optimization run, as well as the raw *RMS* values, are shown in Tables 6.3, 6.4, and 6.5.

Table 6.3 Optimization output using method 1

Event Number		1	2	3	4	5	6	7	8
1 min	*A*	5	5	20	10	90	10	10	40
	b	2.2	2.2	2.1	2.2	1.1	2	2.2	1.7
	RMS	8.67	6.67	5.7	7.47	2.55	6.42	6.75	6.34
3 min	*A*	5	10	10	10	110	5	20	50
	b	2.2	1.9	2	2.2	1.2	2.2	2	1.6
	RMS	6.42	5.22	4.71	4.86	1.56	4.25	4.64	5.43
5 min	*A*	5	30	10	10	50	20	10	40
	b	2.2	1.6	2	2.2	1.5	1.6	2.1	1.7
	RMS	5.63	4.52	4.53	4.65	1.51	4.12	4.59	4.92
10 min	*A*	5	20	5	20	60	5	30	30
	b	2.3	1.8	2.4	1.9	1.4	2.2	2.2	1.8
	RMS	4.52	3.76	3.99	4.68	1.6	3.98	5.16	4.62

Figures 6.4, 6.5, and 6.6 show examples of rain-gauge intensity versus radar intensities for three storm events according to the optimum parameters obtained. As shown on the three figures, the scatter of the gauge/radar pairs is reduced when increasing the accumulation period for any of the methods used. This can be related mainly to the TB sampling errors in short accumulation intervals. Correction of

sampling errors explains some of the variability (i.e., reduces the scatter) as shown when using method 2 & 3 when using the same accumulation interval. In addition, the following points summarize the results of the sampling errors analysis:

Table 6.4 Optimization output using method 2

Event Number		1	2	3	4	5	6	7	8
1 min	*A*	30	5	20	10	140	10	20	40
	b	1.5	2.2	2.2	2.1	2.1	2	2.2	1.7
	TS1	-2	1	5	-1	1	0	2	0
	RMS	5.87	6.65	5.22	6.09	1.68	6.42	4.7	6.35
3 min	*A*	10	10	20	10	70	5	40	30
	b	2	1.9	2	2.2	1.4	2.2	2	1.8
	TS1	-2	0	1	0	1	0	2	1
	RMS	4.2	5.22	3.75	4.86	1.42	4.25	4.39	5.17
5 min	*A*	10	10	10	10	60	10	15	30
	b	2.2	2	2.2	2.2	1.5	2	2.2	1.8
	TS1	-2	1	1	0	1	1	1	2
	RMS	4.11	4.61	4.55	4.65	1.42	3.98	3.46	4.85
10 min	*A*	10	10	10	10	60	5	20	30
	b	2.2	2.2	2.2	2.2	1.4	2.2	2.2	1.8
	TS1	-2	0	-2	1	0	0	1	0
	RMS	4.32	3.89	3.5	4.59	1.64	3.98	4.53	4.64

1- Regardless of the accumulation method used, increasing the accumulation period reduces the *RMS* with respect to 1 min values as reference (refer to Tables 6.3, 6.4, and 6.5). This can be related to the fact that TB rain-gauge sampling errors decrease when increasing the accumulation period. The average increase in *RMSRED* due to using different accumulation intervals

with respect to 1 min *RMS* as reference is shown in Figure 6.7. In other words, Figure 6.7 shows the effects of the different accumulations intervals on reducing the variations between radar and rain-gauges. It can be concluded that increasing the accumulation period from 1 to 10 minutes reduces the scatter by 30% on average in terms of the root mean square error.

Table 6.5 Optimization output using method 3

Event Number		530	531	602	609	804	901	908	922
1 min	*A*	Similar to method 2 by definition							
	b								
	TS2								
	RMS								
3 min	*A*	20	10	10	10	60	20	20	40
	b	1.6	1.9	2.2	2.2	1.3	1.7	2	1.7
	TS2	-2	1	0	-1	1	-1	0	2
	RMS	4.14	4.39	3.81	4.89	1.25	3.91	3.75	4.59
5 min	*A*	20	10	20	20	60	20	10	30
	b	1.6	2	1.7	1.9	1.5	1.6	2.1	1.8
	TS2	-3	1	-1	-2	-1	-1	-1	1
	RMS	3.7	4.25	4.6	4.7	1.1	3.75	2.75	4.71
10 min	*A*	50	40	20	20	50	10	10	60
	b	1.2	1.4	1.8	1.8	1.4	2	2.1	1.5
	TS2	-2	1	-1	4	-2	4	-2	4
	RMS	2.94	3.03	4.01	5.01	1.31	3.58	3.83	4.59

2- Regardless of the accumulation period used, the corrections for sampling errors reduce the *RMS* (i.e., increase the *RMSRED*). Note the reduction in

RMS values after using methods 2 & 3 (refer to Tables 6.3, 6.4, and 6.5) for the same accumulation period. Figure 6.8 shows the average increase in *RMSRED* due to using methods 2 & 3 with respect to method 1 as a reference. The reduction in the gauge/radar variability is approximately 20% on average in terms of the root mean square error.

3- Given that the calibration is unconditional (zero values from both sensors are used), the estimated optimal parameters showed neither clear dependence on the accumulation period nor the method followed for accumulating rainfall depths. In addition, changes in the optimal parameters from event to event are minimal as shown in Tables 6.3, 6.4, and 6.5 even though cases of convective and widespread rainfall are used. Table 6.6 shows a weighted average for the Z-R parameters of the storm analyzed (weighted according to the number of Z-R pairs in each storm) based on method 3.

Table 6.6 Average Z-R Parameters obtained using data from 1989

Period	A	b
3 min	26	1.8
5 min	25	1.8
10 min	40	1.6

It should be noted that the Marshal&Palmer (M&P) relation (A = 200, b = 1.6) (Marshal,and Palmer, 1948) is currently used by King City radar for rainfall conversion. Accordingly, the use of Marshal&Palmer relation is clearly

biased and can lead to a serious underestimation of rainfall rate in the study area. This result will be verified using recent data from years 2000 and 2001 in section 6.8.

4- An inspection sensitivity of the parameters is performed by observing the variation of the objective function (i.e., the *RMS*) around the optimal value. This means observing the *RMS* sensitivity corresponding to changing the value of one parameter and keeping the other parameters at their optimal values. The procedure is done by sorting all possible combinations of the parameters in ascending order according to the *RMS* values. In the region of the lowest *RMS* values, the parameter with the smallest variation is then observed and selected as the most sensitive parameter. The results showed that rainfall estimation for 5 and 10 minute accumulations is more sensitive to the exponent *b*, while for shorter accumulation periods, the estimation is more sensitive to the time shift.

6.7 High Resolution Radar Data

In the one minute optimization done above, the number of data pairs used for one event is equal to the number of radar scans. This means that for each radar scan, only one value from each rain-gauge, which corresponds to the value of the radar value above, is used. Although this rain-gauge temporal averaged value may be shifted in time according to methods 2 & 3 it is still only one value. The reason for this, as mentioned above, is to standardize the number of data points to enable the

comparisons between the different accumulation intervals and the different accumulation methods. In this section, 10 pairs (i.e., one minute values from radar and gauge) can be extracted for each radar scan. This is accomplished by advecting the radar rainfall field according to the velocity vector in every minute. The value of the radar pixel above the rain-gauge and its corresponding value from the gauge (shifted in time by *TS2*) are extracted. Hence, the total number of data pairs for each storm in this calibration process is ten times the number of pairs in the calibrations done in the previous section. Table 6.7 shows the optimum parameters obtained (based on one minute rainfall intensities) using this method of calibration. The optimum Z-R parameters, as shown in the table, are close to those obtained in the previous section and both show departure from Marshal&Palmer equation.

Table 6.7 Optimization output using one minute advected data

Event Number		1	2	3	4	5	6	7	8
1 min	*A*	30	10	10	10	30	10	10	20
	b	1.5	1.9	2.1	2.2	2	2	2.1	2
	TS2	-2	0	-1	-1	-2	-1	-1	-2
	RMS	7.27	6.76	7.7	7.2	3.3	7.13	7.3	7.1

One minute hyetographs can be extracted from the radar scans by using the methodology of advecting the rainfall field in each one minute according to the velocity vector. The obtained optimal Z-R parameters are used. Figures 6.9, 6.10, and 6.11 present an example (Sept. 8, 1989) comparison of rainfall hyetographs extracted from radar and rain-gauge data. Figure 6.9 shows the rainfall hyetographs recorded

at the rain-gauge network, and Figure 6.10 presents the corresponding one minute hyetographs extracted from radar scans by correcting for advection. Figure 6.11 shows the advance of the storm event as recorded by radar scans. As shown on Figures 6.9 and 6.10, and using the visual inspection of the rest of the storm events, the one min hyetographs obtained from radar data by correction for advection agree with those obtained from rain-gauges in terms of shape, time to the centre of gravity of the hyetographs, and volume of rainfall (from table 6.7, the average root mean square error = 6.72 mm/hr). This RMS value indicates that a convective storm of 10 minutes duration will have an average error less than 1.12 mm in the estimated total volume (i.e. depth) of rainfall between radar and gauges. It should be noted that the one minute radar extracted hyetographs underestimate the peaks of rainfall intensities obtained by the rain gauges. The peak intensities, which are important in "flash flood" conditions are smoothed out in the radar scans. For example, as shown in Figures 6.9 and 6.10, the radar extracted peaks at the locations of HAR and DAF are 25 and 20 mm/hr while the rain-gauges values are 80 and 65 mm/hr respectively. With improved radar rainfall estimation (via the correction for the measuring errors as recommended in section 8.3), the agreement between the two sensors would increase and the data would be appropriate for high resolution hydrological applications. This is also due to the additional advantage of the spatial detailing of radar detected rainfall fields that are useful for distributed hydrological modelling. This spatial detailing can not be obtained using rain-gauge networks unless a very dense rain-gauge network is used. It should be noted that this result is conditioned on the unbiased calibration of radar

rainfall estimation of rainfall. However, the improvements that radar high resolution data can provide in watershed modeling must be evaluated through hydrological modelling to establish a general conclusion. The most recommended approach is a study using a distributed hydrological model and sufficient data (i.e., rainfall data from gauges and radar and the corresponding runoff for different watersheds). This recommended study will require parameters optimization to eliminate the effects of the other hydrological parameters (i.e., infiltration, land use, and travel time parameters and their estimation methodologies....etc). For example, half of the events for each basin may be used for parameters optimization of the distributed model and the other half for establishing the conclusion.

6.8 Accuracy Assessment of King City and Exeter Regional Radars

Since the calibration performed in the sampling errors analysis has shown serious underestimation (approximately 30-40% of the rain-gauge rainfall, refer to table 6.6) of the classical Marshal&Palmer equation $Z=200R^{1.6}$ using data from 1989, and since the Canadian National radars use this equation for rainfall conversion , it is essential to verify this result using recent radar and gauge data. The classical M&P equation is used world wide (Illinois, New York, Oklahoma, Finland, England, and other areas) in many radar systems for various storms types (Collier, 1989). As emphasized by Austin (1987), the extent to which results from one study can be applied to other geographical locations is questionable. Accordingly, one relationship may not be used successfully for all Canadian sites without being adequately verified.

Several investigators have analysed the relationship between radar and rain gauge precipitation totals for various locations (Woodley and Herndon, 1970; Wilson and Brandes, 1979; Austin, 1987; Brandes and Wilson, 1988; Wilson et al., 1997; and others). Woodley et. al. (1975) recommended $Z=300R^{1.4}$ which is known as the Fort Collins equation which is recommended in Florida for showers and thunderstorms. Wilson and Brandes (1979) suggested that even for similar type storms in the same geographical area, variations in the Z-R relationship may exist. Thus, an average empirical Z-R relationship must be used. Austin (1987) recommended the standard $Z=300R^{1.3}$ (the default Z-R relation is the precipitation processing subsystem followed in NEXRAD in the United Sates) for intense convective cells . However, many researchers have reported that the standard Z-R relations ($Z=300R^{1.4}$, $Z=400R^{1.3}$, and $Z=200R^{1.6}$) are underestimating rainfall rate (Woodley and Herndon 1970; Smith et al., 1996; and others), which supports the results obtained in the previous sections. Blanchard (1953) recommended $Z=31R^{1.71}$ for orographic rain in Hawaii. Accordingly, based on the previous studies, one can conclude that a single Z-R relationship may not be adequate to provide the appropriate conversion for all precipitation types that occur in various geographical areas. Geographic variability of the Z-R relations for the United States are discussed by Smith and Krajewski (1993).

This section proposes an analysis to assess the accuracy of two Canadian radars (King City and Exeter) in terms of rainfall estimation. Two questions are discussed in this part: (1) is there a significant difference in rainfall estimated from the two radars; and (2) what is the most appropriate Z-R conversion for use in southern

Ontario by the two radars? In section 6.8.1, an intercomparison between the two radars is performed while in section 6.8.2 the two Canadian radars are calibrated by performing a radar-gauge comparison using a network of gauges in southern Ontario.

6.8.1 King City Radar Versus Exeter Radar

King City and Exeter radars are located in southern Ontario, (79.5742W, 43.96389N) and (81.3842W, 43.37027N) respectively. The circles of the two radars intersect making a common area that is covered by both radars as shown in Figure 6.12. The main objective of this part is to check the hypothesis that there is no significant difference in rainfall estimates from both radars. Rainfall estimates by the two radars in their common area are to be compared in order to achieve this task. The comparison will be based on the criterion described in the following subsection.

6.8.1.1 Data and Comparison Criterion

The test radar data cover 4 events in 2000 and 6 events in 2001, i.e., 1440 CAPPI scans from both King City and Exeter Radars (refer to Table 6.8).

Table 6.8 Rainfall events used in 2000 and 2001 from King City and Exeter

Event	1	2	3	4	5	6	7	8	9	10
Year	2000	2000	2000	2000	2001	2001	2001	2001	2001	2001
d\m	10\5	11\5	12\5	13\5	28\5	3\6	10\6	10\7	20\7	2\8
Type	w/c	w	w/c	w	w	c	c	w	c	w

w = Widespread rain

c = Convective

w/c = Mixed-type

In order to explain the comparison procedure, let $\Re$ denote a common domain between the coverages of the two radars. Let I_k and I_c denote instantaneous rainfall intensity from King City and Exeter radars respectively, which are taken at the same nominal time at an arbitrary point belonging to $\Re$. The comparison between the two radar scans at a nominal time is done by comparing the absolute error, bias , and correlation coefficient calculated using all possible pairs (I_k , I_c) in $\Re$, that fall within a range of 150 km from both radars. The average absolute error, bias, and correlation coefficient (CC) are calculated by summing over all possible King-Exeter intensity pairs in the common area as following:

$$Absolue\ Error = \frac{1}{n}\sum_{\Re}|I_k - I_c| \tag{6.15}$$

$$bias = \frac{\sum_{\Re} I_k}{\sum_{\Re} I_c} \tag{6.16}$$

$$CC = \frac{\frac{1}{n}\sum_{\Re}(I_k - \bar{I}_k)(I_c - \bar{I}_c)}{\sigma_{I_k}\sigma_{I_c}} \tag{6.17}$$

Where:

n = Number of included King City/Exeter pairs in the common area.

σ_{I_k} = Standard deviation of King City estimation of rainfall in the common area.

σ_{I_c} = Standard deviation of Exeter rainfall estimation in the common area.

It should be noted that the calculations of the absolute error and bias are conditional (zero values are not included), whereas in the case of the correlation coefficient, the calculation is unconditional (zero values are included).

6.8.1.2 Results.

At each nominal time the rainfall fields obtained from both radars are clipped inside the common domain and equations 6.15, 6.16, and 6.17 are applied. Rainfall conversion is accomplished by using ($Z=30R^{1.6}$) based on the results obtained in the previous sections. The calculated bias (eq. 6.16) can be seen as the slope of the regression line of a scatter plot between King City and Exeter estimated intensities at this nominal time while the correlation coefficient (eq. 6.17) conveys the degree of linear relationship of this scatter. An example of such scatter is shown in Figure 6.13. In order to summarize a full event the absolute error, bias, and correlation values are calculated for each time step (10 minutes spacings) and plotted with respect to time on the X-axis. Examples of such event-plots are shown in Figures 6.14 and 6.15. Each point in these event plots represents a separate scatter plot similar to Figure 6.13. The event plots show small variations, with respect to time, in the bias around a mean value close to one, indicating small overall bias between the two radars. Table 6.9 shows the average overall statistics considering all events. The average overall bias is 1.066 with standard deviation 0.24. Statistically and assuming normal bias distribution these values indicate that King City estimation is different than Exeter estimation at the statistical significant level (95 % significant level for example). This

can be obtained by constructing a test of hypothesis with null hypothesis (Bias = 1) and a sample size of 1440 scans. However, and from the practical significance point of view, the departure of 1.066 from one has little "engineering significance" with regard to areal rainfall estimation. In addition, the correlation value slightly varies around an average of 0.62, which considerably high compared to the typical average correlation coefficient between two consecutive scans from the same radar. Accordingly, and based on the storms analyzed, it can be concluded that there is good agreement between rainfall fields estimated from both radars and it is expected that both radars should use similar Z-R conversions.

Table 6.9 Overall statistics between King City and Exeter radars

Statistic	Average	Std. Deviation
Overall Bias	1.066	0.24
%Absolute Error	29.3	28
Correlation	0.62	0.11

It should be noted that the quality of Exeter data suffers less from ground and clear air echoes than King City radar. Hence, for Hamilton-Wentworth Region, it is recommended to use data from Exeter for real-time applications. Data from Exeter are also recommended because the majority of rainfall storms advance from the west and south west region, which is covered by Exeter radar as shown in Chapter 3.

6.8.2 Z-R Calibration of the Canadian Radars (King City and Exeter)

The rainfall events shown in Table 6.8 are used to calibrate the two radars. In addition to these 10 events, 15 rainfall events from the summer of 2001 are used to increase the data set for King City radar. Rain-gauge data were obtained from a network of 12 gauges in southern Ontario (Figure 6.16). The network is operated by Environment Canada. The temporal resolution of the gauge data was integrated to 10 minutes. The purpose of this section is to calibrate the Z-R parameters of both radars and to verify the results obtained using the data from 1989 (refer to Table 6.6). The following points summarize the calibration process:

- Eight gauges are used for King City calibration and seven gauges are used for Exeter calibration. The number of common gauges between the two radars is four gauges.
- The calibration of both radars is conditional for the 10 minutes calibration (i.e., gauge values less than 8 mm/hr are excluded), and unconditional for the hourly calibration. The times where there is radar data contamination are excluded from the calibration.
- The calibration is done using non-linear regression by determining the Z-R parameters that minimize the *RMS* between rainfall intensities from the radars and gauges. Since the effect of sampling errors on the radar calibration results is negligible when bigger accumulation intervals are used (refer to section 6.6), a stationary rainfall field with no timing errors is assumed for simplicity. Hence, the *RMS* is calculated from equation 6.13 whereas rainfall intensities

from radar and gauges are calculated from equations 6.4, and 6.5.

- The calibration is done using rainfall intensities based on two accumulation periods (10 minutes, and 1 hr) in order to explore the effect of increasing the accumulation interval up to 1 hr.

The results of the 10 minutes comparisons for both radars (based on the 10 events shown in Table 6.8) are shown on Figures 6.17, 6.18, 6.19 and the results for the 1-hr calibration are shown in Figures 6.20, and 6.21. For King City radar, the 15 additional events in year 2001 are added to 10 events shown in Table 6.8 to produce Figures 6.19 (for 10 minutes accumulation interval) and 6.21 (for 1 hr accumulation interval). The upper figure in Figures 6.17, 6.18, and 6.19 shows gauge intensity versus radar reflectivity plotted on a logarithmic scale, the middle figure plots radar intensities (calculated using M&P equation) versus gauge intensity. The lower figure shows radar intensity (calculated using the calibrated Z-R equation) versus gauge intensity. As shown on all figures, there is clear evidence to support the results obtained from the analysis done on data from 1989 (Table 6.6) that M&P equation is biased and can lead to underestimation of rainfall. In addition, the effect of increasing the accumulation interval on the calibration results is negligible. It is recommended for King City to use $Z = 40R^{1.65}$, and $Z = 40R^{1.77}$ should be used for Exeter. Based on the radar/rain-gauge data comparisons by using a 8 mm/hr threshold, an average Z-R relation is $Z = 40R^{1.7}$, which is recommended for unbiased rainfall conversion for both radars. This equation is very similar to Blanchard (1953). Additional data will eventually refine these coefficients and their variances.

The reason for advocating the linear approach between log Z and log R is the theoretical background that is based on a spatiotemporal constant drop size distribution. In reality, the drop size distribution is not constant over space and time and can vary with the degree of rainfall intensity, therefore the linear approach is not strictly applicable (refer to Collier, 1989). It should be noted that the apparent variation (shown on the top figures of 6.17, 6.18, and 6.19) especially at low intensities is attributed to the gauges sampling mechanism (in addition to other sources of measuring and sampling errors) and not to additional non-linearities between log Z and log R (refer to Chapter 2 and section 6.1 for a list of these errors). The threshold value is 8 mm/hr (points under this threshold value are removed - the proposed model is not totally independent of the threshold value). The inclusion of these points to the figures will add additional variation and the false non-linearity that one may observe on the top figures between log Z and log R will disappear (refer to Figure 6.1 for a schematic explanation). The first part of this chapter established a methodology to address the effects of the sampling errors. Similar studies are recommended to account for the measuring errors in order to improve radar rainfall estimation by further reducing the scatter variance (a recommended approach is presented in section 8.3).

For the 10 minutes calibration King City bias is less than Exeter bias (from Figures 6.17 & 6.18: King/Exeter ratio = 0.306/0.535 = 0.62) when using the M&P equation which seems to contradict the results obtained in their comparison in section 6.8.1.2 (King/Exeter ratio = 1.066). On the other hand when calculating King/Exeter

ratio using the calibrated equations (from Figures 6.17 & 6.18: King/Exeter ratio = 0.9997/0.96 = 1.04), the ratio is consistent with the results obtained from the comparison in section 6.8.1.2 (that was done using parameters close to the optimal values). This shows clearly the non-linear effect of the Z-R conversion.

6.9 Summary

In this study, radar data are compared to rain-gauge data for different short term accumulation periods (1, 3, 5, and 10 minutes) to study the effects of the sampling errors. The results showed that correction for timing errors, wind drift, and advection reduces the difference between the two sensors. The sampling errors can be said to account for 20% on average of the scatter between the two sensors for short accumulation intervals (3, 5, or 10 minutes). The parameters of the Z-R relationship show no clear dependence on the accumulation period used for the calibration and/or the correction of sampling errors. One way to calibrate radar is to use 1 min advected values in between radar scans. The advantage of this technique is that it increases the number of data pairs used for regression, but correction for advection is essential in this case.

This chapter shows that, given that the Z-R relation is unbiased and that correction of advection is employed, one minute rainfall hyetographs can be extracted from radar data with minimum overall bias. There is relatively good visual agreement between radar extracted one minute hyetographs and rain-gauge hyetographs. This agreement raise confidence in the applicability of radar data for high resolution

hydrological applications. This is also due to the additional advantage of the spatial detailing of radar detected rainfall fields that is useful for distributed hydrological modelling. This spatial detailing can not be obtained from rain-gauge networks unless a very dense network is used. The expected improvements that this procedure can provide in watershed modeling in small basins should be evaluated through hydrological modelling.

Finally, it is shown that there is relatively good agreement between rainfall fields estimated by King City radar and Exeter radar. In addition, the analysis proves that the classical M&P equation used by the National Canadian radars is biased and can lead to serious underestimation of rainfall. The equation with the coefficients A=40 and b=1.7 fit better the present data but these coefficients are not statistically different than those of other equations and are very similar to Blanchard (1953) (the data used included 8 medium-to-high intensity rainfall events in 1989 in an event-by-event comparison, 25 low-to-medium intensity events from King City in 2000 and 2001 in one overall comparison, and 10 low-to-medium intensity events from Exeter in 2000 and 2001 in one overall comparison). The results of the radar calibration obtained in this chapter are required for the analysis of the next chapter. In the next chapter, the problem of rainfall prediction will be studied. This requires an unbiased estimation of rainfall fields for proper projection into the future.

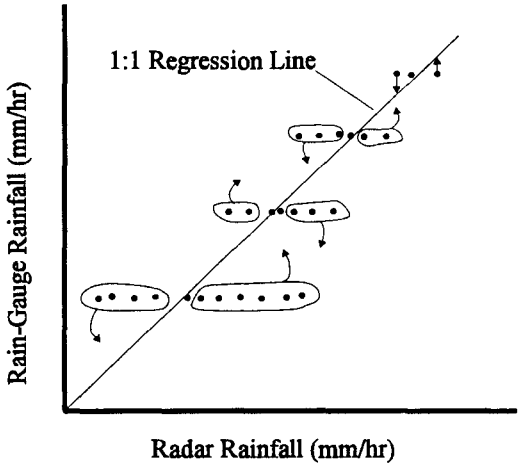

Figure 6.1 Schematic diagram showing the error caused by uncertainty of the tipping bucket mechanism.

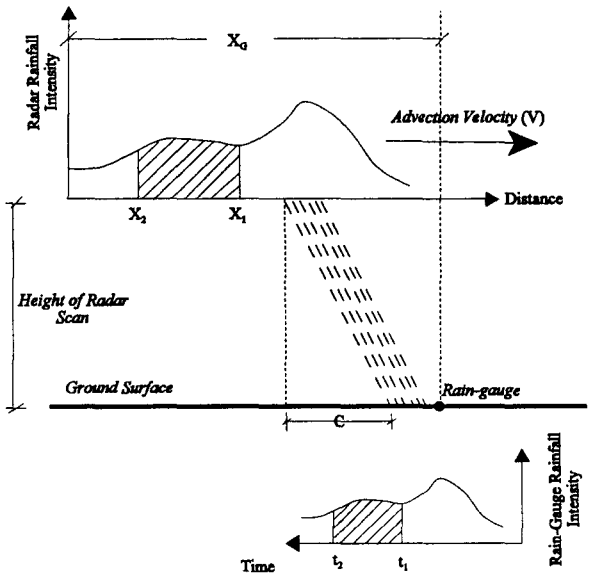

Figure 6.2 Schematic diagram showing the theory followed to account for sampling errors.

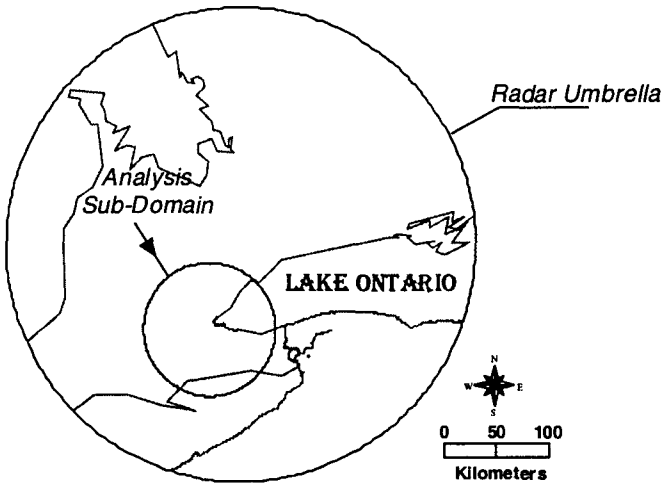

Figure 6.3 The sub-domain used for estimating the velocity vector of rainfall using the cross correlation technique.

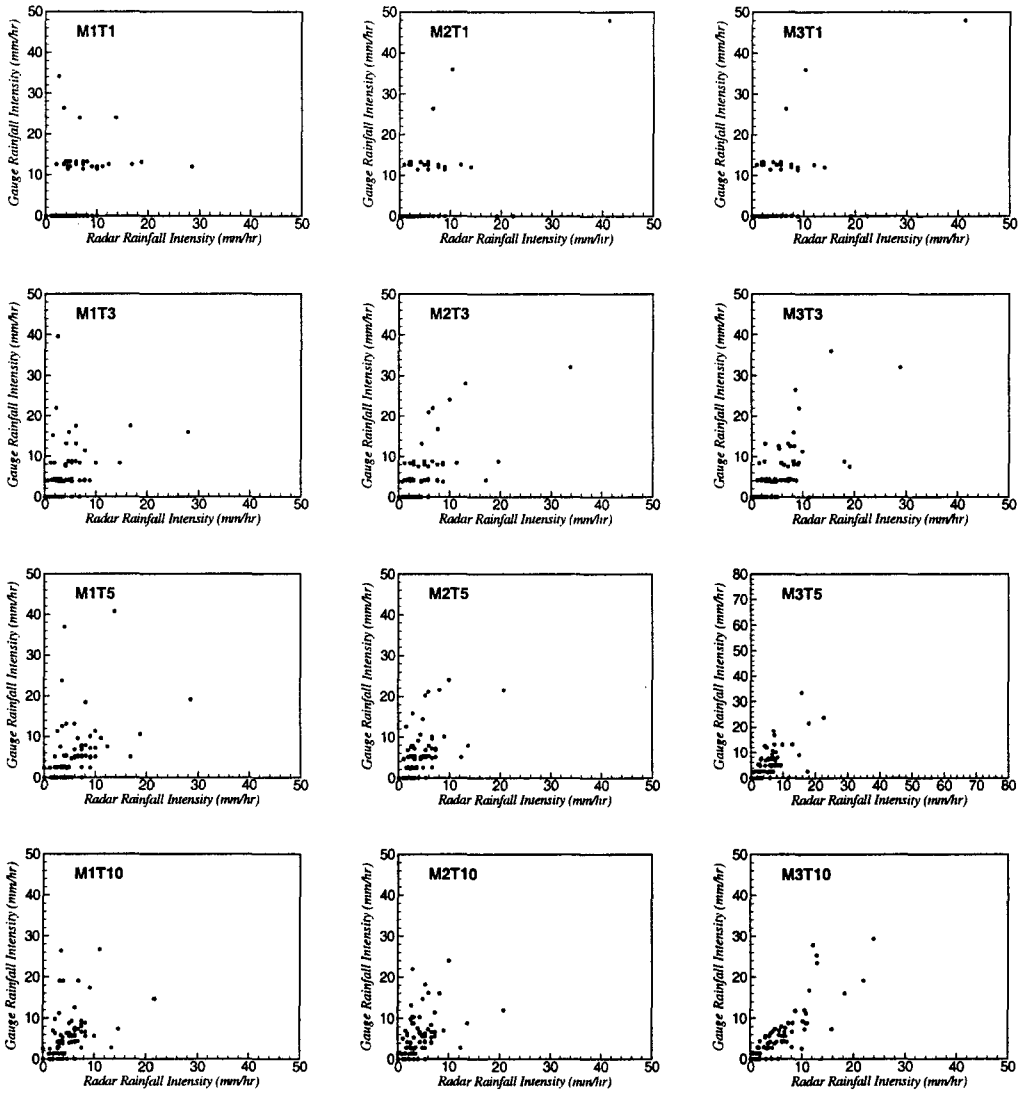

Figure 6.4 Test case of 30/05/1989. The left panel is for method 1; the middle panel represents method 2; and the right panel is for method 3.

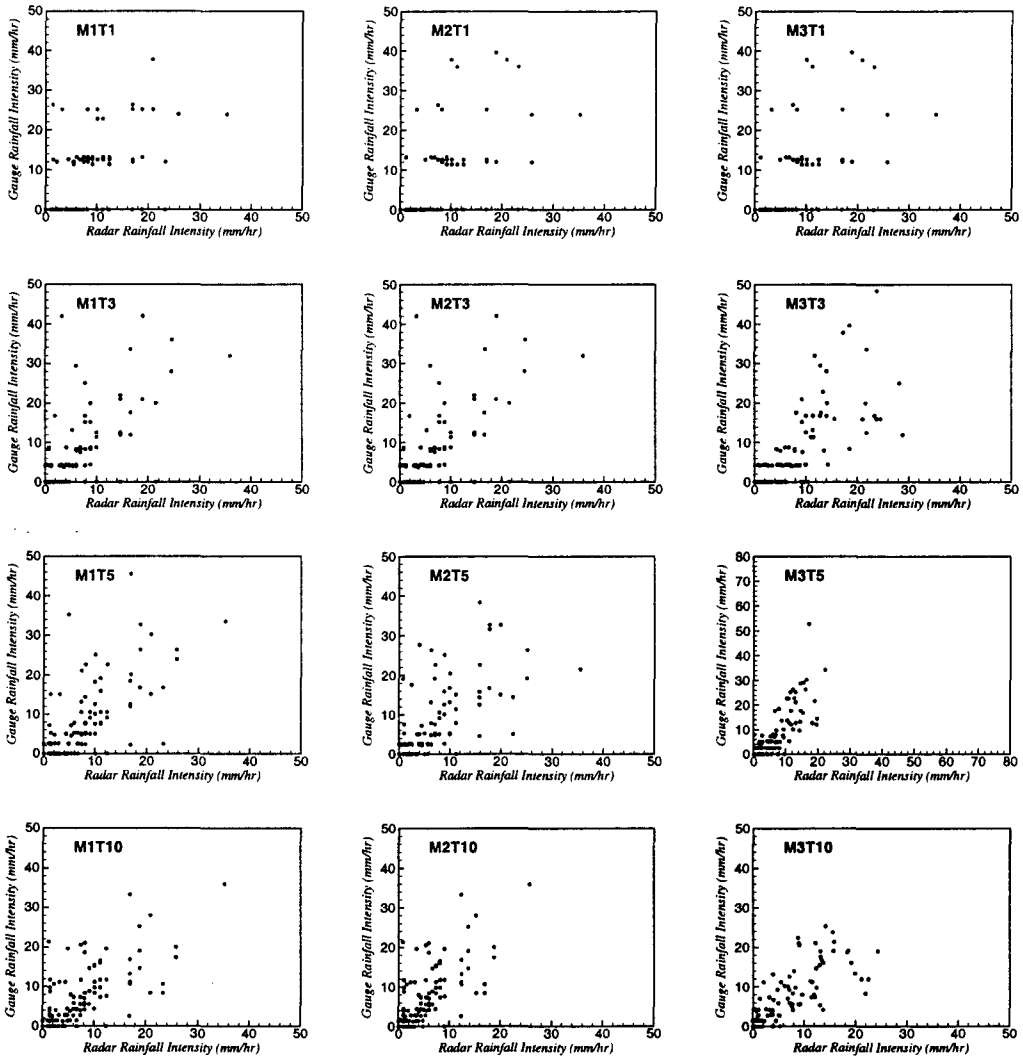

Figure 6.5 Test case of 31/05/1989. The left panel is for method 1; the middle panel represents method 2; and the right panel is for method 3.

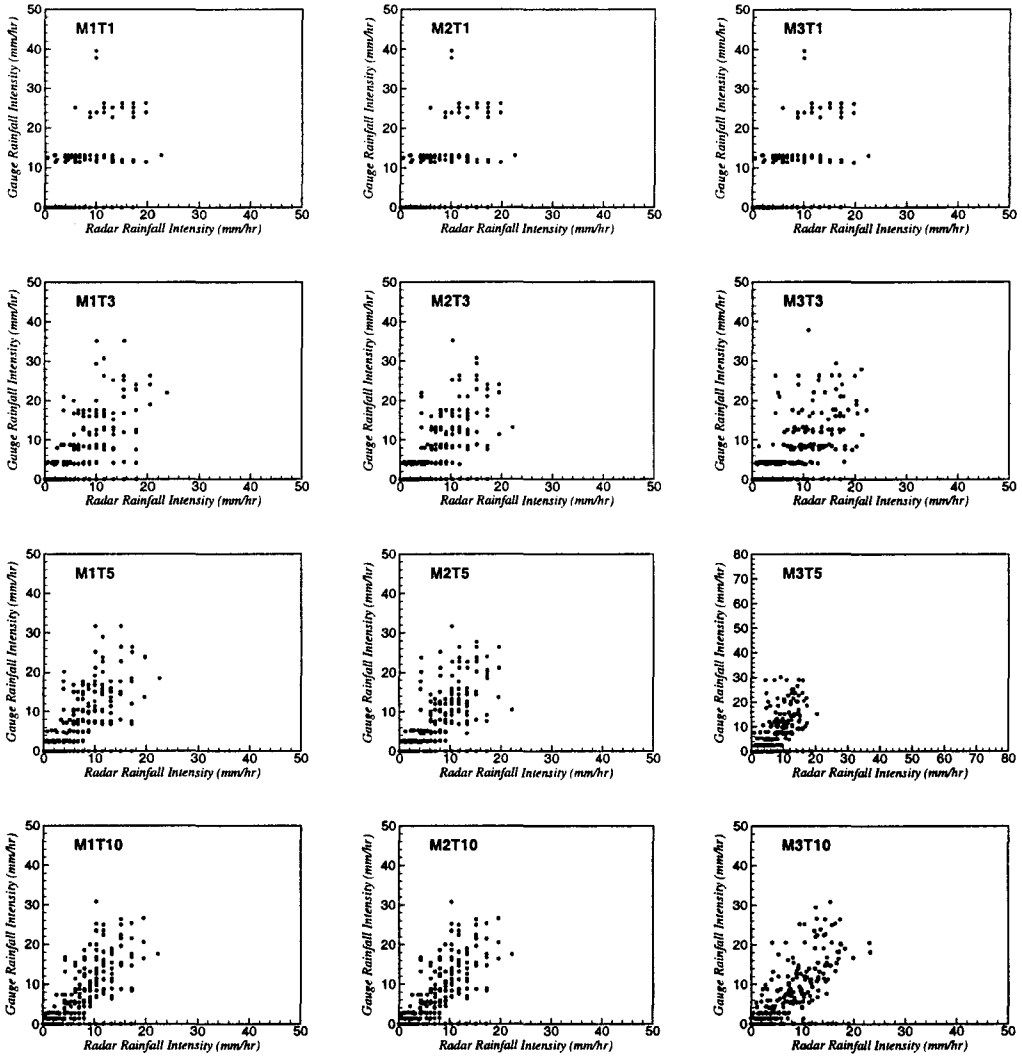

Figure 6.6 Test case of 22/09/1989. The left panel is for method 1; the middle panel represents method 2; and the right panel is for method 3.

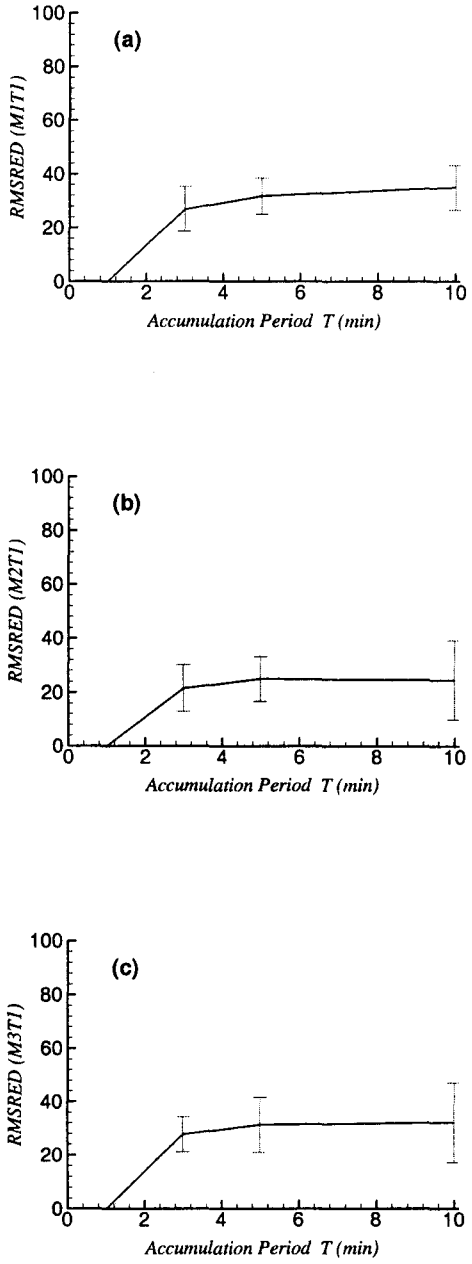

Figure 6.7 Effect of increasing the accumulation interval on the relative reduction in the room mean square error (*RMSRED*) by using: (a) method 1, (b) method 2, and (c) method 3.

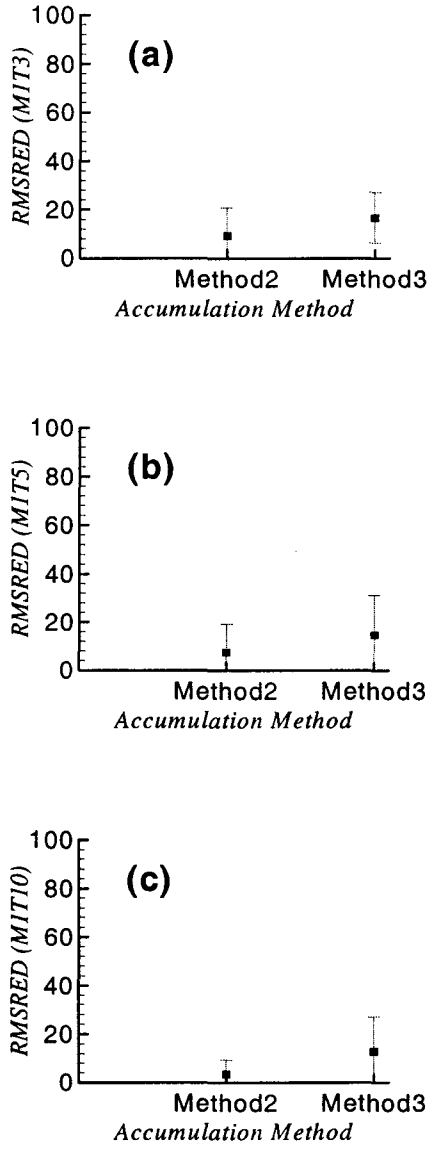

Figure 6.8 Effect of using the different methods of accumulating radar rainfall depths on the relative reduction in the room mean square error (*RMSRED*) by using: (a) 3 minute accumulation period, (b) 5 minutes, and (c) 10 minutes.

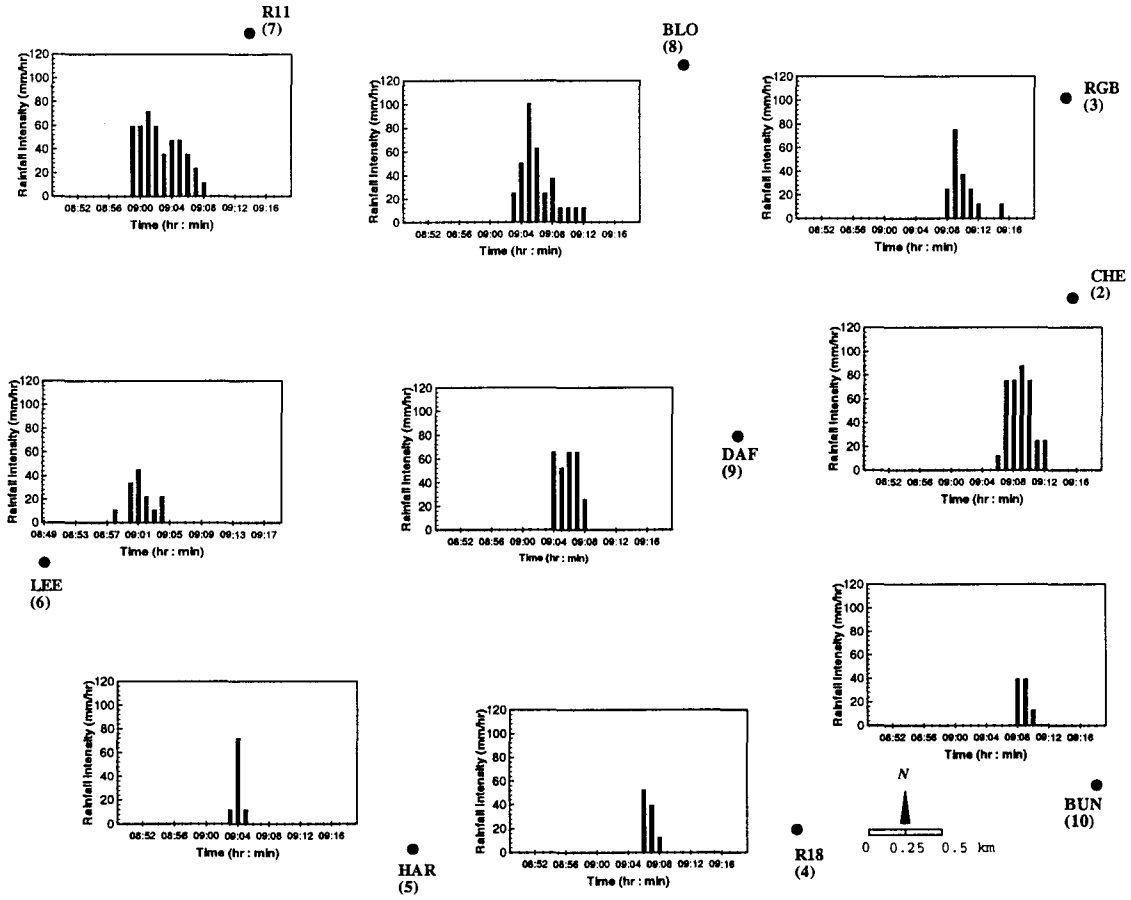

Figure 6.9 One minute rain-gauge measured hyetographs (Sept 8, 1989).

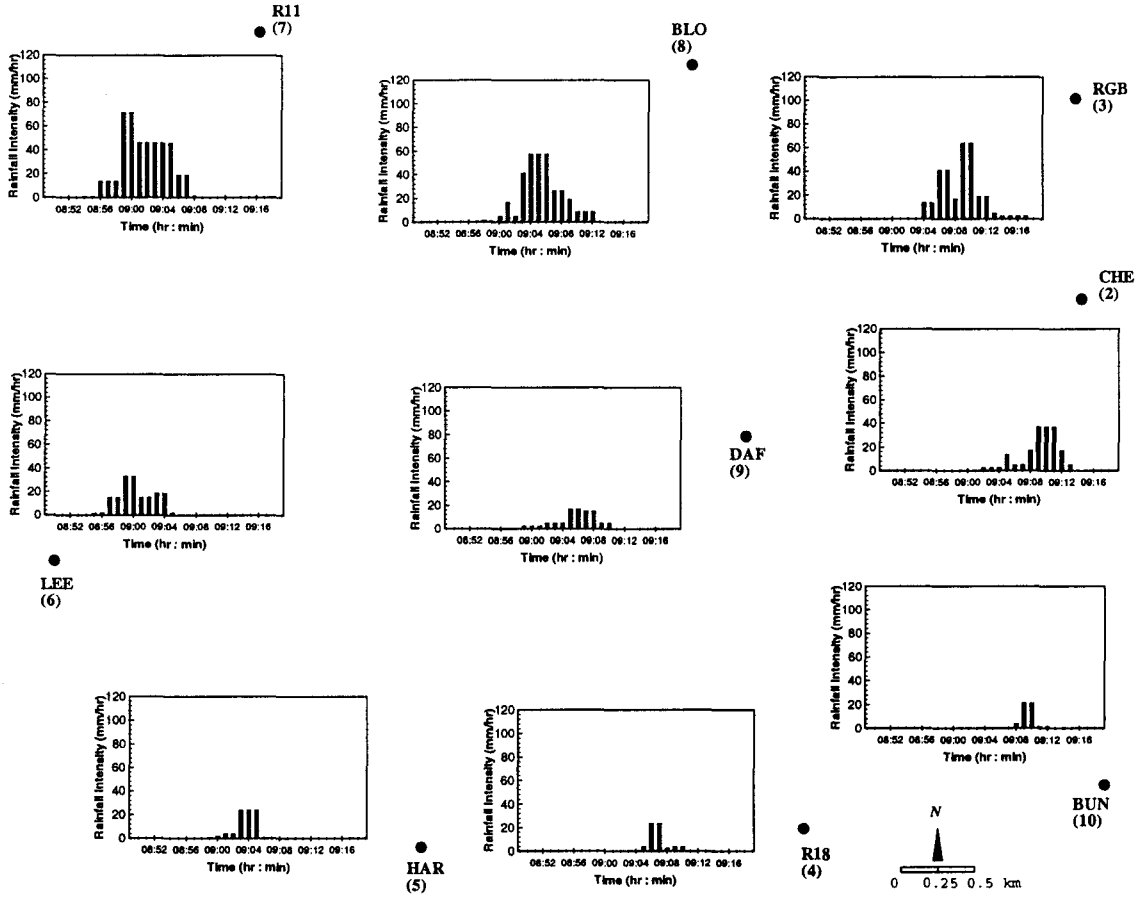

Figure 6.10 One minute radar extracted hyetographs (corresponding to Figure 6.9) developed using method 3 for the event of Sept 8, 1989.

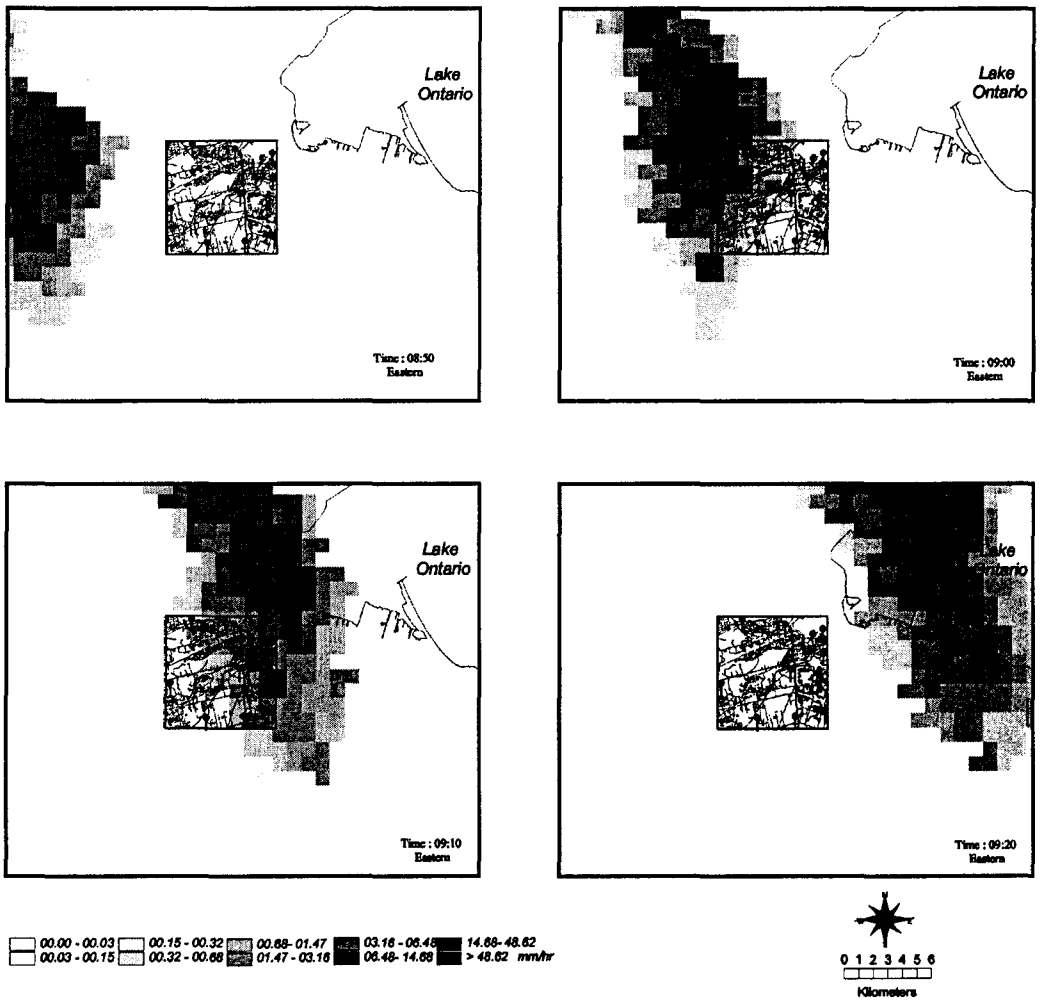

Figure 6.11 A series of radar grids (1 km^2) depicting the 10 minutes radar scans for the storm event of Sept. 8, 1989.

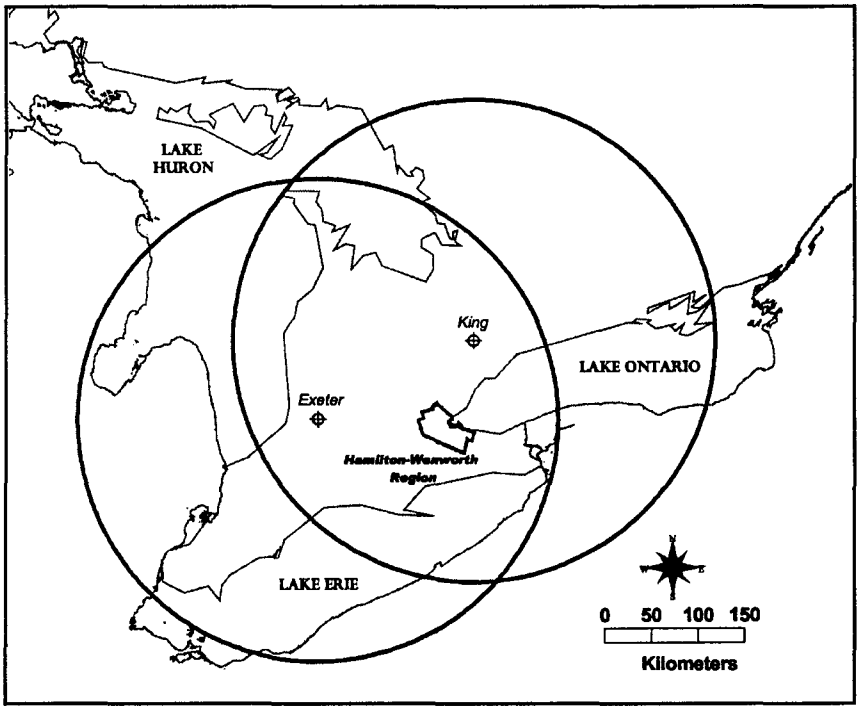

Figure 6.12 The common area between the coverages of King City and Exeter radars.

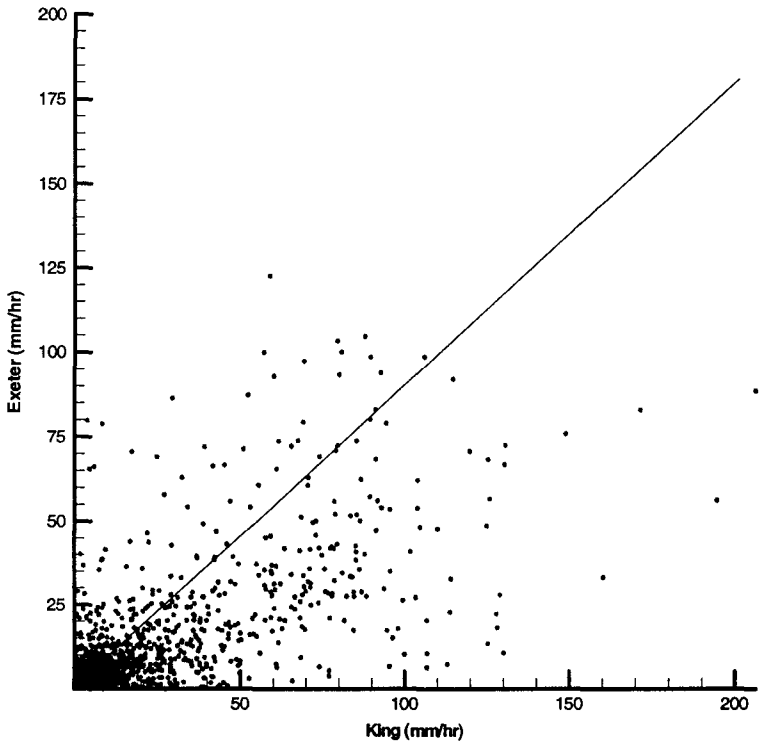

Figure 6.13 Example of a scatter plot from the two radars in the common area at nominal time 200005120930 EST.

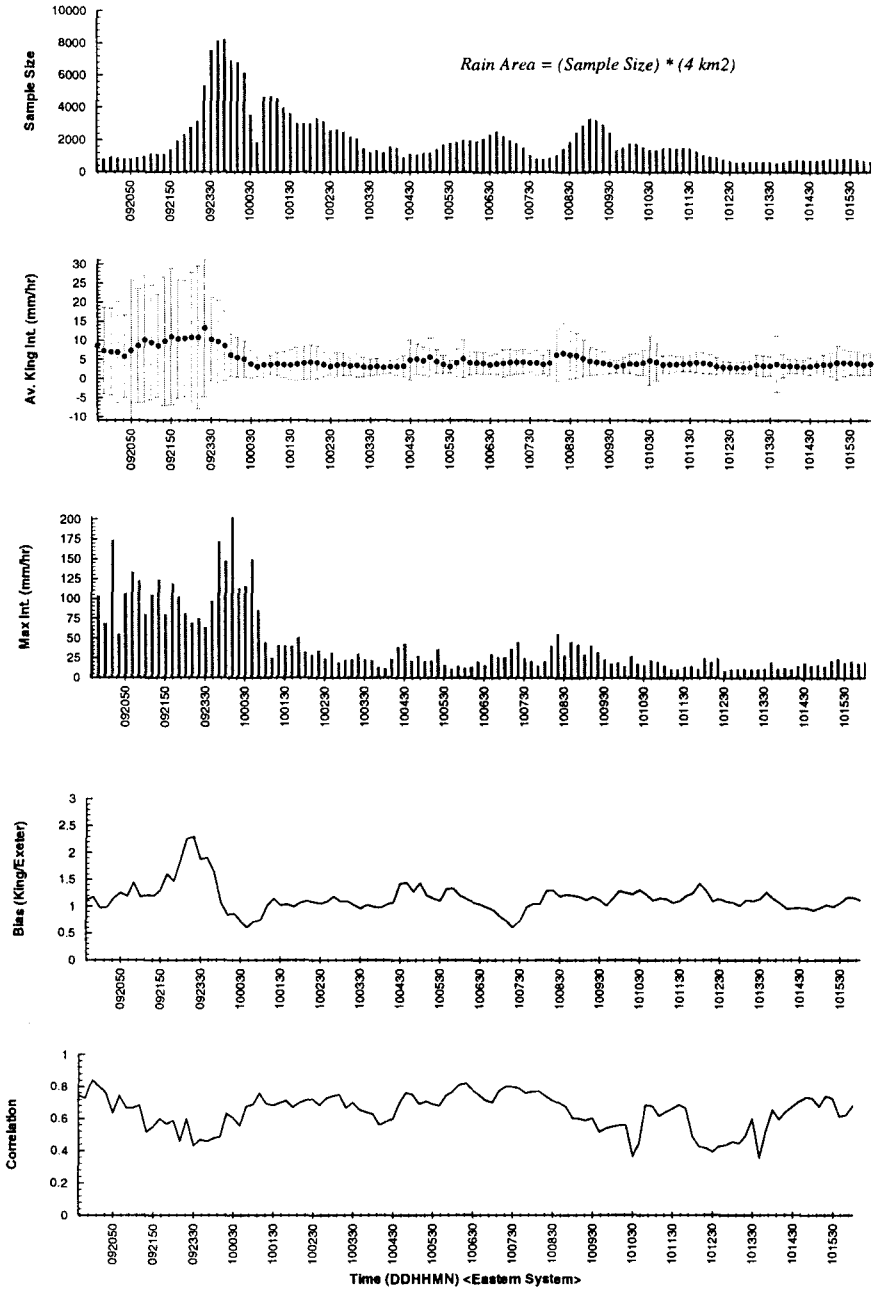

Figure 6.14 Summary of May 10, 2000 event. The plot is a full event , the X-axis is the time during the day. Each point on the curves represents a scatter plot like the one showed in Figure 6.14.

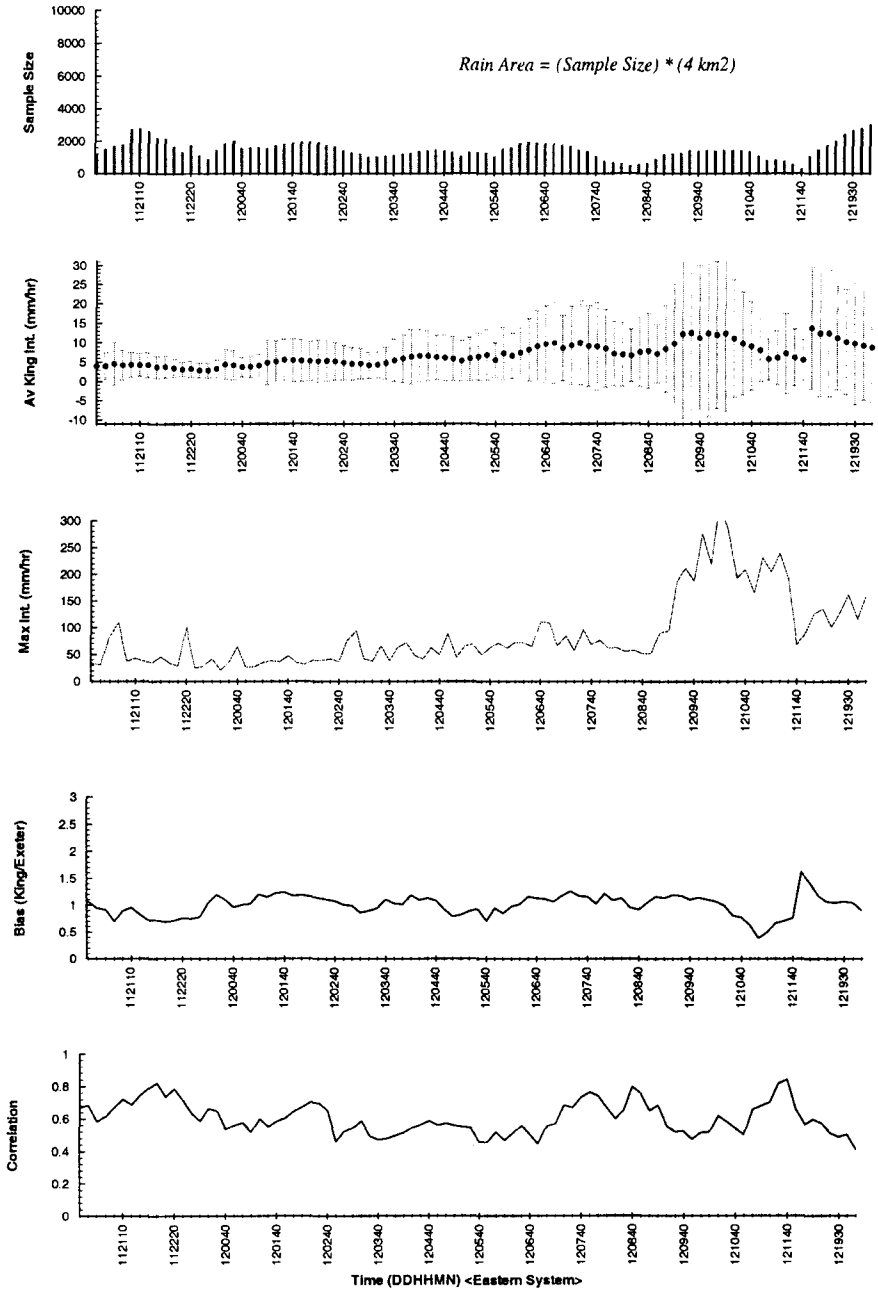

Figure 6.15 Summary of May 12, 2000 event. The plot is a full event , the X-axis is the time during the day. Each point on the curves represents a scatter plot like the one showed in Figure 6.14.

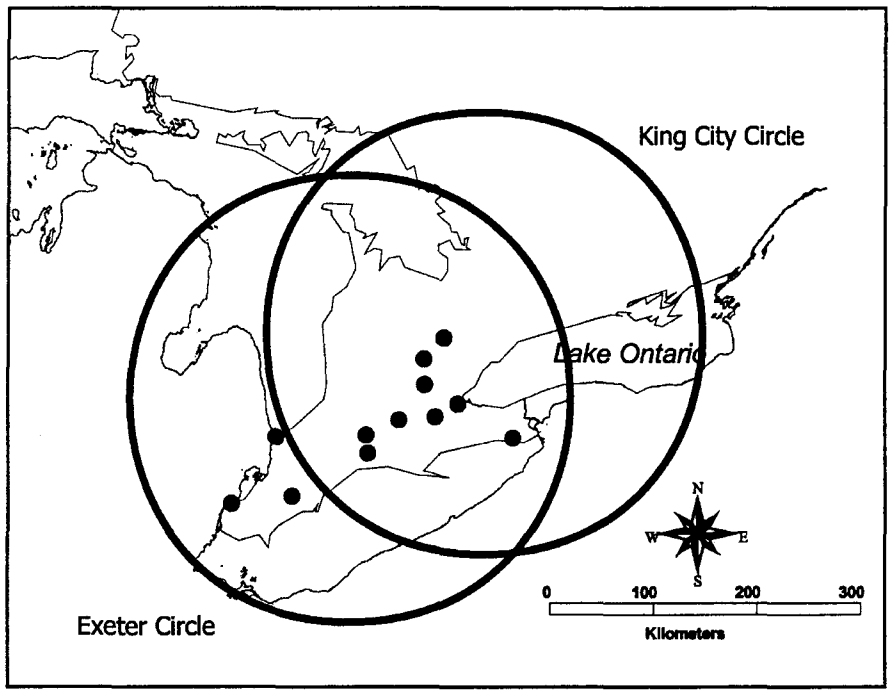

Figure 6.16 Locations of the rain-gauge network with respect to King City and Exeter Radar Sites. The rain-gauge network is operated by Ontario Climate Center. The data used are from years 2000 and 2001.

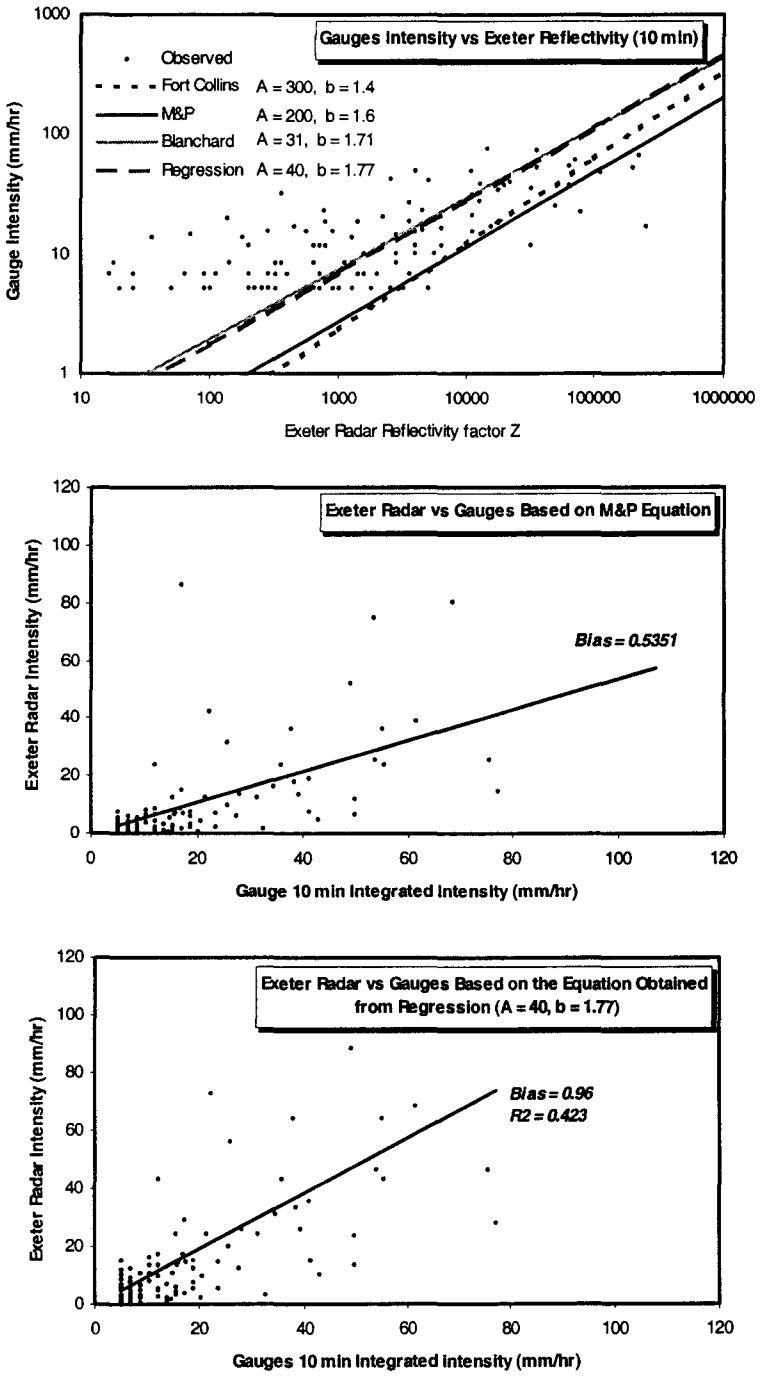

Figure 6.17 Exeter radar intensity versus rain-gauge intensity based on 10 minute accumulations. The top figure uses radar reflectivity drawn on log scale. The figures are produced using data from the 10 events in 2000 and 2001.

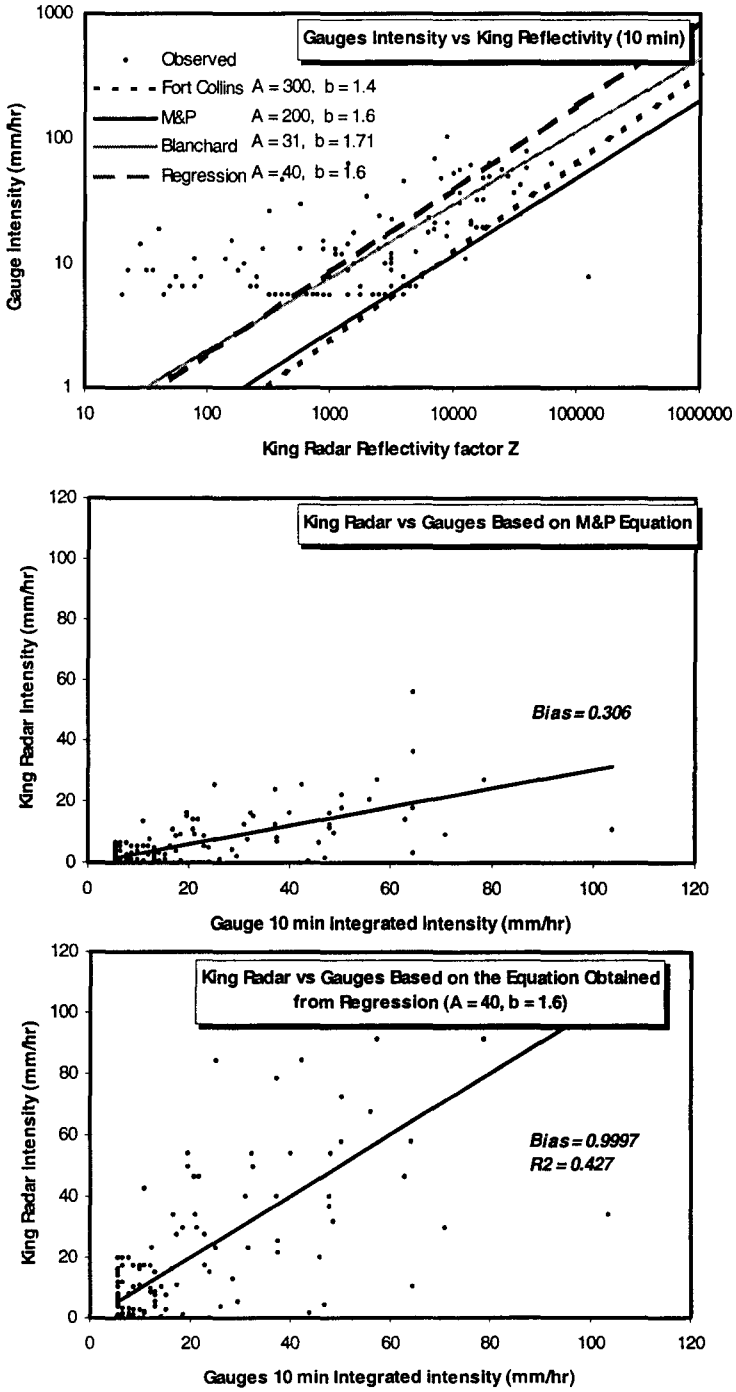

Figure 6.18 King radar intensity versus rain-gauge intensity based on 10 minute accumulations. The top figure uses radar reflectivity drawn on log scale. The figures are produced using data from the 10 events in 2000 and 2001.

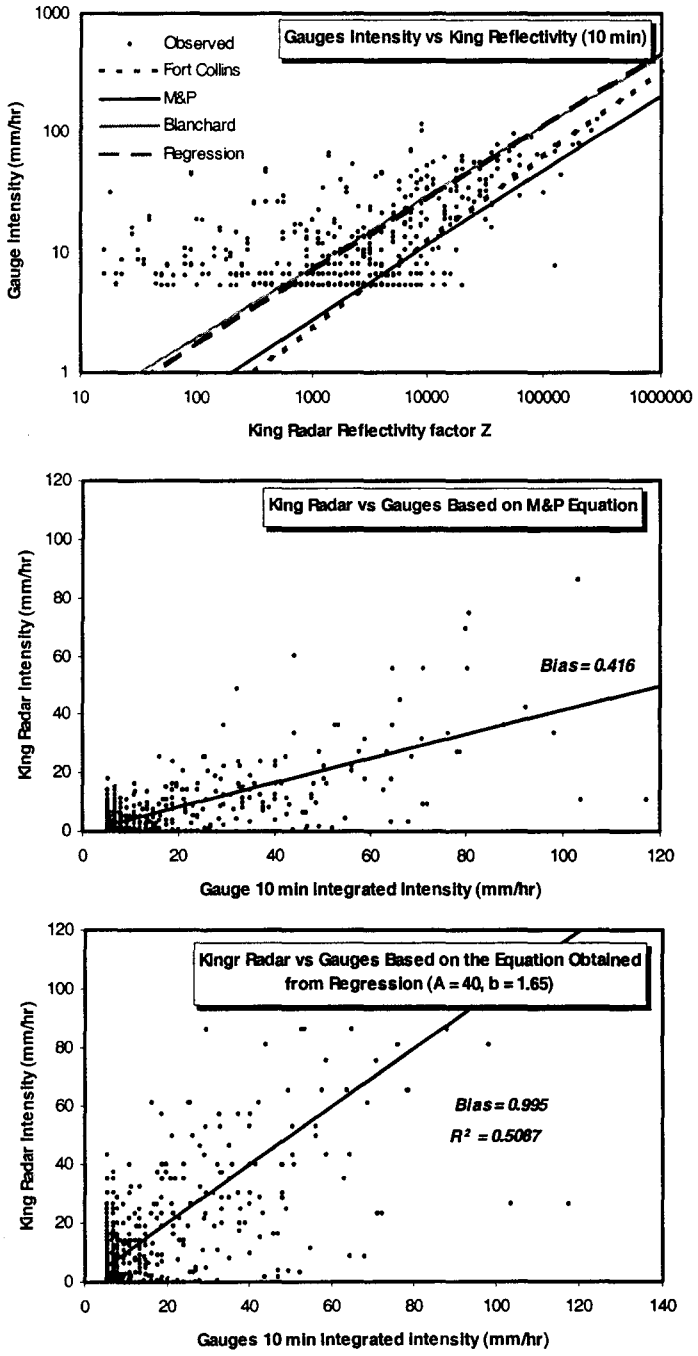

Figure 6.19 King radar intensity versus rain-gauge intensity based on 10 minute accumulations. The top figure uses radar reflectivity drawn on log scale. The figures are produced using data from the 25 events in 2000 and 2001.

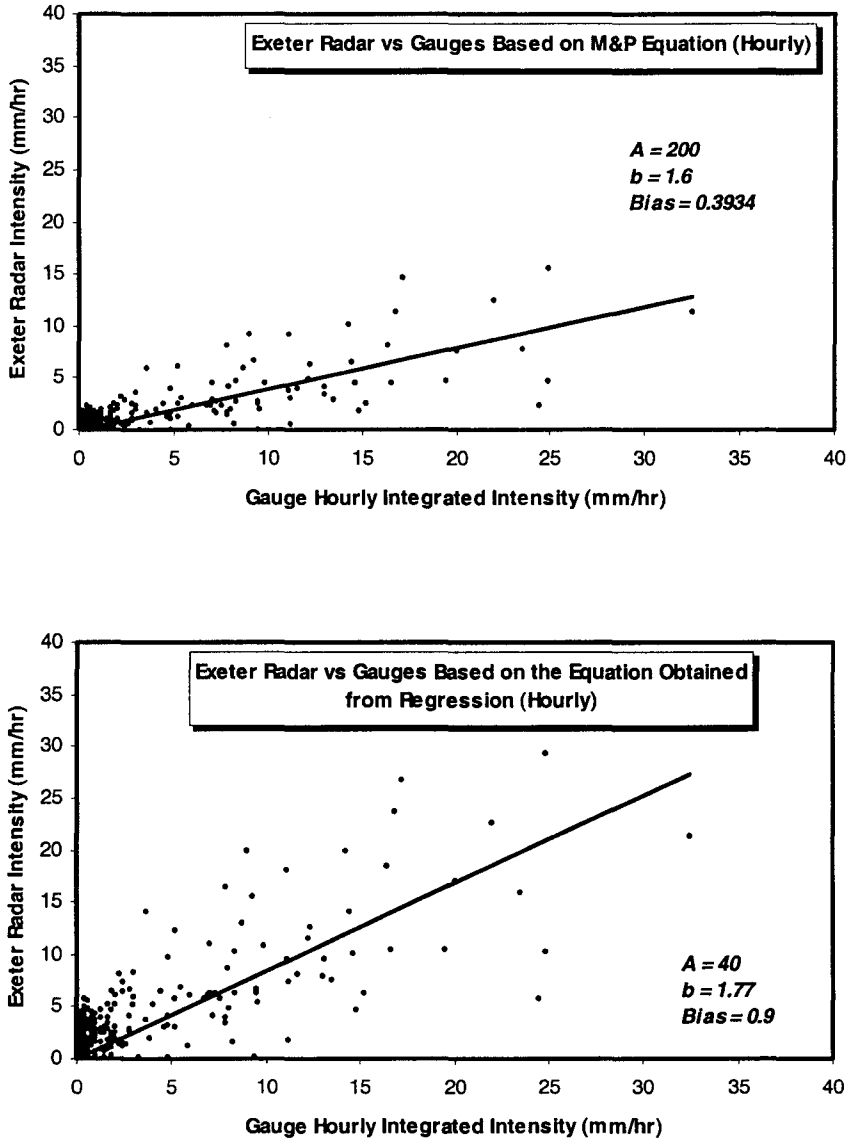

Figure 6.20 Exeter radar intensity versus rain-gauge intensity based on hourly accumulations. The figures are produced using data from the 10 events in 2000 and 2001.

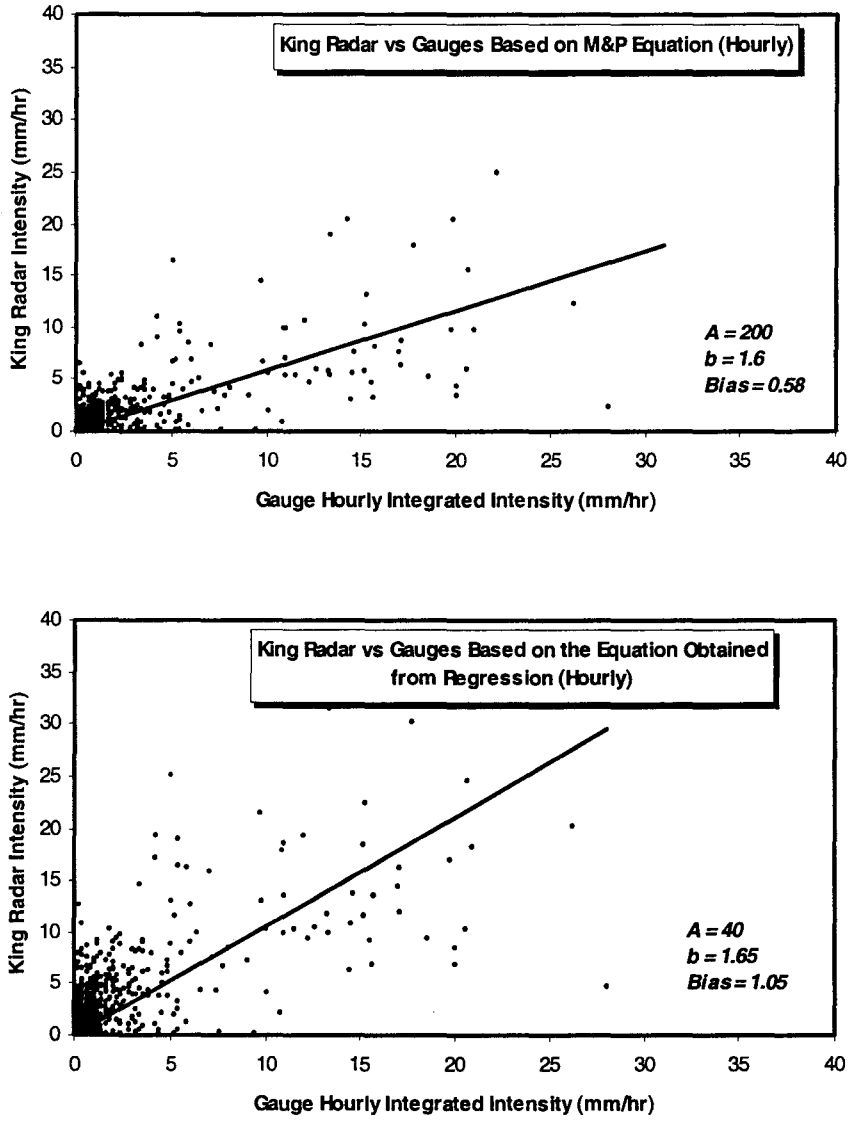

Figure 6.21 King radar intensity versus rain-gauge intensity based on hourly accumulations. The figures are produced using data from the 25 events in 2000 and 2001.

CHAPTER 7

REAL-TIME RADAR RAINFALL SHORT-TERM TRACKING AND FORECASTING

7.1 Background

Rainfall is one of the most difficult elements of the hydrological cycle to forecast. This is due to the tremendous variability it displays, both in space and time, over a wide range of scales. The forecasting problem becomes more difficult when forecasts of rainfall at scales of interest to urban hydrology are required. The "short-term prediction" of rainfall fields means tracking the time-space behavior of these fields at each time step (10 minutes, for example), then forecasting the space-time behavior of these fields for a certain lead time in the future (1 hour, for example).

In the last decade a requirement for the short-term spatially and temporally detailed quantitative precipitation forecast (QPF) has emerged from research on real-time control of sewer systems. For reasons such as storm water problems, which affect both water quantity in the sewer network and water quality of the receiving waters, urban combined drainage systems must be controlled. Detailed reviews of operational procedures for QPF are available in the literature in Chapter 2. Other

reviews can be found in Georgakakos and Hudlow (1984), Brown (1987), Georgakakos and Kavvas (1987), and Browning and Collier (1989).

The Canadian short-term prediction model, developed by Bellon and Austin (1976), is called the Short-Term Automated Radar Prediction (SHARP) model. This model utilizes cross-correlation analysis to track rainfall fields over the entire radar scan in order to obtain a translation vector (the cross-correlation analysis is described in section 7.3.1). The obtained translation vector is then used to extrapolate the motion into the future (for more details refer to Bellon and Austin, 1976). This model is in operational use by different Canadian radar groups. The SHARP model requires considerable run time, which limits the real-time application of the model. In addition, the changes in rainfall intensities over time are not modelled. Accordingly, the SHARP model is useful for off-line tracking applications of rainfall fields, where the changes in rainfall intensities within the rainfall fields are not pronounced. The model would provide less accurate forecasts in cases of severe convective storms, such as multicell storms and squall lines, where there are pronounced changes in rainfall intensity.

This chapter presents an improved radar-based extrapolation model, developed for the short-term prediction of the evolution of rainfall fields in time and space. The developed model employs a new optimization strategy for performing the cross-correlation analysis using minimum trial shifts, which reduces the run time significantly and makes the technique attractive for real-time applications. In addition, the new strategy allows for increasing the tracking accuracy by using high

resolution radar grids. The increase in the tracking accuracy and the run time reduction are useful in different applications that use the cross-correlation technique for rainfall tracking (i.e., historical kinematic analysis, correction for advection, rainfall forecasting...etc).

The changes in rainfall intensities of existing rainfall structures are considered in the new forecasting model. The new model is called AARS (Adaptive Automated Rainfall Simulator) model. In this chapter the AARS model is evaluated and quantitatively compared to two alternative forecasting schemes, the PERSISTENCE and the SHARP models. The developed model is used to assess the accuracy of forecasts in the Hamilton-Wentworth region.

7.2 Model Structure

The basic components of a short-term rainfall prediction scheme are: (1) the detection of rainfall fields on the radar time-space grids, (2) the tracking of rainfall fields to identify the parameters of their evolution, and (3) the use of the identified parameters to extrapolate the tracked rainfall fields into the future. Accordingly, the AARS model can be divided into two main modules. The first module is responsible for tracking rainfall fields to identify the speed and direction of rainfall patterns. The tracking module is described in section 7.3. The second module (the forecasting module) models rainfall evolution (growth and decay) and uses the output of the tracking module to extrapolate rainfall fields into the future. The forecasting module is described in section 7.4. A simple user manual that shows an example of running

the model is provided in Appendix V.

7.3 The Tracking Module

The idea of the tracking module is based on the cross-correlation method. This method determines the velocity vector from the optimum spatial shift ΔS_{opt} required to maximize the correlation coefficient ρ between two successive scans separated by time interval Δt. Hence the velocity vector V is obtained from:

$$\vec{V} = \frac{\Delta \vec{S}_{opt}}{\Delta t} \tag{7.1}$$

$$\Delta S_{otp} = \sqrt{XShift_{opt}{}^2 + YShift_{opt}{}^2} \tag{7.2}$$

In order to find the optimum spatial shift ΔS_{opt}, the common procedure is to try all possible shifts, the spatial shift that corresponds to the maximum correlation is then selected. If there are significant differences in the motion of the patterns due to the wide area covered under a radar umbrella, the rainfall domain is sub-divided into sub-domains (boxes) and the correlation technique is applied separately on each box (refer to the TREC method in Chapter2, section 2.5.1). Care should be taken due to the effect of the arrival/departure of rainfall patterns on the estimation of the correlation coefficient, as this may lead to erroneous estimation of the velocity vector. Ambiguities found in some references concerning this problem make representation of the cross-correlation method essential in this study.

7.3.1 The Cross-Correlation Methodology

In order to overcome the effect of arrival and departure of rainfall on the calculations, the correlation domain (the domain on which the technique is applied) has to be smaller than the radar domain by a margin M, greater than or equal to the maximum allowable speed multiplied by the time difference between the two scans. Two consecutive radar grids, denoted *Grid 1* and *Grid 2* and separated by time interval Δt, are given. The correct methodology is as following (refer to Figure 7.1):

1- Specify a domain to perform the cross-correlation (satisfying the margins condition). Then clip the radar data from *Grid 2* which fall inside the domain.

2- Find the optimum spatial shift ΔS_{opt} by trying all possible shifts as following:

$\rho_{max} = -1$

FOR each possible ΔS_i

- Shift "back" the cross-correlation domain and the clipped *Grid 2* by a spatial shift ΔS_i.
- Locate a copy of the shifted domain on *Grid 1* then clip the data inside the shifted domain.
- Overlay the clipped and shifted data from *Grid 2* on the clipped data from *Grid 1* then calculate the corresponding correlation coefficient ρ_i.
- **IF** ($\rho_i > \rho_{max}$) then

$$\rho_{max} = \rho_i$$

$$\Delta S_{opt} = \Delta S_i$$

END IF

END FOR

3- The optimum spatial shift is then ΔS_{opt} and the corresponding maximum correlation is ρ_{max}.

The main limitation of the cross-correlation technique is the run time required to try all possible shifts in cross-correlating the two grids. The run time requirements increase significantly when the time separation between scans increases (as in cases of missing scans) and/or the grid domain is subdivided into multiple sub-domains, which requires that the cross-correlation is to be done separately for each sub-domain. This problem constitutes a limitation especially when working in real-time. Different search strategies have been developed for this purpose. These search strategies are described in the next section (section 7.3.2). The run time of a cross-correlation routine is dependent on the programing environment and methodology in addition to the amount of data in the analysis.

The main factor influencing the amount of time to perform one trial cross-correlation results from the floating point arithmetic operations (Donaldson, N., 2001). Because of the run time requirements, operational techniques use some approximations based on fast integer matrix manipulations to avoid dealing with a great deal of floating point arithmetic (Donaldson, N., 2002). For example, the operational Canadian cross-correlation routine, which is being used by the different

radar groups, uses only 8-16 levels of data instead of using the whole data range to convert to integer matrix manipulations (this routine was developed at McGill University by Aldo Bellon). This avoids doing the cross-correlation summation on a cell by cell basis and the correlation summation is done according to the number of data levels. In addition, the Canadian cross-correlation routine uses radar grids of 2 km resolution instead of 1 km resolution (i.e., manipulating 2 resampled arrays each of 240×240 instead of 480×480). The reduced grids are resampled from the original grids using a resampling method, i.e., a nearest neighborhood or bilinear resampling. These "tricks" reduce the run-time (Donaldson, N., 2002).

The use of only 8-16 data levels may result in a loss of the detail in the rainfall field leading , in turn, to a wrong answer in some cases for the derived rainfall motion. This problem is dangerous when using a small correlation domain (a box 20 km by 20 km in size for example). In this case the whole box may fall within only one data level and a maximum correlation of unity may be found with different shifts leading to ambiguity in finding the correct answer (especially in cases of widespread rainfall in which rainfall differences are very small on large areas). This might constitute one additional reason for the significant noisy velocity vectors obtained by a tracking model such as the TREC model, as it performs the correlation on small portions of the radar umbrella (refer to Chapter 2, section 2.5.1, for the details of the TREC model). In addition, using 2 km resolution radar grids instead of 1 km grids reduces the tracking accuracy.

7.3.2 Review of the Search Strategies

It is economically unwise to attempt to calculate ρ for all possible shifts in both Cartesian directions. Hence, researchers have followed different strategies to save computer cost and time. Austin and Bellon (1974) suggested saving the trials by taking the displacement of the centre of gravity of the two grids as an initial guess, translating one grid over the other by that amount, then calculating a cross-correlation matrix around this initial displacement. This strategy reduces the run time, although it is still considerably large depending on the size of the correlation matrix. However, the main problem of this strategy is caused by the effect of the arrival and departure of echoes at the edges of the radar domain, which can mislead the calculations of the centre of gravity, in turn, leading to an erroneous velocity vector. The effect of this problem appears clearly when using small correlation domains in which the rainfall pattern extends beyond the boundary of the domain (refer to Figure 7.2 for an example). The upper two circles in Figure 7.2 represent two consecutive radar grids. The rectangle inside each circle represents a stationary analysis domain. Note that the rainfall pattern extends beyond the boundary of the analysis domain and, as a result, the centres of gravity of rainfall inside the analysis domain in the two consecutive scans are almost at the same location. Accordingly, an erroneous zero or small initial displacement will be estimated even though there is, in fact, a considerable initial shift. By making an incorrect estimate of the initial displacement, the cross-correlation matrix will be located far from the true optimum. Austin and Bellon (1974) stated that in order to overcome this problem they were "zeroing out

undesired data", a term not completely understood. In order to use a proper methodology for calculating the centre of gravity the pattern in the two scans should be located inside the correlation domain, which requires more time for processing as well as the use of a non-stationary spatial domain.

In an improvement of the TREC model by Li et al. (1995) the number of trials was reduced by specifying a circular search area for all possible shifts. The radius of this area is equal to the maximum possible velocity (V_{max}) multiplied by the time interval Δt (i.e, $r = V_{max} \times \Delta t$), where V_{max} may be determined from meteorological information or from the knowledge that one would reasonably expect to occur in a given situation. However, the number of possible shifts used in this strategy is still large, even if we add minimum velocity constraint. For example (refer to Figure 7.3), the two axes represent the possible Cartesian shifts in the X and Y directions by which the current rainfall grid may be translated before cross-correlating with the previous grid. Here we assume that V_{max} = 90 km/hr, V_{min} = *12* km/hr, Δt = 10 minutes, and 1 km resolution. Accordingly, r_{max} = 1.5 km/min × 10 min = 15 km, and r_{min} = 2 km. The number of possible shifts within the two circles is 688. Based on experience in running the correlation analysis on PIII-800 Mhz-256MRam-PC using the GIS programming language (Avenue), it takes approximately 1-2 second to perform the cross-correlation between two successive full scans for one shift (using cell by cell cross-correlation, i.e. using floating point arithmetic). This time (i.e., 1-2 seconds) can be explained by how GIS handles grids, which is relatively slower than other programming languages (refer to Chapter 5, section 5.10.2 for more

details). Accordingly, it would take 11-22 minutes to calculate all possible shifts using GIS, a time that is already bigger than the time separation between the two scans (10 minutes). In case of missing data (Δt = 30 minutes, for example), the number of possible shifts, as well as the run time, increase dramatically. It should be noted that storm speeds can reach up to 120 km/hr, which adds more possible shifts (Tsanis et al, 2002). In order to verify this running time using another programming language a correlation routine, employing normal floating point operations, was written using C++. The routine was tested on PIII-800 Mhz-256MRam-PC. The average time taken by this routine to perform one trial cross-correlation between two full scans is 0.80045 seconds. Hence, the total time required to perform 688 shifts (full enumeration) would be 9.18 minutes, which is still very high. In addition, this number will increase in cases of missing scans and/or when increasing the maximum velocity constraint.

Tsanis et al. (2002) used another strategy, which performs the full search within the r_{max} and r_{min} constraints in the beginning. In subsequent scans the search is focused 90 degrees around the optimum direction obtained in the previous scan. In cases when the correlation value seems low, a full search is performed. This strategy reduces the run time to one fourth with respect to a full search. The Canadian radar groups follow a similar strategy for performing the cross-correlation analysis in which the search is done in matrix constructed around the optimum point obtained in the previous scan. If a maximum is found on a search area boundary, the area is expanded in that direction. In cases when the correlation value seems low, a full

enumeration search is performed. The problem with these two strategies appears in a few cases, in which considerably sudden changes of the rainfall kinematics may occur. In some cases, for example, significant directional changes in the rainfall kinematics may suddenly occur. In such cases, the true optimum may fall outside the search region constructed around the previous optimum. The number of possible shifts is still large, using these two strategies, depending on the size of the correlation matrix. In addition, a full search must be performed when initializing the tracker and/or the maximum correlation seems low.

Based on the discussion above it can be concluded that the available search strategies are time consuming, and robustness may be lacking in some cases, as they involve searching a large space for the parameters. At the same time, none of these strategies are based on a systematic optimization methodology, that guides the search in the right direction. Employing a systematic and successful optimization methodology may significantly reduce the run time and improve the tracking accuracy.

In this study a new optimization search strategy is developed to reduce the computational burden of the cross-correlation technique. The real-time optimization problem is a maximization problem searching for the optimum spatial shift that maximizes the correlation coefficient between two rainfall grids using the minimum possible trial shifts. Hence, the parameters here are two, i.e., two shifts in the Cartesian directions (*XShift*, and *YShift*). The objective function is the correlation coefficient ρ.

7.3.3 The Cross-Correlation Surface

The main step in any optimization problem is to explore the degree of difficulty expected in the surface of the objective function. The cross-correlation surface represents the values of the correlation coefficient with respect to all possible shifts in the two Cartesian directions. A sample of 290 CAPPI scans is selected from 15 events covering the summer of 1989. The objective in this section is to explore the possibility of "mountainous terrain" (the existence of more than one region of attraction in the cross-correlation surface), "non-unimodality" (the existence of more than one peak in a region of attraction), and any other difficulties that may be found in the cross-correlation surface from the perspective of an objective function. A region of attraction is defined as any "mountain" in the cross-correlation surface that can attract a simple ascending search strategy. Two correlation domains are used for this analysis (as shown in Figure 7.5). Domain 1 represents, as much as possible, the whole umbrella of King City radar, whereas domain 2 is a smaller circular domain (radius = 64 km) centered at Hamilton-Wentworth, Ontario, Canada. The reason for using the small domain is to explore the effect of reducing the correlation domain , as in the TREC method, on the characteristics of the cross-correlation surface.

From the 290 cases, 6% contained mountainous terrains. Non-unimodality were found in 5% of the cases. Examples of these problematic cases are shown in Figures 7.6, 7.7 , 7.8, and 7.9, which were selected from different rainfall types. Such cases are problematic because of the existence of more than one region of attraction and/or local peaks that may mislead a simple search strategy away from the global

optimum. In cases of local optimality, a simple ascending search strategy may converge to a local peak instead of the global one. This is because, in the ascending search strategies, the criterion for judging a solution is that it has to be higher than its neighbors.

It should be noted that the data set used for this study covers cases of convective and widespread rainfall. The following points summarize the characteristics of the cross-correlation surface obtained by the inspection of the 290 cases considered:

1- The cross-correlation surface is smooth and not spiky.

2- In some cases in the small correlation domain, when the rainfall pattern extends along and beyond the boundary, false regions of attraction "small mountains" may exist (refer to Figure 7.7 for an example). This example represents a squall line that has regularly spaced storm cells along it. There are two false regions of attractions at the dominant storm cell spacings, which is not the true line motion. The region of attraction of the true solution (true region of attraction) can be distinguished by its relatively higher peak.

3- The size and dimensions of the surface is related to the spatial extent and dimensions of the rainfall pattern which explains why the cross-correlation surface in cases of convective rainfall is more steep than cases of widespread rainfall.

4- Reducing the cross-correlation domain increases the chances of local optimality in the cross-correlation surface.

7.3.4 Selection of the Optimization Strategy

Different optimization techniques have been developed in the last four decades for the purposes of process optimization. These techniques may be divided into five main classes: (1) Deterministic search techniques; (2) Pattern search techniques; (3) Probabilistic search techniques; (4) Evolutionary Techniques; and (5) Stochastic approximation techniques. Each main class contains different methods. For more details, refer to a textbook on optimization such as Fu and Hu (1997), Belegundu and Chandrupatla (1999), and others. General comparisons between different techniques in terms of bias, variance, and computational complexity are not possible. A few studies rely on computer simulations to compare different techniques in terms of accuracy and number of iterations. However, it can be expected that no single technique can work effectively (i.e., solve the problem globally) and/or efficiently (i.e., uses minimum run time) in all cases.

The best optimization technique for a specific problem should overcome the degree of difficulty of the specific global optimization problem with the least amount of computational effort and cost. Dixon and Szego (1978) related the degree of difficulty in solving a global optimization problem to the dimensionality of the problem and the characteristics of the objective function. Duan et. al. (1993) indicated that there are five major characteristics of the objective surface that can complicate the solution process. In general, they are:

1- There may be several major regions of attraction to which a simple search strategy may be attracted.

2- Each major region of attraction may contain numerous (possibly uncountable) local peaks.

3- The surface of the objective function in multi-parameter space may not be smooth and may not even be continuous.

4- The parameters may exhibit varying degrees of sensitivity and a great deal of interaction and compensation.

5- The response surface near the true solution may be non-convex (minimization) or non-concave (maximization).

Refer to Duan, et al. (1993) for more details.

Probabilistic search techniques, such as random search or the pure adaptive and hit-and-run search techniques, select trial points governed by a scan distribution, which is the main source of randomness. Unfortunately, these techniques cannot determine the location of the optimum value of the objective function, which in this study is as important as the value of the objective function itself.

Evolutionary Techniques (Simulated Annealing and the Genetic techniques for example) allow ascent of a random population of points (not a single point) to move in order to escape any local optimum. A price is paid, however, in terms of a large increase in the computational time required; a global (i.e., true) optimum may require a long time to be found. These techniques use the ideas of evolution to optimize a system that is usually too difficult for traditional optimization techniques. In this study a deterministic, or pattern search method was recommended for the following reasons:

1- The cross-correlation surface is a relatively simple surface. The surface usually consists of one main region of attraction, which contains no or few local peaks.

2- The deterministic or pattern search methods are the fastest in terms of convergence.

Accordingly, two methods were considered as they are considered to be the most suitable for type of objective function. They are: (1) the response surface analysis and (2) the simplex method (Spendley et al. 1962; Nelder and Mead 1965; Wright 1996; and others). Though the two methods work on a continuous parameter space they can be modified to work on a discrete space. Because the dimensions of the problem include only two parameters (shifts in X and Y directions), the response surface method is chosen because of its simplicity and adaptability to a discrete space. The approach chosen for this study is a modification of the response surface analysis (RS) combined with the concept of tabu search (TS).

7.3.5 Description of Tracking Module

It is important to introduce the ideas used for the response surface search (RS) and tabu search (TS) strategies before proceeding with the combinatory strategy.

7.3.5.1 The Response Surface Strategy

The modification of the RS (response surface search) method used in this study will be presented in this section. This method is used usually for process

optimization to reduce the number of experiments required to optimize a certain process. The original method and more details concerning the response surface experimental designs and analyses can be found in Khuri and Cornell (1998). This experimental design is used to "climb" the surface of the objective function (the cross-correlation surface) from a starting point on a grid of points (representing possible shifts in the X and Y directions). At the starting point (denoted *CurrentPoint*) the eight grid points (the neighborhood) around *CurrentPoint* are tested (box design). Note that for each point a correlation analysis is performed between the two scans in order to calculate the corresponding correlation coefficient. The direction of steepest ascent is then determined as following:

1- Find the highest point (i.e., shift) in terms of cross-correlation (denote this point as *NextPosition*) in the neighborhood of *CurrentPoint* (i.e., one of the 8 box points).

2- Find the lowest point in terms of cross-correlation (denote this point as *LowestPoint)* in all 9 points (i.e., the neighborhood including *CurrentPoint*).

3- The direction of steepest ascent is defined as the direction of the line joining *LowestPoint* to *NextPosition.*

4- The search then moves to *NextPosition* and continues in the direction of steepest ascent by using the following increments:

$$DeltaX = XShift_{NextPosition} - XShift_{LowestPoint}$$

$$DeltaY = YShift_{NextPosition} - YShif_{LowestPoint}$$

5- Trials runs are then made along the direction of steepest ascent until no

improvement in the correlation value is achieved. Another box is then constructed around the highest point reached so far and a new steep path is determined, i.e., set *CurrentPoint* as the highest point reached and repeat from step number one.

The process continues until the RS halting condition is encountered. The RS halting condition is reached when all eight box points are less than the middle point in terms of correlation. Figure 7.10 shows the idea of the RS method. The disadvantage of this strategy is that it may fail to converge to the global optimum in cases when local peaks exists (refer to the small domain cases in Figures 7.6, 7.7 , 7.8, and 7.9). It should be noted here that the RS strategy, as it will be concluded in the test cases in section 7.3.5.5, succeeded in obtaining the global solution of the cross-correlation surface in cases of subsequent scans despite of the disadvantage mentioned above. However, there is still a danger of converging to the wrong answer if there are multiple local maxima. This case is possible for example when a line of storms has regularly spaced cells along it. There could be a local maximum at the cell spacing, which is not true line motion (refer to Figure 7.7). Hence, it was decided to implement another strategy (the tabu search strategy) in conjunction with the RS strategy to overcome the effect of local optimality that might appear in few cases.

7.3.5.2 The Tabu Search Strategy

The tabu search (TS) is a technique that is frequently used to escape local optimums. Following Glover (1990) and Glover and Laguna (1993), tabu search has

its antecedents in methods designed to cross boundaries of feasibility or local optimality standardly treated as barriers. Most early references of tabu search in its present form are works of Glover distinguishing him as the inventor of what currently is known as tabu search. Further on, there are a number of contributions that have influenced the development of tabu search. The tabu search, although still in its infancy, has been reported in the literature during the last few years as providing successful solution approaches for a great variety of problem areas. The method is still actively researched, and is continuing to evolve and improve. The tabu method was partly motivated by the observation that human behavior appears to operate with a random element that leads to inconsistent behavior given similar circumstances. The tabu method operates in this way with the exception that new courses are not chosen randomly. Instead the tabu search proceeds according to the supposition that there is no point in accepting a new (poor) solution unless it is to avoid a path already investigated. This insures new regions of a problems solution space will be investigated with the goal of avoiding local minima and ultimately finding the desired solution.

Although a tabu search is conceptually simple, any implementation of an efficient tabu search algorithm is problem specific, and no generic tabu search software is available at this time. The tabu search algorithm combines, in general, a few simple ideas into a remarkably efficient frame-work. Among the main elements of this framework are:

- A neighborhood local search; the next solution is usually the best not-yet

visited solution in the current neighborhood. The term "best" refers usually to the neighbor with the highest objective function even if it is less than the current solution.

- A mechanism (tabu lists) discouraging or preventing returns to recently visited solutions.
- A mechanism that changes the solution path when no progress has been made for a long time or when the current path seems unpromising.

The tabu search used in this paper implements these elements in a robust and efficient way designed to escape local optimality of the cross-correlation surface.

In this study the TS explores the neighborhood (box of 8 points) around a feasible solution (peak) that was obtained using the RS. The TS starts at this feasible solution then proceeds (i.e., the next move) by moving to the highest point in the neighborhood (the best neighbor) even if this results in a deterioration of the correlation value. The new position is then considered a current position (i.e., perform exchange) and the search moves to one of its neighbors. The process continues in this manner until the halting condition of the TS is encountered. Solutions that were examined by any of the RS and TS are declared tabu (taboo, i.e., visited points) in order to avoid cycling. Two running memory storage lists are required to save the visited points (a tabu list and an absolute tabu list). The tabu list includes the history of all points visited by any RS or TS since the beginning of process. The absolute tabu list includes the peaks found and other special points

which are visited twice (these special points are called freed points). The details of the two lists and these special points will be described later in this section. The advantage of implementing the TS with the RS is that if a higher value (higher than the maximum peak found) is found through a TS, a new climber using the RS strategy can be re-initialized at this point. The TS can be described in details in the following steps:

Given that the RS has reached a feasible solution termed *OptimumPosition*, with an objective function value termed *MaxCorrelation* :

1- Add *OptimumPosition* to the absolute tabu list.

2- Set the current search position to this feasible solution:

CurrentPosition= OptimumPosition

CurrentCorrelation= MaxCorrelation

3- Examine the neighborhood of *CurrentPosition* (the neighborhood is a box of 8 grid points around *CurrentPosition*). The new move is to one of the 8 neighbors (*NextPosition*), which satisfies the following conditions:

a- The highest correlation value in the neighborhood even if it is less than *CurrentCorrelation*.

b- It has never been visited before by any of the RS or the TS (i.e., a new point, i.e., not included in the tabu list). In the case where all of the neighbors were visited before (i.e., taboo)

then free the highest neighbor and move to it as long as it is not an absolute taboo point.

4- Add any newly visited points to the tabu list or add the freed point to the absolute tabu list. Note that the two cases can not happen at the same time (i.e., if there are new points in the neighborhood, there will be no freed points).

5- Set the new position as current position (i.e., *CurrentPosition* = *NextPosition*) and repeat from step number three. In case this path seems unpromising (i.e., when TS "finds out that it is going to move" to a point less than a predefined minimum percent, denoted η , of the feasible solution) then change the solution path. This is done by going back to the feasible solution and choosing the next highest direction (i.e., just repeat from step number two).

The process continues until the TS halting criterion is encountered, if a value higher than *MaxCorrelation* is found in any of the TS moves, a new RS climber is restarted at this point. The TS halting criterion is encountered in either of the following two cases:

- The number of examined solution paths (denoted *Max_N_Paths*) exceeds a predefined number (three paths in this study), or
- All neighbors are absolute taboo.

The purpose of the tabu list is to record the history of the visited points since the start of the process to prevent the TS to move to them again. In the case where all

neighbors are taboo , i.e. a trapped point (this case happens for example when the TS starts after the RS reaches a feasible solution), one of the taboo neighbors is then freed and the search moves to it. The absolute tabu list is required in this case to record the history of the freed points to avoid cycling within paths.

The search method used in this paper is a combination of the RS and TS techniques and will be described in details in the following section. The search method used is the same for both initialization and subsequent scans. The only difference is that the starting point in subsequent scans is determined according to the velocity vector obtained in the previous scan. In addition, in subsequent scans, there is an option to cancel TS.

7.3.5.3 The Search Method

The method in general can be described as a starting large scale search (i.e., using low resolution, 4 km for example) followed by a final small scale search (i.e., using high resolution, 1 km for example). The large scale search is done using a combination of the RS and TS. The large scale search recommends the area where the global solution is expected. The final small scale search climbs in this area using the RS. The steps of the method can be described in the following:

1- Choose a starting point. In case of initialization, the operator may use a "meteorological value" or any fixed or random point can be chosen. In subsequent scans, the starting point is determined automatically according to the previous velocity vector.

2- The starting search climbs the surface from the starting point using the RS (using large scale search resolution denoted *Start_Res*) until a feasible solution is found.

3- Once an optimum is found in step 2, the starting search continues using TS using the same resolution (*Start_Res*). The correlation value at each move is compared to the feasible solution obtained in step 2 as following:

If a higher value (higher than the feasible solution) is found at a point, the RS is restarted again at this point using the same large scale resolution. Else, the TS continues searching. The starting search stops when TS encounters its halting criterion.

5- Once the starting search stops, the final small scale search is performed. The final search is done by restarting an RS (using the finest resolution possible; *Final_Res* = 1 km in this study) at the highest solution found in the starting search. The final RS stops when it reaches an optimum. This optimum is considered the global solution.

Refer to Figure 7.11 for a schematic flow chart of the optimization methodology. Appendix IV includes a pseudo code for the method.

7.3.5.4 Technical Notes

The tabu list and the absolute tabu list are the search guides. It is important to formulate the rules that decide how the search moves:

1- TS can NOT move to any point from the absolute tabu list to avoid cycling within paths.

2- TS can NOT move to any point from the tabu list to avoid cycling within points except for only one exception. This exception is when a TS is at a point (trapped point) where all neighbors were visited before (i.e., declared taboo). In this exception, the highest (non-absolute taboo) point of the neighborhood is freed and the TS moves to the freed point. The freed point is then declared absolute taboo.

2- RS is allowed to use points from the tabu and absolute tabu lists to save run time.

3- Both RS and TS can not move to or visit a point outside the boundary of the maximum speed constraint (i.e., circle). Note that when the search moves close to the boundary, the neighborhood is reduced to the possible points. I.e., only points contained inside the circle are visited and the remaining of the 8 neighbors are neglected.

4- The halting criterion of the TS is encountered when the number of solution paths examined is equal to *Max_N_Paths* OR when all neighbors are absolute taboo.

The method requires the specification of 6 parameters. Table 7.1 shows the recommended values used in this study for these parameters.

Table 7.1 Recommended values for the Technical Parameters of the Tracker

Technical Parameter	Convective	Widespread	General
Max Speed (V_{max})	*140 km/hr*	*140 km/hr*	*140 km/hr*
Perform TS in subsequent scans? *(Perform_TS)*	*Yes*	*Yes*	*Yes*
Starting search resolution *(Start_Res)*	*4 km*	*6 km*	*4 km*
Minimum Percent for changing TS Paths (η)	*40-60%*	*50-70%*	*50%*
Halting TS criterion *(Max_N_Paths)*	*3*	*3*	*3*
Final search resolution *(Final_Res)*	*Max (1 km)*	*Max (1 km)*	*Max (1 km)*

There is an option to cancel the TS in the case of subsequent scans, as specified in the *Perform_TS* parameter. In this case only two parameters are required and should be set to the following values:

1- *Start_Res* = The maximum resolution possible, i.e., 1 km in this paper.

2- *Perform_TS* = No.

When TS is canceled, the method uses the TS in initialization. Then in subsequent scans, it climbs the surface from the global optimum obtained in the previous scan (using the finest resolution possible) and stops without performing a TS. However, there is a possibility of converting to a wrong answer if the TS is canceled in subsequent scans. Hence, canceling the TS in subsequent scans is not recommended.

The values of the parameters shown in Table 7.1 were specified based on the

characteristics of the cross-correlation surface. For example, a search resolution of 4 km is expected to be smaller than the dimension of the true region of attraction (i.e., 4 km would not miss a true region of attraction). At the same time, using TS on this resolution is expected to sufficiently escape a false region of attraction or a local peak. A 50 % criterion for changing TS paths means that the search has moved outside the top region of the surface (in which the global solution exists). Finally, a TS halting criterion of 3 paths is considered to be sufficient to explore the area around a feasible solution. It is important to note that this number (i.e., *Max_N_Paths* = 3 paths) is critical and should not be reduced as it can seriously affect the robustness of the method. This is because the search will be limited to one or two directions. This may only explore the wrong directions from the feasible solution. Certainly, the maximum value of this technical parameter is 8. Increasing this number to more than 3-4 will not significantly increase the run time or the robustness, as might be expected. This is because the search will proceed in a tabu area which is already available in the tabu list (i.e., it will only lead to converting the taboo area to an absolute taboo).

The optimization method is computationally fast and straight forward in terms of programming, although the steps of the method may seem long (Appendix-IV presents a detailed pseudo code to facilitate reproduction of the method).

7.3.5.5 Test Cases

The method developed in this study was tested on a sample of 290 radar scans from King City radar in Southern Ontario. The verification was accomplished by comparing the optimum spatial shifts obtained to the true optimums (i.e., those obtained by performing a full enumeration search). The following points summarize the results:

- The developed method is robust. In all cases the search converged to the true optimum (i.e., the optimum obtained by performing a full enumeration search).
- The run time is reduced on average by 96±1.5 % with respect to the time required to perform a full enumeration search inside the maximum speed constraint (using 1 km grid resolution). In other words, for example, a 12 minutes full search is reduced to 30 seconds on average. Also note that addition run time reduction will result in the cases of missing scans.
- The second fastest and robust method (denote this method method-2) that can be recommended is to perform a starting full enumeration search on large scale (i.e., using 4 km resolution) then perform a climbing search (i.e., RS using maximum resolution) from the highest point found in the starting search. Based on the test cases, the run time reduction using the method developed in this paper with respect to method-2 is approximately 60%. This number will also increase in cases of missing scans.
- The new method is insensitive to the starting point in terms of robustness. In

terms of run time, the starting point has a small effect on reducing the run time.

- The new method is flexible to allow for sudden changes in the kinematic properties of rainfall, unlike previous techniques that limit their search in an area constructed around the solution obtained in the previous scan.
- The increase in the tracking accuracy and the significant run time reduction are useful for different applications that use the cross-correlation technique for rainfall tracking (i.e., historical kinematic analysis, correction for advection, rainfall forecasting...etc).
- Another advantage of this method is that it can be modified to work in an unconstrained space (i.e., without the maximum speed constraint). This is because the method is adaptive and adopts itself to search in the regions of high correlation values only. This can allow for higher speeds to be detected, which can not be achieved by using any of the previous techniques.

7.4 The Forecasting Module

Detailed reviews of the operational procedures for QPF and their advantages and disadvantages are presented in Chapter 2 (Section 2.5). The first step in developing a rainfall forecasting algorithm is to select a model that is believed to describe the rainfall process being observed on the radar scans. The chosen model in this study is a deterministic polynomial function of the time t. This polynomial has been observed in the presence of additive random errors (Chen and Kavvas, 1992).

As the Weierstrass approximation theorem states, any continuous function can be approximated by polynomials over a finite interval to any degree of precision. The polynomials can be used for smoothing over sufficiently short intervals with very little knowledge of the true process. A second order degree polynomial quadratic is chosen to describe rainfall evolution. The model is applied on a cell-basis, i.e., each rainfall cell of the radar grid is modelled independently to allow growth and decay of rainfall at the finest resolution possible. The horizontal motion of rainfall patterns is modelled using a semi-lagrangian frame of reference so that the spatial two dimensional computational domain translates according to the velocity vector.

7.4.1 Forecasting Methodology

Let *R(t)* denote rainfall intensity at a certain grid cell at time *t*. The chosen model can be represented in the differential form as:

$$\frac{d^3}{dt^3} R(t) = 0 \tag{7.3}$$

Let *A(c)* denote the state-vector of the rainfall intensity at the grid cell at a certain time *c*. The state-vector is :

$$A(c) = \begin{pmatrix} A_0 \\ A_1 \\ A_2 \end{pmatrix} = \begin{bmatrix} R(t) \\ \frac{d}{dt} R(t) \\ \frac{d^2}{dt^2} R(t) \end{bmatrix} \tag{7.4}$$

The state-vector $A(c)$ can be seen as the Taylor series expansion coefficient vector of the polynomial. Hence, the forecasting solution can be written in the vector form as following:

$$A(c+t) = M(t)A(c) \tag{7.5}$$

where $A(c+t)$ is the forecasted state-vector using forecasting lead time t and $M(t)$ is called the transition matrix and is defined as:

$$M(t) = \begin{pmatrix} 1 & t & t^2/2 \\ 0 & 1 & t \\ 0 & 0 & 1 \end{pmatrix} \tag{7.6}$$

Equation 7.5 is called the transition equation. Once the estimation of the state-vector $A(c)$ at the current time c is obtained, the forecasted state-vector $A(c+t)$ after lead time t can be obtained by the transition equation. The forecasting methodology is applied on a per cell-basis, i.e., the rainfall variable $R(t)$ can be seen as a matrix of $n \times n$ observations representing the grided radar rainfall values. The state-vector A may be seen as a vector of corresponding matrices.

7.4.2 Real-Time Parameter Estimation

An adaptive exponential smoothing scheme (Brown, 1963) is chosen to estimate the model's parameters. A similar scheme was used by Chen and Kavvas (1992) to forecast locations of the vertices of a polygon model approximating the rainfall contours.The adaptive exponential smoothing filter employs the concept of

negative feedback where the new forecast is adjusted for the error committed in the previous forecast while allowing the option for varying the relative weight given to recent versus past observations. This is important in cases of convective rainfall in which the rainfall evolution may require focussing primarily on recent observations in stable rainfall fields and on old observation for noisy and unstable fields. In addition, the scheme requires very little storage memory, since only the current observation and the previous forecast of the parameters are required, to produce a new forecast.

The real-time parameter estimation procedure amounts to the estimation of the state-vector, i.e., Taylor series expansion coefficients of the polynomials representing the evolution of the radar rainfall pixels. The estimated parameters are required to be stable in the presence of noise. At the same time, the scheme should detect any rapid change in the process and respond to this change quickly. These two requirements are often conflicting. Therefore, a compromise has to be made. The adaptive exponential smoothing scheme can easily deal with both stability and flexibility. It puts more weight on the most recent observation. The influence of observation errors on the estimation decreases rapidly with the age of the observation. Hence, the adaptive exponential smoothing can be considered as a weighted least-square fitting with exponentially discounting weighting factors (Brown, 1963).

Suppose that the analysis domains (the analysis domain can be a partition of the radar umbrella) consists of m rainfall cells, where m equals the number of grid

cells in the analysis domain. Accordingly, a number of *m* independent filters can be used to estimate the *m* state-vectors of the *m* rainfall cells to describe their evolution as being observed on the radar scans. These filters are identical and completely disconnected. Thus, only one filter is described in the following paragraph.

From the theory of Adaptive Exponential smoothing (Brown, 1963), the updated state-vector at the current time $A(c)$ can be estimated from the previous state-vector $A(c\text{-}t)$ by:

$$A_{c,c} = M(t)A_{c-t,c-t} + H'E_C \tag{7.7}$$

where:

$$H' = \begin{bmatrix} 1-(1-\beta')^3 \\ 3/2\beta'^2(2-\beta') \\ \beta'^3 \end{bmatrix} \tag{7.8}$$

$$E_c = R(c) - R_{c,c-t} \tag{7.9}$$

where:

$A_{c,c}$ = Updated state-vector at time *c*. This state-vector will be used for forecasting the next forecast using the transition equation (equation 7.6).

$A_{c\text{-}t,c\text{-}t}$ = State-vector at the previous time step.

H' = Smoothing coefficient vector.

E_c = The error between the observed value $R(c)$ at time c and the t-step ahead forecast $R_{c,c-t}$, made at time c-t.

$R(c)$ = Rainfall observation obtained at the current time c.

$R_{c,c-t}$ = The t-step ahead forecasted value made at time c-t.

β' = Exponential smoothing coefficient.

The values of the $\boldsymbol{M(t)}$ matrix and the $\boldsymbol{H'}$ vector are set in the initialization of the model. They are then fixed throughout the forecasting operation. The choice of the value of the exponential smoothing coefficient β' is based on the stability of the rainfall field. If the evolution of the rainfall field being observed on the radar scans is very unstable, a smaller value of β' (0.1-0.3) should be chosen so that more weight is put on older observations. Although this makes the algorithm less sensitive to rapid changes, smoother estimates will be obtained in the presence of small scale noise . If the rainfall pattern is stable, a larger β' (0.3-0.5) can be taken to make the algorithm respond quickly to slow changes. Also, for long lead time forecasting (60 and 120 minutes), a smaller value of β' (0.05-0.15) should be chosen to give more weight on older observations to avoid overestimating or underestimating the forecasted rainfall field due to the effect of quick responses to newer observations on the long term extrapolation.

In the initialization of the model and in the case of newly appearing rainfall cells or disappearing cells, the initial values of the state-vector (equation 7.4) are set by neglecting the higher order terms. For example, for the first time step or for the

first time a rainfall pixel appears, A_o is set to the observation value *R(1)* at time 1, while A_1 and A_2 are set to zeros. For the second time step, A_o is set to *R(2)* , A_1 may be set to *[R(2) - R(1)]* or simply to zero, and A_2 is set to zero. The updated estimates of the state-vector are then obtained directly from equation 7.7 for subsequent time steps.

7.5 Model Output

The developed AARS is applied at a temporal resolution equal to that of the radar scans, that is, every 10 minutes, and spatial resolutions of 1 km for tracking and 3 km for forecasting. At each time step the AARS model produces two spatial fields of forecasted rainfall: (1) a forecast valid at the time of the next observation (updating forecast). This forecast is used to update the model to obtain an optimal estimate of the state-vector of each rainfall cell of the radar grid with respect to the moving computational domain; and (2) a forecast valid at the required lead time (for example: 10, 30, 60, and 120 minute lead times, or any other user specified lead time). This lead time forecast is not used in the updating process. It serves only as a source of forecast information (informative forecast).

It should be noted that negative values are allowed to appear in the updating forecast. On the other hand, negative values are replaced by zero values in the informative forecast. In addition, when updating the model, the filter is discontinued and reinitialized at any zero observation.

7.6 Model Performance

The prediction performed in this study is not only in time but also in space. Therefore, the grids employed are three-dimensional time-space grids, which have a time increment of 10 minutes and any space resolution chosen in order to predict the highly variable rainfall structure. In order to evaluate the performance of a forecasting scheme, it should be tested in terms of: (1) requiring the least run time, which essentially is the result of the fewest computations and the smallest amount of computer memory required; (2) being adaptable to the evolution of the highly variable nature of the rainfall field; and (3) yielding the best forecast in terms of the performance measures. Accordingly, the performance of the AARS model will be compared to two alternative forecasting schemes, PERSISTENCE and SHARP.

7.6.1 Performance Measures

The performance measures used to evaluate the model are: (1) the average error in rainfall rate between the forecasted and observed fields (*Ferr*); (2) the root mean square error between the forecasted and observed fields (*FRMS*); and (3) the cross-correlation between observed and forecasted fields (*FCC*). The three measures are calculated from:

$$Ferr = \frac{1}{n}\sum_{i=1}^{n}(I(i)_f - I(i)_o) \tag{7.10}$$

$$FRMS = [\frac{1}{n}\sum_{i=1}^{n}(I(i)_f - I(i)_o)^2]^{1/2} \tag{7.11}$$

$$FCC = \frac{\frac{1}{n}\sum_{i=1}^{n}(I(i)_f - \bar{I}_f)(I(i)_o - \bar{I}_o)}{\sigma_{I_f}\sigma_{I_o}} \tag{7.12}$$

where:

$I(i)_o$ = Observed rainfall intensity at grid cell i.

$I(i)_f$ = Forecasted rainfall intensity at grid cell i.

n = Number of grid cells in the domain used for the analysis.

$\bar{I}_o$ = Average value of the observed rainfall field.

$\bar{I}_f$ = Average value of the forecasted rainfall field.

σ_{I_o} = Standard deviation of the observed rainfall field.

σ_{I_f} = Standard deviation of the forecasted rainfall field.

7.6.2 Test Cases

The test cases include King City radar scans covering eight storm events in year 1989. This data set is characterized as having quality controlled radar data from King City radar. The 8 events are those used for the sampling error analysis in Chapter 6 (refer to Table 6.2). In this section the AARS model is evaluated and quantitatively compared with two alternative forecasting schemes, namely the PERSISTENCE and SHARP models (refer to Chapter 2, and section 7.1). With PERSISTENCE the latest available radar observations are the forecasted rainfall field. Thus, in PERSISTENCE, there is no translation of the field in space and neither growth nor decay of rainfall intensity in time.

The analysis domain is a stationary squared area (300×300 km^2) centered at

the radar location. The analysis is applied at a temporal resolution equal to that of the radar observations, that is every 10 minutes. The spatial resolution used for performing the tracking is 1 km to achieve maximum tracking accuracy whereas the forecasting is applied on 3 km spatial resolution grids to minimize the effect of small-scale variations of rainfall. The 3 km resolution grids are re-sampled from the original 1 km fields using a bilinear re-sampling methodology. Figures 7.12 to 7.15 show a comparison between the three forecasting schemes for the Aug. 15, 1989 test case using different forecasting lead times (10, 30, 60 , and 120 minutes respectively). The AARS is slightly better than the SHARP in terms of the forecasting measures in Figures 7.12 and 7.13 (i.e., for the 10, 30 minutes lead times) and almost the same in Figure 7.14 and 7.15 (i.e., for the 60 and 120 minutes lead times). Figure 7.16 presents the overall average performance for the 8 events studied. As shown on figures 7.12 to 7.16, both the AARS and SHARP forecasting models are significantly better than the PRESISTENCE scheme. The AARS model is slightly better than the SHARP model in terms of overall accuracy for lead times up to 30 minutes and approximately equal to the SHARP model for longer lead times. The slight improvements in the forecasting accuracy using the ARRS over the SHARP model in the 10 minutes and 30 minutes lead times (Figures 7.12 and 7.13) are attributed to modelling the growth and decay of "existing" rainfall structures. The equality between the two models for longer lead times can be explained as a result of the inability of both models to predict the "birth" of new rainfall cells. This is a more dominant feature in these forecast horizons than the growth and decay of

rainfall in the "vertical" direction. This decreases the forecasting accuracy especially when the forecasting lead time exceeds the characteristic life time of convective storms, which is on the order of 30-45 minutes. The AARS, because of the fast and robust search strategy it employs for the tracking, is superior to the SHARP model in terms of run time. In summary, it can be concluded that there are some minor improvements in terms of forecasting accuracy for short lead times (10 and 30 minutes), although these are not remarkable. In addition, the AARS model significantly requires less run time.

It should be noted again that in order to use the AARS model for long lead times more than 30 minutes, a small value of the exponential smoothing coefficient should be used to reduce the effect of the polynomial extrapolation on a long extrapolation lead time (i.e., give more weight on older observations in the least square fitting). The AARS is able to predict the disappearance of existing rainfall structures. On the other hand the AARS model, similar to other extrapolation forecasting models, can not predict the "birth" of new rainfall cells. This aspect remains a difficult future challenge especially on this fine spatiotemporal scale. The lack of a complete understanding of the rainfall producing mechanism and the available remote sensing technology make the problem more complicated.

7.7 Assessment of the Forecasting Accuracy in Hamilton Region

In order to test the portability of the model and assess the quality of rainfall forecasting in the Hamilton-Wentworth Region, the AARS model is applied to recent

data from Exeter Radar covering 4 events. Each event represents a continuous day (refer to Table 7.2). As concluded in Chapter 3, rain storms in Hamilton-Wentworth Region normally originate from the west. Exeter Radar covers the west of Hamilton-Wentworth Region , which makes it more desirable than King City radar for forecasting purposes in this region (refer to Figure 6.13 for the location of Hamilton-Wentworth Region with respect to Exeter Radar). Also, as concluded in Chapter 6, data from Exeter suffers less from clear air and ground contaminations.

Table 7.2 Events Used from Exeter Radar for the Forecasting Assessment in Hamilton-Wentworth Region

Event No.	1	2	3	4
Day\Month\Year	10\05\2000	13\05\2000	10\06\2001	20\07\2001
Type	w/c	w	w/c	w/c

w = Widespread Rainfall

c = Convective

w/c = Mixed

In addition to the performance measures introduced in section 7.6.1, an additional measure is used for assessing the quality of forecasts in Hamilton-Wentworth Region. This performance measure is known as the Critical Success Index (*CSI*) and can be calculated from:

$$CSI = \frac{n_1}{n_1 + n_2 + n_3} \times 100 \qquad (7.13)$$

Where n_1, n_2, and n_3 are the number of grid cells (pixels), which are defined in Table 7.3 .

Table 7.3 The Critical Success Index (CSI) Definition

		Forecasted	
		Rain	No rain
Measured	Rain	*n1*	*n2*
	No rain	*n3*	--

The tracking and evaluation strategies in this section are relatively different:

1- Different correlation domains are used for the tracking module. The tracking module uses the full radar domain in its initialization to determine the average storm direction. A smaller sub-domain (200×200 km^2) is then placed in the direction from which rainfall advances towards Hamilton-Wentworth Region. The tracking module performs the tracking inside this sub-domain.

2- Only the grid cells contained within a box representing the boundary of Hamilton-Wentworth Region are considered for calculating the forecasting measures (the evaluation area is shown in Figure 7.17).

3- The AARS is initialized at the beginning of each day and run on a continuous basis. Because the evaluation area is small it may not be subjected to rainfall in all time steps. Accordingly, only those runs producing rainfall inside the evaluation area are considered for calculating the performance measures of the forecasts.

In order to summarize the evaluation of the forecasts in Hamilton-Wentworth Region, refer to Table 7.4. This table shows the overall average of the performance measures inside the evaluation area obtained from 76 scans reporting rainfall. Note that the forecasting error *Ferr* is calculated as a percentage of the average observed rainfall. The averaging neglects the underestimation or overestimation (i.e., the average of the absolute values of *Ferr*).

Table 7.4 Overall Forecasting Accuracy in Hamilton-Wentworth Region

	30-Min Forecasts		60-Min Forecasts	
Measure	**Average**	**Std. Dev.**	**Average**	**Std. Dev.**
CSI	65%	10%	51%	16%
%Ferr	27%	29%	42%	34%
FCC	0.45	0.12	0.3	0.14

Figure 7.18 shows a continuous time sample from May, 10, 2000. The figures show the values of the forecasting measures during a continuous time period, reporting rainfall inside the evaluation area. Figures 7.19 to 7.24 compare a sample of forecasted rainfall fields generated by the model with those measured by Exeter radar in the area surrounding Hamilton-Wentworth Region. Using the visual comparison between forecasted rainfall fields and the measured field in Figures 7.19 to 7.24, it is evident that there is agreement in terms of the rainfall pattern location with respect to the Municipality of Hamilton-Wentworth. This spatial agreement means a corresponding agreement in the timing of rainfall given that the location of

rainfall defines the timing of rainfall. Using the information presented in Table 7.4 in an engineering context a 51% average success in determining the rainy area on this small scale with 42% expected error in the average areal rainfall can, however, provide useful 1-hr ahead detailed rainfall field with good timing accuracy. This forecast can then be used for the different flood forecasting applications. For example, given the expected dry/wet condition of a combined sewer system after 1 hour and using the forecasted rainfall field as input to a distributed hydrological/hydraulic model, an estimate of the flows at the key points of the system can be obtained. This estimate can be used at the current time to prepare the system (preparing the system involves controlling the gates and reservoirs) for the coming event after one hour in order to optimize its performance. Future research will have to quantify the gain. One of the objective functions that can be used to optimize a combined sewer system is minimizing the volume of untreated sewage in the receiving water bodies. This control process can be done in an automatic mode using minimum manual interaction.

7.8 The Operational Implementation of The AARS Model

The operational implementation of the AARS model can provide support for different applications that require quantitative precipitation forecasts. In this section some recommendations for the operational implementation of the AARS model are discussed.

The operational AARS model is recommended to run on a main workstation (The Processing Workstation), which will act as a server for the different users. This Processing Workstation may be located at McMaster University for example. Figure 7.25 provides a schematic diagram of the operational implementation of the AARS model. The real-time delivery of rainfall forecasts to the remote users can be accomplished in three real-time concurrent (i.e., parallel) stages:

Stage 1 (Transmitting the raw radar data to the Processing Workstation):

In this stage, the raw radar data files are transmitted from the radar processing unit to a remote workstation (The Processing Workstation) using an automatic FTP (File Transfer Protocol). The received raw data, in the Processing Workstation, goes directly to a "current" directory in which all the data for the current day (or couple of hours) are saved for the purpose of updating the AARS model. When the data are one day (or couple of hours) old, they are then moved to a tree storage directory that uses the following terminology: "OldData/year/month/day/". It should be noted that the old data are "packed up" every certain period (a year for example).

Stage 2 (Updating the AARS model using the latest data and producing forecast products):

This stage runs in the Processing Workstation. After initialization, the AARS model is updated every 10 minutes using the latest data in the "current" directory and produces the following recommended set of products:

- Severe storm warnings and graphical displays such as forecasted images and animations that are placed in a web folder for the public to access through the Internet.
- Numerical products in the form of grided precipitation rates or accumulations. These products are saved in different automatic FTP user folders, which are accessed remotely by specific organizations. These numerical products should be in the format and specifications required by each organization.

Once these products are old (one day old for example) they should be moved from the user/public permissible directories to archiving places.

Stage 3 (Delivering the AARS products to the users):

The operational ARRS model is recommended to produce two types of products: (1) products of graphical displays and severe storm warnings and (2) numerical products, as mentioned in the previous stage. The graphical display and sever storm warning products should be available to the public through the Internet by accessing a specific web site. The laptop computer shown in Figure 7.25 provides an example of such public user.

The second group of products (numerical products) are available for specific organizations through automatic FTP. Two examples of this type of delivery are shown in Figure 7.25. In the first example (the PC Running a Flood Warning System) the delivered numerical product can be used as input to a hydrological/hydraulic

model in order to produce flood forecasts. In the second example (i.e., the Workstation Supervising an operational RTC (Real Time Control) System), the delivered products can be used as input to the RTC system to optimize the performance of the sewers network.

7.8 Summary

This chapter introduces an improved extrapolation model to real-time short-term rainfall forecasting. The two main contributions of the new model are: (1) significant improvement in run time requirements, which makes the new model attractive for real-time application; and (2) simulation of the growth and decay of existing rainfall structures on cell by cell basis.

The new model is called AARS (Adaptive Automated Rainfall Simulator) and consists of two modules, the tracking module and the forecasting module. The tracking module employs the cross-correlation analysis with a new search strategy based on optimization. The new tracking strategy significantly reduces tracking run time. This run time reduction provides improvement for many applications, including forecasting, that use the cross-correlation technique for estimating rainfall kinematics. The forecasting module simulates the growth and decay of rainfall on a cell by cell basis (i.e., only in the vertical direction) using a second degree polynomial model. The real-time estimation of the parameters is done by using an adaptive exponential smoothing algorithm. The developed AARS is applied at a

temporal resolution equal to that of the radar scans, that is, every 10 minutes, and spatial resolution of 1 km for the tracking and 3 km for forecasting to minimize the effect of small scale noise. At each time step the AARS model produces two spatial fields of forecasted rainfall. The first is a forecast valid at the time of the next observation; this forecast is used to update the model to obtain an optimal estimate of the state-vector of each rainfall pixel of the radar grid with respect to the moving computational domain. The second is the forecast that is for the user specified lead time. This lead time forecast is not used in the updating process, and it serves only as a source of information (the forecast to the user).

The AARS model is evaluated and quantitatively compared to two alternative forecasting schemes, namely the PERSISTENCE and the SHARP models. The results show that AARS and SHARP are significantly better than PERSISTENCE. The ARRS model is slightly better than the SHARP model in terms of overall accuracy up to 30 minutes lead forecasting time. It is concluded that modelling the growth and decay of rainfall on cell by cell basis has shown no practical improvements over the traditional advection forecasting methodology followed in the SHARP model. This insignificant difference between the two methodologies can be related to the inability of both methodologies to predict the birth of new rainfall cells. This ability is particularly important given the characteristic life time of convective rainfall (30-45 minutes). In terms of the amount of time to track events and the tracking accuracy, the AARS is superior.

The ARRS model is used to assess rainfall forecasting in Hamilton-Wentworth Region. The results are promising for lead times up to 60 minutes. The average critical success index is 65±10% and 51±16% for 30 , and 60 minutes forecasting lead times respectively. The average forecasting error in Hamilton-Wentworth Region is 27±29% and 42±34% for the 30 and 60 minutes forecasting lead times respectively. The average correlation coefficient between the forecasted and measured fields is 0.45±0.12 and 0.3±0.14 for the 30, and 60 minutes lead times.

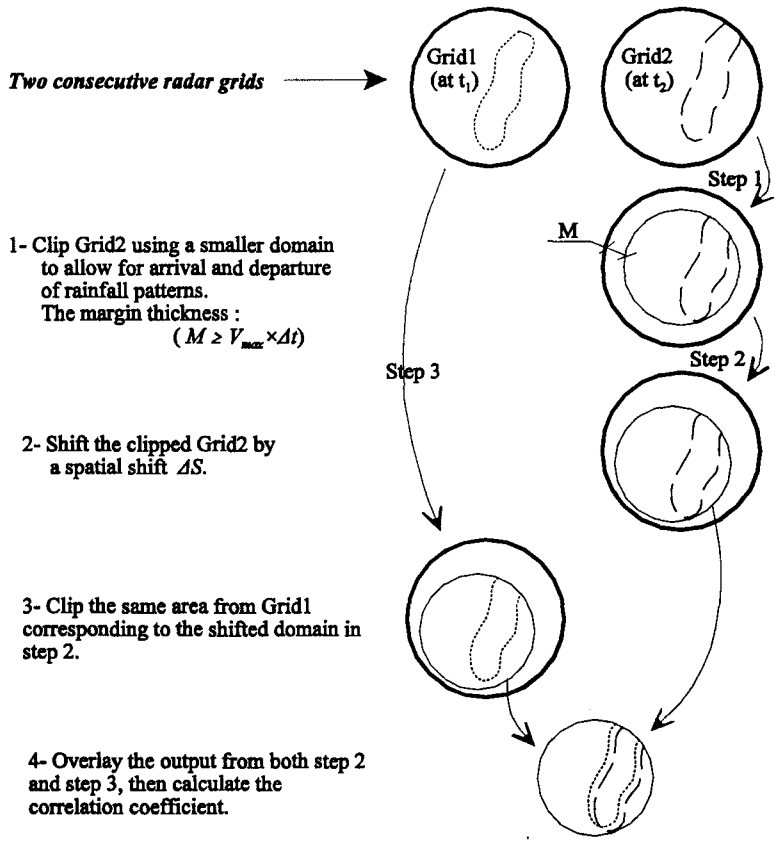

Figure 7.1 The methodology for cross-correlating two consecutive radar rainfall grids.

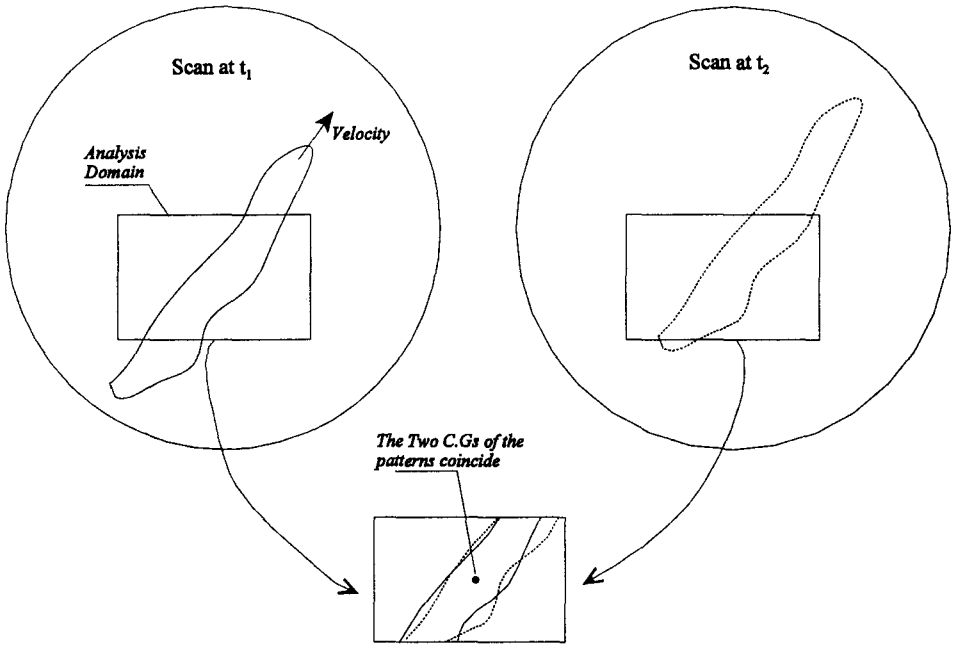

Figure 7.2 A schematic diagram explaining the problem in using the displacement of the centre of gravity to estimate the initial shift when using small domains. Accordingly, an erroneous zero or small initial displacement will be estimated even though there is, in fact, a considerable initial shift. By taking a wrong initial displacement the cross-correlation matrix will be located far from the true optimum.

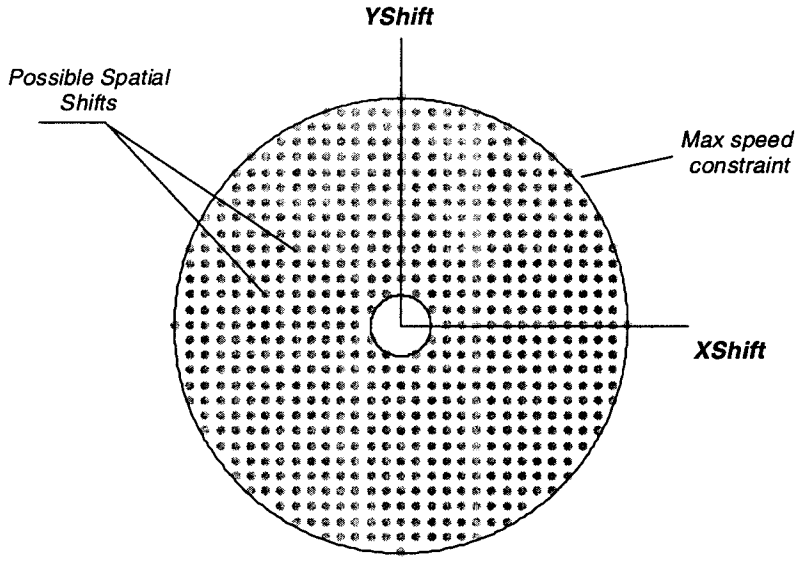

Figure 7.3 Number of possible shifts using V_{max} = 90 km/hr , V_{min} = *12* km/hr, Δt = 10 minutes, and 1 km resolution. Each point represents a possible shift.

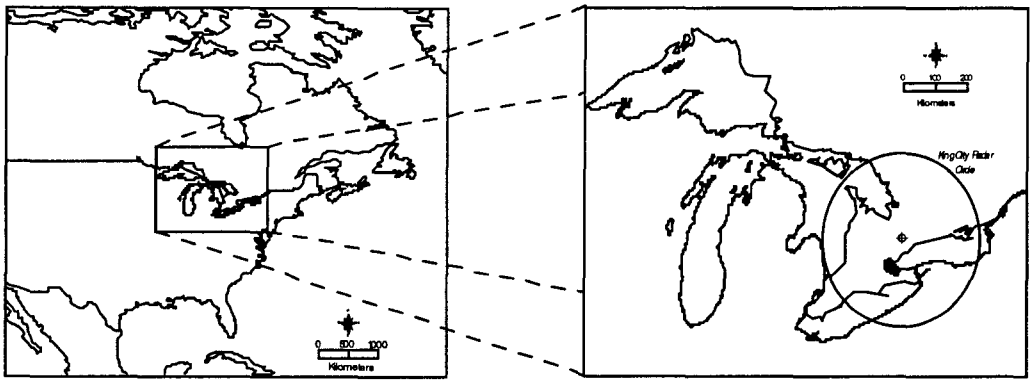

Figure 7.4 Location of King City Radar site.

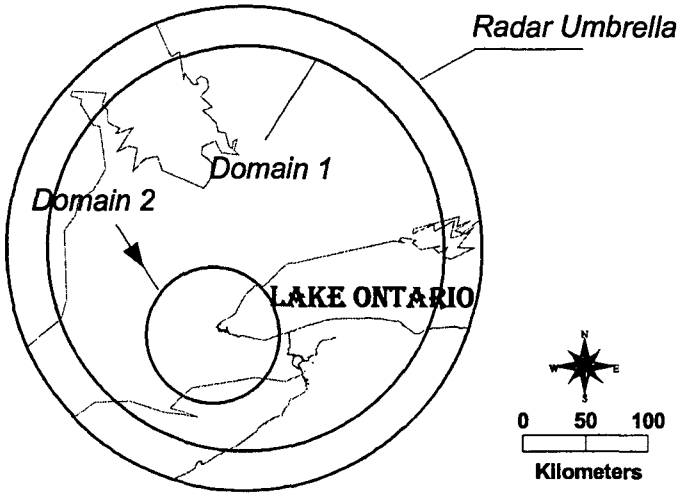

Figure 7.5 Two domains used for performing the cross-correlation in Southern Ontario. Domain 1 covers the maximum area of the radar umbrella, while domain 2 is a smaller domain (radius = 64 km) centred approximately at Hamilton, Ontario, Canada.

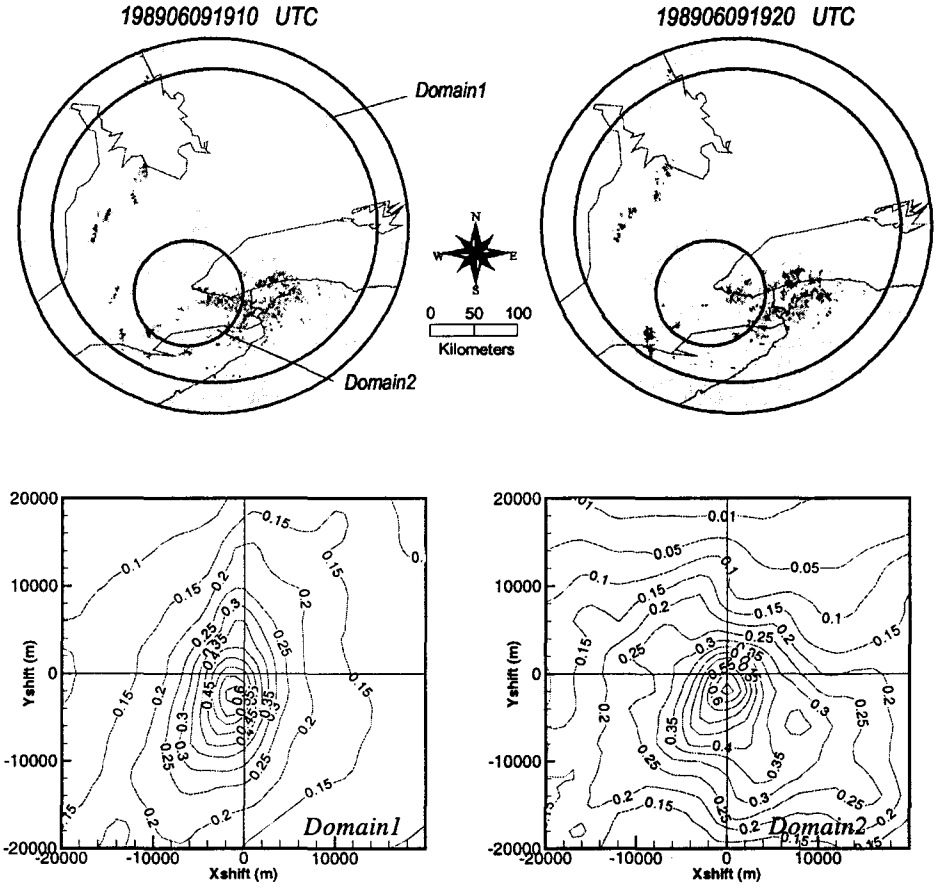

Figure 7.6 Example of a problematic correlation surface (convective rain type). The two figures at the top are two consecutive radar scans. Lower left is the corresponding correlation surface using domain1. Lower right uses domain 2. Note the scaling effect in the appearance of a local optimum (non-unimodality) at contour 0.35 using domain 2.

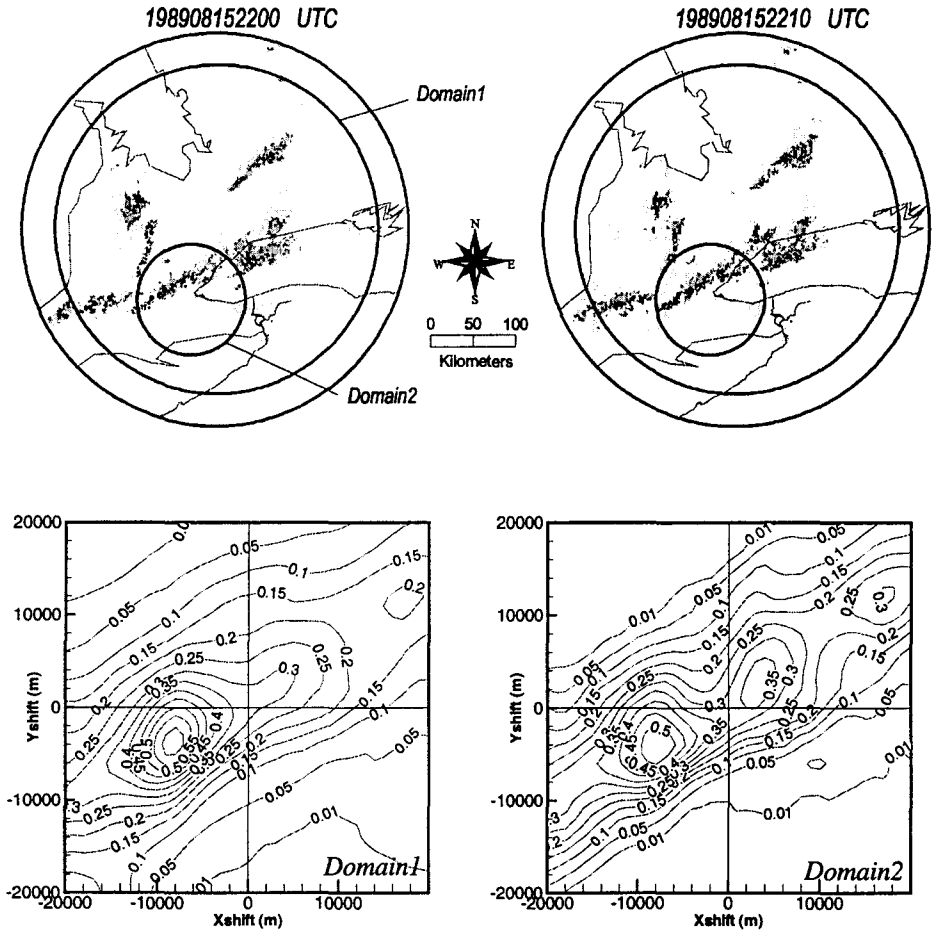

Figure 7.7 Example of a problematic correlation surface (frontal squall lines). The two figures at the top are two consecutive radar scans. Lower left is the corresponding correlation surface using domain 1. Lower right uses domain 2. This case presents one of the most difficult cases for optimization due to the appearance of 2 local regions of attraction (mountainous terrain) when using domain 2.

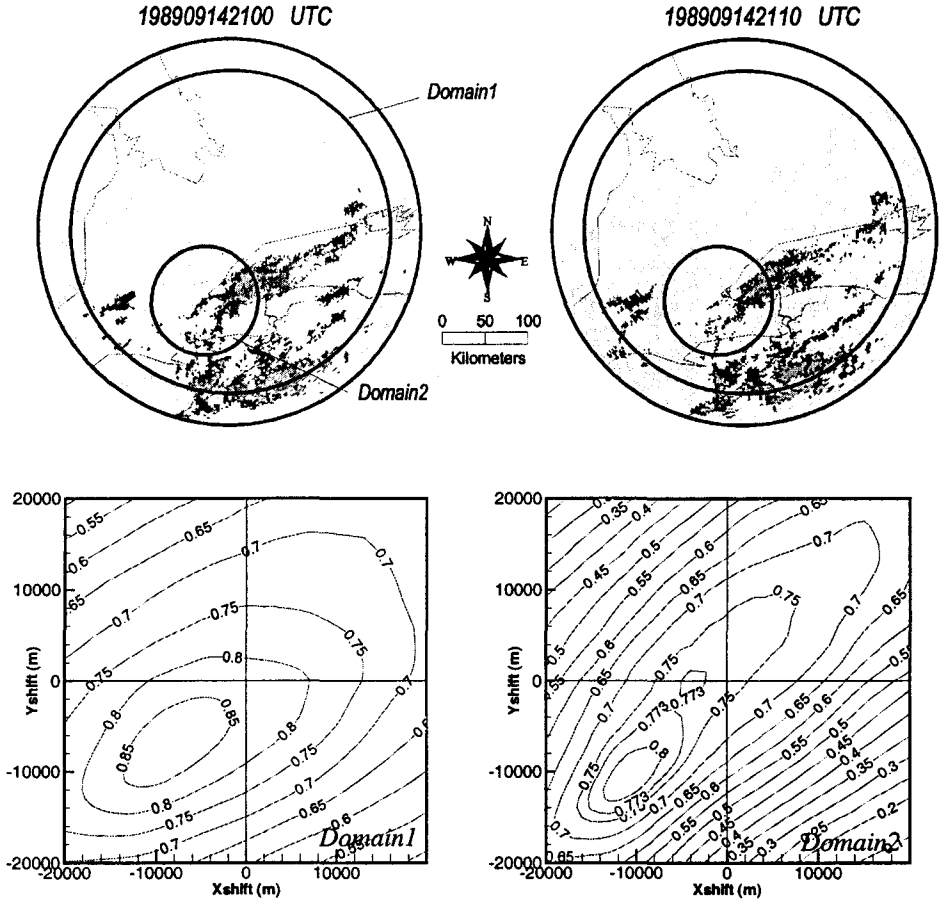

Figure 7.8 Example of a problematic correlation surface (widespread rainfall). The two figures at the top are two consecutive radar scans. Lower left is the corresponding correlation surface using domain1. Lower right uses domain 2. Note the local optimum at contour 0.773 using domain 2.

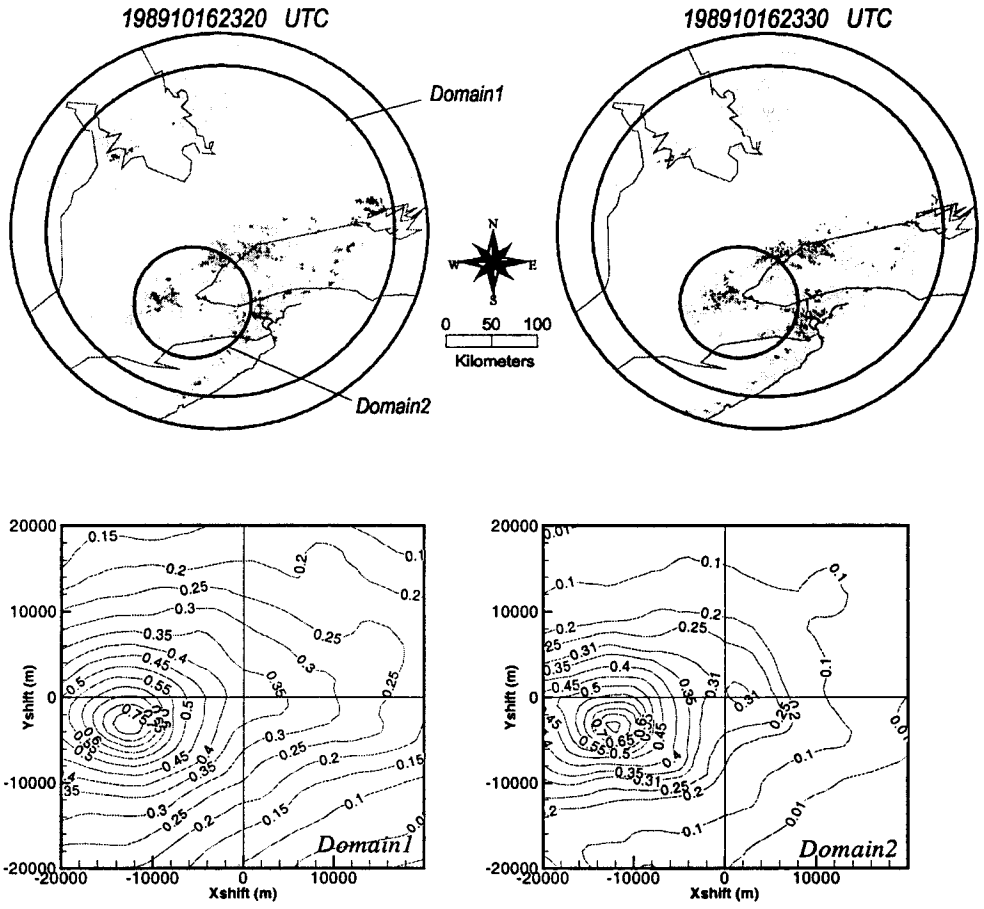

Figure 7.9 Example of a problematic correlation surface (frontal rainfall). The two figures at the top are two consecutive radar scans. Lower left is the corresponding correlation surface using domain 1. Lower right uses domain 2. Note the local optimum at contour 0.31 using domain 2.

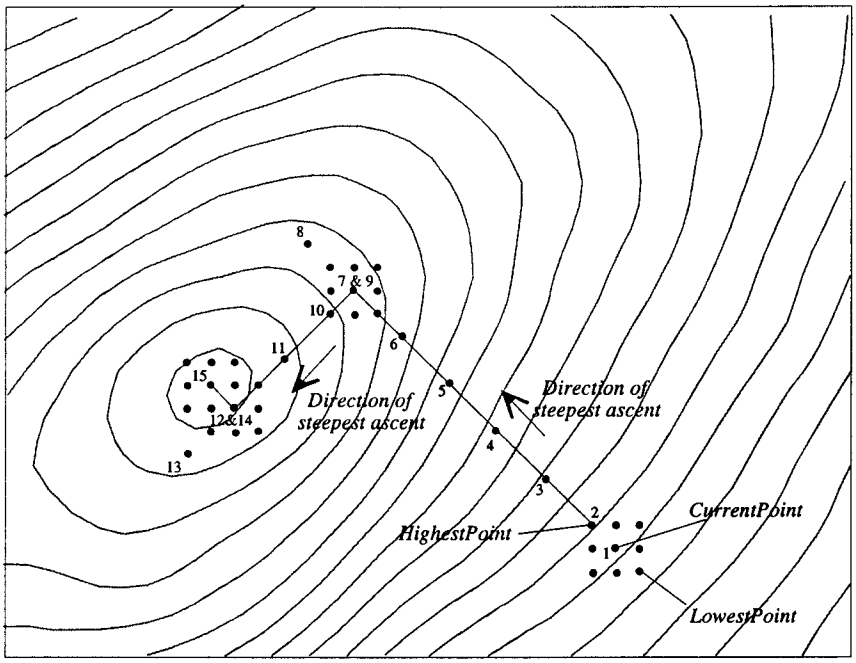

Figure 7.10 The Response Surface (RS) search strategy used in this study. The search starts according to a box design and proceeds in the direction of steepest ascent.

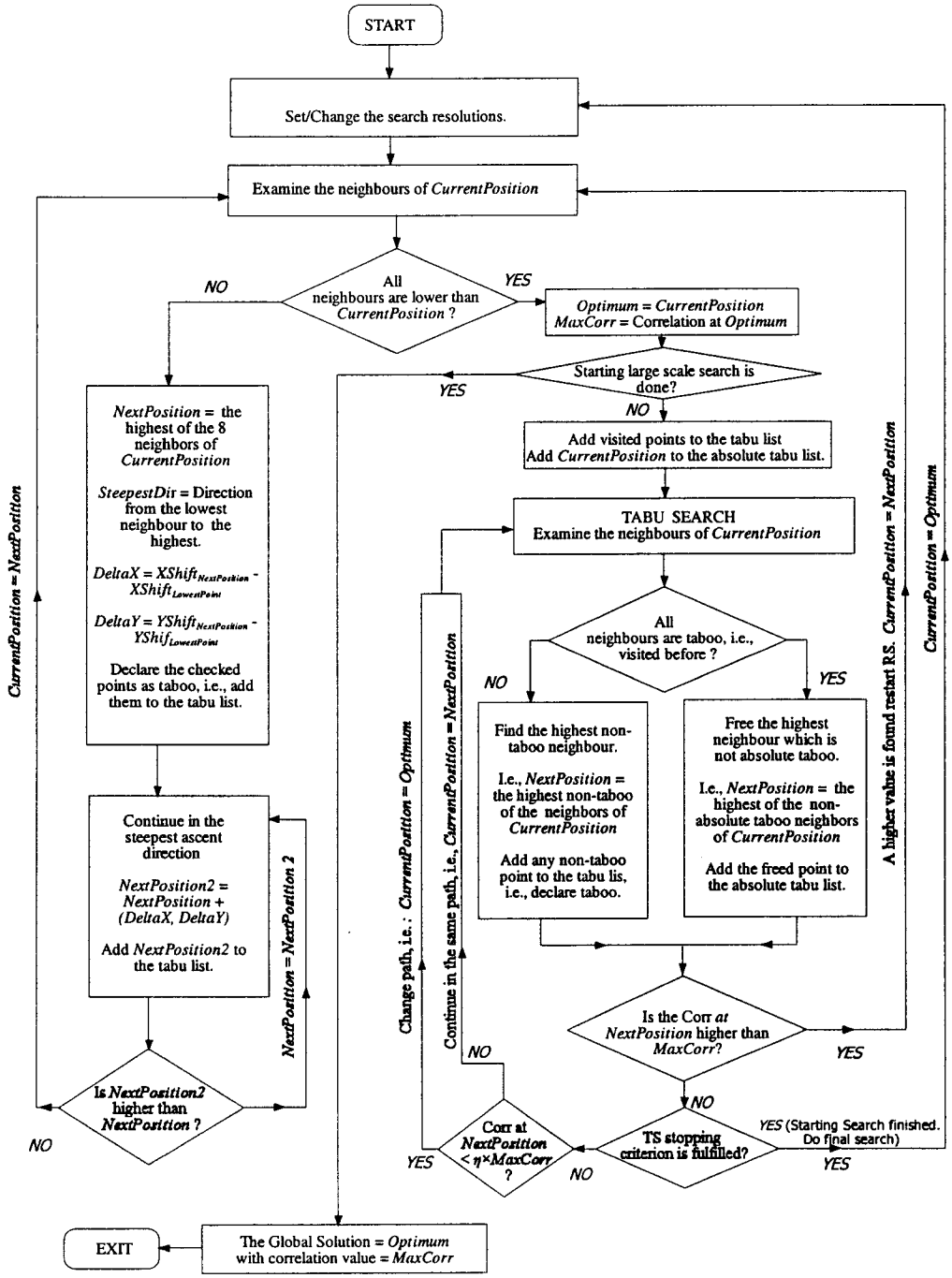

Figure 7.11 The optimization methodology used for the global maximization of the correlation surface.

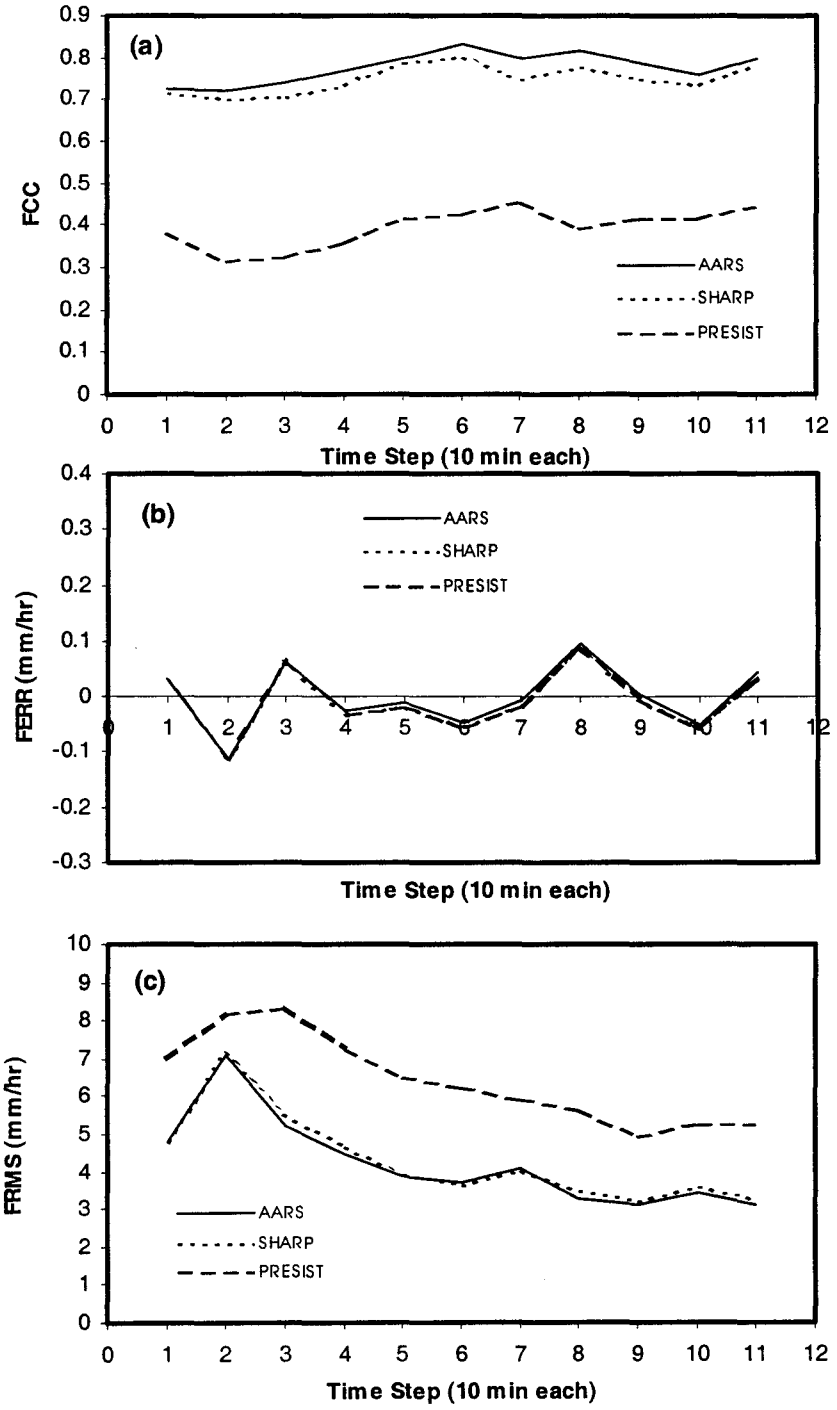

Figure 7.12 Model performance for 10 minute forecasting lead time. Storm on 15/08/1989 starting time 16:10 UTC. (a) correlation ; (b) average error; and (c) root mean square error.

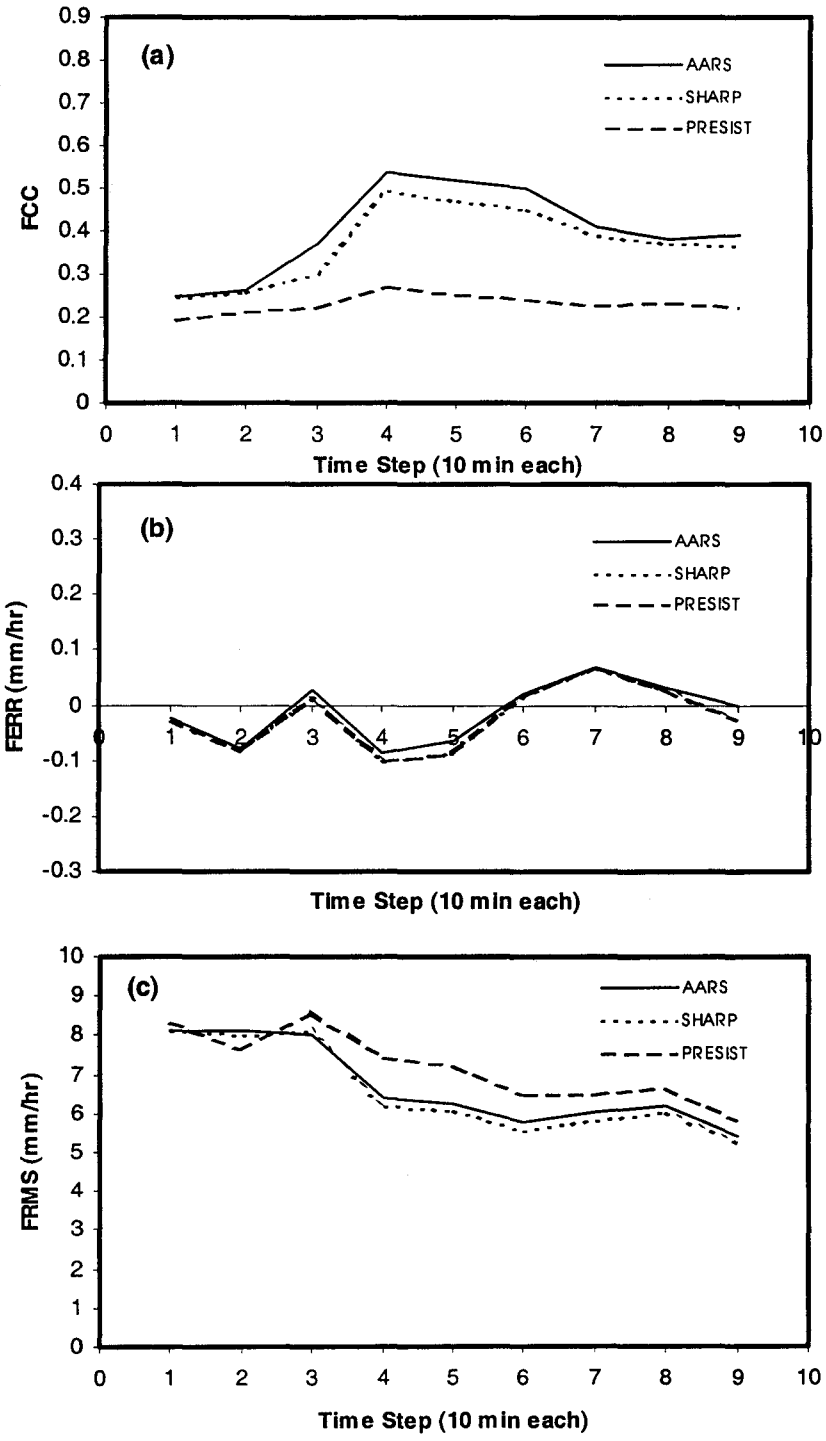

Figure 7.13 Model performance for 30 minute forecasting lead time. Storm on 15/08/1989 starting time 16:10 UTC. (a) correlation ; (b) average error; and (c) root mean square error.

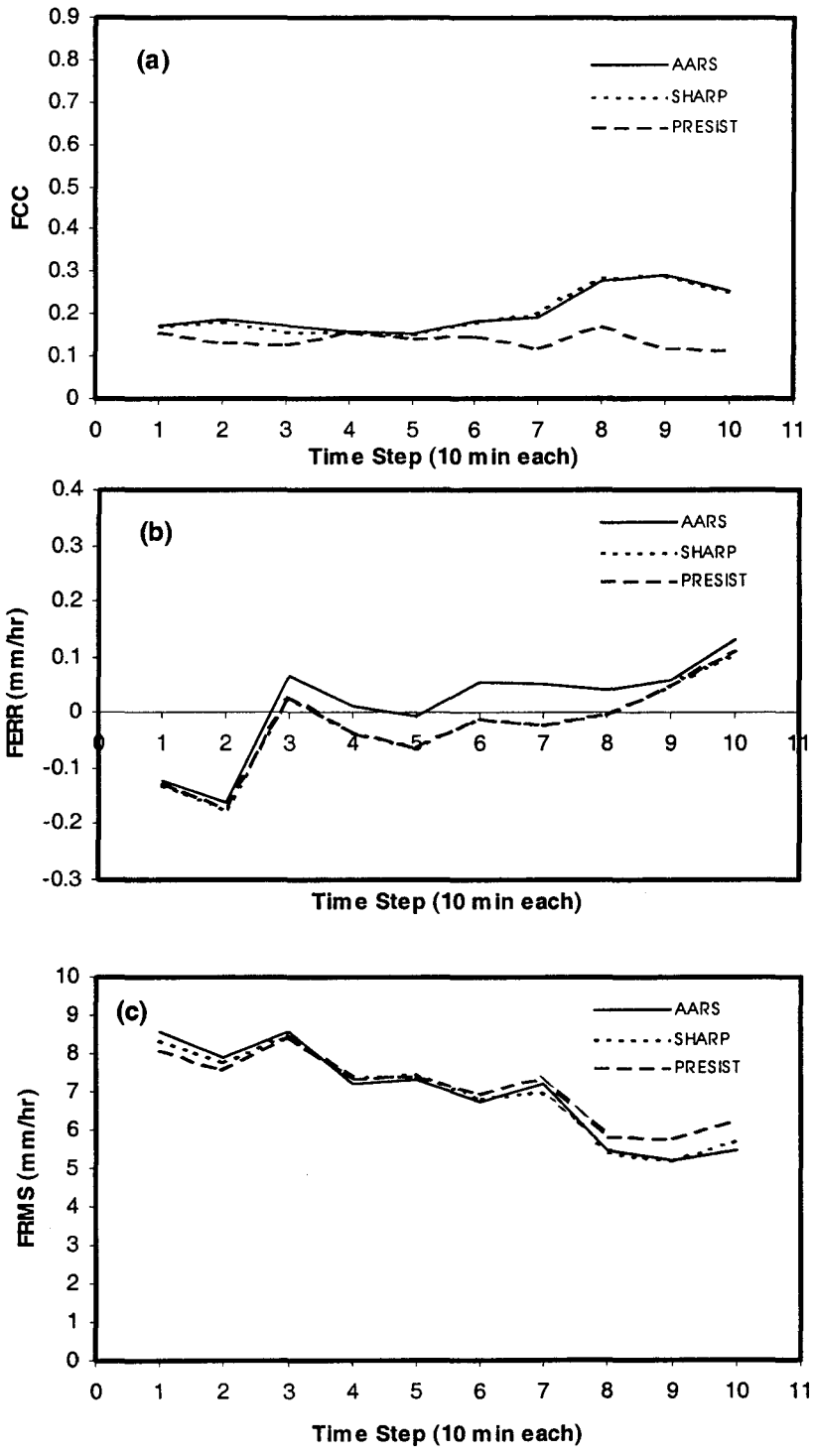

Figure 7.14 Model performance for 60 minute forecasting lead time. Storm on 15/08/1989 starting time 16:10 UTC. (a) correlation ; (b) average error; and (c) root mean square error.

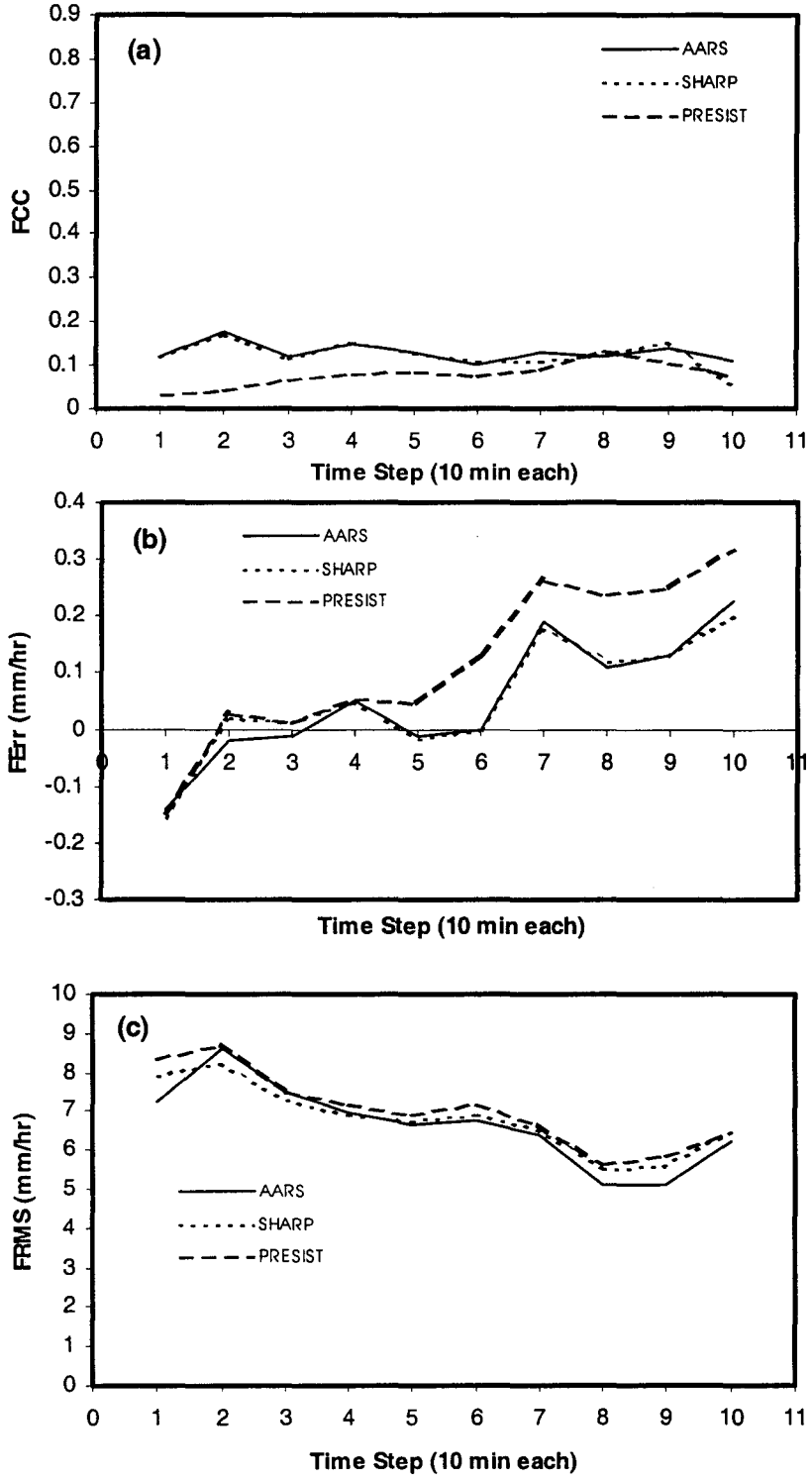

Figure 7.15 Model performance for 120 minute forecasting lead time. Storm on 15/08/1989 starting time 16:10 UTC. (a) correlation ; (b) average error; and (c) root mean square error.

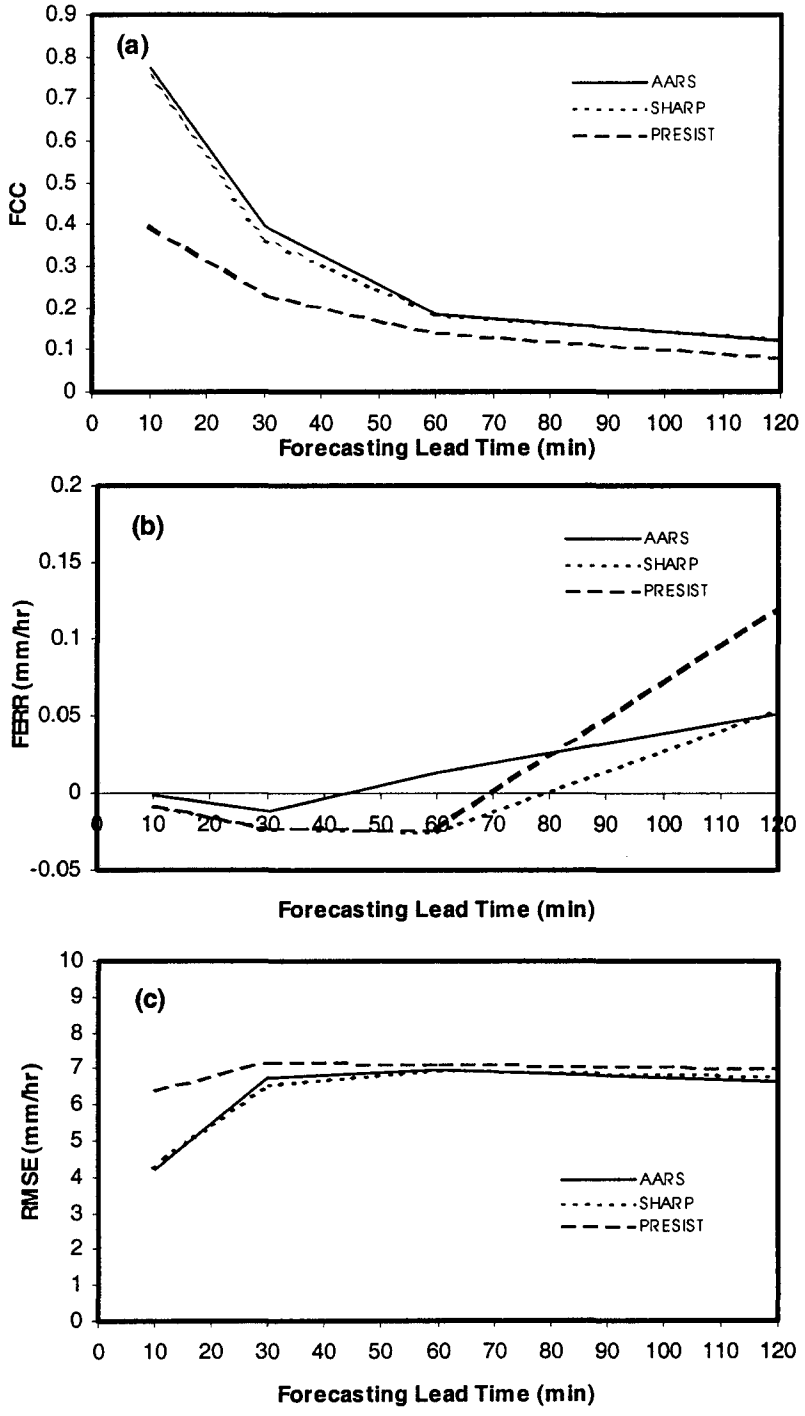

Figure 7.16 Overall model performance based on 8 storm events from King City radar in 1989: (a) correlation ; (b) average error; and (c) root mean square error.

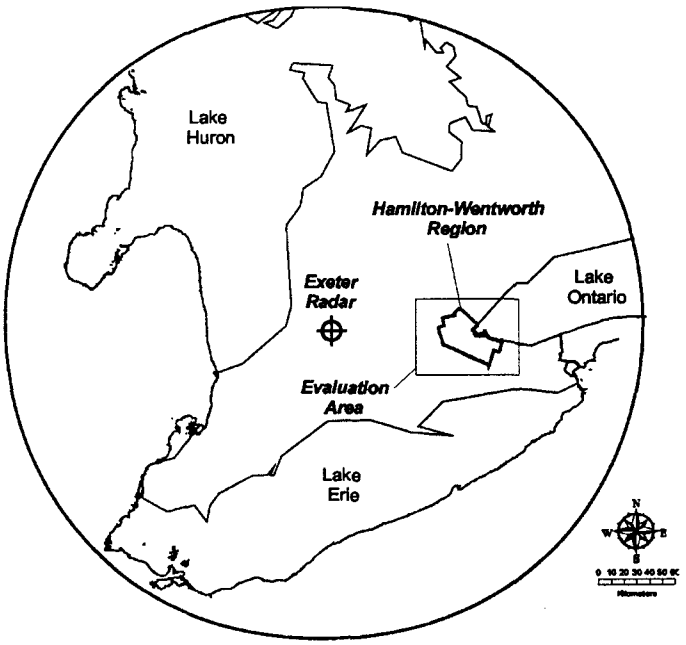

Figure 7.17 Exeter radar and the evaluation area used to assess the forecasting in Hamilton-Wentworth Region.

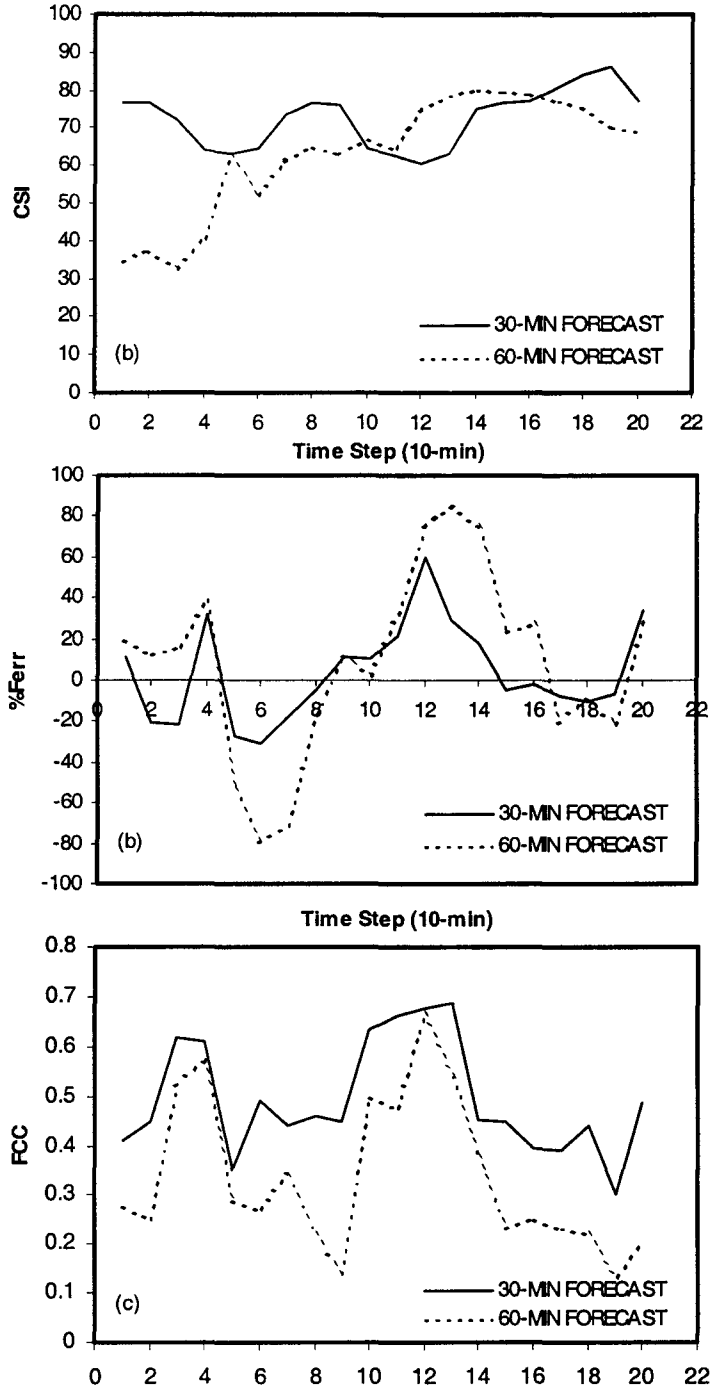

Figure 7.18 Model Performance in Hamilton-Wentworth region using data from Exeter. Event May 10, 2000: (a) critical success index; (b) percentage error; and (c) correlation.

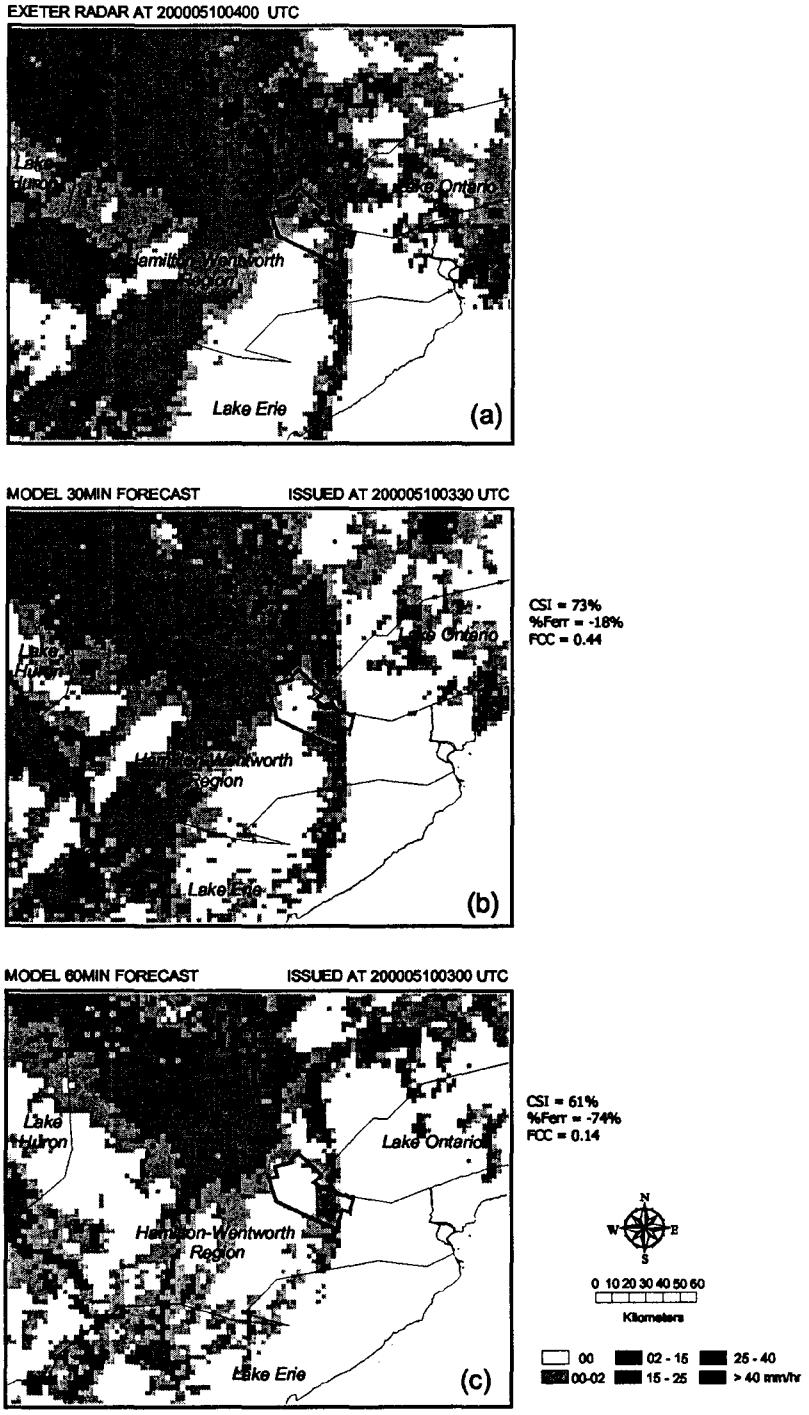

Figure 7.19 Forecasted rainfall fields versus measured field. Event May 10, 2000, 04:00 UTC : (a) Exeter measured field; (b) 30 minute forecasted field; and (c) 1 hour forecasted field.

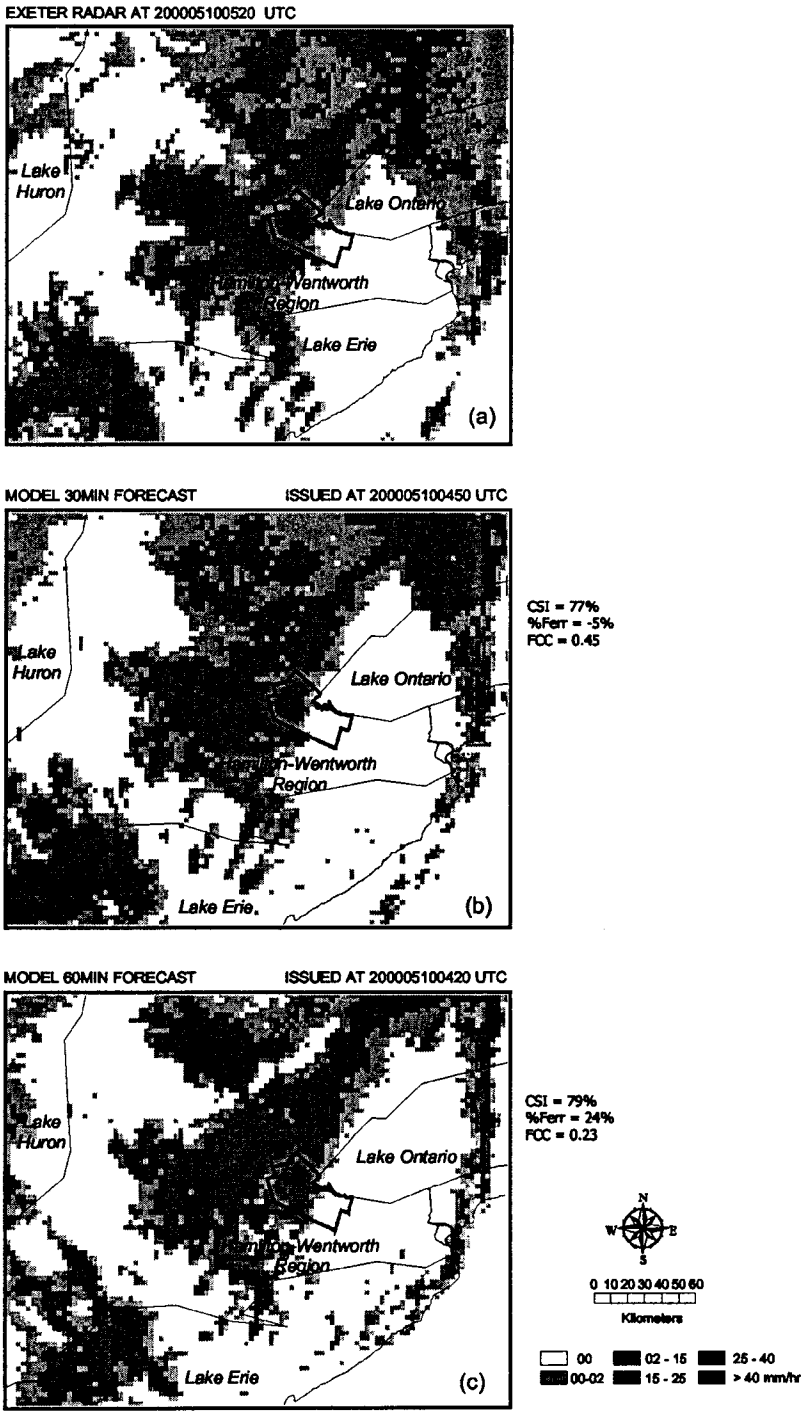

Figure 7.20 Forecasted rainfall fields versus measured field. Event May 10, 2000, 05:20 UTC : (a) Exeter measured field; (b) 30 minute forecasted field; and (c) 1 hour forecasted field.

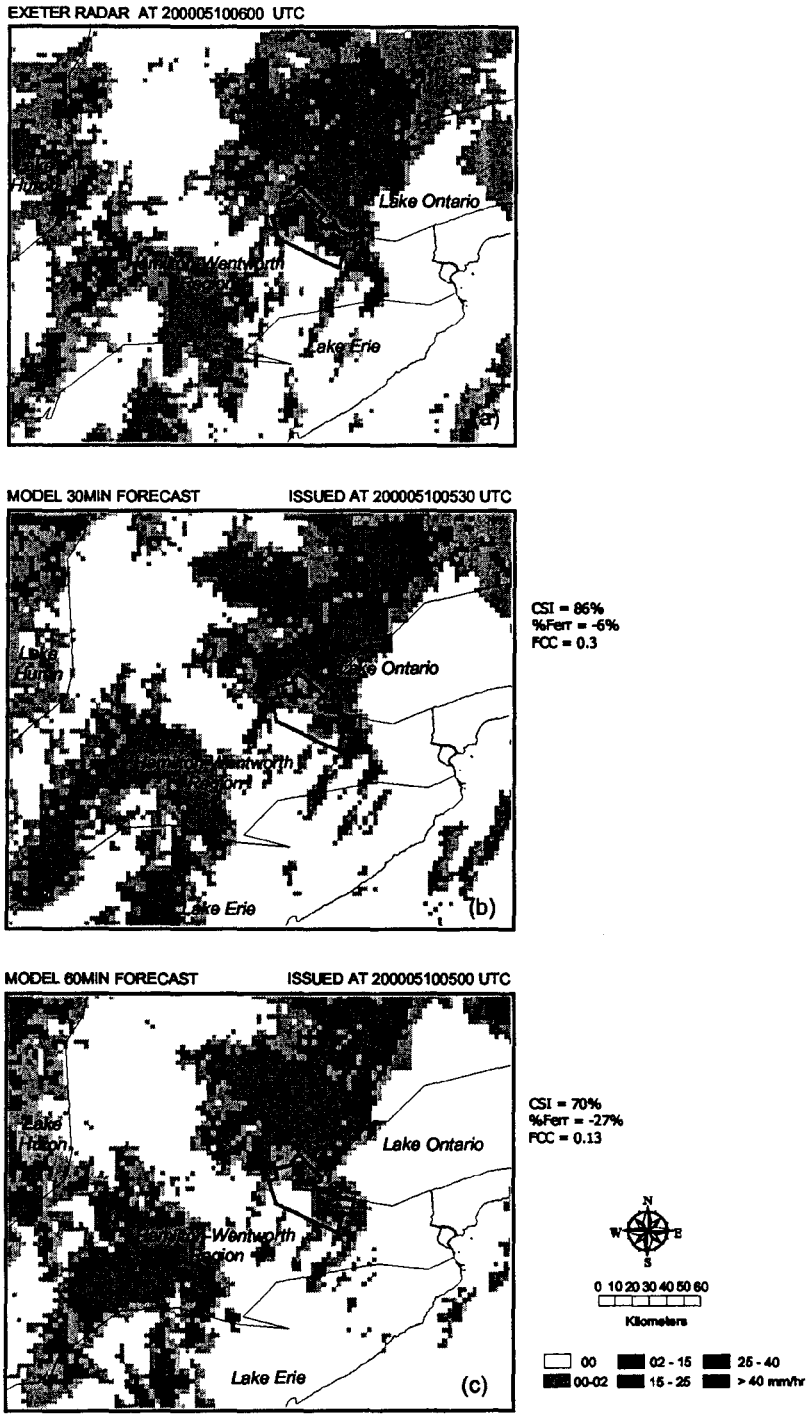

Figure 7.21 Forecasted rainfall fields versus measured field. Event May 10, 2000, 06:00 UTC : (a) Exeter measured field; (b) 30 minute forecasted field; and (c) 1 hour forecasted field.

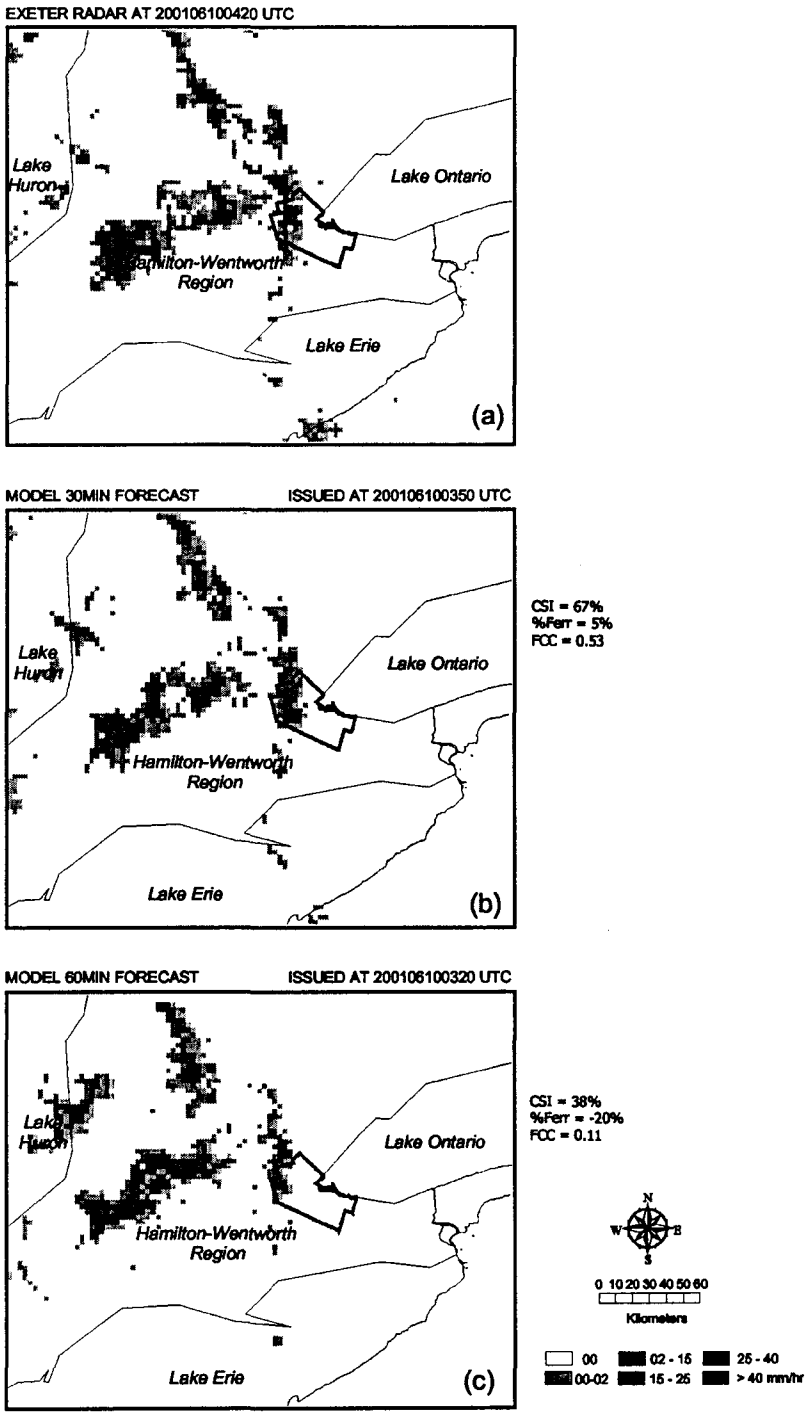

Figure 7.22 Forecasted rainfall fields versus measured field. Event June 10, 2001, 04:20 UTC : (a) Exeter measured field; (b) 30 minute forecasted field; and (c) 1 hour forecasted field.

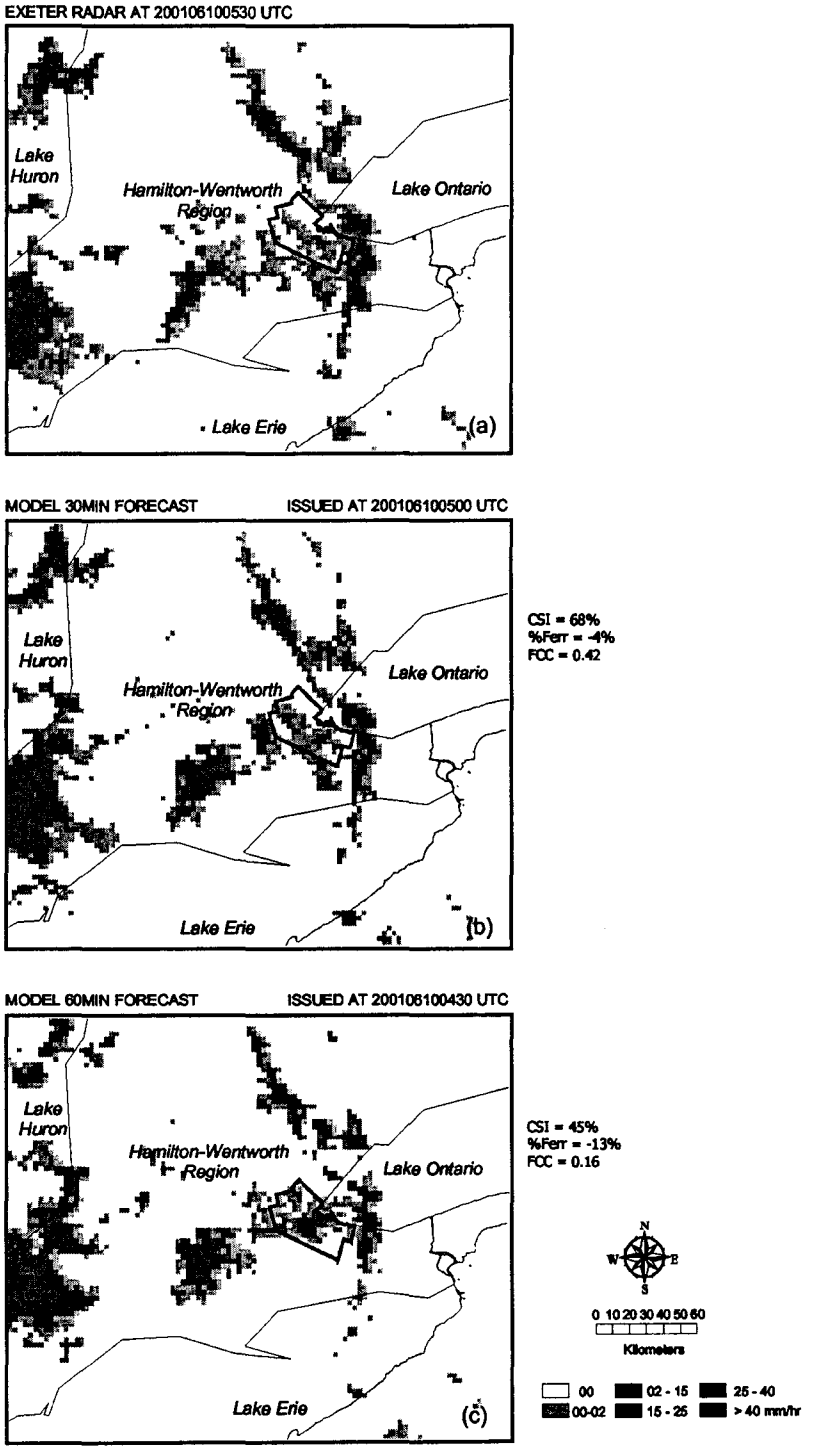

Figure 7.23 Forecasted rainfall fields versus measured field. Event June 10, 2001, 05:30 UTC : (a) Exeter measured field; (b) 30 minute forecasted field; and (c) 1 hour forecasted field.

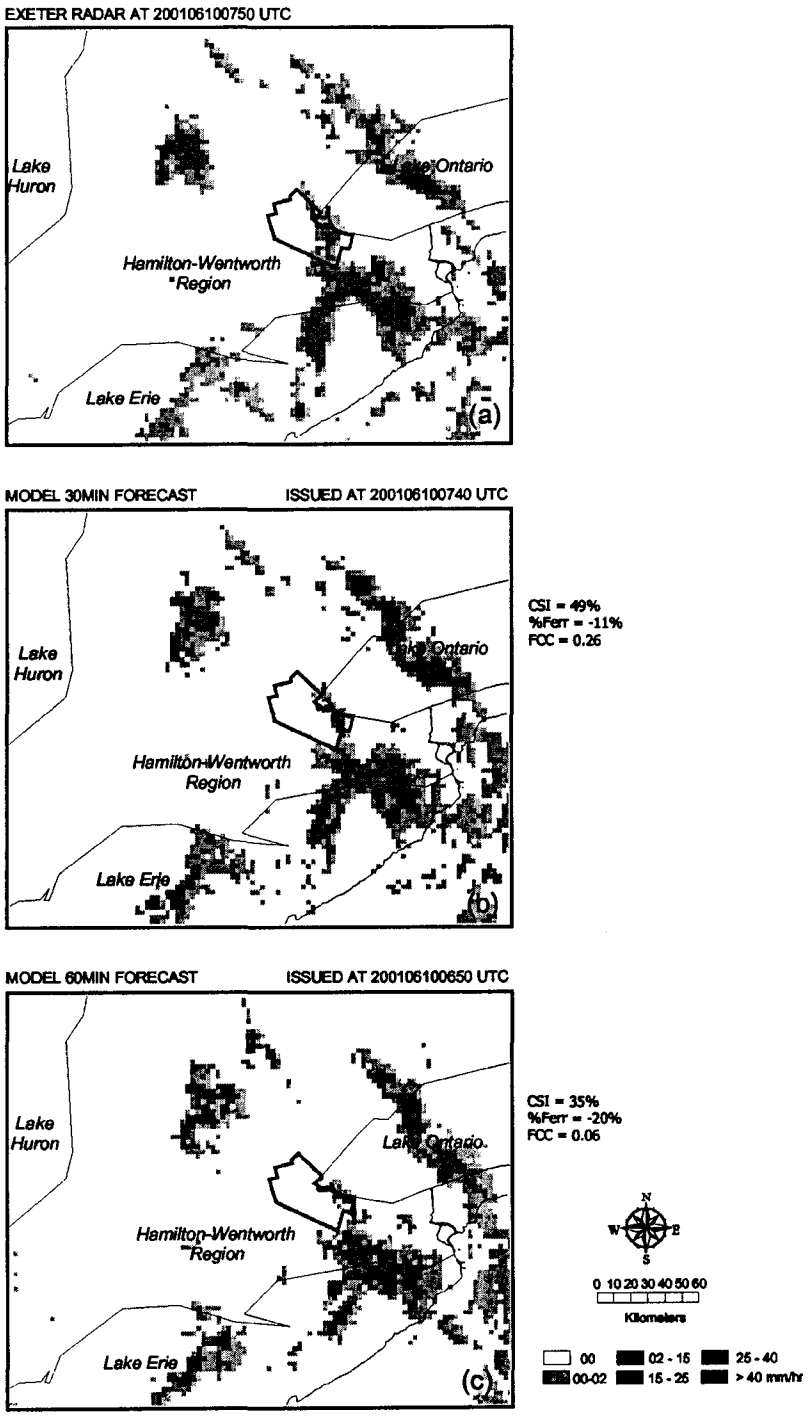

Figure 7.24 Forecasted rainfall fields versus measured field. Event June 10, 2001, 07:50 UTC : (a) Exeter measured field; (b) 30 minute forecasted field; and (c) 1 hour forecasted field.

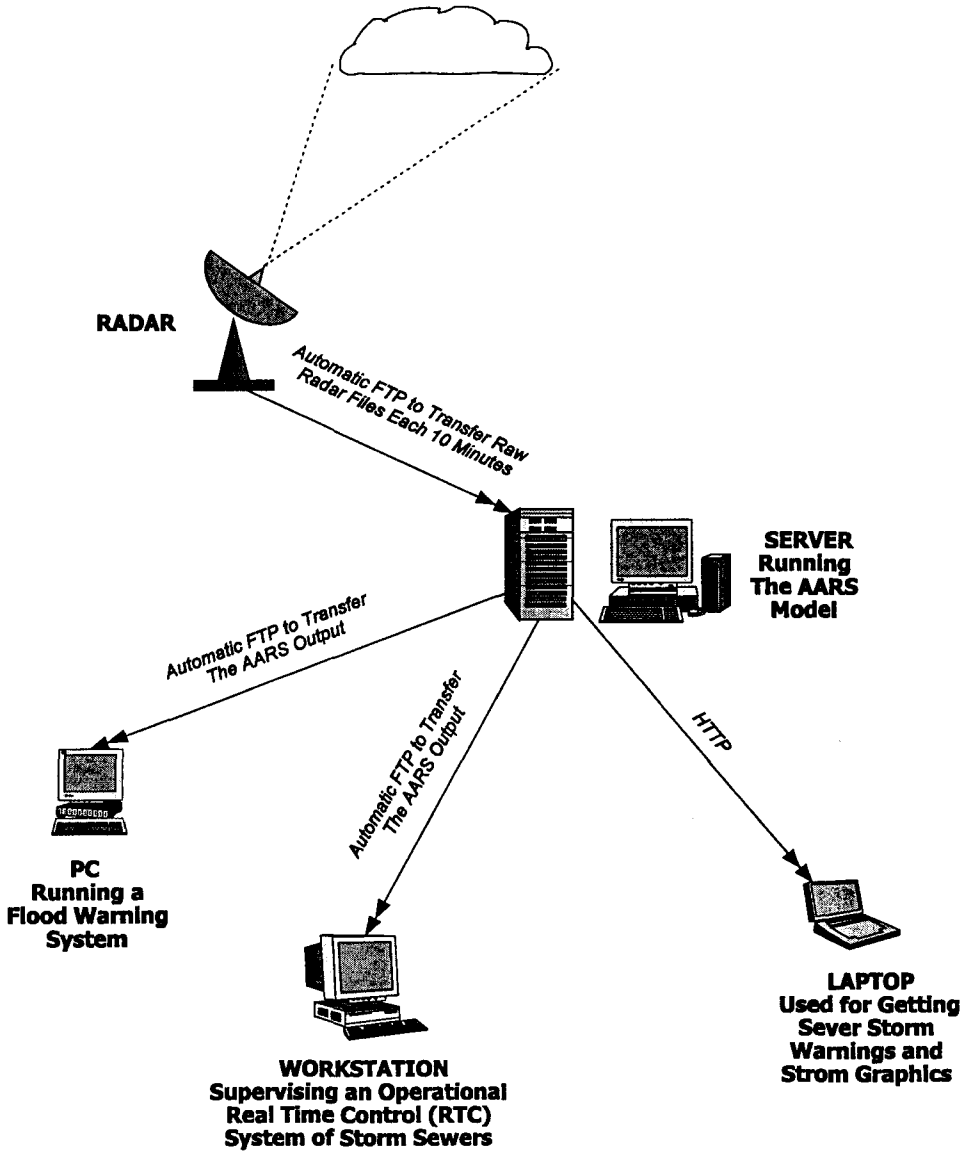

Figure 7.25 The operational implementation of the AARS model.

CHAPTER 8

SUMMARY, CONCLUSIONS,

AND FUTURE RESEARCH

8.1 Summary

The primary purposes of this research are improvements in the estimation and forecasting of precipitation using weather radar. Accurate measurements of rainfall duration, timing, location, and intensity are important for different water resources applications. Weather radars can provide valuable information on the space-time variations of rainfall. However, there are uncertainties in the radar measurements of precipitation. Hence, rain-gauges are commonly used to calibrate Z-R relationships, which are used to convert from radar reflectivity Z to rainfall rate R. Sampling errors cause differences between rainfall estimated by radar and that estimated by rain-gauges. These errors constitute a limitation for use of radar data for high resolution applications such as urban runoff modelling.

Rainfall is one of the most difficult elements of the hydrological cycle to forecast. This is due to the tremendous variability it displays, both in space and time, over a wide range of scales. The forecasting problem becomes more difficult when

forecasts of rainfall fields at scales of interest to urban hydrology are required. The "short-term prediction" of rainfall fields includes tracking the time-space behavior of these fields at each 10 minute time increment, then forecasting the space-time behavior of these fields for a certain lead time.

The main aspects and contributions of the research include: (1) the development of a rain-gauge method for tracking of rainfall patterns (*Chapter 3*); (2) the study of the predominant storm characteristics in Hamilton-Wentworth Region (*Chapter 3*); (3) the investigation of the problem of geo-referencing rainfall data from multi-sensors (*Chapter 4*); (4) development of a multi-component GIS interface for the analysis of rainfall data from multi-sensors (*Chapter 5*) ; (5) the study of the sampling errors of the radar and rain-gauges and their effects on the radar-gauge comparisons and on the radar Z-R calibration (*Chapter 6*) ; (6) development of a procedure to correct for sampling errors in order to enable the extraction of high temporal resolution radar derived rainfall data (*Chapter 6*); (7) a comparative study between the two Canadian radars (King City, and Exeter) in terms of rainfall estimation (*Chapter 6*); (8) the calibration of the two Canadian radars using rain-gauge data (*Chapter 6*); (9) the development of a short-term tracking and forecasting model for quantitative rainfall forecasting (*Chapter 7*); and (10) assessment of the accuracy of short-term rainfall forecasting in Hamilton-Wentworth region (*Chapter 7*).

8.2 Conclusions

This research focuses on issues related to precipitation estimation and forecasting using data from radar and rain-gauges. Within this main framework, other generally related problems, such as geo-referencing rainfall data from multi-sensors and studying the predominant storm characteristics in Hamilton-Wentworth Region, are investigated. Accordingly, the main conclusions of this research can be classified into three main groups: (1) general conclusions, (2) conclusions related to the radar-rainfall estimation problem, and (3) conclusions related to short-term quantitative rainfall forecasting.

(1) General Conclusions

- A simple and efficient rain-gauge tracking technique is developed for the purpose of estimating the kinematics of rainfall using any number of tipping bucket rain-gauges. The rain-gauge tracker is verified using a radar cross-correlation tracker.
- Convective type rainfall and widespread rainfall are the most common types in the Hamilton-Wentworth Region. Based on the analysis of 39 storm events in 1989 and 1990, the predominant storm direction ranges from 202.5 to 292.5 degrees ,i.e., within the S-W quadrant with an average speed of 58 ±15 km/hr. The expected size of a single storm cell is 3.94 ±1.3 km in diameter. Storm speeds can reach up to 120 km/hr.

- A spheroid-based projection method (*GPP*) is developed in this study for the purpose of evaluating different sphere-based projection methods in terms of the accuracy of locating rain-gauges with respect to radar rainfall data. The different sphere-based planar projections give approximately similar results to the *GPP* if the geodetic coordinates are converted to geocentric ones before projection into the radar coordinate system. If the geodetic coordinates are not converted to geocentric ones before using any sphere-based planar projection, an error in locating the rain-gauge can be introduced. This, in turn, may affect the results of the radar-gauge comparison.
- The GPP projection method developed in this study is ellipsoid based and recommended for referencing data from multiple radars into any ellipsoid based common coordinate system.
- A polar Stereographic projection (83 W) is suggested as a common coordinate system to geo-reference data from multiple radars and GOES-8 satellite data for tracking and forecasting purposes in the Great Lakes area. The parameters of the raster to real-world conversion of the satellite images are determined.
- A GIS multi-component interface is developed for the analysis of weather radar precipitation data. The interface is a valuable tool that facilitates the exploration and analysis of radar data.

(2) Conclusions Related to the Radar-Rainfall Estimation Problem

- Correcting for sampling errors can reduce the variation between radar and rain-gauges estimated rainfall rates. Based on the analysis of the root mean square error between radar and rain-gauges for 8 storm events in 1989, the sampling errors can be said to account for 20% on average of the scatter between the two sensors for short accumulation intervals (3, 5, or 10 minutes).
- Correcting for sampling errors has a minor effect on the results of Z-R calibration.
- If correction for advection is employed and if the Z-R relationship is unbiased, then high temporal resolution radar rainfall data can be extracted. One minute rainfall hyetographs can be extracted from radar data with a good degree of accuracy (average RMS = 6 mm/hr) suitable for high resolution hydrological applications such as urban applications.
- The comparison between rainfall fields estimated by two Canadian radars (King City and Exeter) shows that there is good agreement between rainfall fields estimated by the two radars. This comparison is based on the analysis of 10 events in the years 2000 and 2001 in terms of overall bias, correlation, and mean field error. In addition, based on 33 events from King City radar (years 1989, 2000, and 2001) and 10 events from Exeter radar (years 2000, and 2001), the comparisons between the two radars and rain-gauges prove that the classical M&P equation used by the National Canadian radars is

biased and can lead to serious underestimation of rainfall. It is recommended that the following Z-R relation ($Z = 40R^{1.7}$) be used by King City and Exeter radars.

(3) Conclusions Related to Short-term Quantitative Rainfall Forecasting

- A new model for real-time tracking and forecasting of rainfall is developed. The new model is called AARS (Adaptive Automated Rainfall Simulator). The AARS employs the adaptive exponential smoothing algorithm for real-time parameters estimation. Performance comparisons between the AARS model and the Canadian short-term prediction model SHARP (Short-Term Automated Radar Prediction) prove that the AARS model is superior in terms of run time and slightly better, or almost the same, in terms of accuracy. It is concluded that modeling the growth and decay of rainfall on cell by cell basis has shown no practical improvements over the traditional advection forecasting methodology followed in the SHARP model. This can be related to the inability of both methodologies to predict the birth of new rainfall cells, which is an influencing factor, especially beyond the characteristic life time of convective rainfall (30-45 minutes).
- The application of the AARS model for rainfall forecasting in the Hamilton-Wentworth Region shows promising results for lead times up to 60 minutes. The average critical success index is 65±10% and 51±16% for 30 and 60 minutes forecasting lead times respectively. The average forecasting error in

the Hamilton-Wentworth Region is 27±29% and 42±34% for the 30 and 60 minutes forecasts, respectively. The average correlation coefficient between the forecasted and measured fields is 0.45±0.12 and 0.3±0.14 for the 30 , and 60 minutes lead times, respectively.

8.3 Future Research

Statistical analysis should be performed to the present data in order to test if the parameters A & b are statistically different than those of M&P and Blanchard models. Bi-linear or second order relations between log Z and log R should be applied to the data in order to examine if a reduction in variance is achieved. Additional data will eventually refine these coefficients and their variances. The dependence of the coefficients A & b on the threshold value of rainfall intensity should be examined. The results should be further evaluated through hydrological modelling. Though the radar calibration analysis of the two regional radars (King City and Exeter) has been successfully developed and implemented, the results can not be generally applied to the whole Canadian Radars Network. The geographic variation must be studied by applying similar analysis on other radars.

Other recommendations include studying the range and attenuation effects on the accuracy of radar rainfall estimation. Assessment of these factors requires a large rain-gauge network that can cover different ranges under the radar umbrella. Although the important role of the Z-R choice is undeniable, there are other factors of radar-rainfall estimation systems that can significantly affect their performance (i.e.,

range and attenuation effects for example) The same calibration methodology presented in section 6.4 is recommended for studying the effect of range and attenuation, or any additional factors, on the accuracy of radar rainfall estimation. This can be achieved by including additional parameters representing these factors. The contribution of the included factors in explaining the variation between rain-gauges and radar can then be evaluated in terms of the reduction of the root mean square error (refer to the calibration methodology described in section 6.4).

Another area with significant implications to all aspects of radar derived rainfall is the lack of ground truth for mean-areal rainfall. Hence, it is important to study the very small-scale structure of precipitation within a radar pixel. Specialized experiments involving radar data and corresponding very high spatial resolution rain-gauge networks, concentrated within a few radar pixels, is the most recommended approach.

A procedure is used in this study for extracting high resolution rainfall data from radar scans by correcting for the advection effect. Study of the improvements that this procedure can provide in watershed modelling for small basins is recommended. This may be achieved by using the developed high resolution product as input to a distributed hydrological model.

A study of the operational implementation of rainfall forecasting products in conjunction with a rainfall-runoff simulation model is required to assess the attainable gain in real-time control of storm sewer systems. This is an is an attractive future area of research.

Finally, predicting the "birth" of new rainfall producing cells is a major challenge to overcome. Its attainment would improve forecast accuracy. Certainly, the exact solution for the forecasting problem is to use the hydrodynamic equations to create a mathematical model of the atmosphere on a high resolution 3D grid, plug in data on the past and current state of the atmosphere, and solve the equations to predict a future state. The lack of data on this level of resolution and of appropriate modelling of cloud physics are the obstacle against this approach in addition to the tremendous computations that would be required. A recommended engineering approach to model the birth of rainfall is to search for meteorological variables (i.e., relative humidity, temperature, and atmospheric lapse rates and instability) that can be highly correlated with the "birth" of rainfall cells. Such an engineering approach has to take into account the non-stationarity (in space and time) of the fields of these meteorological variables. Such a study would require the availability of data for these meteorological variables with sufficient spatiotemporal resolution. Use of output (which includes data assimilation and parameterization) from numerical weather prediction models (NWP) may provide some data alternatives. However, for the time being, interpolation and extrapolation techniques would have to be used to overcome the poor temporal resolution of such models. A study of the small scale spatial variability of these meteorological variables is required to assess the suitability of the spatial resolution of NWP products.

REFERENCES

Ahnert, P., Hudlow, M., johnson, E., Greene, D., Dias, M., 1983. "Proposed on-site processing system for NEXRAD". *Proc. of the 21st conf. on radar meteorology*. Am. Met. Soc., pp. 378-385.

Alaka, M.A., Elvander, R.C., and Saffle, R.E., 1979. *Nowcasts and short-range (0-2 hour) forecasts of thunderstorms and severe convective weather for use in air traffic control*. U.S. Dept. of Transportation, Rep. No. FAA-RD-79-98, 31 pp.

Amorocho, J. and Wu, B., 1977. "Mathematical models for simulation of cyclonic storm sequences and precipitation fields". Journal of Hydrology, vol 32, pp. 329-345.

Anagnostou, E. N, and Krajewski, W. F., 1999. "Uncertainty Quantification of Mean-Areal Radar-Rainfall Estimates". J. Atmo. And Oceanic Tech. Vol 16, pp. 206-215.

Anagnostou, E. N., 1997. Real-Time Radar Rainfall Estimation. Department of Civil and Environmental Engineering, The University of Iowa. Iowa City, Iowa. Ph.D. Thesis.

Andrieu, H., French, M.N., Thauvin, V., Krajewski, W., 1996. "Adaptation and application of a quantitative rainfall forecasting model in mountainous region". J. of Hydrology, vol. 184, pp. 243-259.

ArcDoc Version 7.0 ,1994. Environmental Systems Research Institute (ESRI). Redlands, California.

Atlas, D., 1964. *Advances in radar meteorology*. Advances in Geophysics, vol. 10, Editors H.E. Landsberg and J. Van Meighen. New York, Academic Press.

Atlas, D., (Editor), 1990. *Radar in meteorology*: Battan Memorial and 40th Anniversary Radar Meteorology Conference. Boston, Amer. Meteor. Soc.

Austin, P.M., 1987. "Relation between measured radar reflectivity and surface rainfall". Mon. Weather Rev., vol. 115, pp. 1053-1070.

Austin, G. L., and Bellon, A., 1974. "The use of digital weather record for short-term precipitation forecasting". Qt. J. R. Meteorol. Soc., vol. 100, pp. 658-664.

Austin, P.M., and Houze, R. A., 1972. "Analysis of the structure of precipitation patterns in New England". Journal of Appl. Meteoro., vol. 11, pp. 926-934.

Bader, M. J., Collier, C. G., and Hill, F. F.,1983. " Radar and rain-gauge observations of a severe thunderstorm near Manchester: 5/6 August". Meteor. Mag., vol. 112, pp. 149-162.

Bankert, R. L., 1994. "Cloud classification of a AVHRR imagery in maritime regions using a probabilistic neural network". J. Appl. Meteor., vol. 33, pp.909-918.

Barclay, P.A, and Wilk, K.E. 1970. Severe Thunderstorm Radar Echo Motion and Related Weather Events Hazardous to Aviation Operations. ESSA Technical Memorandum No. ERLTM-NSSL 46.

Battan, L.J., 1981. *Radar observation of the atmosphere*. Chicago, Univ. of Chicago Press.

Belegundu A., and T. Chandrupatla, 1999. *Optimization Concepts and Applications in Engineering*, Prentice Hall.

Bellon, D.E, and Austin, G.L., 1976. "SHARP (Short-term automated radar prediction) on a real time test". 17th Conf. on radar meteor., Seattle, Washington. American Meteorol. Soc., Boston, pp. 522-525.

Bellon, A., and Austin, G.L.,1984. " The accuracy of short-term radar rainfall forecast". Journal of Hydrology, vol. 70, pp. 35-49.

Bjerkaas, C.L., and Forsyth, D. E., 1980. *An automated real-time storm analysis and storm tracking program (WEATRK).* AFGL-TR-80-0316, Air Force Geophysics Laboratory.

Blanchard, D.C., 1953. "Raindrop size distribution in Hawaiian rains". J. Meteor., vol 10, pp. 457-473.

Blanchet, B., Neuman, A., Jacquet, G. and Andrieu, H., 1991. " Improvement of rainfall measurements due to accurate synchronization of raingauges and due to advection use in calibration". In: I.D. Cluckie and C.G. Collier (Editors),

Hydrological application of weather radar. Ellis Horward, Chichester, pp. 213-218.

Brandes, E., and Wilson, J. 1988. " Measuring storm rainfall by radar and rain gauge". Instruments and Techniques for Thunderstorm Observation and Analysis. University of Oklahoma Press, pp. 171-186.

Briggs, B.H., Phiillips, G.J. and Shinn, D.H., 1950. " The analysis of observation on spaced receivers of the fading of radio signals". Proc. Phys. Soc., London, Ser. B, 63: pp. 106-121.

Brooks, H. E., and Doswell C., A. III, 1997. *Precipitation Forecasting Using a Neural Network.* Internal document. NOAA/ERL/National Severe Storms Laboratory, NOAA/NWS West Gulf River Forecast Center, Norman, Oklahoma.

Brown, R., Sargent, G.P., Newcomp, P.D., Cheung-Lee, J., and Brown, P.M., 1991. "Development of the FRONTIERS precipitation nowcasting system to use mesoscale model products". Preprints, 25th Conf. on radar Meteorology, 24-28 June 199, Paris, France, American Meteorological Society, Boston, pp 79-82.

Brown, R.G., 1963. *Smoothing, forecasting and prediction of discrete time series.* Prentice Hall Inc., Englewood Cliffs, NJ.

Brown, J.A., Jr., 1987. " operational numerical weather prediction". Rev. Geophys., vol. 25(3), pp. 312-322.

Browning, K.A., 1987. "Towards the more effective use of radar and satellite imagery in weather forecasting". *Weather radar and flood forecasting.* Ed. by V.K. Collinge and C. Kirby, John Wiley and Sons, pp. 239-269.

Browning, K.A., and Collier, C.G., 1989. "Nowcasting of precipitation systems". Rev. Geophys., vol.27(3), pp. 345-370.

Browning, K.A., 1980. "Local weather forecasting". Proc. R. Soc. London, ser. A371, pp. 179-211.

Bugayevskiy, L. M., and Snyder, J. P., 1995. *Map projections - a reference manual.* Taylor & Francis Ltd. British Library Cataloguing in Publication Data.

Burgess, D., and Ray, P.S.,1986. *Principles of radar in mesoscale meteorology and forecasting.* Ed P.S. Ray, American Meteorological Society, Boston

Massachusetts, Chapter 6, pp.85-117.

Chen, Z-Q., and M.L. Kavvas, 1992. "An automated method for representing, tracking and forecasting rain fields of severe storms by doppler weather radars". Journal of Hydrology, vol. 132, pp.179-200.

Ciach, G.J., and Krajewski, W.F., 1999. "On the Estimation of Radar Rainfall Error Variance". Advances in Water Res., vol 22, pp. 585-595.

Clayton, A. J. and Deacon, R.C., 1971. "The investigation of local patterns of precipitation and storm movements using computer techniques". Bristol University, Dept. Civ. Eng., pp . 1-42.

Cluckie, I.D.,Yuan, J., Norreys, R., Shepherd, G., and Tyson, J. ,1995. "Real-time control of large urban drainage systems using weather radar". 3rd Int. Symp. on Hydrol. Applications of Weather Radar. Sao Paolo, Brazil.

Collier, C.G., 1989. *Applications of weather radar systems.* Ellis Horwood Serious in Space and Technology.

Collier, C.G., 1999. "The impact of wind drift on the utility of very high spatial resolution radar data over urban areas". Phys. Chem. Earth (B), vol 24, pp. 889-893.

Collier, C.G., 1986. "Accuracy of rainfall estimates by radar, part I: calibration by telemetering raingauges". J. Hydrology, vol. 83, pp. 207-223.

CompuServe, Incorporated, 1987. *Graphics Interchange Format (GIF87).* Technical Manual.An H&R Block Company 5000 Arlington Centre Blvd. Columbus, Ohio 43220.

Conway, B.J., and Browning, K.A., 1988. "Weather forecasting by interactive analysis of radar and satellite imagery". Philos. Trans. R. Soc. London Ser. A, vol. 324, pp. 299-315.

Cornelius, R., R. Gagnon, and F. Pratte, 1995. *Optimization of WSR-88D clutter processing and AP clutter mitigation.* Final Report to the Operations Support Facility (OSF), 182 pp.

Cotton, W.R., and Anthes, R. A., 1989. *Storm and Cloud Dynamics.* International Geophysics Series, vol. 44.

Dingman, S.L.D.,Seedy-Reynolds M., and Reynolds, R.C. III., 1988. "Application

of kriging to estimating mean annual precipitation in a region of orographic influence". Water Resources Bulletin, vol(24), pp.329-339.

Dixon, L. C. W., and Szego, G. P., 1978. "The global optimization problem: an introduction". Towards Global Optimization 2, Edited by L.C.W Dixon, and G.P. Szego, North-Holland, Amsterdam, Holland, pp.1-15.

Donaldson, N.R., 1990. "An example of attenuation by wet snow on a radar dome". Atmosphere-Ocean, vol. 29, pp. 699-711.

Donaldson, N., 2001. Personal communication.. Atmospheric Environment Service of Canada, Meteorological Research Branch, Cloud Physics Research Division,4905 Dufferin St., Downsview, Ontario, Canada, M3H 5T4.

Donaldson, N., 2001. *Great circles, heights and radar projections*. Technical report. Atmospheric Environment Service of Canada, Meteorological Research Branch, Cloud Physics Research Division,4905 Dufferin St., Downsview, Ontario, Canada, M3H 5T4

Donaldson, N., 2002. *McGill Correlation Calculation*. Technical report Atmospheric Environment Service of Canada, Meteorological Research Branch, Cloud Physics Research Division,4905 Dufferin St., Downsview, Ontario, Canada, M3H 5T4

Doviak, R.J. and D.S. Zrnic, 1993. *Doppler radar and weather observations (2nd Edition)*. San Diego, Calif., Academic Press.

Drufuca, G. and Rogers, R.R., 1978. "Statistics of rainfall over paths from 1 to 50 km". Atmospheric Environment, Great Britain, vol. 12, pp. 2333-2342.

Duan, Q. Y., Gupta, V. K., and Sorooshian, S., 1993. "Shuffled complex evolution approach for effective and efficient global minimization". J. of Optimization theory and Application, Vol. 76, No. 3, pp. 501-521.

Duda, R. O., and Blackmer, R. H., 1972. *Application of pattern recognition techniques to digitised weather radar*. Report (Contract No. 1-36072). SRI project No. 1287. Stanford research Institute, Menlo Park, California.

Einfalt, T., Denoeux, T., and Jacquet, G. ,1990. "A radar rainfall forecasting method designed for hydrological purposes". J. Hydrology, vol. (114), pp. 229-244.

ESRI , 1998[1]. ARC-INFO, version 7.2.1 - Discussion on Interpolation Techniques.

ESRI , 1998[2].. "ESRI Shapefile Technical Description". An ESRI White Paper. Environmental Systems Research Institute (ESRI). Redlands, California. July-1998.

Ewing, C.E., and Mitchell, M. M., 1970. *Introduction to geodesy*. American Elsevier Publishing Company, Inc. New York.

Fabry, F., Bellon, A., Duncan M.R., and Austin, G.L, 1994. "High resolution rainfall measurements by radar for very small basins: the sampling problem reexamined". Journal of Hydrology, vol. 161, pp. 415-428.

Felgate, D.G. and Read, D.G., 1975. "Correlation analysis of the cellular structure of storms observed by rain gauges". Journal of Hydrology, vol. 24, pp.191-200.

Fiore, J.F., Fransworth, R.K., and Huffman, G.J., 1986. "Quality control of radar data with satellite data". *Prepr. 23rd Radar meteorol. conf.,* Snow Mass, AMS, Boston, Mass., pp. JP15-JP18.

FMH: Federal Meteorological Handbook No. 11, 1991. *Doppler Radar Meteorological Observations-Part C-WSR88D Products and Algorithms.* U.S Department of Commerce/ National Oceanic and Atmospheric Administration. Washington D.C.

Foroud, N., Broughton, R.S. and Austin, G.L., 1984. "The effects of a moving rainstorm on direct runoff properties". Water Resources Bulletin, vol. 20 (1), pp. 87-91.

Franke, R., 1982. "Smooth interpolation of scattered data by local thin plate splines. Comp. & Maths. with App., vol. 8(4),. pp. 237 - 281. Great Britain.

French, M.N., Krajewski, W.F., and Cuykendall, R.R., 1992. "Rainfall forecasting in space and time using a neural network". J. of Hydrology, vol. 137, pp. 1-31.

French, M.N., and Krajewski W.F, 1994[1]. "A model for real-time quantitative rainfall forecasting using remote sensing, part-1: formulation". Water Resources Res, vol. 30(4), pp.1075-1083.

French, M.N and Krajewski, W.F., 1994[2]. "A model for real-time quantitative rainfall forecasting using remote sensing part-2: case studies". Water Resources Res., vol. 30(4), pp. 1085-1097.

Fu M., and J-Q. Hu,1997. *Conditional Monte Carlo: Gradient Estimation and*

Optimization Applications. Kluwer Academic Publishers.

Gad, M.A., and Tsanis, I.K., 1999. *RAINPRO: A GIS method for estimating storm kinematics*. Technical Manual. Civil Eng. Dept., McMaster University, Hamilton, ON, L8S 4L7.

Gad, M.A., and Tsanis, I.K., 2001. "Geo-Referencing Radar Rainfall Data". ASCE Journal of Hydrologic Engineering. (Submitted).

Gad, M.A, and Tsanis, I.K.,2002[1] . "A GIS Methodology For The Analysis of Weather Radar Precipitation Data. J. Hydroinformatics (Accepted for publication).

Gad, M.A., and Tsanis, I.K, 2002[2]. "Use of optimization in cross-correlating radar detected rainfall patterns". Weather and Forecasting, American Met. Soc. (Submitted)

Gad, M.A., and Tsanis, I.K., 2002[3]. *RAINPLAT : A GIS platform for rainfall data from Multi-Sensor*. Technical Manual. Civil Eng. Dept., McMaster Univeristy, Hamilton, ON, L8S 4L7.

Gebhardt, K., Bohn, C. and Gordon, N.,1988. *Estimating daily precipitation in the Northern Great Basin*. Saval ranch Research and Evaluation Project Final Report, Bureau of Land Management, Reno, NV, 4-25.

Georgakakos K.P., and Hudlow, M.D., 1984. "Quantitative precipitation forecast techniques for use in hydrologic forecasting". Bull. Am. Meteorol. Soc., vol. 65(11), pp. 1186-1200.

Georgakakos, K.P., and Bras, R.L., 1984[2]. "A hydrologically useful station precipitation model , part II , applications". Water Res. Res., vol 20(11), pp. 1597–1610.

Georgakakos, K.P., and Bras, R.L., 1984[1]. " A hydrologically useful station precipitation model , part I , formulation". Water Res. Res., vol 20(11), pp. 1186-1200.

Georgakakos K.P., and Kavvas M.L, 1987. "Precipitation analysis modeling and prediction in hydrology". Rev. Geophys., vol. 25(2), pp.163-178.

Glover, F., 1990. "Tabu search - part II". ORSA Journal on Computing vol 2, pp.4 - 32.

Glover, F. and Laguna, M., 1993. "Tabu search". In: C.R. Reeves (ed.) Modern Heuristic Techniques for Combinatorial Problems. Blackwell, Oxford, pp.70 - 150.

GOES I-M DataBook, 1996. *Technical Report.* National Aeronautics and Space Administration. Goddard Space Flight Center. Greenbelt, Maryland 20771. Contract NAS5-29500

Goldhirsh, J., Krichevsky, V., and Gebo, N. E., 1992. ''Rain-rate duration statistics and fade distributions at 20 and 30 GHz derived from a net-work of rain gauges in the Mid-Atlantic coast over a five-year period.'' IEEE Trans. Antennas Propagation, vol. 40(11), pp. 1408–1415.

Green, M.J., 1991. "Real-time control of urban drainage systems: advantage or disadvantage". *Hydrological Applications of Weather Radar.* I.D. Cluckie and C.G. Collier (Editors), Ellis Horwood..

Grimes, D.I.F., Milford, J.R and Dugdale G., 1993. "The use of satellite rainfall estimates in hydrological modelling". Presented at the first international conference of the African Met. Soc. Nairobi, Kenya.

Gupta, V. K. and Waymyre, E.C., 1979. " A stochastic kinematic study of subsynoptic space-time rainfall ". Water Resources Research , vol 3(15), pp. 637-644.

Habib, E., Krajewski, W. F., and Kruger, A., 2001. "Sampling errors of tipping-bucket rain gauge measurements". J. Hydrologic Eng, vol 6 (2), pp. 159-166.

Hamilton, E., 1992. *JPEG File Interchange Format Version 1.02.* Technical Report. C-Cube Microsystems. 1778 McCarthy Blvd. Milpitas, CA 95035.

Hardaker, P.J., and Collier C.G., 1995. "Radar and storm model-based estimation of probable maximum precipitation in tropics". 3rd Int. Symp. on Hydrol. Applications of Weather Radar. Sao Paolo, Brazil.

Heiskanen, W. A. and Moritz, H., 1967. *Physical Geodesy.* A series of Books in Geology, Ed. Gilluly, J. and Woodford, A. O. W.H. Freeman and Company.

Hill, F. F., Whyte, K. W., and Browing, K. A., 1977. "The contribution of a weather radar network for forecasting frontal precipitation; a case study". Meteor. Mag., vol. 106, pp. 68-89.

Hindi, W.N.A., and Kelway, P.S., 1977. " determination of storm velocities as an aid to the quality control of recording rain gauge data". J. of Hydrology, vol. 32, pp. 115-137.

Hoke, J.E., Hayes, J.L., and Renninger, L.G., 1981. Map projections and grid systems for meteorological applications. Air Force Global Weather Central, Offutt Field, Neb.

Hudlow, M. D., 1973. "Use of digital radar data in operational hydrology". National Water Resources Engineering Meeting, Am. Soc. of Civil Eng., Washington, D.C.

Huff, F.A., Vogel, J. L., and Changnon Jr., S.A, 1981. "Real-time rainfall monitoring - prediction system and urban hydrologic operations". Journal of the Water Resources Planning and Management, ASCE, vol. 107(WR2), pp. 419-435.

Huff, F.A., 1967. " Time distribution of rainfall in heavy storms". Water Resources Res., vol. 3, pp.1007-1019.

Ishizaki, K., Yoshino, F., Takeuchi, K., and Yoo, A., 1989. "A study on short-term rainfall prediction by radar raingauge". Proc. Of Symp. during third Scientific Assembly of IAHS, May 1989, Baltimore, MD. IAHS Publ. No. 181, IASH Press, Institute of Hydrology, Wallingford.

James, W. and Scheckenberger, R.B., 1983. "Storm dynamics model for urban runoff". International Symposium on Urban Hydrology, Hydraulics and Sediment Control, University of Kentucky, Lexington, Kentucky, July 25-28.

Joss, J., and A. Waldvogel, 1990. "Precipitation measurement and hydrology". *Radar in meteorology*. Ed. Atlas,D. Amer. Meteor. Soc., pp. 577-606.

Kendall, G.R. and Petrie, A.G., 1962 "The Frequency of thunder storm days in Canada", Meteorological Branch, Department of Transportation; CIR-3688, TEC-418, June 1962.

Khuri, A.I., Cornell, J.A., 1996. *Response surfaces: designs and analyses*. 2nd edition, Marcel Dekker, Inc., New York, NY.

Kitchen, M, and Blackall, R.M., 1992. "Representative errors in comparisons between radar and rain-gauge measurements of rainfall". J. Hydrology, vol. 234, pp.13-33.

Krajewski, W. F., 1987. "Co-kriging of radar-rainfall and raingage data". J.

Geophys. Res. vol. 92(D8), pp. 9571-9580.

Landel, G., J. A. Smith, M. L. Baeck, and M. Steiner, 1999. "Radar studies of heavy convective rainfall in mountainous terrain". J. of Geophysical Research, vol.104(D24), pp. 31451-31465.

Lee, T.H., and Georgakakos, K.P., 1991. *A stochastic-dynamical model for short-term quantitative rainfall prediction.* Tech. Rep.349. Iowa Inst. Hydr. Res., University of Iowa.

Lee, T.H., and Georgakakos, K.P., 1990. "A two dimensional stochastic dynamical quantitative precipitation model". J. Geophys. Res., vol. 95(D3), pp. 2113-2126.

Li, L., Schmid, W., Joss, J., 1995. " Nowcasting of motion and growth of precipitation with radar over a complex orography". J. Applied Meteo., vol 34, pp. 1286-1300.

Marshal R.J., 1980. "The estimation and distribution of storm movement and storm structure, using correlation analysis technique and rain gauge data". J. of Hydrology, vol. 48, pp. 19-39.

Marshal, J.S., and Palmer, W., 1948. "The distribution of raindrops with size". J. Meteorol., vol. 5, pp. 165-166.

Marzban, C. And G. J. Stumpf, 1996. "A neural network for tornado prediction based on doppler radar-derived attributes". J. Appl. Meteor., vol. 35, pp.617-626.

Matheron, G.,1971. " The theory of regionalized variables and applications". Cahiers du centre de Morphologie Mathematic Ecole des Mines, Fountainbleau, France, 211 pp.

Mitas, L., and Mitasova, H., 1998. "General variational approach to the interpolation problem". Comput. Math. App., vol 16(12), pp. 983-992. Great Britain.

Montmollin, F.A., Olivier, R.J., Simard, R.G. and Zwahlen, F.,1980. "Evaluation of a precipitation map using a smoothed elevation-precipitation relationship and optimal estimates (kriging)". Nordic hydrology, vol.11(3-4), pp.113-120.

Murray, J.D., and Vanryper, W., 1996. *Graphic File Format.* 2nd Edition.

Naoums S., Tsanis, I.K., and Gad M.A., 2002. "Short-term rainfall

interpolation".Departmental Report. Civil Engineering Dept., McMaster University, Hamilton, ON, L8S 4L7.

National Weather Service, Meteorological Service Division, 1981. *Two-to-six hour probabilities of thunderstorms and severe local storms*. National Weather Service, National Oceanic and Atmospheric Administration, Silver Spring, Maryland, Tech. Procedures Bull. Ser. No. 295, 133pp.

Nelder, J.A., and Mead, R., 1965. "A simplex method for function minimization". Computer Journal, vol.7, pp.308-313.

Newsome, D.H., and Collier, C.G.,1991. "COST 73: possible hydrological applications of weather radar in Western Europe". *Hydrological Applications of Weather Radar*. I.D. Cluckie and C.G. Collier (Editors), Ellis Horwood., pp. 623-635.

Ngirane-Katashaya, G.G. and Wheater, H.S., 1985. "Hydrograph sensitivity to storm kinematics". Water Resources Research, vol. 21 (3) pp. 337-345.

Niemczynowicz, J., 1987. "Storm tracking using rain gauge data". J. of Hydrology, vol. 93 pp. 135-152.

Niemczynowicz, J., and Dahlblom, P., 1984. "Dynamic properties of rainfall in lund". Nordic Hydrology, vol. 15, pp. 9-24.

Niemczynowicz, J., and Jönsson, O., 1981. "Extreme rainfall events in lund 1979-1980". Nordic Hydrology, vol. 12, pp. 129-142.

Nimmrichter, P., 1986. *Dynamics of storms on the western shore of lake ontario*. Department of Civil Engineering, McMaster University.

Nystuen, J. A., and Proni, J. R.,1996. ''A comparison of automatic rain gauges.'' J. Atmospheric and Oceanic Technol, vol. 13, pp. 62–73.

Ogden, F.L., Richardson, J.R. and Julien, P.Y., 1995. "Similarity in catchment response: 2. Moving rainstorms". Water Resources Research, vol. 31 (6), pp. 1543-1547.

Orlanski, I., 1975. "A rational subdivision of scale of atmosphereic processes". Bull. Am. Meteorolo. Soc. , vol 56, pp. 572-530.

Philip, G.M. and Watson, D.F.,1982. "A precise method for determining contoured surfaces.' Australian Petroleum Exploration Association Journal, vol. 22,

pp.205-212.

Pick, M., Picha, J., and Vyskocil, V. ,1973. *Theory of the Earth's gravity field.* Ed. Academician Tibor Kolbenheyer. Elsevier Scientific Publishing Company.

Pielke, R. A., 1984. *Mesoscale meteorological modeling.* Academic, San Diego, Calif., 612 pp.

Pratte, F., D. Ecoff, J. VanAndel, and R.J. Keeler, 1997. "AP clutter mitigation in the WSR-88D". Preprints, 28th Radar Meteor. Conf., AMS, Austin, TX, 7-12 Sep. 1997.

Press, W. H., Teukolsky, S. A., Vetterling, W. T., and Flannery, B. P., 1999. *Numerical Recipes in C - The Art of Scientific Computing.* Second Edition. Cambridge University Press, Melbourne 3166, Australia.

Probert-Jones, J.R., 1962. "The radar equation in meteorology". Quart. J. Roy. Met. Soc., vol.88, pp. 485-495.

Reed, S. M., and Maidment, D. R.,1999. "Coordinate transformations for using NEXRAD data in GIS-based hydrologic modeling". Journal of Hydrologic Engineering, vol.4(2), pp.174-182.

Reed, S. M., and Maidment, D. R. ,1995. *A GIS procedure for merging NEXRAD precipitation data and digital elevation models to determine rainfall-runoff modeling parameters.* Department of Environmental and Water Resources Engineering. University of Texas, Austin, Texas. Departmental Report.

Rinehart, R.E., 1991. *Radar for meteorologists.* Grand Forks, N. Dakota, U.S.A., Univ. of N. Dakota, Dept. Atmos. Sci.

Rinehart, R. E., 1981. "A pattern matching technique for use with conventional weather radar to determine internal storm motions". Recent Progress in Radar Meteorology. Atmos. Technol., pp. 119-134.

Rinehart, R. E., and Garvey, 1978. "Three dimensional storm motion detection by conventional weather radar". Nature, vol (273), pp.287-289.

Sachidananda, M., D.S. Zrnic, R.J. Doviak, and S. Torres, 1998. *Signal Design and Processing Techniques for WSR-88D Ambiguity Resolution, Part 2.* National Severe Storms Laboratory, June 1998, 105 pp.

Sargent, D.M., 1981. "An investigation into the effects of storm movement on the

design of urban drainage systems: Part 1". The Public Health Engineer, vol. 9, pp. 201-207.

Sargent, D.M., 1982. "An investigation into the effects of storm movement on the design of urban drainage systems: Part 2". Probability analysis. The Public Health Engineer, vol. 10 (2), pp.111-117.

Sauvageot, H. ,1982. *Radarmeteorologie*. Paris, Eyrolles.

Scheckenberger, R., 1983. *Dynamically spatially variable rain models for stormwater management*. M. Eng. Thesis, McMaster University, Hamilton, Ontario, L8S 4L7.

Seed, A.W., Nicol J.G.L., Austin, C.D., Bradley, S.G., 1995. "A physical basis for parameters selection for Z-R relationships". *3rd Int. Symp. On Hydrol. Appl. of Weather Radar*, Sao Paolo, Brazil, 1995.

Seo, D. J., Krajewski, W. F., Azimi-Zonooz. A, and Bowles, D.S., 1990[2]. "Stochastic interpolation of rainfall data from rain gages and radar using cokriging 2. results". Water Resources Research, vol. 26 (3), pp. 469-477.

Seo, D.J., and J.A. Smith, 1992. "Radar-based short-term rainfall prediction". J. of Hydrology, vol.131, pp.341-367.

Bengtsson. L., 1985. "Medium-range forecasting at the ECMWF". Adv. Geophys., vol. 28(B), pp. 3-54.

Seo, D.J., .Krajewski, W.F. and Bowles, D.S. ,1990[1]. "Stochastic interpolation of rainfall data from rain gages and radar using cokriging, 1, design of experiments". Water Resources Research, vol. 26 (3), pp.469-477.

Sevruk, B., and Lapin, M., Eds. 1993. ''Precipitation measurement & quality control''. Proc., Int. Symp. on Precipitation and Evaporation. Vol. 1, Slovak Hydrometeorological Institute, Bratislava, Slovakia.

Shaw, E.M. and Lynn, P. P., 1972. "Areal evaluation using two surface fitting techniques". Bull. Int. Assoc. Sci. Hydrol., vol. 18(4), pp. 419-433.

Shaw, S.R., 1983. "An Investigation of the Cellular Structure of Rainfall Using Correlation Technique". Journal of Hydrology, vol. 62, pp. 63-79.

Shearman, R.J., 1977. " The speed and direction of storm rainfall patterns with reference to urban storm sewer design". Hydrological Science-Bulletin-des

Sciences Hydrologiques, XXII,3 , pp. 421-431.

Shed, R., Smith J. A., and Walton, M. L., 1991. "Sectorized hybrid scan strategy of the NEXRAD precipitation-processing system". *Hydrological Applications of Weather Radar.* Ed. I.D., Cluckie, and C.G., Collier, Ellis Horward.

Shtifter, Z., 1981. *A kinematic storm model for urban drainage studies.* M. Eng Thesis, McMaster University, Hamilton, Ontario, L8S 4L7.

Singh, V.P. ,1992. *Elementary Hydrology.* Department of Civil Engineering, Louisiana State University. Prentice Hall, Englewood Cliffs, NJ.

Singh, V.P., 1998. "Effect of the direction of storm movement on planar flow". Hydrological Processes, vol 12(1), pp. 147-170.

Skolnik, M. (Editor), 1970. *Radar Handbook.* New York, McGraw-Hill.

Smith, J. A., and Krajewski W. F., 1993. "A modelling study of rainfall rate: Reflectivity relationships". Water Res. Res., vol. 29, pp. 2505-2514.

Smith, J.A., Seo D.J., Baeck M. L., Hudlow M. D., 1996. "An intercomparison study of NEXRAD precipitation estimates". Water Res. Res., vol (32)(7), pp. 2035-2045.

Snyder, J.P., 1987. "Map Projections-a working manual". Professional paper 1395, US Geological Survey, Washington, D.C.

Spendley, W.,Hext, G.R., and Himsworth, F.R., 1962. "Sequential application of simplex designs in optimisation and evolutionary operation". Technometrics, vol.4, pp.441-461.

Steiner, M. ,1996. ''Uncertainty of estimates of monthly areal rainfall for temporally sparse remote observations.'' Water Resour. Res., vol. 32(2), pp. 373–388.

Tabios III, G.Q. and T.D. Salas, 1985. "A comparative analysis of techniques for spatial interpolation of precipitation". Water Resources Bulletin, vol.21(3), pp.365-380.

Theissen, A. H., 1911. " Precipitation averages for large areas". Monthly Weather Rev., 39, 1082-1084.

Tsanis, I.K., Gad, M.A. and Donalson, N , 2002. "A comparative analysis of rain-gauge and radar techniques for storm kinematics". Advances in Water

Resources, vol 25 (3), pp. 305-316.

Tsanis, I.K. and Gad, M. A. 1999. *Real-Time Rainfall Prediction and Storm tracking For Hamilton-Wentworth Region.* Technical Report. The Regional Municipality of Hamilton-Wentworth. 35 King Street East, Main Floor, Hamilton, Ontario L8N 4A0.

Tsanis, I.K. and Gad, M. A. 2001. "A GIS Precipitation Method for Analysis of Storm Kinematics", Journal of Environmental Modelling & Software, 16, pp. 273-281.

Vicente, G.A., R.A. Scofield & W.P. Menzel 1998. "The operational GOES infra-red estimation technique". Bull. Amer. Meteor. Soc., 79, 1883-98.

Watson, D.F. and Philip, G.M.,1985. "A refinement of inverse distance weighted interpolation" .Geo-Processing, vol. 2, pp.315-327.

Wilk, K. E., and Gray, K. C., 1970. "Processing and analysis techniques used with the NSSL weather radar system". *Preprint volume 14, Conf. on Radar Meteorology.* American Meteorological Society, Boston, Massachusetts, pp. 369-374.

Wilson, J., and Brandes, E., 1979. "Radar measurement of rainfall - a summary". Bulletin of American Meteorological Society, vol. 60 (9), pp.1048-58.

Wilson, J. W. 1966. *Movement and predictability of radar Echoes.* Report , U.S Weather Bureau Contract CWB-11093, the Travelers Weather Research Center, Hartford, Connecticut.

Wilson, W., French, M., Bhaskar, N., and Anderson, R. 1997. "Rain gage and WSR-88D rainfall accumulation comparison in Jefferson county, Kentucky". Proceedings of the American Meteorological Society13th Conference on Hydrology.

Woodley, W., and Herndon, A. 1970. "A raingauge evaluation of the Miami reflectivity-rainfall rate relation". Journal of Applied Meteorology, vol (14), pp. 909-28.

Woodley, W. L., Olsen, A. A., Herndon, A., and Wiggert, V., 1975. "Comparison of gauge and radar methods of convective rain measurements". J. App. Meteorol., vol (14), pp. 909-928.

Wright, M.H., 1996. *The Nelder-Mead method: numerical experimentation and*

algorithmic improvements. Technical report, AT&T Bell Laboratories, Murray Hill, New Jersey, USA.

Yoshino F., and Kozeki, D., 1985. *Study on short-term forecasting of rainfall using radar rain-gauge*. Report, Hydrology Division, Public Works Research Institute, Ministry of Construction, Japan.

Yu, B., Ciesiolka, C. A. A., Rose, C. W., and Coughlan, K. J. , 1997. ''A note on sampling errors in the rainfall and runoff data collected using tipping bucket technology." Trans. ASAE., vol. 40(5), pp. 1305–1309.

Zawadzki, I., 1984. "Factors affecting the precision of radar measurements of rain".Preprints, 22d Conf. on Radar meteorology, Zurich, Switzerland, Amer. Meteor. Soc., pp. 251-256.

Zawadzki, I. I., 1973. "Statistical properties of precipitation patterns". J. Applied Meteorology, vol 12, pp. 459-472.

Zittel, W. D., 1976. "Computer Applications and Techniques for Storm Tracking and Warning". *Preprint volume, 17th conf. on radar meteorology*, Seattle, Washington. American Meteorological Society, Boston, Massachusetts, pp. 514-521.

APPENDIX I
DERIVATION OF THE GPP INVERSE TRANSFORMATION

This appendix derives the inverse transformation of the GPP projection method, which is developed in Chapter 4. The inverse transformation means that, given the radar location $O\ (\lambda_o\ ,\ \Phi_o)$ and the Cartesian coordinates of an arbitrary point $P\ (x_p\ ,\ y_p)$, the corresponding longitude and latitude $(\lambda_p\ ,\ \Phi_p,)$ are to be calculated. Refer to Chapter 4, Figure 4.9, Figure 4.10, and the list of symbols for the definition of the symbols and triangles.

The calculation of the longitude does not require iterations and can be obtained as following: From the two triangles, $Q_pN\,u_p$, and $Q_pP\,u_p$, shown in Figure 4.10:

$$\frac{n_p u_p}{y'_p \sin\phi_o} = \frac{Q_p u_p}{Q_p u'_p} = \frac{P u_p}{x_p}$$

$$P u_p = \frac{x_p}{y'_p \sin\phi_o} \times n_p u_p \qquad \text{(a.1)}$$

Form the third triangle Pn_pu_p:

$$\lambda_p = \lambda_o + \Delta\lambda = \lambda_o + tan^{-1}\frac{x_p}{y'_p \sin\phi_o} \qquad \text{(a.2)}$$

Then to solve for latitude, consider triangle $Q_p n_p u_p$

$$n_p u_p = (H_p + \Delta H_p) \tan \theta_p$$

$$= (H_p + \Delta H_p) \times \frac{y'_p \sin \phi_o}{h_N + \Delta H_p - y'_p \cos \phi_o}$$

$$= \frac{H_p}{1 - e^2} \times \frac{y'_p \sin \phi_o}{h_N - y'_p \cos \phi_o + H_p \dfrac{e^2}{1 - e^2}} \qquad \text{(a.3)}$$

then, form triangle $P n_p u_p$:

$$R^2{}_p = \overline{n_p u_p}^2 + \overline{P u_p}^2 \qquad \text{(a.4)}$$

Substituting from (a.1) into (a.4), then substituting from (a.3):

$$R^2{}_p = \frac{[(y'_p \sin \phi_o)^2 + x_p{}^2] \times H_p{}^2}{(1 - e^2)^2} \times \frac{1}{[(h_N - y'_p \cos \phi_o) + H_p \times \dfrac{e^2}{1 - e^2}]^2}$$

$$= \frac{1}{1 - e^2} \times \frac{c_2 H_p{}^2}{(c_3 + c_4 H_p)^2} \qquad \text{(a.5)}$$

Where R_p can also be obtained from the meridional ellipse equation as following:

$$R_p{}^2 = \frac{1}{1 - e^2} [a^2 (1 - e^2) - H_p{}^2] = \frac{1}{1 - e^2} [c_1 - H_p{}^2] \qquad \text{(a.6)}$$

Hence, equating equations (a.5) and (a.6) and rearranging:

$$AH_p^4 + BH_p^3 + DH_p^2 - EH_p - G = 0 \tag{a.7}$$

Where:

$$A = c_4^2 , \quad B = 2c_3c_4 , \quad D = c_2 + c_3^2 - c_1c_4^2$$
$$E = 2c_1c_3c_4 , \quad G = c_1c_3^2 \tag{a.8}$$

APPENDIX II
A LIBRARY FOR LOADING RADAR DATA

It is essential to provide the utility required for loading radar data into ArcView GIS separately from the interface because of its importance. The code described here is generalized so that it can be used independently for any application that requires loading radar data into ArcView GIS. The source code is provided in this appendix so that the reader needs only to compile it and run it without the need to obtain the RAINPLAT installation package. The source code consists of two components: (1) A dynamic link library "*cappiload.dll*" and (2) an avenue script that calls this library "*Rad_Load_Binary.ave.*".

- The full details of the code are commented inside the body of the code below.
- The process runs from inside ArcView. In order to do this assign the action of the script to a button or a menu item in your view then simply run it by clicking the button or the menu item (refer to the end of this appendix for step by step instructions).
- Make sure to set up your working directory before you start. Also, make sure to save the compiled dynamic link library "cappiload.dll" inside your working directory (refer to the end of this appendix for step by step instructions).
- A file that contains the grid properties should be inside the working directory. This file is given a name "afterc.hdr" inside the script code. The contents of this file is shown at the end of the appendix.
- When the script runs a series of dialogs prompts the user to select the output type, the time system, and a set of radar files to be loaded. I recommend to load the files of each day (240 files) into a separate view.
- Note that the DLL is written using C++ and requires Microsoft Visual C++ 4.0 or later version for compilation.

- The loaded grids are referenced in radar coordinates, i.e., the origin of the Cartesian coordinate system is at the radar location.
- The source code provided in this appendix is modified so that it can be used independently without the need to install the RAINPLAT package developed in Chapter-5.
- Refer to Chapter 5 (section 5.4.1) for additional information.

The Avenue Script (Rad_Load_Binary.ave.)

```
'*****
 'Author:          Mohamed Gad
' Title:           Rad_Load_Binary.ave
'  Description:   This script loads the radar binary CAPPI files. Simply attach it to any button or menu item in
'                  your view and run it.
'                 The script requires a dynamic link library cappiload.dll. Here for simplicity, the dynamic link
'                  library has to be placed in your working directory.
'                 When run, the script prompts the user using a dialog to select any group of radar files to be
'                  loaded in the view.
' Results:        The selected radar files will be added to the view and named according to the time system you
'                  specify in the dialogs.
'  Dependencies:  1- cappiload.dll  (A dynamic link Lib)
'                 2- afterc.hdr  (this file holds the grid  preperties such as number of rows and columns,
'                    this file should be in your working directory)


'          ********** START OF SCRIPT**********

outtype = MsgBox.ChoiceAsString ({"N","DBZ","Z","RAIN"},"Select the required output type","Loading Binary Radar
Data")

if (outtype = nil) then
   exit
end


if (outtype = "RAIN") then
   labels = {"Time System Difference.(hrs)  ", "  (Z-R parameter)        A       ", "  (Z-R Parameter)        b     "}
   defaults = {"4", "40","1.7"}
   TheUserlist = MsgBox.MultiInput( "Input:", "Loading Binary Radar Data", labels, defaults )
   if (TheUserlist.Count = 0) then
     exit
   end

   timediff = TheUserlist.Get(0).AsNumber
   A = TheUserlist.Get(1).AsNumber
```

```
    b = TheUserlist.Get(2).AsNumber

else
    labels = {"Time System Difference.(hrs)"}
    defaults = {"4"}
    TheUserlist = MsgBox.MultiInput( "Input:", "Loading Binary Radar Data", labels, defaults )
     if (TheUserlist.Count = 0) then
      exit
    end
    timediff = TheUserlist.Get(0).AsNumber


end

'* Get view
workdir = av.GetProject.GetWorkDir
theview = av.GetActiveDoc

'* Define the DLL and the add procedure
myDLL = DLL.Make((workdir.AsString+"\cappiload.dll").AsFileName)
add = DLLProc.Make(myDLL, "Loadbindata", #DLLPROC_TYPE_VOID,{})

'* Get radar files from the user using a dialog
thefilelist = FileDialog.ReturnFiles ({"*.num","*.txt"}, {" Radar Data","Txt Files"}, "Select the Radar files", 0)
thecount = thefilelist.Count
progress = 1


For each fle in thefilelist

'* Show a progress indicator
indication = av.SetStatus((progress/thecount)*100)

    '* Copy the original radar file from the original location to the work dir and use it as input to the Dll.
          ' the DLL's output is a fixed name file "afterc.flt".
          origradarfile = fle.GetName.AsFileName
    radarfile = (workdir.AsString+"\copiedfile.num").AsFileName
    File.Copy (origradarfile,radarfile)
    TheTempRadfle = LineFile.Make(radarfile,#FILE_PERM_READ)

    '* Read Valid Time from the input file
    While (TRUE)
        thedatestrg = TheTempRadfle.ReadElt
        if (thedatestrg.Contains("Valid Time")) then
          allstr = thedatestrg.Right(12)
          TheTempRadfle.Close
          break
        else
          continue
        end
    end
```

```
workdir.SetCWD
theinputfile = (workdir.AsString+"\afterc.flt").AsFileName

'* Call the add procedure from the DLL. The DLL will format the original file and output it
      ' in "afterc.flt" which will be used as an external grid data set.
         add.Call({})
indication = av.SetStatus((progress/thecount)*100)

       '* Create a grid theme from the dll output.
        thegrid = Grid.MakeFromFloat(theinputfile)

'* Perform untis conversion

      if (outtype = "N") then
            theoutgrid = thegrid
      elseif (outtype = "DBZ") then
            DBZGrid = (0.5.AsGrid*thegrid) - 32.AsGrid
            theoutgrid = DBZGrid
      elseif (outtype = "Z") then
            DBZGrid = (0.5.AsGrid*thegrid) - 32.AsGrid
            ZGrid = (10.AsGrid)^(0.1.AsGrid*DBZGrid)
            theoutgrid = ZGrid
      elseif (outtype = "RAIN") then
            DBZGrid = (0.5.AsGrid*thegrid) - 32.AsGrid
            ZGrid = (10.AsGrid)^(0.1.AsGrid*DBZGrid)
            RainGrid = (ZGrid/(A.AsGrid))^((1/b).AsGrid)
            theoutgrid = RainGrid
      else
            MsgBox.Info("Specify the Output type please: either","Warning")
      end


thegtheme = Gtheme.Make(theoutgrid)

 '* This part is for time system conversion.
       '* Now get the time from the file name for simplicity.
          themonth = allstr.Middle(4,2)
 theday = allstr.Middle(6,2)
 hrstrUTC = allstr.Middle(8,2)
 mininboth = allstr.Middle(10,2)

 hrEST = hrstrUTC.AsNumber - timediff

'* Set the name of the Grid theme.
if (hrEST < 0) then
    hrEST = hrEST + 24
end

       if (hrEST < 10) then
   hrstrEST = "0"+hrEST.AsString
```

```
    else
       hrstrEST = hrEST.AsString
    end

    if (timediff > 0) then
          theoutstr = hrstrEST+ " : " + mininboth
    else
      theoutstr = hrstrUTC+ " : " + mininboth
    end

    thegtheme.SetName(theoutstr)
    thelegend = thegtheme.GetLegend

'* Use a colour legend to colour your gtheme. I did not put this legend file as dependency because you can create
'  your own clour legend and use it. Just remember to save it in your working directory.
    thelegend.Load ((workdir.AsString+"\Legend3.avl").AsFileName, #LEGEND_LOADTYPE_ALL)
    thegtheme.SetLegendVisible(FALSE)
    indication = av.SetStatus((progress/thecount)*100)

   '* Add the grid theme to the view
    theview.AddTheme(thegtheme)
    progress = progress + 1

end

'* Clear progress indicator from the screen.
av.ClearStatus

'********************** END OF SCRIPT**************************
```

The Dynamic Link Library "cappiload.dll"

```
// Author:        Mohamed Gad
//Title:          cappiload.dll
//Description:    This is a dynamic link library that can be linked in run time to any application including ArcView
                  GIS. The library formats radar data into a GIS compatible format.

#include <windows.h>
#include <stdio.h>
#include <ctype.h>


void Loadbindata(void);

// Attaching and detaching procedures for the dll.

BOOL WINAPI DllEntryPoint (HINSTANCE hDLL, DWORD dwReason, LPVOID Reserved)
{
        switch (dwReason)
```

```
        {
        case DLL_PROCESS_ATTACH:
                {
                        break;
                }
        case DLL_PROCESS_DETACH:
                {
                        break;
                }
        }
        return TRUE;
}


// The loading procedure of the radar data starts here.
void Loadbindata(void)
{
FILE *fp1,*fp2;
unsigned char value;
int c,row,knt;
int i,text[6];
float valuef;

// the following is Input and output files. Note that these names are compatible with those in the
// calling script. If you change them, make sure to change them in both the dll and the calling script.
fp1 = fopen("copiedfile.num","r+b");
fp2 = fopen("afterc.flt","w+b");

//This following character array corresponds to '#DATA-', which is the last string
//before the radar data binary section

text[0]=35;
text[1]=68;
text[2]=65;
text[3]=84;
text[4]=65;
text[5]=45;

// scan along until string #DATA- is matched
i=0;
while( (i<6) ){
        c=fgetc(fp1);
        if(c==text[i]){
                i++;
        }
        else{
                i=0;
        }

}
```

```
// the start of DATA found ...start inputting and outputting
// Read last raw from input file and output it
// as first raw in output file
// I am assuming the radar file is the standard 480*480 size. If not change 480 to
// the number of rows and columns.


for (row=1;row<=480;row++)
{
                    // you can check for errors and add Windows API messages here if you want.


        if(ferror(fp1)){
                            break;
        }

        if(ferror(fp2)){
                            break;
        }

        fseek(fp1,-480*row*sizeof(unsigned char),SEEK_END);
        knt=1;
        while (knt <= 480)
        {

                fread(&value,sizeof(unsigned char),1,fp1);
                valuef = value+0;
                fwrite(&valuef,sizeof(float),1,fp2);
                knt++;

        }


}
fclose(fp1);
fclose(fp2);
}
```

The header file "afterc.hdr"

```
ncols 480
nrows 480
xllcorner -240000
yllcorner -240000
cellsize 1000
nodata_value -999
byteorder Lsbfirst
```

Step-by-step Instructions for Setting up ArcView for Loading Radar DAta

This process requires a dynamic link library "*cappiload.dll*", a calling script "*Rad_Load_Binary.ave*", and a header file "*afterc.hdr*". Compile the Dynamic link library provided in this appendix using Microsoft Visual C++ 4.0 or later version. A compiled version can be obtained by contacting the author or the Water Resources Laboratory at McMaster University. The steps for loading the data are:

- Create a new directory on the hard drive to be used as a working directory for your case. Let us say "*C:\demo*".

- Save the compiled link library "*cappiload.dll*"and the header file "*afterc.hdr*" inside the new directory "*C:\demo*".

- Open ArcView GIS from the Windows start menu.

- Open a new view in ArcView by double licking on the "Views" icon. ArcView will respond by opening a new view "View1".

- Set up ArcView working directory by clicking the "File" menu then click "Set Working Directory". In the dialog that appears enter "C:\demo". Then save the project.

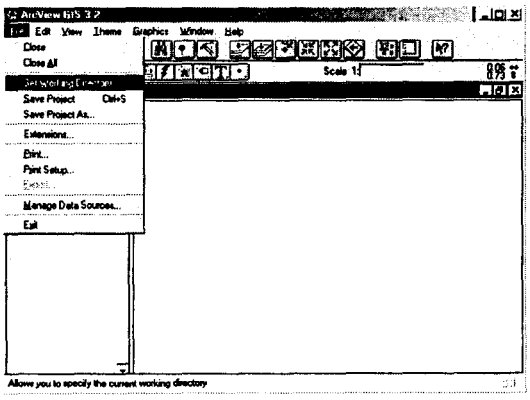

- Close the view "view1" and open a new script editor by double clicking on the "Scripts" icon.

- Load the script "*Rad_Load_Binary.ave.*". This can be done by clicking the "Script" menu then selecting "Load Text File".

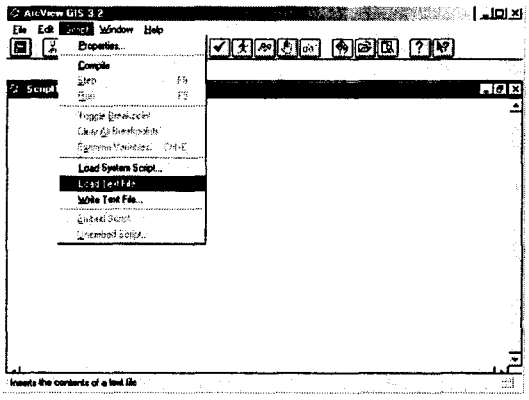

- Rename the script to *Rad_Load_Binary* by selecting "Properties" from the "Script" menu.

- Compile the script by clicking "Compile" from the "Script" menu then close the script editor.

- Attach the action of the script to a button in your view or a menu item. In this example, we will use a menu item. In order to achieve this we will add a new menu to ArcView GIS interface then add an item inside this menu. The new menu will be called "RADAR" and the item will be called "LOAD":

    - Go back to View1 then double click anywhere in the gray area in ArcView interface. You should receive the following customize dialog.

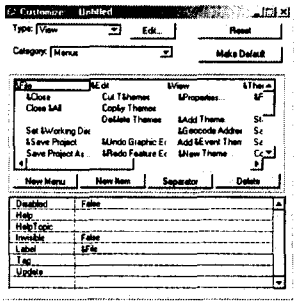

- Click the "New Menu" button to add a new menu to ArcView interface then click the "Label" property to change its name to RADAR.

- Click the "New Item" button to add a new item under the RADAR menu then click the "Label" property to change its name to LOAD.

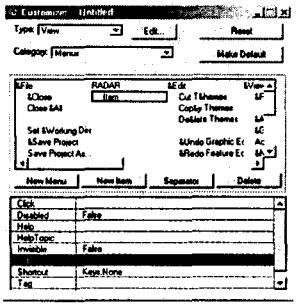

- Assign the action of the LOAD item to the *Rad_Load_Binary* script. This can be done by clicking the "Click" property then in the dialog that appears browse to select *Rad_Load_Binary* script then press "Ok".

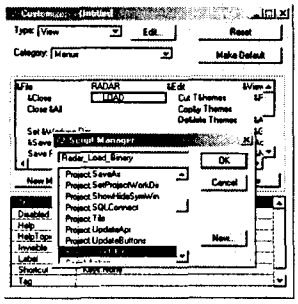

- Close the customize dialog. Now you should have a new menu RADAR added to ArcView interface with a menu item LOAD added under it.

- Load the Spatial Analyst Extension. To do this go to the "File" menu then select "Extensions". Browse and check the Spatial Analyst Extension then press "Ok". ArcView is now ready to load radar data. Save the project.

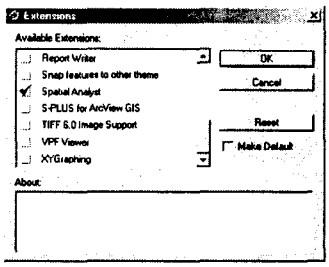

- In order to load the data go back to "View1" and go to the "RADAR" menu and click the "LOAD" item. You will receive a file dialog prompting to select radar files.

- Browse to the location on the hard drives where the data is. Hold down the "Shift" key then select with the mouse (or with the keyboard arrows) any number of radar files you want to load then press "Ok".

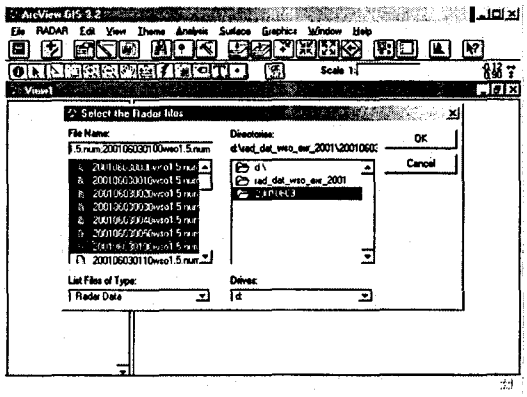

- Now the process of setting ArcView and Loading the data is finished. ArcView interface after loading the data should look similar to the following figure.

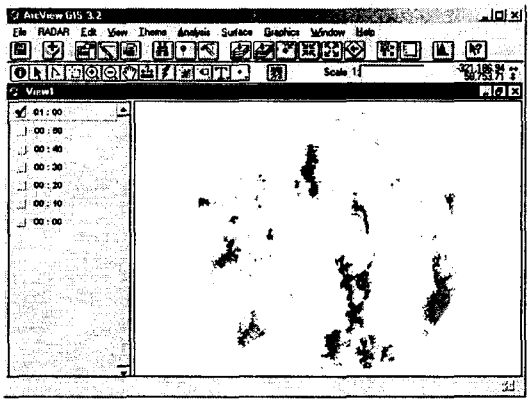

APPENDIX III
A LIBRARY FOR RADAR PROJECTION

Two programs are provided in this appendix for the purpose of projection using the developed GPP projection method. The two programs are written using C/C++ to provide utilities for projecting a set of points from geodetic coordinates to radar coordinates or vice versa. They can be used, in the current form, as separate executables or they can be modified to be used as dynamic libraries that can be linked to any applications. The first program, *GPPForward* is for the forward transformation and the second, *GPPInverse* , is for te inverse transformation.

- The *GPPForward* requires an input ASCII file that contains both the geographical coordinates of the radar location (longitude and latitude in degrees) as well as the coordinates (longitudes and latitudes in degrees) of the set of points required to be projected into the radar coordinate system. Note the radar coordinates (longitude and latitude) should be written in the first line in the input file. An example of the input file is provided at the end of this appendix.

- The *GPPInverse* requires an input ASCII file that contains both the geographical coordinates of the radar location (longitude and latitude in degrees) as well as the Cartesian coordinates (x and y in meters) of the set of points required to be projected from radar coordinates to geodetic coordinates. Note the radar coordinates (longitude and latitude) should be written in the first line in the file. An example of the input file is provided at the end of this appendix.

- Both programs write the projected coordinates in an output file in the same sequence they are in the input file. The name of the output file is fixed "*output.txt*". It can be changed inside the code to any other name or to be a variable that the main function can receive from the command line.

GPPForward

```
#include <stdio.h>
#include <math.h>
#include <stdlib.h>


// This program projects a set of points from geodetic coordinates into radar
// coordinates using the GPP forward transformation.

// The variables are named exactly according the names
// used in the thesis to simplify linking the code and equations.

// Declare global array to store projected coordinates. This array is used also to pass values between
procedures.
double arr[2];



// The following functions are for the three methods : GPP, conventional, and conventional with
// pre-conversion from geodetic to geocentric, respectively.
// All these procedures take the geographic coordinates of the radar and the point
// being projected as arguments.
// The procedures then save the projected coordinates of the points in a global array
// that get accessed from the main.
double * GPP(double lndao,double phio,double lndp,double php);
double * convential(double lndo,double phio,double lndp,double php);
double * convential2(double lndo,double phio1,double lndp,double phip1);

// The following functions are used by the code to convert from geodetic to geocentric,
// calculate range, and to calculate beam height, respectively.
double * geocenteric(double lndo,double phio1,double lndp,double phip1);
double calcrkm(double lndo,double phio1,double lndp,double phip1);
double calchcappi(double rkm);



int main(int argc, char *argv[])
{
        FILE *fp1,*fp2;
        char *filename;
        filename = argv[1];
        int i;
        double lndo,phio,lndp,phip,pi,x,y,*thpt;
        double lndodeg,phiodeg,lndpdeg,phipdeg;
        pi = 3.1415927;

        fp1 = fopen(filename,"r");
        fp2 = fopen("output.txt","w");

        // Read radar coordinates.
```

```
        fscanf(fp1,"%lf", &lndodeg );
         fscanf(fp1,"%lf", &phiodeg );

        // NOTE: you have to have the radar coordinates as the first
        // point in your input file.

        // Get the radar coordinates lando, and phio.
        lndo = lndodeg*(pi/180);
        phio = phiodeg*(pi/180);


        // loop through the number of points in the input file
        // you can change the loop size according to the number
        // of points in your input file.

        for (i=1;i<=441;++i)
        {

        // Read the point coordinates.
        fscanf(fp1,"%lf", &lndpdeg );
        fscanf(fp1,"%lf", &phipdeg );

        // Convert to radians.
        lndp = lndpdeg*(pi/180);
        phip = phipdeg*(pi/180);



        // Now call the projection routine to project the point.
        // I am using the GPP now.
        thpt = GPP(lndo,phio,lndp,phip);
        //thpt = convential(lndo,phio,lndp,phip);
        //thpt = convential2(lndo,phio,lndp,phip);
        //thpt = geocenteric(lndo,phio,lndp,phip);

        // Get the projected coordinates from the global array.
        x = thpt[0];
        y = thpt[1];

        // Write the projected coordinates in the output file.
        fprintf(fp2," % 10.9lf",x);
        fprintf(fp2," % 10.9lf\n",y);
        }

        return 0;

}


double * GPP(double lndo,double phio,double lndp,double phip)
{
        double a,e,ro,phidasho,ho,hn,rp,phidashp,hp,deltahp,rkm,newrkm,theerr;
        double e2,pi,qp,thetap,deltalnd,ydash,alpha,x,y,hcappi,conic;

        a = 6378137; e = .081819; pi=3.1415927;
        e2 = pow(e,2);

        rkm = calcrkm(lndo,phio,lndp,phip);


        while (1)
        {

                // conic is the elevation angel.
                // hcappi is the beam height.
                conic = calchcappi(rkm);
```

```
                hcappi = rkm * tan(conic);

                ro = (a*cos(phio))/(sqrt(1-(e2*pow(sin(phio),2))));
                phidasho = atan((1-e2)*tan(phio));
                ho = ro*tan(phidasho);
                hn = (ro+(ho*tan(phio))+(hcappi/cos(phio)))/(tan(phio));

                rp = (a*cos(phip))/(sqrt(1-(e2*pow(sin(phip),2))));
                phidashp = atan((1-e2)*tan(phip));
                hp = rp*tan(phidashp);
                deltahp = hp*tan(phip)*((1/tan(phidashp))-(1/tan(phip)));
                qp = rp/cos(phip);
                deltalnd = lndp - lndo;
                thetap = atan ((rp*cos(deltalnd))/(hp+deltahp));

                ydash = (hn+deltahp)*((sin(thetap))/(sin(phio+thetap)));
                alpha = asin(rp*sin(deltalnd)/qp);

                x = (hn+deltahp)*(tan(alpha))*((sin(phio))/(sin(phio+thetap)));
                y = (ro/sin(phio))+(hcappi/(tan(phio)))- ydash;

                newrkm = sqrt(x*x + y*y);
                theerr = fabs(newrkm - rkm);

                if (theerr < 50)
                        break;
                else
                        rkm = newrkm;

        }
// Now fill the global array with the projected coordinates and go back to main.
arr[0]=x;
arr[1]=y;
return arr;

}


double * convential(double lndo,double phio,double lndp,double phip)
{
        double R,d,theta,deltalnd,sina,cosa,x,y;
        R = 6371200;
        deltalnd = lndp - lndo;
        theta = acos((sin(phio)*sin(phip))+(cos(phio)*cos(phip)*cos(deltalnd)));
        d = R*theta;
        sina=(cos(phip)*sin(deltalnd))/(sin(theta));
        cosa=((cos(phio)*sin(phip))-(sin(phio)*cos(phip)*cos(deltalnd)))/(sin(theta));
        x = d*sina;
        y = d*cosa;
        // Now fill the global array with the projected coordinates and go back to main.
        arr[0]=x;
        arr[1]=y;
        return arr;

}



double * convential2(double lndo,double phio1,double lndp,double phip1)
{
        double R,d,theta,deltalnd,sina,cosa,x,y;
        double phio,phip,a,e,e2;
        R = 6371200;

        a = 6378137; e = .081819;
        e2 = pow(e,2);
```

```
        phio = atan((1-e2)*tan(phio1));
        phip = atan((1-e2)*tan(phip1));
        deltalnd = lndp - lndo;
        theta = acos((sin(phio)*sin(phip))+(cos(phio)*cos(phip)*cos(deltalnd)));
        d = R*theta;
        sina=(cos(phip)*sin(deltalnd))/(sin(theta));
        cosa=((cos(phio)*sin(phip))-(sin(phio)*cos(phip)*cos(deltalnd)))/(sin(theta));
        x = d*sina;
        y = d*cosa;
        // Now fill the global array with the projected coordinates and go back to main.
        arr[0]=x;
        arr[1]=y;
        return arr;

}


double * geocenteric(double lndo,double phio1,double lndp,double phip1)
{
        double x,y;
        double phip,a,e,e2,pi;
        pi=3.1415927;

        a = 6378137; e = .081819;
        e2 = pow(e,2);
        phip = atan((1-e2)*tan(phip1));

        x = lndp*(180/pi);
        y = phip*(180/pi);


        // I am just using the global array to pass the geocentric coordinates back to the calling procedure.
        arr[0]=x;
        arr[1]=y;
        return arr;

}


double calchcappi(double rkm)
{

        double kingelev[] =
        {0.3,0.5,0.7,0.9,1.1,1.4,1.7,2.0,2.4,2.9,3.4,4.1,4.8,5.6,6.6,7.7,9.0,10.4,12.1,14.1,16.3,18.7,21.5,24.6};
        double elev,bmht,degtorad,capht,hcab,hant,close,conic,diff,cosq,sinn,elevdeg;
        int el;

        close = 9999999;
        conic = -9;
        degtorad = 3.1415927/180;
        capht = 1500;
        hant = 390;


        for (el=0;el<24;++el)
        {
                elevdeg = kingelev[el];
                elev = elevdeg * (degtorad);
                cosq = (cos(elev)) * (cos(elev)) / 16980000.0;
                sinn = sin(elev);
                bmht = (rkm*rkm*cosq) + (rkm*sinn);
                diff = fabs(bmht-capht);

                if (diff < close)
```

```
                {
                        close = diff;
                        hcab = bmht;
                        conic = elev;
                }
        }

        return conic;
}


double calcrkm(double lndo,double phio1,double lndp,double phip1)
{
        double degtorad,capht,hant,close,conic,rkm;
        double R,theta,deltalnd;
        double phio,phip,a,e,e2;
        R = 6371200;

        a = 6378137; e = .081819;
        e2 = pow(e,2);

        close = 9999999;
        conic = -9;
        degtorad = 3.1415927/180;
          capht = 1500;
        hant = 390;
        phio = atan((1-e2)*tan(phio1));
        phip = atan((1-e2)*tan(phip1));
        deltalnd = lndp - lndo;
         theta = acos((sin(phio)*sin(phip))+(cos(phio)*cos(phip)*cos(deltalnd)));
        rkm = R*theta;
        return rkm;
}
```

GPPInverse

```
#include <stdio.h>
#include <math.h>
#include <stdlib.h>


// Declare global array to store projected coordinates. This array is used also to pass values between
double arr[2];


// This program projects a set of points from radar coordinates into
// geodetic coordinates using teh developed GPP ellepsoid method.

// The variables are named exactly according the names
// used in the thesis to simplify linking the code and equations.

// The following procedure  takes the radar geodetic coordinates and the point radar cartesian
// coordinates as arguments. It then projects the points coordinates into geodetic and
// pass them back to the calling main.

void GPPInverse(double lndo,double phio,double x,double y);

int main(int argc, char *argv[])
{
```

```
        FILE *fp1,*fp2;
        char *filename;
        filename = argv[1];
         int i;
        double lndo,phio,pi,x,y;
        double lndodeg,phiodeg,lndpdeg,phipdeg;
        pi = 3.1415927;

        fp1 = fopen(filename,"r");
        fp2 = fopen("output.txt","w");

        //Read radar coordinates.

        fscanf(fp1,"%lf", &lndodeg );
        fscanf(fp1,"%lf", &phiodeg );

        // Convert to radians.
        lndo = lndodeg*(pi/180);
        phio = phiodeg*(pi/180);

        // scan along teh input file to read each point and project it
        for (i=1;i<=30;++i)
        {
        // Read the point cartesian coordinates.
         fscanf(fp1,"%lf", &x );
         fscanf(fp1,"%lf", &y );

        // Call the GPP projection procedure.
        GPPInverse(lndo,phio,x/1000,y/1000);

        // Get the projected coordinates from the global storage.
        lndpdeg = arr[0];
        phipdeg = arr[1];

        // Write projected values into the output file.
        fprintf(fp2," % lf",lndpdeg);
        fprintf(fp2," % lf\n",phipdeg);
        }

        return 0;

}



void GPPInverse(double lndo,double phio,double x,double y)

{

        double a,e,ro,phidasho,ho,hn;
        double e2,pi,ydash,hcappi;
        double rp,phip,phipdeg,deltalnd,lndp,lndpdeg;
        double ratio,numb,c1,c2,c3,c4,A,B,D,E,G,h,h2,f,fdash;
        int j;

        hcappi=1.500;
        a = 6378.137; e = 0.081819; pi=3.1415927;
        e2 = pow(e,2);

        ro = (a*cos(phio))/(sqrt(1-(e2*pow(sin(phio),2))));
        phidasho = atan((1-e2)*tan(phio));
        ho = ro*tan(phidasho);
        hn = (ro+(ho*tan(phio))+(hcappi/cos(phio)))/(tan(phio));
        ydash = (ro/sin(phio)) + (hcappi/tan(phio)) - y;
```

```
        ratio = x/(ydash*sin(phio));
        numb = sqrt(1+pow(ratio,2));


        // Calculate the parameters of the polynomial.
        c1= pow(a,2)*(1-e2);
        c2= pow((numb*sin(phio)*ydash),2)/(1-e2);
        c3= hn-(ydash*cos(phio));
        c4= e2/(1-e2);

        A = pow(c4,2);
        B = 2*c3*c4;
        D = c2 + pow(c3,2) - (c1*A);
        E = 2*c1*c3*c4;
        G = c1*pow(c3,2);


        // Start solving using Newton Raphson.

        f = 300000;
        h = ho;

        // Allowable error in the function is 200000
        // which corresponds to an error of less than 1 meter
        // in the height.
        while(fabs(f)>200000)
        {
                f = pow(h,4)*A + pow(h,3)*B + pow(h,2)*D - h*E - G;
                fdash = 4*A*pow(h,3) + 3*B*pow(h,2) + 2*h*D - E;
                h2 = h-(f/fdash);
                h = h2;
        }

        // Newton Raphson is done. Start finding the geographical coordinates.
        rp= sqrt((c1-pow(h2,2))/(1-e2));
        phip = atan(h2/(rp*(1-e2)));
        deltaInd = atan(ratio);
        Indp = Indo+deltaInd;
        Indpdeg = Indp*(180/pi);
        phipdeg = phip*(180/pi);

        // Now fill the global array with the projected coordinates and go back to main.
        arr[0]=Indpdeg;
        arr[1]=phipdeg;

}
```

Example input coordinates file for the forward transformation

```
-79.5728 43.9635
-79.5728 44.25
-79.5728 44.5
-79.5728 44.75
-79.5728 45
-79.5728 45.25
-79.5728 45.5
-79.5728 45.75
-79.25 43.9635
-79.25 44.25
-79.25 44.5
-79.25 44.75
```

```
-79.25 45
-79.25 45.25
-79.25 45.5
-79.25 45.75
-79 43.9635
-79 44.25
-79 44.5
-79 44.75
-79 45
-79 45.25
-79 45.5
-79 45.75
-78.75 43.9635
-78.75 44.25
-78.75 44.5
-78.75 44.75
-78.75 45
-78.75 45.25
-78.75 45.5
-78.75 45.75
-78.5 43.9635
-78.5 44.25
-78.5 44.5
-78.5 44.75
-78.5 45
-78.5 45.25
-78.5 45.5
-78.5 45.75
-78.25 43.9635
-78.25 44.25
-78.25 44.5
.
. And so on...
```

Example input coordinates file for the inverse transformation

```
-79.5728 43.9635
-208972.0333 -274734.5368
-188080.0141 -275324.7782
-167186.3576 -275852.8865
-146291.2458 -276318.8624
-125394.8608 -276722.7067
-104497.3845  -277064.4201
-83598.9988 -277344.0030
-62699.8856  277561.4559
-41800.2269  277716.7792
-20900.2044  277809.9731
0.0000  277841.0377
20900.2044 277809.9731
41800.2269 277716.7792
62699.8856 277561.4559
.
.
...And so on...
```

APPENDIX IV

PSEUDO CODE FOR THE GLOBAL MAXIMIZATION OF THE CORRELATION SURFACE

This appendix contains a detailed pseudo code for the optimization methodology used for the global maximization of the correlation surface to facilitate reproduction in different programming language. The methodology is described in Chapter 7, section 7.3.5.

The Pseudo Code:

Set the values of the 6 technical parameters (refer to Table 7.1).
Initialize a tabu lis, an absolute tabu list, and a peaks list.
Res = *Start_Res* (set the search resolution according to the value in Table 1)

IF (Case of initialization) **THEN**

- *CurrentPosition* = any position (*XShift* , *Yshift*).
- *TS* = "Yes"

ELSE

- *CurrentPosition* = According to the velocity vector obtained in the previous scan.
- **IF** (*Perform_TS* = "No") **THEN**

  TS = "No"

  ELSE

  TS= "Yes"

  ENDIF

ENDIF

CurrentCorrelation = the correlation value corresponding to *CurrentPosition*

WHILE (TRUE)

/*Examine all the neighbourhood (box) around *CurrentPosition*. If all neighbours are less than *CurrentCorrelation* start a TS because a peak is found. Else go in the direction of the steepest ascent. This is shown in the following main IF statement.*/

- **IF** (the correlation values of all neighbours are less than *CurrentCorrelation*) **THEN**
  - *OptimumPosition* = *CurrentPosition*
  - *MaxCorrelation* = *CurrentCorrelation*
  - **IF** (*TS* = "No") **THEN**
    - BREAK /*This will exit the whole process*/
  - **ENDIF**
  - Declare the visited new points as taboo (i.e., add them to the tabu list).
  - *N_Paths = 0*
  - **WHILE** (*TS* = "Yes") /*This is the tabu search while loop*/

    /*Examine the neighbourhood (box) around *CurrentPosition.* If all neighbours are taboo, free one which has the highest correlation. Else find the highest new point. This is performed in the following IF statement*/
    - **IF** (all neighbours are less than *CurrentCorrelation*) **THEN**
      - Add *CurrentPosition* to the Peaks list.

      ENDIF
    - **IF** (all neighbours are Taboo) **THEN**
      - **IF** (all neighbours are Absolute taboo) **THEN**
        - *CurrentPosition* = *OptimumPosition*
        - *TS* = "No" /* Large scale search is done*/
        - *Res* = *Final_Res* /*change to the final search resolution*/
        - BREAK /* The Starting search is done, do final search*/

        ENDIF
      - *NextPosition* = Free one of the neighbourhood which has the highest correlation value even if the correlation is less than *CurrentCorrelation*. Make sure that this point is not already absolute taboo (i.e., not included in the absolute tabu list).
      - *NextCorrelation* = the correlation value corresponding to *NextPosition*.
      - Add the freed point to the absolute tabu list.

      ELSE (at least one of the neighbours is not taboo)
      - *NextPosition* = One of the new points (i.e., non-taboo) which has the highest correlation value even if the correlation is less than

CurrentCorrelation.

- *NextCorrelation* = the correlation value corresponding to *NextPosition.*
- Declare the new visited points from the neighbourhood as taboo (i.e., add them to the tabu list).

ENDIF

/*Check if *NextCorrelation* is higher than the maximum solution found so far:*/

- **IF** (*NextCorrelation* > *MaxCorrelation*) **THEN**
  - *CurrentPosition* = *NextPosition*
  - BREAK the TS while loop which will move control to the beginning of the main RS while loop. I.e., restart RS climber at *CurrentPosition.*

ENDIF

/*Check if TS stopping criterion is fulfilled*/

- **IF** (*N_Paths* = *Max_N_Paths*) **THEN**
  - *TS* = "No" /* Large scale search is done*/
  - *Res* = *Final_Res* /*change to the final search resolution*/
  - *CurrentPosition* = *OptimumPosition*

ELSE

- **IF** (*NextCorrelation* < $\eta \times$ *MaxCorrelation*) **THEN**
  - *CurrentPosition* = *OptimumPosition*
  - *N_Paths* = *N_Paths*+1

ELSE

- *CurrentPosition* = *NextPosition*

ENDIF

ENDIF

END WHILE /*End of the tabu search while loop*/

ELSE (at least one of the neighbours is higher, hence go in the direction of steepest ascent)

- *NextPosition1* = one of the neighbours which has the highset correlation value.
- *LowestPoint* = one of the neighbours (here including the current point) which has the lowest correlation value.
- *NextCorrelation1* = the correlation value corresponding to *NextPosition*1.
- *SteepestDirection* = the extension of the line joining *LowestPoint* to *NextPosition.* This can be obtained from:

$$DeltaX = XShift_{NextPosition} - XShift_{LowestPoint}$$
$$DeltaY = YShift_{NextPosition} - YShift_{LowestPoint}$$

- **WHILE** (TRUE) /*This while loop to perform runs on the steepest direction*/
  - *NextPosition2 = NextPosition1 + (DeltaX, DeltaY)*
  - *NextCorrelation2* = the correlation value corresponding to *NextPosition2.*
  - **IF** (*NextCorrelation2* < *NextCorrelation1*) **THEN**
    - *CurrentPosition* = *NextPosition1*
    - *CurrentCorrelation* = correlation corresponding to *CurrentPosition*
    - BREAK /*I.e., stop going in a line and go to the beginning of the main RS while loop to construct a box again around the last point reached. I.e., restart RS climber at *CurrentPosition.*/

    ELSE
    - CONTINUE this while loop (the line while loop) , i.e., keep going in a line.
    - *NextPosition1 = NextPosition2*

    ENDIF

END WHILE /*This is the end of the steepest direction while loop*/

ENDIF /*This is the end of the main IF statement*/

END WHILE /*This is the end of the main While loop, i.e. the RS while loop*/

APPENDIX V
SIMPLE USER MANUAL FOR THE RAINPLAT-GIS PACKAGE

This appendix provides a simple manual for using the main components of the RAINPLAT-GIS package developed in Chapter 5 of this thesis. This package requires ArcView GIS version 3.0, 3.1, or 3.2. The RAINPLAT-GIS software is available on a compact disk (CD), which can be obtained by contacting the author or the Water Resources Laboratory at McMaster University. The package includes three GIS extensions (the Radar, Rain-Gauge, and Satellite extensions). Refer to Chapter 5 for more details on the theories of the different modules. The three extensions can be used independently, i.e., it is not essential to load the Radar Extension before using the Satellite Extension for example. Additional details on the three extensions are available in the software manual, which is provided in PDF format with the installation CD.

V.1 Installing The RAINPLAT-GIS Package

1- Insert the RAINPLAT-GIS CD in the CD drive.

2- Click the Windows "Start" main menu then select "Run".

3- Browse to the CD then double click the "rainplat_setup.exe" in the RAINPLAT-GIS CD.

4- Follow the simple instructions on the screen until the installation finishes. Then check that the directory "C:\Rainplat" has been created. This directory contains all the files required by the RAINPLAT-GIS modules.

In case you have different versions of ArcView on the same Widows system and you want to install the package on all the versions follow the same steps mentioned above. In addition, copy the three extension files from the "Ext32" folder on the CD to the "$AVHOME\AV_GIS30\ARCVIEW\EXT32" folders of each ArcView version, where "$AVHOME\" denotes ArcView installation folder.

V.2 The Radar Extension

V.2.1 Installing The Radar Extension

After installing the RINPLAT-GIS package, follow the following steps to load the Radar Extension:

1- Open ArcView.

2- Go to the "File" menu then select "Extensions".

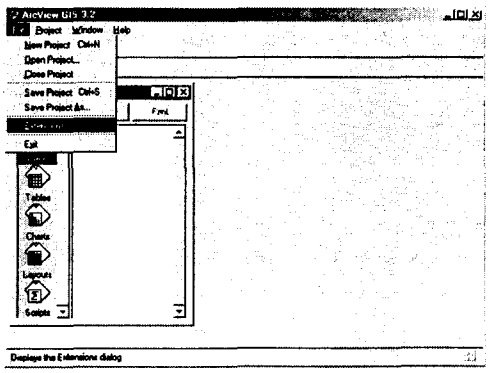

3- In the dialog that appears check the "Radar" Extension.

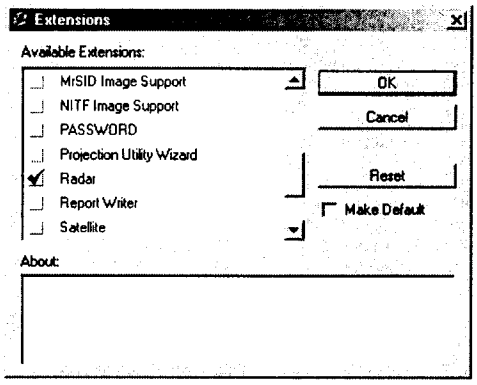

After Loading the "Radar" Extension. Open a new view. The view interface will have a new "Radar" menu added as shown in the following figure.

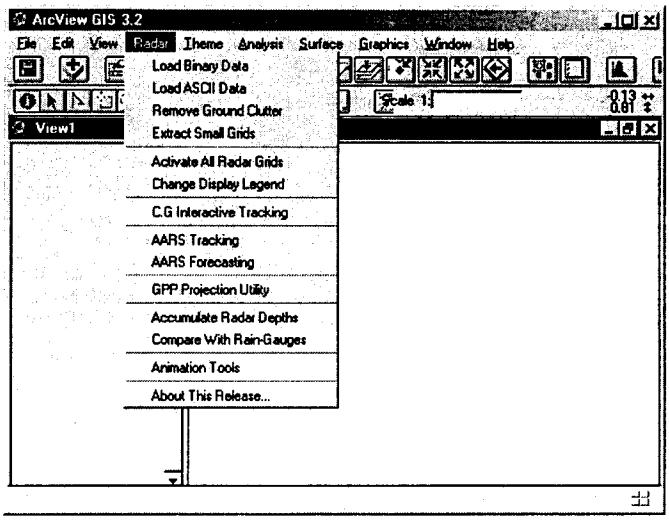

V.2.2 Loading Radar Data

V.2.2.1 Loading Binary Data

The current data provided by the Radar Groups of Environment Canada is in binary format and in the IRIS-N units. In order to load the data into ArcView GIS follow the following steps:

1- Go to the "Radar" menu then select "Load Binary Data".

2- A dialog appears prompting the user to select the type of output units from a drop down list. Choices are: N, DBZ, Z, or RAIN. N is the reflectivity in IRIS values, DBZ is the reflectivity in decibels, Z is the reflectivity in mm3/m6, and RAIN is the rain rate in mm/hr. Select the output units then press "Ok".

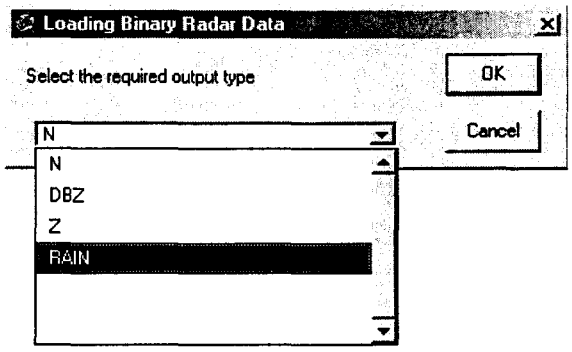

3- A second dialog appears prompting the user to enter the time difference with the UTC (Greenwich) System in hours. For example, if you want the data to be loaded in ArcView in Eastern time System, enter 4 hours in the summer or 5 hours in the winter (zero value will keep the data in UTC system). In case you have selected RAIN units, the same dialog will ask for two additional parameters for the Z-R conversion. These two parameters are the A and b of the Z-R

conversion. Enter the values then press "Ok".

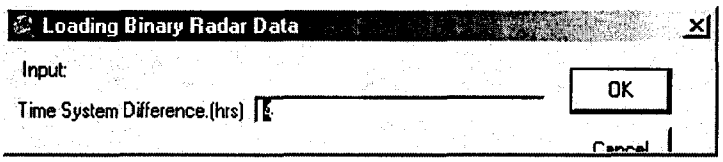

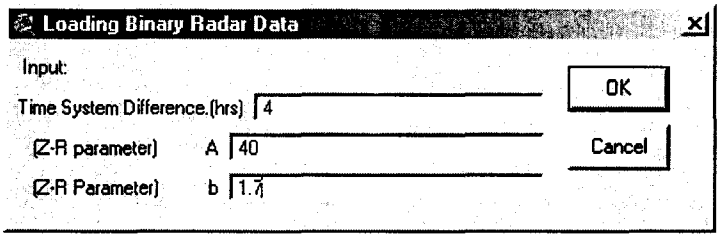

4- A file dialog appears prompting the user to select the radar files to be loaded. Browse to the location on the hard drives where the data is (a permissible network drive can be used) . Hold down the "Shift" key then select with the mouse (or with the keyboard arrows) any number of radar files you want to load then press "Ok".

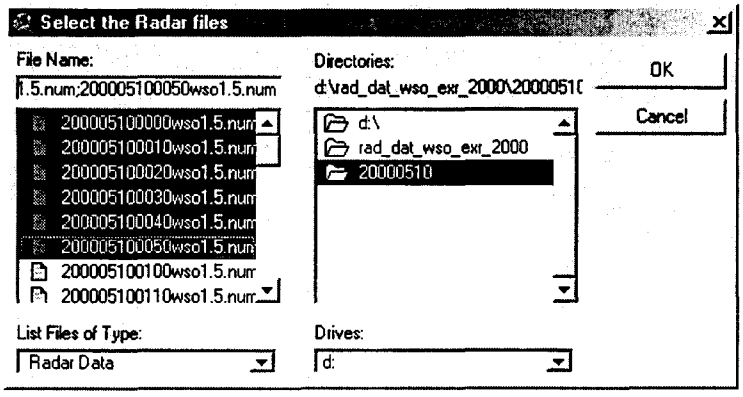

The process of loading the binary data is finished. The radar grids will be loaded in your view. It is recommended to load each event or day (240 files per day)

in a separate view. Note that the loaded data are referenced and displayed in radar coordinate system. I.e., the coordinate system is a Cartesian coordinate system in meters units having its origin at the centre of grid (the radar location).

V.2.2.2 Loading ASCII Data

It is uncommon to receive radar data in ASCII format because of the file sizes. However, the interface provides also an option for loading ASCII radar data. The ASCII data provided by Environment Canada is assumed to be in DBZ units. The process of loading the data in ASCII format is very similar to that of the binary data. In order to load the ASCII data follow the following steps:

1. Go to the "Radar" menu then select "Load ASCII Data".

2. A dialog appears prompting the user to select the type of output units from a drop down list. Choices are: N, DBZ, Z, or RAIN. N is the reflectivity in IRIS values, DBZ is the reflectivity in decibels, Z is the reflectivity in mm3/m6, and RAIN is the rain rate in mm/hr. Select the output units you want then press "Ok".

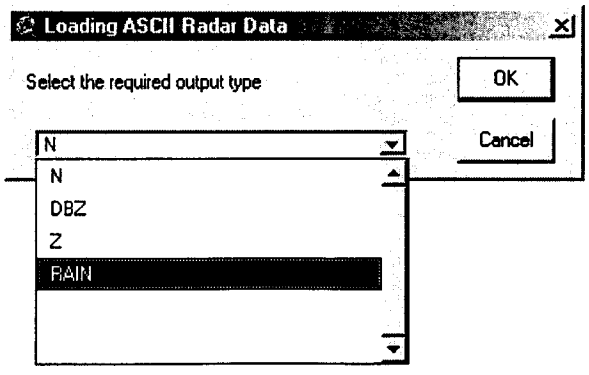

3. A second dialog appears prompting the user to enter the time difference with the UTC (Greenwich) System in hours. For example, if you want the data to be loaded in ArcView in Eastern time System, enter 4 hours in the summer or 5 hours in the winter. In case you have selected RAIN output units, the same dialog will ask you for two additional parameters for the Z-R conversion. These two parameters are the A and b of the Z-R conversion. Enter the values then press "Ok".

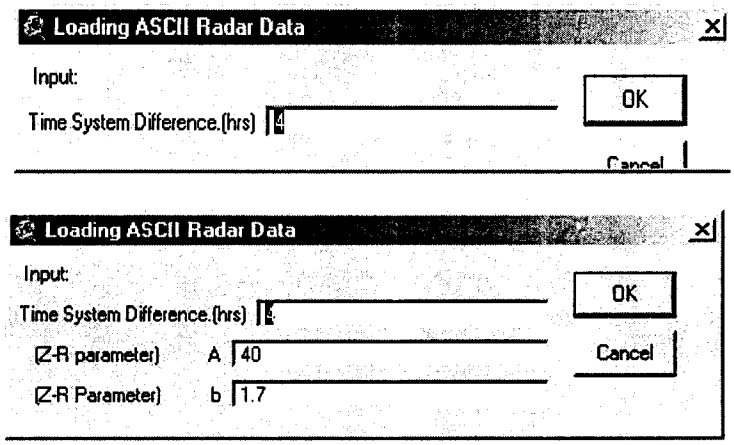

4. A file dialog appears prompting the user to select the radar files to be loaded. Browse to the location on the hard drives where the data is. Hold down the "Shift" key then select with the mouse (or with the keyboard arrows) any number of radar files you want to load then press "Ok".

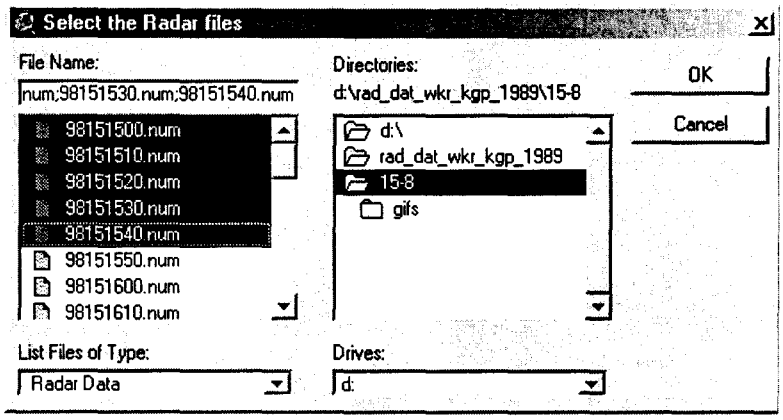

The process of loading the ASCII data is finished. You will find the radar grids loaded in your view. It is recommended to load each event in a separate view. Note that the loaded data are referenced and displayed in a radar coordinate system. I.e., the coordinate system is a Cartesian coordinate system in meters units having its origin at the centre of grid (the radar location).

V.2.3 Ground Clutter Removal

An automated clutter cancellation routine is used to suppress clutter from the raw scans. This procedure removes ground clutter in two stages: (1) Where radar reflectivities in a raw image are less than those in a clutter map, the former are deleted; (2) Any remaining reflectivity in the radar image which correspond to instantaneous rainfall rates less than a threshold value (usually equivalent to 1/32 mm/hr) are deleted. The procedure is fully automatic, requiring only an average ground clutter map collected during dry days. In order to run this routine:

1. Load a set of raw radar files in your view as described in the previous

sections. Remember to write down the output units you used because the clutter map you will use must be in the same units.

2. Add a grid theme to the view representing the clutter map. One simple way of doing this is to use one of the existing dry radar grids which have been previously loaded. To do this copy and paste this grid to replicate it then change its name to any other name to differentiate it from the radar grids.

3. Activate the radar grids you want to suppress their clutter. If all the grids will be corrected you can use the menu item "Activate All Radar Grids" to save time.

4. Go to the "Radar" menu then select "Remove Ground Clutter". A dialog appears prompting to select the clutter grid from a drop down list. Note that you have to use the same units the radar grids are in then press "Ok".

5. After the routine runs the activated radar grids will be replaced by a corrected version in the same view. Note that the old raw grids will be totally deleted.

V.2.4 Running the Interactive Center of Gravity Tracking

The interactive Center of Gravity (C.G) Tracker runs in an interactive mode. The user delineates the storm clusters under investigation in consecutive radar scans then the module calculates the average speed and direction together with their

standard deviations.

1- Load a set of radar files in your view as described in the previous sections. Remember to specify "RAIN" as your output type then remove ground clutter if required. You may use ArcView zooming tools to zoom to the storm clusters under investigation.

2- In order to launch the main dialog of the C.G Tracker go to the "Radar" menu then select "C.G Interactive Tracking". The main dialog of the C.G Tracker appears as shown in the following figure. This dialog is floating so that the user can move it anywhere in the display, even outside the ArcView menu, in order to facilitate the delineation of echoes. In order to perform a tracking session, follow the following steps.

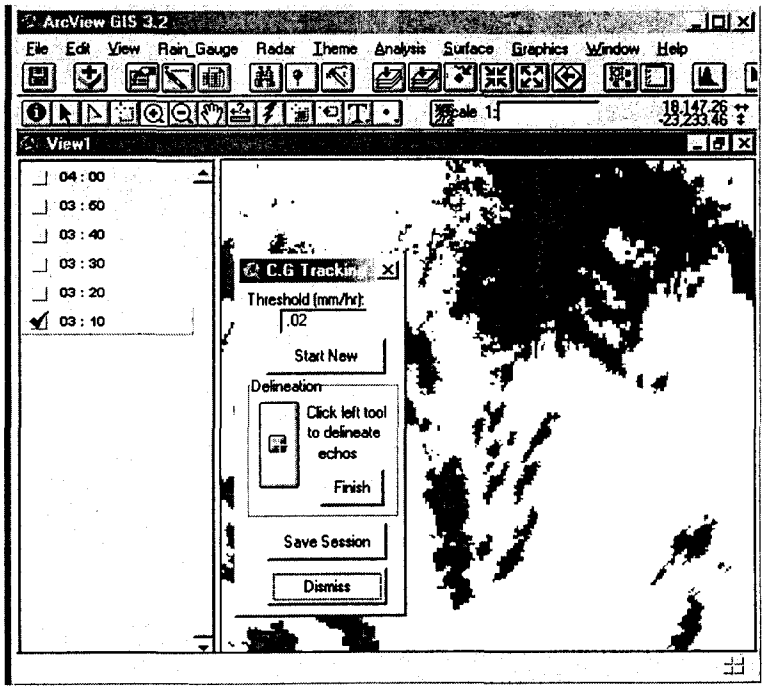

3- Click the "Start New" button.

4- Activate the first radar grid you want to work on. In the previous figure the time "03 : 10" is activated.

5- Press the left tool (the delineation tool) in the delineation part of the dialog. Move the mouse to the view and delineate the cluster under interest by drawing a polygon around it. To finish drawing the polygon double click the left button of the mouse at the last point of the polygon. In case you make an error click the "Start New" button to start again.

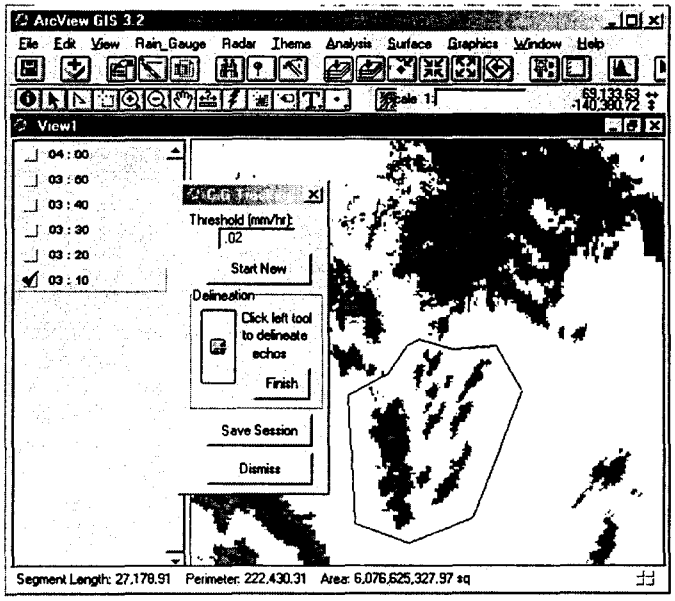

6- Activate the next radar grid in the view. In this example it is at time "03 : 20" then delineate te same cluster again as in the previous step.

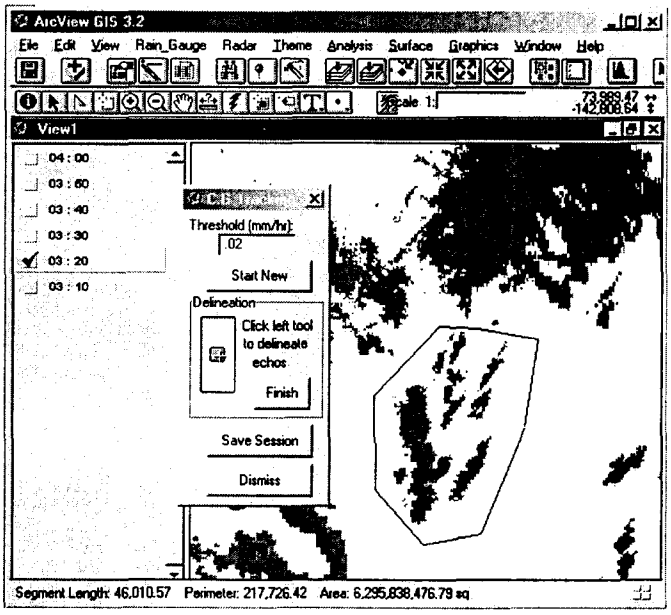

7- Continue the same process of activating the consecutive grids and delineating the same storm clusters in the subsequent grids. When finished click the "Finish" button to display the results. A dialog appears to display a quick summary of the tracking process.

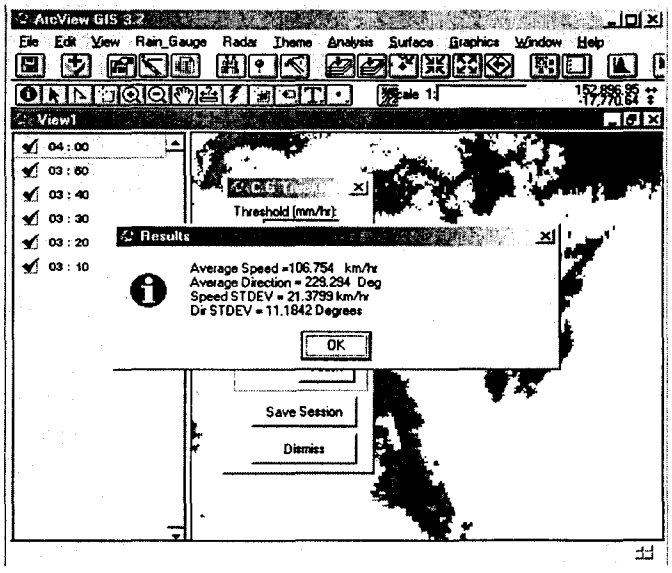

8- Press the "Save Session" button if you want to save a detailed summary of your tracking process, which includes the positions of the centre of gravity as well as the speed and direction at each time step. A file dialog appears prompting for a name for the output text file that will contain the detailed summary.

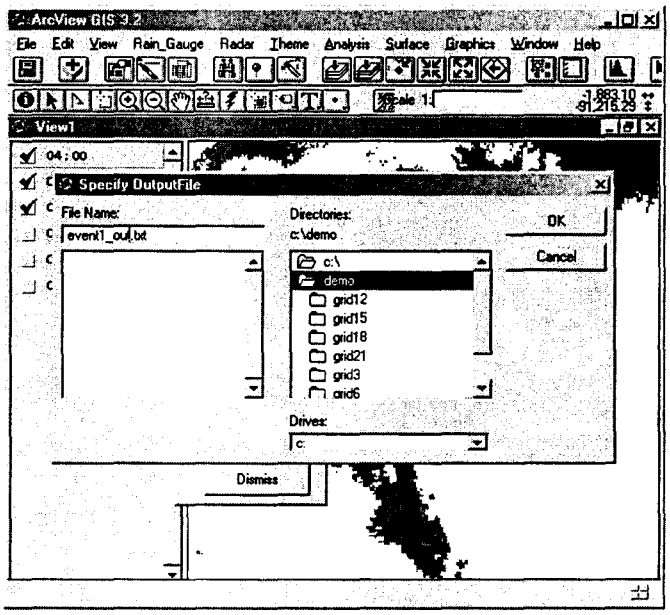

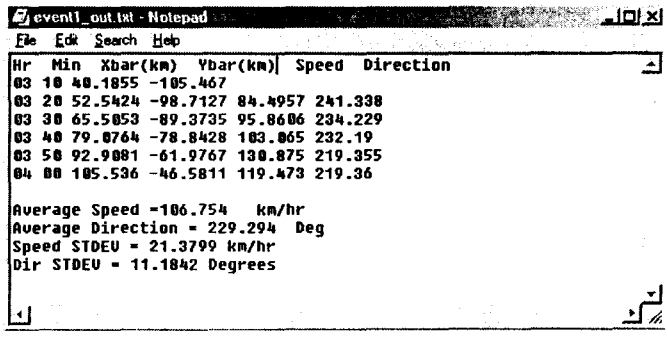

V.2.5 Running The AARS Tracking and Forecasting

The AARS tracking and forecasting module run automatically, i.e., the user activates the radar rainfall grids at the different times and the module moves from one scan to the next until it finishes all rainfall grids within the activated time period. Load a set of radar files in your view as described in the previous sections and remove clutter if required. Remember to specify "RAIN" as your output type. The AARS tracking and forecasting modules provided in this interface is designed to run independently for off-line research purposes that may require running each component separately.

V.2.5.1 Running the AARS Tracking Module

In order to run the AARS tracking module, follow the following steps:

1- Add a polygon theme to the view to be used as a sub-domain for performing the tracking. This theme can have multiple polygon shapes. Select the shape you will use as sub-domain as shown in the following figure. As shown in the following figure, the circle having Idpoly = 2 is selected.

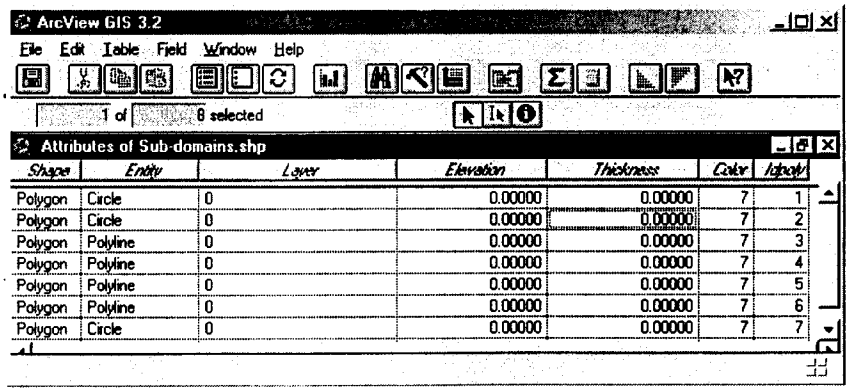

Shape	Entity	Layer	Elevation	Thickness	Color	Idpoly
Polygon	Circle	0	0.00000	0.00000	7	1
Polygon	Circle	0	0.00000	0.00000	7	2
Polygon	Polyline	0	0.00000	0.00000	7	3
Polygon	Polyline	0	0.00000	0.00000	7	4
Polygon	Polyline	0	0.00000	0.00000	7	5
Polygon	Polyline	0	0.00000	0.00000	7	6
Polygon	Circle	0	0.00000	0.00000	7	7

2- Activate the radar themes you want to include in your tracking run as shown in the following figure. Note that the polygon theme "Sub-domains.shp" is shown on this figure as well.

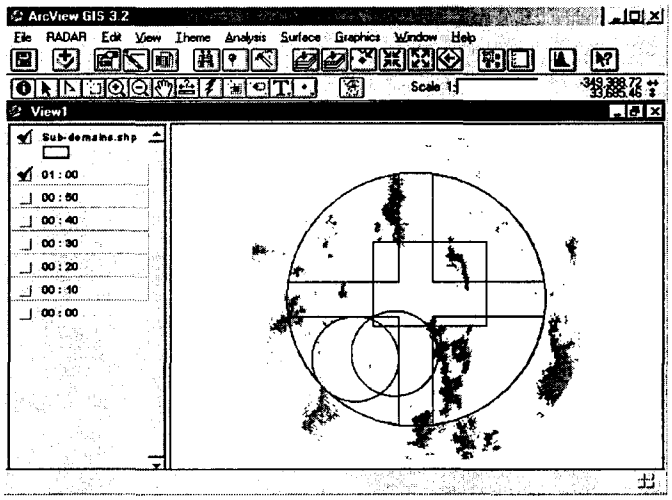

3- Go to the "Radar" menu and click the "AARS Tracking" item to run the AARS tracking module. A dialog prompts for selecting a polygon theme that represents the analysis domain. Select the polygon theme then press "Ok".

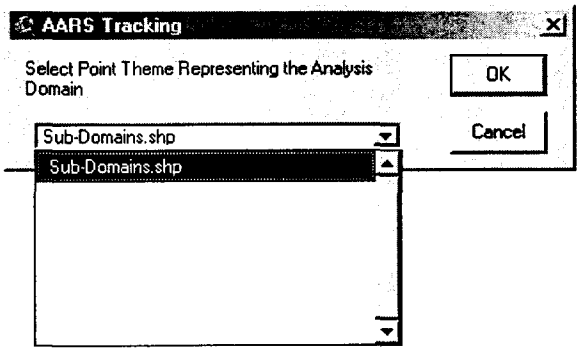

4- A dialog prompts for selecting any filed (column) from the attribute

table of the domain theme to be used as ID for the domain shape. Select one them press "Ok".

5- An output file dialog appears to prompt for a name for the output text file that will hold the tracking output. Type the name and location where you want to save this output file then press "Ok".

6- After the module finishes the run open the output text file using WordPad, it should look similar to the following figure.

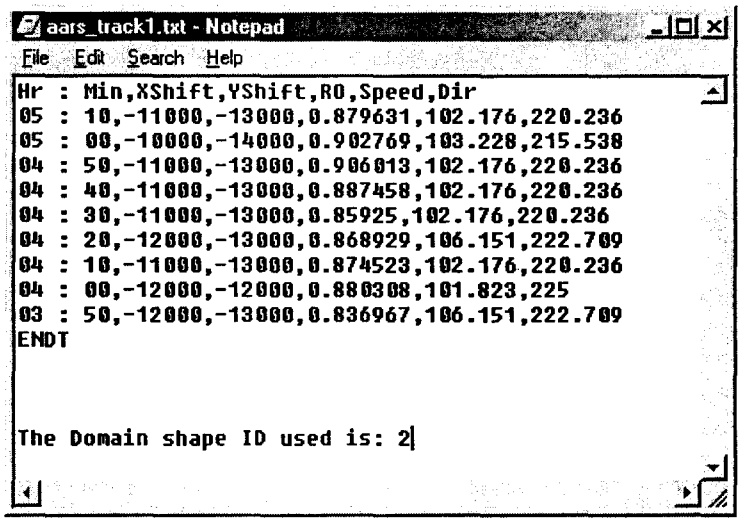

The ID column in the output file represents the Idpoly number of the polygon shape used as a sub-domain.

V.2.5.2 Running the AARS Forecasting Module

1- Activate the radar themes you want to include in your forecasting run as shown in the following figure. Note that the forecasting module uses the output of the tracking module. Hence, the activated themes must have corresponding values in the output file created by the tracking module otherwise an error message will appear.

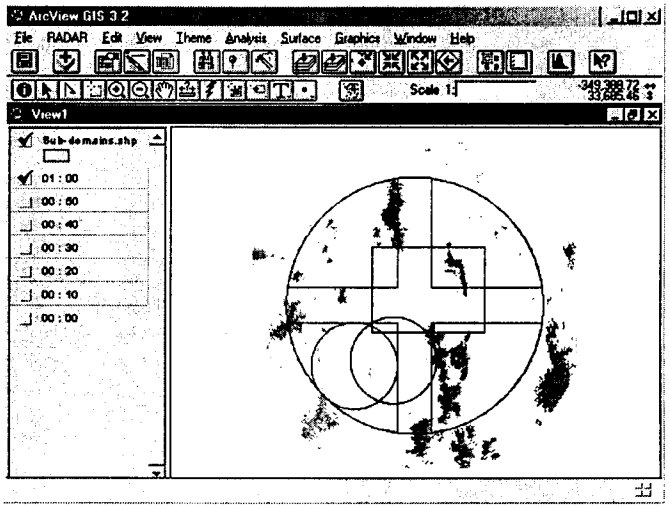

2- Go to the "Radar" menu and click the "AARS Forecasting". A file dialog appears prompting to select the text file created by the tracking module, which holds the velocity vector information. Browse and select the file developed from running the tracking module then press "Ok".

3- Another dialog appears to prompt the user to enter the forecasting parameters as shown in the following figure. The forecasting steps

should be an integer representing the number of time step ahead (each time step is 10 minutes). The following figure shows a lead time of one hour. The smoothing coefficient represents β' (i.e, the exponential smoothing coefficient described in Chapter 7).

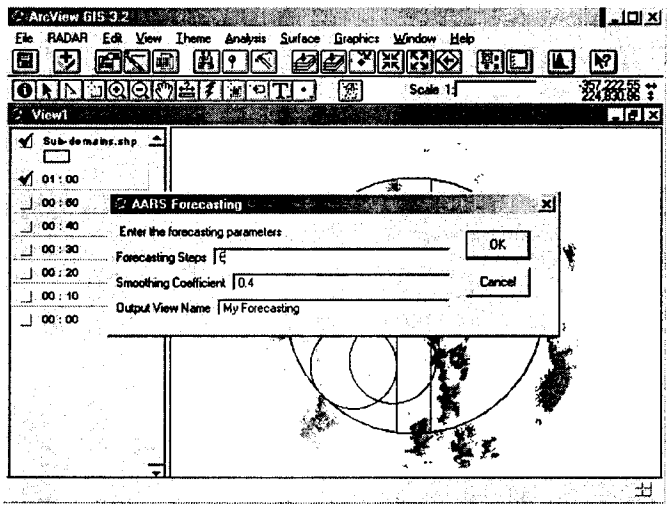

4- Enter the parameters then press "ok". The module will run and a new view will be created in your project. This view takes the name you entered in previous dialog. The forecasted rainfall fields will be placed in this new view.

V.2.6 Accumulating Radar Depths

When the user specifies "RAIN" as an output units for loading radar data , the loaded radar grids represent instantaneous rainfall intensity maps in mm/hr. In order to accumulate grids of rainfall depths a method for accumulation is required. The three methods described in (Chapter-5) are used to accumulate incremental grids of

rainfall depths. The following steps describe the use of this utility:

1- Go to te "Radar" menu then select "Accumulate Radar Depths".

2- In the drop down list choose the method to be used in accumulating grids of radar rainfall depths in mm.

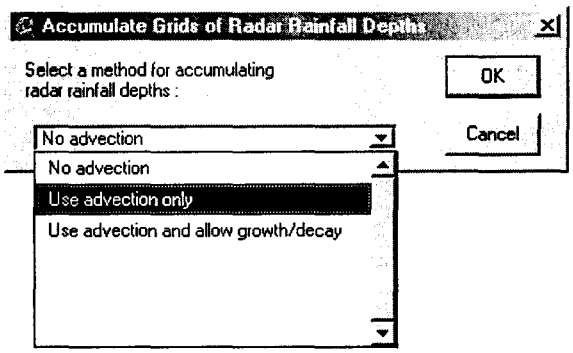

3- A dialog box appears prompting for the starting time, ending time, the time step between output grids (i.e., the accumulation interval in minutes), and a name for the output view that will hold the output grids. If method 2 or 3 are used, an additional input is require to specify the analysis step for advection correction. If zero value is entered in this box, the module determines the analysis step automatically from the velocity vector information. It is recommended that you enter zero and leave this job to the module.

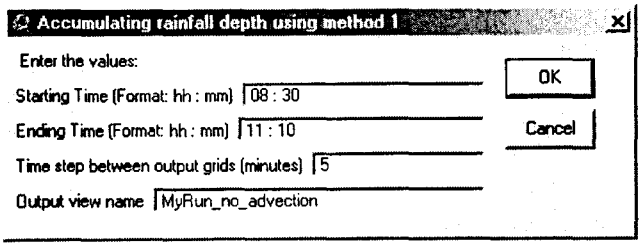

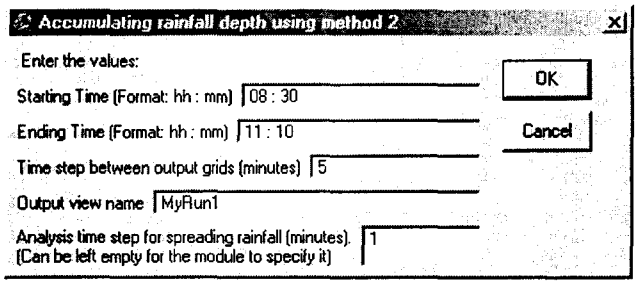

4- If method 2 or 3 are used an additional file dialog appears to get the text file holding the velocity vector information, the format of this text file is comma separated. Each line contains the time and the corresponding velocity vector information (i.e., Xshift, and Yshift in meters). The output file of both the AARS Tracking and the C.G tracking modules is compatible and can be used directly as is.

V.2.7 The GPP Projection Utility

The loaded radar data, as mentioned above, is in the radar coordinate system. The radar coordinate system is a Cartesian coordinate system (meters units) having its origin at the center (i.e., the middle) of the squared radar grid (i.e., the radar location). The GPP projection utility is provided for the purpose of locating rain-gauges or other geographical features with respect to this coordinate system, i.e. for projecting geographical features into/from the radar coordinate system using the GPP method developed in Chapter 4. In other words, this projection utility is for the forward/inverse transformations between two coordinate systems: the radar coordinate system (meters units) and the ellipsoidal geodetic systems (longitudes and latitudes). The forward transformation is used for converting the geographical features or locations from longitudes and latitudes to radar coordinates so that it can be aligned accurately in the view. The inverse transformation is used to export the

locations from the view back to longitudes and latitudes. The following steps describe the use of the forward transformation, the inverse steps are similar except that the input coordinates in this case are radar coordinates and the output is long. and lat.

In order to use the forward transformation, make sure that the geographical features you are going to load into your view are in geographical coordinates (i.e., longitudes and latitudes). The features can be either point coordinates text file or any other shape file (point, line, or polygons features). To use the forward transformation follow these steps:

1- Go to the "Radar" menu then select "GPP Projection Utility". In the dialog that appears select "Forward Transformation".

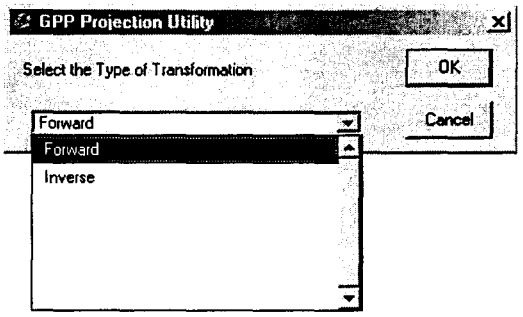

2- Enter the longitude and latitude of the radar location in the next dialog.

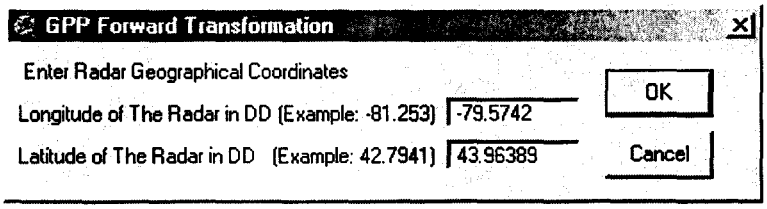

3- Select the type of input you are going to use from a drop down list. the Shape file choice is the standard shape file format of ArcView GIS vector data and the points text file is the other option.

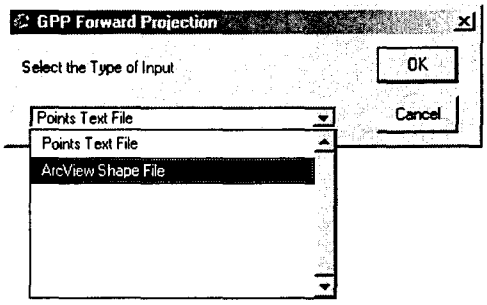

If you are going to use point text file the coordinates have to be written in the format of long. and lat. separated by one space and each point in a separate line as shown in the following figure.

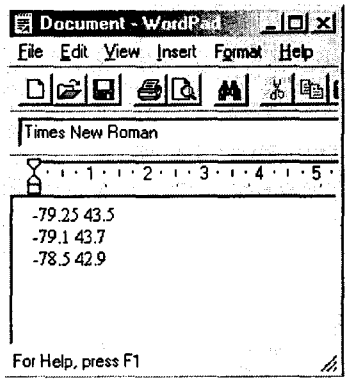

4- Two file dialogs appear to prompt for the input and output files respectively. Specify them then press "Ok". After the projection is done, a message will ask if it is required to add the projected data into the view.

The steps of the inverse transformation is similar to the forward transformation case. But in this case the input coordinates are radar Cartesian coordinates (x and y) in meters and the output coordinates are longitudes and latitudes in decimal degrees. Also, if you are going to use point coordinates in an input text file, the format are space delimited and each line contains the x and y coordinates of a point in meters.

V.2.8 Comparison With Rain-Gauges

This utility extracts a series of radar values at the locations of the rain-gauges. It requires a point theme, representing the locations of the rain-gauges, loaded in the view. The point theme must be in radar coordinates to align properly with the loaded radar data. You may use the projection utility described in the previous section or any other projection software to project point themes from longitudes and latitudes to radar coordinates. Once the gauges theme is loaded in the view use the following steps:

1- Activate the radar grids in the period you want to extract data for.

2- Go to the "Radar" menu then select "Compare With Rain-Gauges".

3- A drop down list appears. Select the point theme representing the rain-gauge locations then press "Ok".

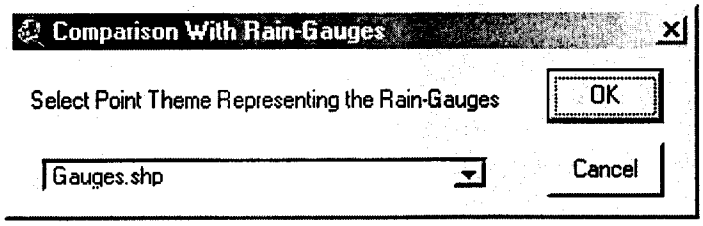

4- A list of the column names in the attribute table of the gauges theme appears in a list box. Select one of theses filed to be used as identification for the gauges. In the output file later, you will identify the gauges using these IDs.

4- A file dialog appears to prompt for the output text file, enter the name then press "Ok".

V.2.9 Radar Menu Additional Features

The "radar" menu contains additional features such as "Changing Display Legend", and "Animation". The module for extracting small grids is useful when exporting radar data inside portions of the radar umbrella. In addition it is more economical to use small grids when it is required to work on smaller areas. Changing display legend is used to change the colour ramps which are used to specify the shades of the grids. The animation module is useful for presentations and for observing storm evolution in different scales. Additional details on these features can be found in the RAINPLAT user manual.

V.3 The Rain-Gauge Extension

The Rain-Gauge Extension is a specific extension for loading and processing rain-gauge data from Hamilton-Wentworth (HW) and Ontario Climate Center (OCC) networks. Hence, it may be limited only to these two networks or similar formats.

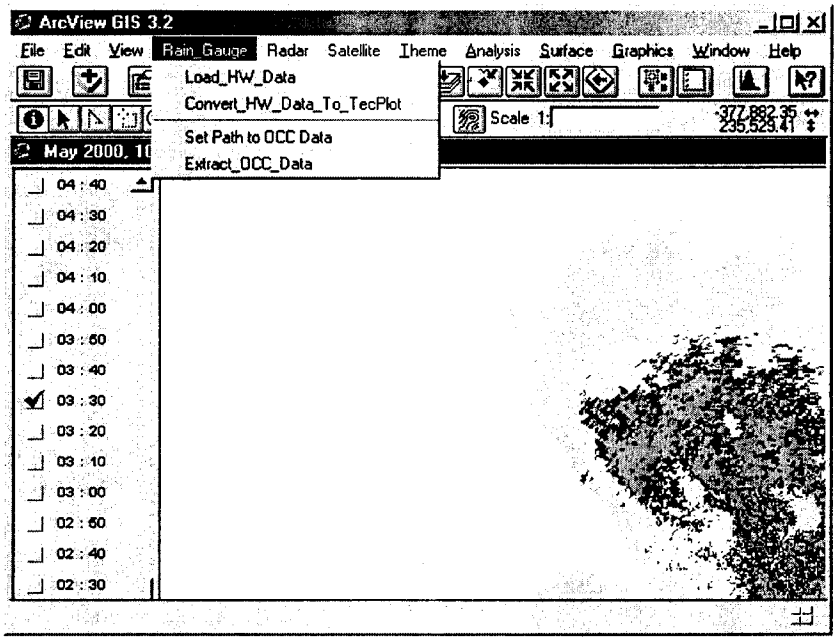

V.4 The Satellite Extension

A Satellite Extension is also available for loading GOES8 satellite data and overlaying it with radar data. The process of loading satellite data is similar to the case of radar data described in the previous sections. In addition, the C.G and AARS tracking modules can be run on satellite data.

V.4.1 Installing the Satellite Extension

Assuming that the RINPLAT-GIS package is installed on the system, follow the following steps to load the Satellite Extension:

1- Open ArcView.

2- Go to the "File" menu then select "Extensions".

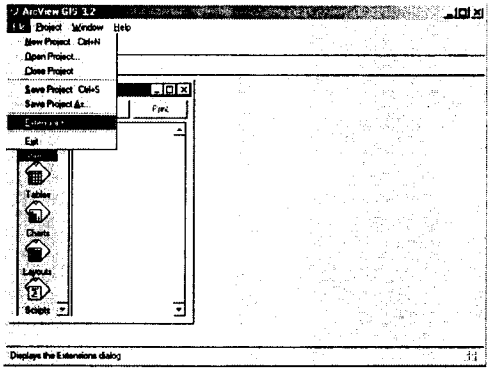

3- In the dialog that appears check the "Satellite" Extension.

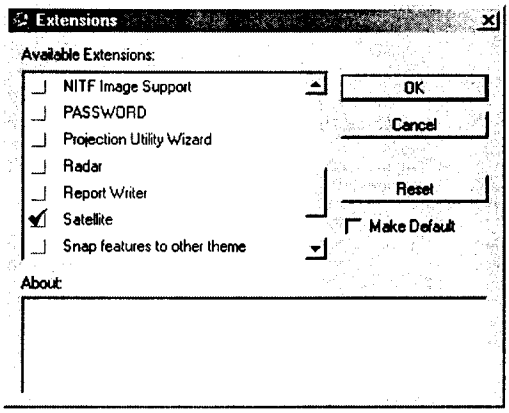

After Loading the "Satellite" Extension. Open a new view. The view interface will have a new "Satellite" menu added.

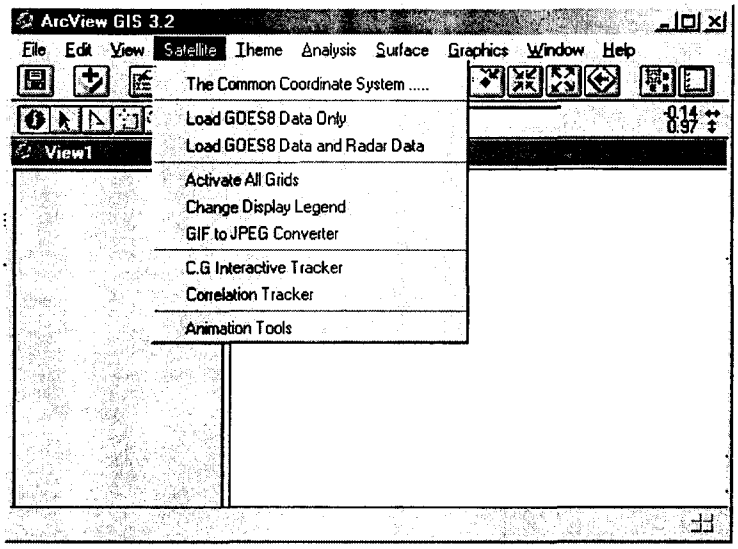

V.4.2 Loading Satellite Data

Note that the raw satellite file names have to start with a string representing the time of the file. For example "200105180420...". However, there is no limitation of the remaining of the file name. For example : "200107192030_anyname.jpg" is a correct file name.

1- Go to the "Satellite" menu then select "Load Satellite Data Only".

2- In the dialog that appears enter the time difference with the UTC (Greenwich) System in hours. For example, if you want the data to be loaded in ArcView in Eastern time System, enter 4 hours in the summer or 5 hours in the winter. Enter zero if you want to leave the data in UTC system.

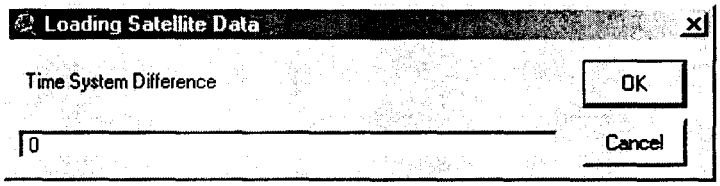

3- A file dialog appears prompting the user to select the satellite JPG files to be loaded. Browse to the location on the hard drives where the data is. Hold down the "Shift" key then select with the mouse (or with the keyboard arrows) any number of the satellite files you want to load then press "Ok".

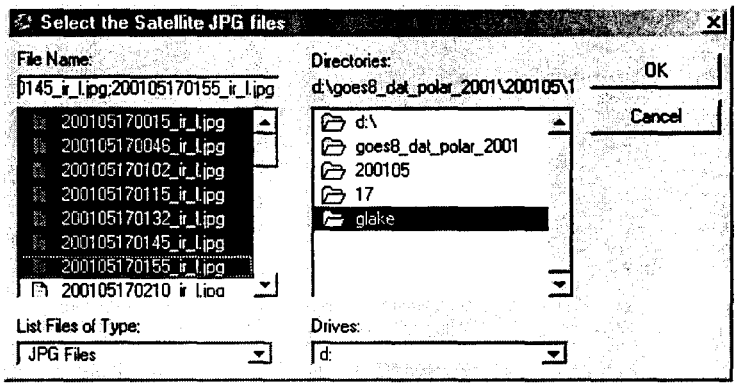

The satellite data will be loaded in the view as ArcView grids as shown in the following figure.

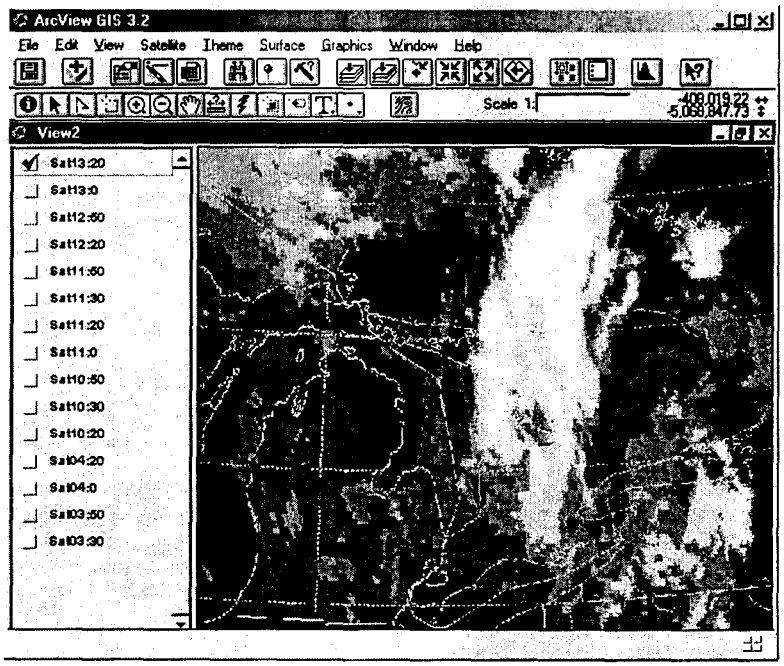

V.4.3 Loading Satellite Data and Radar Data

The common coordinate system in which the satellite data is referenced is a polar Stereographic projection. In order to properly overlay the radar data with the satellite data, the radar data should be projected in the same coordinate system. For this purpose ArcInfo-GIS is used.

I.V.4.3.1 Projecting Radar Data Using Arc/Info-GIS

To do this follow the following steps:

1- Load the radar data into ArcView using the radar extension and use UTC time system, i.e., specify time difference of zero. (Note that the grid data sets will be located in your working directory).

2- Export the radar data to IEEE grids. This can be done from the

"File" menu by using "Export".

3- Close ArcView. Open ArcInfo and import the data you have exported using ArcInfo command "Import". The grids will be imported to ArcInfo.

4- Then Use Arc/Info projection command "Project" to project the imported grid data set from (King or Exeter) projections to the polar Stereographic common coordinate system. You will need the following projection files to define the projection for each of King City and Exeter when using ArcInfo:

King City Arc/Info Projection File:

```
INPUT
PROJECTION AZIMUTHAL
UNITS METERS
PARAMETERS
0
-79 34 22.188
43 57 48.6
0
0
OUTPUT
PROJECTION STEREOGRAPHIC
UNITS METERS
PARAMETERS
1
6371200
-83.00
90.00
0
0
END
```

Exeter Arc/Info Projection File:

```
INPUT
PROJECTION AZIMUTHAL
UNITS METERS
PARAMETERS
0
-81 23 00
43 22 00
0
0
OUTPUT
PROJECTION STEREOGRAPHIC
UNITS METERS
PARAMETERS
1
6371200
-83.00
90.00
0
0
END
```

5- Once you finished projecting the grids, export the grids back to IEEE format using ArcInfo command "Export".

V.4.3.2 Loading The Data

1- Go the "Satellite" menu then select "Load Satellite Data and Radar Data".

2- Two file dialogs will appear, the first prompts to select all the satellite files required. The second file dialog prompts to select where is the location of the projected radar data (exported from ArcInfo). Select the files in the first dialog then browse to the location of the projected radar data folder

and select only one file (any file) from there then press "Ok".

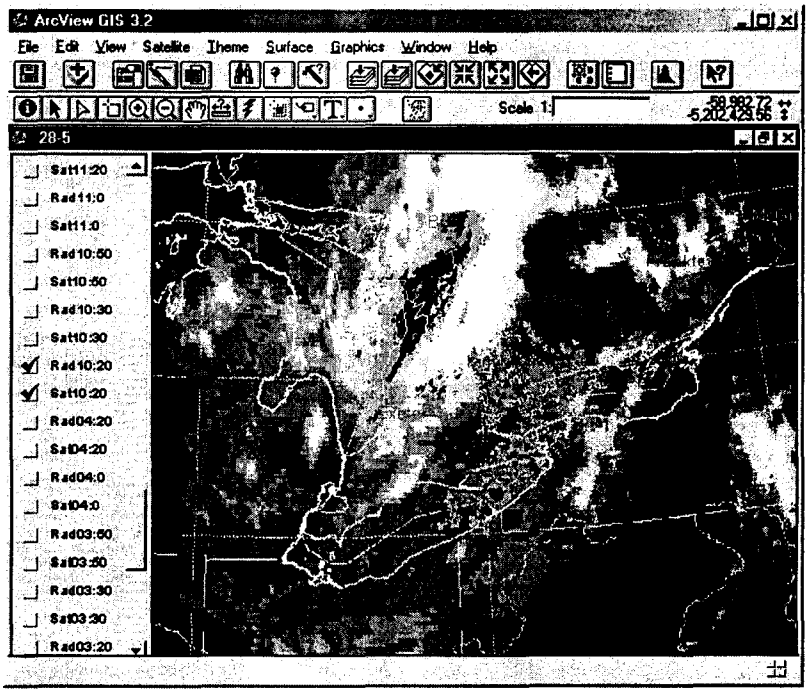

V.4.4 Satellite Menu Additional Features

The "Satellite" menu contains additional features such as the tracking items, "Changing Display legend", and a GIF to JPG converter. The usage of the tracking modules on satellite data is similar to the case of radar data described in sections V.2.4 and V 2.5.1. Changing display legend is used to change the colour ramps which are used to specify the shades of the satellite grids. The GIF to JPG converter is used to convert the raw satellite data from GIF to JPG format if required. Additional details on the extension can be found in the RAINPLAT user manual.